

**A Thesis Submitted for the Degree of PhD at the University of Warwick**

**Permanent WRAP URL:**

<http://wrap.warwick.ac.uk/89185>

**Copyright and reuse:**

This thesis is made available online and is protected by original copyright.

Please scroll down to view the document itself.

Please refer to the repository record for this item for information to help you to cite it.

Our policy information is available from the repository home page.

For more information, please contact the WRAP Team at: [wrap@warwick.ac.uk](mailto:wrap@warwick.ac.uk)

# Lightweighting of Stiffness Critical Advanced High Strength Steel Structures using Fibre Reinforced Plastics

by

Elspeth Macgregor Keating

A thesis submitted in partial fulfilment of the requirements for the degree of  
Doctor of Philosophy in Engineering

University of Warwick, Warwick Manufacturing Group

October 2016

## TABLE OF CONTENTS

Table of contents.....	ii
Table of figures.....	vi
Table of tables.....	xii
Table of equations.....	xv
Acknowledgements.....	xvi
Declaration of authorship.....	xvii
Abstract.....	xviii
Abbreviations and terminology.....	xix
1 Introduction.....	1
1.1 Drivers of the lightweighting trend.....	3
1.2 Automotive lightweighting context .....	4
1.2.1 Raw material costs .....	6
1.2.2 Change in design mentality.....	6
1.3 Scope of the project and novel contribution .....	7
1.4 Layout of the document .....	8
2 Literature review.....	11
2.1 A focus on the automotive industry .....	11
2.2 Steel-FRP hybrid automotive applications.....	13
2.3 Other hybrid applications.....	20
2.4 Joining mechanisms for dissimilar materials .....	22
2.5 Theoretical analysis of the materials.....	24
2.6 Purpose of this research .....	26
3 Materials and methods .....	29
3.1 Steel DP600 .....	29

3.1.1	DP600 properties.....	30
3.1.2	DP600 coating.....	31
3.2	Composite .....	32
3.2.1	PA6 GF60 – Glass Fibre .....	33
3.2.2	PA6 CF60 – Carbon Fibre .....	35
3.3	Adhesive .....	36
3.3.1	Alpha Adhesives S10 and SAS 272.....	37
3.3.2	Sika 490 C.....	38
3.4	Testing.....	40
3.4.1	Equipment .....	40
3.4.2	Standards.....	44
3.5	Simulation program .....	44
3.5.1	Element Selection and Meshing.....	45
3.5.2	LS-DYNA .....	47
3.5.3	Genesis.....	48
3.5.4	Optimisation Concept .....	49
4	Coupon program .....	50
4.1	Testing.....	50
4.1.1	Sample production and hybrid preparation .....	50
4.1.2	Three-point bend instrumentation.....	58
4.1.3	Benchmarking .....	59
4.1.4	Hybrid .....	60
4.2	Simulation.....	63
4.2.1	FEA Model Creation in LS-DYNA .....	65
4.2.2	FEA Model Creation in GENESIS .....	70
4.3	Results and Discussion .....	76

4.3.1	Expressing the results.....	76
4.3.2	Full Results and Discussion .....	78
4.4	Conclusions.....	96
Chapters 5 and 6; a brief introduction.....		99
5	Component program – Experimental approach .....	100
5.1	Geometry and dimensions.....	100
5.2	Testing.....	101
5.2.1	Sample production .....	102
5.2.2	Instrumentation set up.....	103
5.2.3	Samples .....	105
5.3	Results.....	107
5.3.1	Topside up.....	107
5.3.2	Topside down.....	114
5.3.3	Discussion .....	119
5.4	Conclusions.....	124
6	Component program – Simulation approach .....	125
6.1	The basic model .....	125
6.2	Study of the loading constraints.....	128
6.3	Local reinforcement .....	134
6.4	Results.....	136
6.4.1	Correlating the 1.6 mm DP600 samples .....	141
6.5	A manual localisation optimisation – pure elastic bending .....	149
6.6	Limitations, Conclusions and Further work.....	153
7	Summary.....	155
7.1	Discussion of outcomes and limitations to the research .....	155

7.1.1	Manufacture of the hybrid materials.....	156
7.1.2	Expressing the stiffness performance.....	157
7.1.3	Quasi-static coupon testing.....	158
7.1.4	Quasi-static component testing.....	163
7.1.5	FEA predictions.....	166
8	Conclusions and Perceived Contribution to Knowledge.....	169
9	Wider implications of FRP steel hybrid uptake in BIW.....	171
10	References.....	174
	Appendix A.....	181
	Appendix B.....	185
	Appendix C.....	187
	Appendix D.....	189

## TABLE OF FIGURES

Figure 1-1: Body-in-white (BIW) representation with steel grades used for different applications [3].....	2
Figure 1-2: An overview of the project.....	10
Figure 2-1: Profile cross-section of a hybrid structure with special structural parts labelled [21] .....	14
Figure 2-2: Load-deformation curve of the various profile sections tested in flexure [21].....	14
Figure 2-3: Load-deflection diagrams comparing an open “U” profile without and with plastic stiffeners [23] .....	15
Figure 2-4: Geometry and location of composite reinforcement [27] .....	16
Figure 2-5: CBS 96, 1 – in-mould surface film, 2 – first fibre layer, 3 – resin core, 4 – second fibre layer [39] .....	19
Figure 3-1: Strength - elongation graph of the different types of steel produced by Tata Steel [81].....	30
Figure 3-2: Micrograph image showing the layup of DP600, SAS 272 and [0,90][90,0] PA6 GF60 .....	34
Figure 3-3: Micrographs showing the depth of peel-ply surface preparation a) top layer of peel-ply surface preparation, b) bottom layer of peel-ply surface preparation .....	35
Figure 3-4: Heat flow curves for S10 adhesive [91] .....	37
Figure 3-5: Lap Shear strength extension curve for the SAS 272 adhesive between a carbon fibre MTM57 and AC600 E coated aluminium [92].....	38
Figure 3-6: Lap Shear strength extension curve for the Sika 490 C adhesive between carbon fibre MTM57 and AC600 E coated aluminium [92].....	39
Figure 3-7: Three-point bend test rig and fixture.....	43

Figure 4-1: Sketch defining fibre directionality in the three-point bending samples (not to scale); from top to bottom 45° (grey), 90° (blue) and 0° (pink).....	54
Figure 4-2. Hybrid Composite/Steel [0,90] <sub>s</sub> ply directionality – not to scale .....	56
Figure 4-3: Hybrid Composite/Steel [90,0] <sub>s</sub> ply directionality – not to scale .....	57
Figure 4-4: Hybrid Composite/Steel [45,-45] <sub>s</sub> ply directionality – not to scale.....	57
Figure 4-5: Micrograph cross section of the hybrid sample DP600 and [0,90] <sub>s</sub> PA6 GF60 .....	58
Figure 4-6: Three-point flexure fixture set up – span length is 40 mm .....	59
Figure 4-7: Quasi-static three-point bend set up with composite face down (S/C) – sample length 60 mm, span 40 mm, width 15 mm .....	61
Figure 4-8: Quasi-static three-point bend set up with steel face down (C/S) – sample length 60 mm, span 40 mm, width 15 mm.....	61
Figure 4-9: LS-DYNA Model showing the directionality of the vectors normal to the shell elements from Primer .....	65
Figure 4-10: Genesis model showing the directionality of the vectors normal to the shell elements.....	65
Figure 4-11: HyperMesh model of the three-point bend test.....	66
Figure 4-12: LS-DYNA model of the three-point bend test, with a single layer of shell elements.....	67
Figure 4-13: Representation of correlation between the experimental (solid lines) and simulated (dotted line) for the hybrid 0.8 mm DP600 GFRP samples .....	68
Figure 4-14: LS-DYNA model with two layers of shell elements: Steel and composite model .....	69
Figure 4-15: Layers modelled individually.....	69
Figure 4-16: Support and loading conditions on the coupon sample in Genesis – showing displacement (mm) .....	71
Figure 4-17: Screenshot of the deflected 0.5 mm DP600 [0,90] <sub>s</sub> specimen – magnitude of deflection (mm).....	72



Figure 4-18: Genesis model of the three-point bend test, with a single layer of shell elements .....	72
Figure 4-19: Genesis model with two layers of shell elements joined by rigid body elements (RBE) – layer thickness shown.....	74
Figure 4-20: Genesis model with two layers of shell elements – focus on RBEs... 74	
Figure 4-21: Specific stiffness diagram for various benchmark materials [87] .....	77
Figure 4-22: Load-extension diagram for the 0.8 mm hybrid coupon samples tested to failure .....	78
Figure 4-23: Elastic region relevant to the project, all 0.8 mm hybrid samples .....	79
Figure 4-24: Specific bending stiffness for all 0.8 mm DP600 GFRP hybrids and steel .....	80
Figure 4-25: Graphical representation of all the hybrid samples .....	81
Figure 4-26: Ludke’s criterion for the steel and GFRP samples, normalised to pure DP600 steel only .....	82
Figure 4-27: Load-extension graph showing the 0.5 and 0.8 mm hybrid samples and the benchmarked 0.8 and 1.6 mm pure steel sample.....	84
Figure 4-28: The performance and weight “improvements” of the GFRP hybrid samples compared to the pure steel ones .....	92
Figure 4-29: The performance and weight “improvements” of the CFRP hybrid samples compared to the pure steel ones .....	93
Figure 4-30: Comparative performance improvements between the GFRP and CFRP hybrids – combination of Figure 4-28 and Figure 4-29 .....	95
Figure 5-1: Selected top-hat geometry from an automotive OEM without backplate .....	100
Figure 5-2: Top hat showing local PA6 GF60 reinforcement on the top of the top-hat – sample is 450 mm in length, 132 mm in width, height ~ 43 mm.....	101
Figure 5-3: Three-point bend fixture set-up for the top-up static bending – sample length 450 mm, width 132 mm and height ~43 mm .....	104

Figure 5-4: Schematic drawing showing the dimensions of the rollers and test set-up .....	104
Figure 5-5: Sample with composite reinforcement in test rig; scenario with top-hat side down .....	106
Figure 5-6: Top-hat samples as tested, with composite reinforcement; a) scenario with top-hat side up; b) scenario with top-hat side down .....	106
Figure 5-7: 0.5 mm DP600, pure steel (a), hybrid (b); 0.8 mm DP600, pure steel (c), hybrid (d) – samples are 450 mm long .....	108
Figure 5-8: ISO view of the deflection region of 0.5 mm DP600 pure (a) and hybrid (b); and 0.8 mm DP600 pure (c) and hybrid (d) .....	110
Figure 5-9: Comparison of plastic hinge area in a) 0.8 mm DP600 pure steel sample and b) 0.8 mm DP600 hybrid sample .....	110
Figure 5-10: Summary of the load-extension curves for all samples tested in the topside up scenario.....	111
Figure 5-11: Load-extension curves for pure steel samples only .....	112
Figure 5-12: Load-extension graphs for hybrid samples only .....	112
Figure 5-13: Topside down 0.8 mm pure steel a) and hybrid samples b).....	114
Figure 5-14: Detail of plastic hinging zone on 0.8 mm DP600 pure steel and hybrid samples for topside down.....	116
Figure 5-15: Load-extension graph for all samples tested topside down.....	117
Figure 5-16: Load-extension graphs for pure steel samples only .....	117
Figure 5-17: Load-extension graphs for hybrid samples only .....	118
Figure 5-18: The performance and weight “improvements” of the hybrid samples compared to the pure steel ones, topside up.....	122
Figure 6-1: Genesis FE model of the beams used in testing .....	125
Figure 6-2: Showing the RBE2 links representing the adhesive bond between the top hat shape and the backplate; a) and b) with and without thickness representation	127
Figure 6-3: Deflection of beam under full nodal force distribution.....	129

Figure 6-4: Roller loading condition.....	132
Figure 6-5: Graphical representation of the effect of the loading conditions of the load-extension performance.....	133
Figure 6-6: Shows the reinforcement locations; a) shows the top reinforcement, b) shows the side reinforcement, c) shows the corner reinforcement .....	135
Figure 6-7: Bar chart showing the beam stiffness k based on steel thickness and composite reinforcement location, topside up .....	137
Figure 6-8: Bar chart showing the sample weights based on steel thickness and composite reinforcement location, topside up .....	138
Figure 6-9: Pure steel and hybrid sample stiffness values in experimental and simulated cases.....	139
Figure 6-10: Correlation of experimental testing from this work (Els 1) and LCVTP sources (14_1 and 14_4) .....	142
Figure 6-11: Quarter-beam model as used in LCVTP .....	143
Figure 6-12: Von Mises stress values at onset of displacement – when impactor first connects with beam.....	143
Figure 6-13: Plastic strain values at onset of displacement – when impactor first connects with beam.....	144
Figure 6-14: Von Mises stress values at onset of displacement.....	145
Figure 6-15: Plastic strain values at onset of displacement .....	145
Figure 6-16: Load-extension graph showing the correlation of the experimental and simulated results.....	146
Figure 6-17: Load-extension graph of the simulated results only.....	147
Figure 6-18: Load-extension graph of the hybrid experimental and simulated results .....	148
Figure 6-19: Localised reinforcement using patches of composite material .....	150
Figure 6-20: Deflection plot for 0.8 mm samples at identical load; a) pure steel, b) top reinforcement, c) local reinforcement – deflections not to scale .....	151

Figure 7-1: The performance and weight “improvements” of the GFRP hybrid samples compared to the pure steel ones (reshown Figure 4-28) .....	160
Figure 7-2: The performance and weight “improvements” of the hybrid samples compared to the pure steel ones – reshow Figure 5-18.....	165
Figure A-1: Optical microscopy image of the cross section of a hybrid DP600 PA6 GF60 specimen showing the adhesive (top) and composite (bottom) layers – scale >500 μm.....	181
Figure A-2: EDS graph showing the elements present in the adhesive .....	182
Figure A-3: Scans showing presence of elements in inclusions .....	184
Figure D-1: Load-extension diagram for the 0.8 mm hybrid coupon samples tested to failure - reshow .....	189

## TABLE OF TABLES

Table 2-1: Specimen dimensions in study by Dlugosch [28] .....	17
Table 3-1: DP600 properties obtained from tensile tests following standard BS EN ISO 6892-1 (2009) [83] .....	30
Table 3-2: Chemical composition of DP 600 as guaranteed by manufacturer [82]	31
Table 3-3: PA6 GF60 properties obtained from tensile and flexure testing [88, 89] .....	34
Table 3-4: PA6 CF60 properties obtained from tensile and flexure testing.....	36
Table 3-5: Variations of hold time, pressure and rate attempted to press samples .	41
Table 3-6: Maximum deflection from scans of samples after forming at varying pressures and hold times .....	42
Table 4-1: Fibre layups considered in study .....	55
Table 4-2: Sizing of 0.8 mm hybrid samples for flexure tests .....	56
Table 4-3: Sizing of 0.5 mm hybrid samples for flexure tests .....	56
Table 4-4. Summary of the coupon samples tested, five repeats each. C/S refers to composite/steel, and S/C to steel/composite .....	62
Table 4-5: Correlation of tested and Genesis simulated load-displacements for the benchmark DP600 material and both hybrids.....	73
Table 4-6: Percentage increase in specific bending stiffness and percentage weight save for the equivalent performance in steel only.....	83
Table 4-7: Summary of all the results obtained in testing and associated simulation .....	85
Table 4-8: Summary of simulated CFRP results.....	86
Table 4-9: Normalised performance of the GFRP 0.5 mm hybrid coupon samples relative to other samples .....	86
Table 4-10: Normalised performance of the GFRP 0.8 mm hybrid coupon samples relative to other samples .....	87

Table 4-11: Further simulated comparison of coupon samples .....	88
Table 4-12: Normalised performance of the simulated CFRP 0.5 mm hybrid coupon samples relative to other samples.....	89
Table 4-13: Normalised performance of the simulated CFRP 0.8 mm hybrid coupon samples relative to other samples.....	90
Table 5-1: Summary of samples tested experimentally and their weights.....	105
Table 5-2: Summary of topside up stiffness values and sample weights.....	113
Table 5-3: Summary of topside down stiffness values and sample weights .....	118
Table 5-4: Summary of topside up and topside down k values, as well as sample weights .....	119
Table 5-5: Comparative figures of the performance of the 0.5 mm hybrid samples to the benchmarked pure steel samples and 0.8 mm hybrid samples.....	120
Table 5-6: Comparative figures of the performance of the 0.8 mm hybrid samples to the benchmarked pure steel samples and 0.5 mm hybrid samples.....	121
Table 6-1: Description of loading conditions trialled .....	129
Table 6-2: Summary of local reinforcement and combinations thereof.....	134
Table 6-3: Summary of the weights of the samples, the “adjusted simulated” weights take into account the estimated weight of adhesive per sample.....	136
Table 6-4: Summary of stiffness values K based on samples make-up – pure DP600 or DP600 with specific reinforcements.....	137
Table 6-5: Stiffness performance of the hybrid samples with local reinforcements compared to the previously tested ones .....	150
Table 7-1: Summary of all fabricated samples .....	157
Table A-1: Element weight distribution in the adhesive layer SAS 272 .....	183
Table B-1: Scans of springback samples, with associated rate, pressure and hold time information.....	185
Table D-1: Notes on sample failure patterns .....	190
Table D-2: Representative failure (photographic documentation).....	190

Table D-3: Image captures of the compressive zone of the samples – fibre overlap show .....	192
--	-----

## TABLE OF EQUATIONS

Equation 2-1.....	25
Equation 2-2.....	25
Equation 2-3.....	25
Equation 2-4.....	25
Equation 2-5.....	26
Equation 4-1.....	82
Equation 4-2.....	82
Equation 4-3.....	86
Equation 5-1.....	120
Equation 5-2.....	120



## ACKNOWLEDGEMENTS

I would like to acknowledge the University of Warwick, EPSRC and Tata Steel for their financial contribution and the opportunity to undertake this research.

Thanks and recognition must be given:

To Dr Darren Hughes and Dr Janka Cafolla for their constant support and guidance; to Prof Richard Dashwood and Dr Iain McGregor for their insight and overview. It has been a privilege to work with you.

To the staff at GRM for their technical support and knowledge.

To Dr Helen Ascroft, Dr Beth Middleton, Zachary Parkinson, Darren Stewardson, Martyn Wilkinson, Dr Neill Raath, Dr Richard Beaumont, Matt Byrne, Rich Powe, Craig Carnegie and Scott Taylor.

To the University of Warwick Sailing Club, that brought me Oliver Newell, Sarah Kent, Ayushi Amin, Louise Jackson, Sophie Hetherton, Thomas Needham, Benjamin Mackley, Chris Gudde and Dr Mathieu Boissaud-Cooke. You were the calming influence, welcome breaks and insanity checks.

To Anne Jacob, for the example of hard work and a dedication to learning

To Rachel Stevenson, Dr Paula Kellett and Dr Charlotte Banks

To Niamh Schutte Byars, Tony Schutte Byars and the members of squadron 221

To John Sheridan, Steffan Chave and Andrew Lang

And finally to my Mother, Father and Sibling, for leading the way.

Thank you, I couldn't have done it without you.

## **DECLARATION OF AUTHORSHIP**

This thesis is submitted in partial fulfilment of the requirements for the degree of Doctor of Philosophy. It describes work carried out from November 2012 to October 2016. Unless otherwise indicated the research described is my own and not the product of collaboration. No part of this thesis has been submitted to any other university, or as any part of any other submission to the University of Warwick.

Signed and dated:

## ABSTRACT

In the drive for lightweighting in many industries, optimum material selection is at the forefront of research. Many solutions are being investigated, including the fabrication of multi-material components. Following a state of the art review of the literature, it has been shown that there is an opportunity to improve basic knowledge and understanding of the characteristics of hybrid steel-FRP materials for lightweight applications. This dissertation explores the potential for designing lightweight automotive steel structures through novel use of lower gauges *combined with* local reinforcement by fibre-reinforced plastics to achieve desired stiffness performances. The main focus of the work is to provide underpinning research to enable the further understanding of the stiffness performance of hybrid steel-FRP materials, both experimentally and in simulation.

This thesis focuses on the characterisation of high strength automotive grade steel (DP600) reinforced with a fibre reinforced polyamide (PA6 GF60) laminate, however, the results are readily applicable for other combinations. The project was achieved through two main phases; each phase consisting of an iteration loop between experimentation and simulation validations. Initial characterisation was achieved using coupon samples in quasi-static three-point bend, cross-validated in simulation providing a trusted material model. Correlating experimental and simulated results showed a potential lightweighting of up to 30 % of a hybrid DP600-GFRP over a DP600 counterpart with a matched stiffness performance. Further characterisation was performed using an idealised automotive component in flexure, confirming a potential lightweighting of up to 30 %. The simulation investigation demonstrated the effect of localised hybrid reinforcements, and identified difficulties in predicting the local geometrical effects of plastic hinging. For an overall application to an automotive body-in-white, these would require further investigating.

This thesis has proven that downgauging steel whilst locally reinforcing (intelligent deployment) with FRP patches provides a significant lightweight solution with a matched stiffness performance. A hybrid material model has been validated and the application to an automotive component investigated. This work provides the basic understanding for a direct application in lightweight automotive designs using computer aided engineering (CAE).

## ABBREVIATIONS AND TERMINOLOGY

AMRC	Advanced Materials Research Centre
BIW	Body In White
C/S	Composite-over-steel testing scenario
CAA	Clean Air Act
CAE	Computer Aided Engineering
CAFE	Corporate Average Fuel Economy
CBS	Car Body Sheet
CFRP	Carbon Fibre Reinforced Polymer
DP	Dual Phase – as in DP600 Steel
E	Young’s modulus
EPA	Environmental Protection Agency
FAT	Forschungsvereinigung Automobiltechn
FEA	Finite Element Analysis
FRP	Fibre Reinforced Polymer
GFRP	Glass Fibre Reinforced Polymer
GHG	GreenHouse Gas
IPA	Iso-propyl Alcohol
ISO	Isometric
k	Gradient of the load-extension curve in the elastic region
LCVTP	Low Carbon Vehicle Technology Project
OEM	Original Equipment Manufacturer

PA 6	Polyamide 6
PA 6.6	Polyamide 6.6
S/C	Steel-over-composite testing scenario
SMC	Sheet Metal Compound
SMMT	Society of Motor Manufacturers and Traders
$\sigma_y$	Yield Strength
UNFCCC	United Nations Framework Convention on Climate Change
UTS	Ultimate Tensile Strength
$\rho$	Material density

# 1 INTRODUCTION

Promoted by a number of worldwide and European treaties and directives, the automotive industry is taking a (forced) stand on the future of automotive design, shifting towards perceived “greener” solutions.

In the automotive market, the use of fibre reinforced plastics, also known as FRP, was historically limited to the predominantly niche market of sports cars, primarily due to the costs associated with those materials [1]. Recent developments in high-end consumer vehicles show a slow emergence of composite materials in automotive structures, with an industry-wide drive for lighter, more efficient and recyclable vehicles [2].

This ever increasing demand for automotive body lightweighting drives the idea of combining the strength provided by advanced high strength steel (AHSS) together with the comparatively light weight of FRP. Together, these hybrid materials can potentially achieve the desired mass reduction whilst maintaining performance – here specifically stiffness – and ideally minimising cost.

This thesis will research the material properties of a combined FRP and low-gauge high strength steel hybrid material focussing on stiffness performance (but lower weight), and investigate the required input data for appropriate finite element simulations. Using the experimental data acquired and a validated simulation model, further work will investigate the “intelligent deployment” of the FRP patches or reinforcements in specific structures representative of “real life” automotive body applications. This project is specifically interested in “higher-strength” steels used in automotive structures as shown in in Figure 1-1 [3]. However, the approach and method is valid for any steel. Due to the large variety of FRP materials, the approach and method for the FRP can be expanded to different materials, with modifications on a case per case basis.

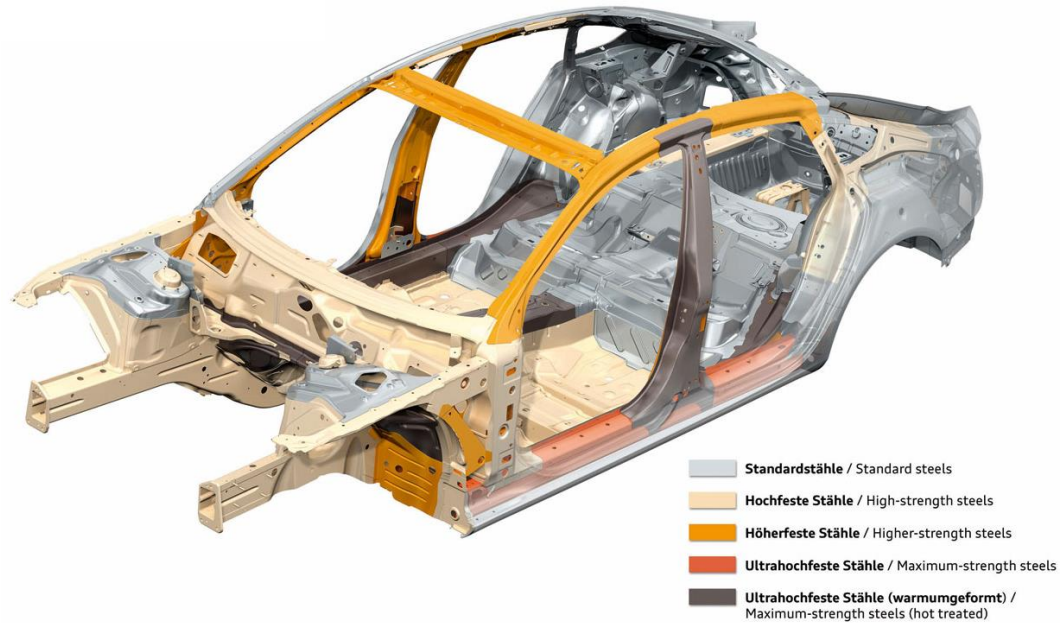


*Figure I-1: Body-in-white (BIW) representation with steel grades used for different applications [3].*

Body-in-white (BIW) stiffness is well known to affect the handling and performance of any vehicle, therefore a focussed study on maintaining stiffness performance whilst providing a weight save would be of value to an automotive manufacturer. Additionally, maintaining the pre-existing steel structure and locally reinforcing it presents manufacturing and cost advantages. This dissertation explores the potential for designing lightweight automotive steel structures through novel use of lower gauges *combined with* local reinforcement by fibre-reinforced plastics to achieve desired stiffness performances. The main focus of the work is to provide underpinning research to enable the further understanding of the stiffness performance of hybrid steel-FRP materials, both experimentally and in simulation.

This project can conceptually be split into several research objectives. The first is to perform a concise, exhaustive and relevant literature review on the subject of lightweight material solutions, FRP reinforcing of steel, joining of dissimilar materials, testing and simulation therefore identifying the research opportunity in this field.

The second objective is to design and manufacture a range of parts for stiffness testing in order to characterise the material. This preliminary material performance data is used in the development of a hybrid material simulation model. Using iterative steps between experimental results and simulation results, the next objective is to validate the simulation model, first at coupon and then at component level. The coupon work focuses on determining the inherent stiffness properties of the hybrid material. The selected component work concentrates on the application of FRP to an automotive top-hat geometry with an application to the BIW.

This chapter introduces the driving factors in the lightweighting trend, including the potential solutions relevant to the automotive industry. The costs associated with the raw materials are discussed and the changes in design mentality that the industry demands are investigated. The scope of the project is also presented in detail, along with the formal thesis structure.

## **1.1 Drivers of the lightweighting trend**

The creation and signing of the United Nations Framework Convention on Climate Change (UNFCCC) [4] in 1992 signalled the start to the writing and implementation of government policies and regulations relating to the emission of greenhouse gases (GHG), namely carbon dioxide, methane, nitrous oxide, sulphur hexafluoride and chlorofluorocarbons (CFC). The Kyoto Protocol (2008-2012) [5], on reversing and reducing greenhouse gas emissions, is one of the most commonly known protocols to have come out of the UNFCCC treaty. Despite its only relative success, it has been largely instrumental in bringing the issue of the environmental impact of industrialisation to the general public. It has since been followed by the signing of the Paris Agreement, which took effect on November 4<sup>th</sup> 2016 and “*brings all nations into a common cause to undertake ambitious efforts to combat climate change and adapt to its effects, with enhanced support to assist developing countries*



*to do so*" [6]. Both the Kyoto Protocol and the Paris agreement have and will be drivers behind individual government policies and regulations regarding greenhouse gas emissions. One such example is the U.S. Environmental Protection Agency's (EPA's) regulation of GHG emissions under the Clean Air Act (CAA) [7]. In the USA again, and running in parallel to treaties focused on environmental impact, the Corporate Average Fuel Economy (CAFE) regulations aim to improve fuel economy of vehicles. Starting at 8.0 mpg in 1978, the standard is 27.5 mpg today and is aiming for 35.0 mpg in 2020 [8]. In the UK, the Society of Motor Manufacturers and Traders, the SMMT, reports European CO<sub>2</sub> emission targets of 130 g/km in 2015 and 95 g/km in 2020 [9]. In the automotive industry, these goals translate in part into weight reducing targets, as approximately every 10 % weight reduction can result in 5 to 10 % greater fuel efficiency [10]. Individual automotive companies have also started setting in-house goals for improved fuel economy. For example, Ford Motor Company has indicated that weight reduction is a key part of its strategy. Plans are to improve fuel economy by 40 % by the year 2020 by reducing vehicle weight by as much as 340 kg [11].

These are just examples of the regulations applied to the automotive industries that all have the same goals: improvement of fuel economy, reduction of emission of polluting gases as well as weight saving targets for light, long-range electric vehicles. They highlight the need within the industry to design and manufacture lighter weight, efficient and optimised vehicles.

## **1.2 Automotive lightweighting context**

There are now recognised solutions to lightweighting a BIW, which include the downgauging of the original material, tailor welded blanks where multi materials are combined, lightweight material substitution such as aluminium or composites, and a BIW redesign [10]. However, despite its high density, there are a number of

advantages to steel as a BIW material, including raw cost, manufacturing ease, recyclability and knowledge-base. This project is specifically investigating the possibility of maintaining the steel BIW base, due to these benefits, whilst downgauging it to reduce mass, and locally reinforcing it with FRP.

In the mid-1990s Messler [12] remarked that metallics and composites are often considered as competitive and unable to “coexist”. In his opinion, researchers are likely to “pick a side” and refuse to consider the hybrid options available. He also highlights that multi-material joining processes are lagging behind in terms of knowledge, performance characterisation and manufacturability compared to monolithic materials. Since then, trends show that FRPs are growingly being recognised as legitimate ways to reinforce metallic structures. Studies show that it is possible, through optimisation and the development of performance indices, to create lightweight multi-material automotive bodies without significant cost increase [13, 14].

There is however a pressing need to develop the knowledge-base surrounding these hybrid materials, ranging from their manufacturing, performance, optimisation, failure modes and range of application.

Work has been done in terms of potential application (see Chapter 2, Literature review), however little work has been carried out towards the understanding of the fundamental properties of steel-FRP hybrid materials. There is a gap in knowledge concerning the basic properties of this material, its performance in stiffness, strength and crash. This thesis will focus on understanding specifically the stiffness of the material, and its potential in terms of replacing steel in a structure whilst ensuring there is no loss in performance.

### **1.2.1 Raw material costs**

Despite the economic downturn of 2008, global trends in raw material costs (metals, composites, fuel) show an average increase in prices over the last two decades. In 2001, the U.S. Department of Energy commissioned a review on “the cost of automotive polymer composites” [15]. It concluded that on a \$/lb basis, the cost of polymer composites is about 2-3 times higher than steel. However, because of the higher weight reduction potential of these composite materials, the value of carbon fibre reinforced plastic (CFRP) weight savings lies in the range of \$1.00 - \$4.00/lb [15].

In addition to this, in 2008, in part due to the global recession, Autodata Corp reported a drop of 18.0 % in new vehicle car and light truck sales in the US compared to 2007 levels. In Europe, 2008 was the worst year for auto sales in 15 years; Spain recorded the highest drop at 28.1 %, and the UK a 11.3 % drop according to the European Automobile Manufacturers Association [16]. These factors combined are drivers in the lightweighting trend [11]. Consumers associate a lighter vehicle with lower start-up costs such as the purchase, taxes and insurance as well as lower running costs; reinforcing the industry’s need to lightweight its fleets.

### **1.2.2 Change in design mentality**

There is a shift in design mentality happening alongside the drive to lightweighting. Optimisation is becoming prominent at every design stage and the use of Life Cycle Analysis points towards a move from empirical based design to a design methodology based on risk and performance.

Companies and universities are building relationships towards working together to educate and train future engineers in the knowledge and skills required to understand and implement optimisation in the automotive industry. It can be applied

at every level of automotive design, from the material characteristics and usage to the overall design. Kelvin Lake, of the University of Wales Trinity Saint David, is, in the UK, pioneering the task of involving industrials in this process and raising awareness as to the gap the current education system leaves as to efficient optimised design in engineering [17]. Research centres, such as the UK's Catapult or Germany's Fraunhofer centres, are also providing a key link between industrials and academics [18].

A recent emphasis on Life Cycle Analysis as a feature of the design process has also influenced the design mentality. This stems partly from government and organisation standards on environmental "friendliness" such as the EU's End-of-Life Vehicles Directive [16] which since 2006 requires that a minimum of 85 % by weight of an end-of-life vehicle is reused or recovered (including 5 % energy recovery) and a minimum of 80 % is reused or recycled. By 2015, reuse and recovery was forecast to increase to 95 % with a 10 % energy recovery and reuse and recycling to increase to 85 % [16]. Life Cycle Analysis is also a tool promoting optimisation, when thought about as a more efficient usage of materials [19].

### **1.3 Scope of the project and novel contribution**

Chapter 2 will highlight the gap in published knowledge relating to the stiffness performance and weight save potential offered by the local patching reinforcement of steels using FRPs over their pure steel counterparts. It is intended that this project will seek to answer some of these questions, by focusing specifically on the stiffness and elastic performance of hybrid steel-FRP materials as well as pure steel and pure composite materials. Other characteristics will be noted throughout and discussed however the focus will remain on the elastic behaviour.

The aim of this project is to study the possibility of achieving an enhanced stiffness of low gauge advanced high strength steel structures using fibre reinforced polymers as *patches*, focusing on the automotive industry but consideration is given to other sectors.

Explicitly not covered within the scope are the detailed study of the material under any other loading than quasi-static three-point bend, manufacturability, cost, recyclability, adhesive bond properties outside of an effective bond under elastic loading.

#### **1.4 Layout of the document**

Chapter 1 has presented the context of the project, including the drivers and justifications behind it. Figure 1-2 presents an overview of the project.

Chapter 2 presents the literature review and state of the art review of the use of steel FRP hybrid materials and shows the opportunity for this work, highlighting the current knowledge gap where hybrid material performance is concerned.

Chapter 3 details the materials and methods used throughout the work. The steel, composite and adhesive are introduced, as well as the hybrid fabrication method for all samples. The instrumentation used in production and physical testing of the samples is also discussed, as well as the standards that guided the work. The finite element simulation software packages are also presented.

Chapter 4 focuses on the coupon work. It discusses coupon manufacture in greater depth and the test regime operated. The physical testing was used in an iterative loop to create a simulation of the material behaviour, which was validated against further testing. From the results, the specific bending stiffness was calculated as well as the potential weight save for an identical performance in stiffness.

Chapter 5 presents the component work, where the knowledge from Chapter 4 was applied to an idealised automotive component. It presents and discusses the experimental testing performed on the component sections and presents the final results in terms of performance and weight improvement comparisons.

Chapter 6 describes the application of the simulation assumptions from Chapter 4 to the component section. It discusses the difficulties encountered and proposes a solution.

Chapter 7 discusses the overall learning outcomes from the research, as well as the wider implications for this work in terms of application to the automotive industry and the further research in hybrid material characterisation. It finalises the work, with a discussion of the results and observations, a definition of the perceived contribution to knowledge, and final conclusions for the thesis.

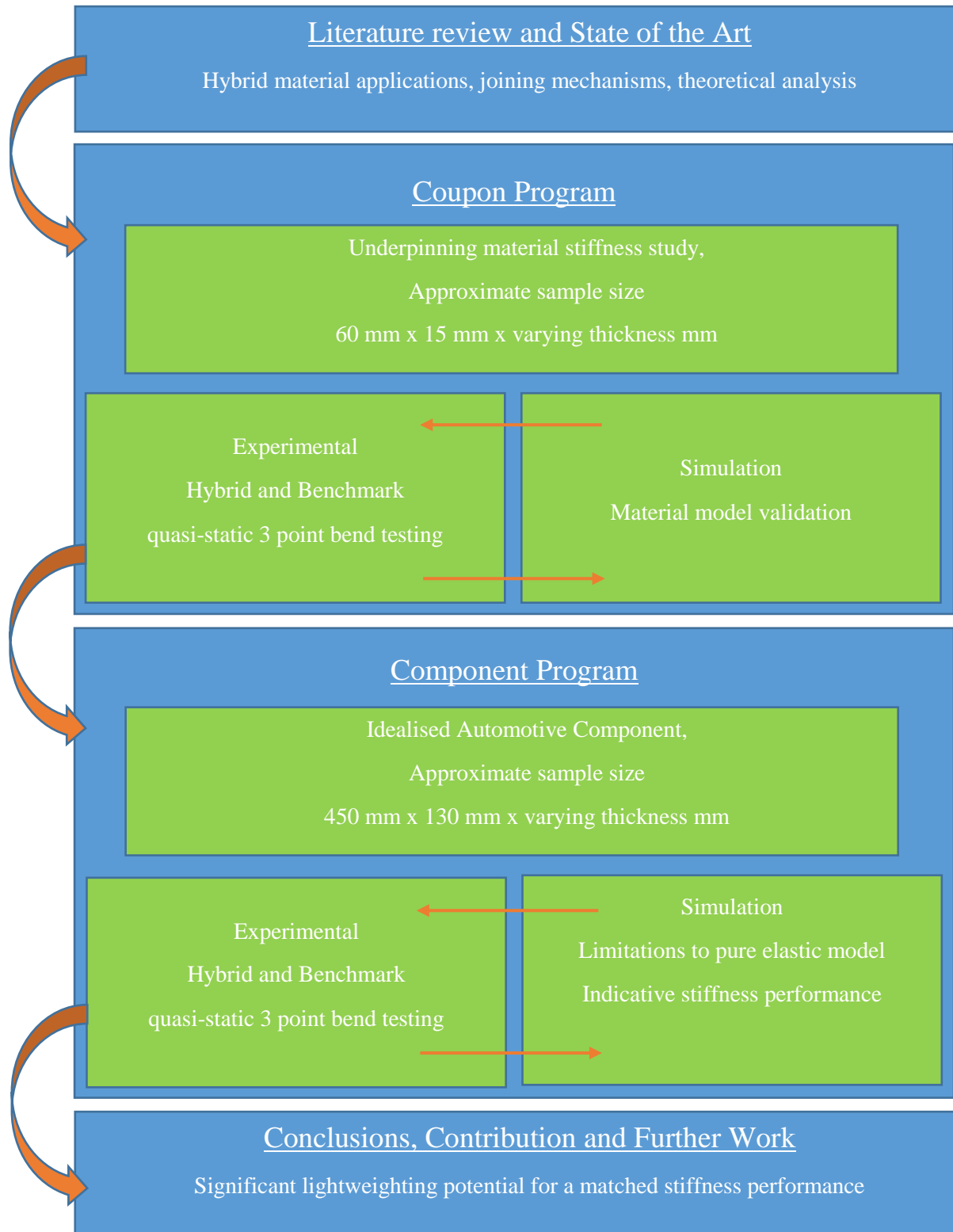


Figure 1-2: An overview of the project

## **2 LITERATURE REVIEW**

This chapter will focus on a literature review and summary of the state of the art research relevant to this thesis. It will start with the introduction of lightweight material options, as currently being researched and published, followed by a presentation of FRP-hybrid materials as an entity, focusing on the current applications and uses, moving on to the challenges of joining dissimilar materials and the methods for simulating this hybrid. Finally, this chapter will identify the opportunities for research and define the perceived contribution to knowledge.

Due to their material characteristics (light, strong, durable) FRPs are increasingly popular as a lightweight solution to repairing or strengthening ageing metallic structures. A large proportion of the research concentrating on the use of FRP/metallic hybrids has been carried out with retrospective reinforcement in mind. However, increasingly stringent demands for lightweight solutions are pushing many designers towards the use of FRP-steel hybrid materials at the design stage. The following sections detail the most relevant research currently on-going in the field of FRP-steel hybrids.

### **2.1 A focus on the automotive industry**

Important design attributes for the vehicle body structure are its static stiffness and frequency response. The static stiffness is determined in both bending and torsion, and depends on the structural configuration, stiffness of the primary components of the body structure, joint design, as well as the joining method. The frequency response is determined using dynamic tests at the engine idling speed (typically 600 to 700 rpm), and depends on both the static stiffness and the mass distribution in the structure. For vibration-free operation, the first natural frequencies for the bending and torsional modes of the BIW must lie within a specific



range. Depending on the vehicle class, each vehicle manufacturer sets target values for the static stiffness and frequency response at the initial design stage and determines them using FEA and laboratory tests as the BIW is developed [20]. The stiffness of the primary components in the body structure depends on their shape and dimensions as well as the material characteristics.

As mentioned previously, a 10 % reduction in vehicle mass leads to fuel savings from 5 to 10 % [10]. The body-in-white (BIW) is typically 20 to 25 % of the vehicle weight. There are recognised solutions to lightweighting an automotive steel structure, which include the downgauging of the original material, tailor welded blanks where multi materials are combined, lightweight material substitution such as aluminium or composites, and a BIW redesign [10]. A brief overview of their advantaged and disadvantages follows.

Material downgauging is commonly defined as reducing the thickness of the material making a part, usually associated with an increase in material properties (different material grade). Advantages: Higher grade of material; Disadvantages: Can lead to decreases in stiffness, as the values of Young's modulus  $E$  are unchanged.

Tailor welded blanks use multiple thicknesses and grades of steel joined together (welded or brazed) then pressed into shape. Advantages: Progressive energy absorption; Disadvantages: Welding different grades of steel, ductility, formability, deflection response depending on weld location.

Lightweight material substitutions use aluminium alloys, FRPs, magnesium alloys, titanium alloys, foams, etc. These include alternatives to monolithic sheet materials such as composite materials and sandwich materials. Advantages: Low density materials implies thicker parts which can match the bending stiffness for a lower mass; Disadvantages: Formability, reduction in strength, stiffness and hardness, difficulties relating to joining.

Finally, BIW redesign consists of redesigning the BIW structure or components of it, for example making space frame structures such as the Audi A2 or the Jaguar X351 and finally the BMW i-series. Advantages: Full control, no restrictions; Disadvantages: Cost.

Steel has historically been the material of choice in automotive structures however, multi-material body-in-white solutions are becoming increasingly prominent. Multi-material cars make up approximately 2 % of production volume worldwide, though public awareness perception is skewed through advertising etc. [1]. Within multi-material cars, hybrid materials, consisting of two (or more) materials can be used in parallel.

The pursuit of a comprehensive lightweight design implies the development of advanced structures that have undergone topological optimisations to fit all the loading requirements making use of the advantages of advanced materials such as composites. Using hybrid steel-FRP materials, it could be possible to find lightweight solutions to a complex set of requirements, taking advantage of the features of both the steel and the FRP that make-up the material. The FRP can be optimised to align its strengths with the load-paths in the structure, the steel can provide the underlying required properties.

## **2.2 Steel-FRP hybrid automotive applications**

It is worth noting from the onset that the studies published in the literature on steel-FRP hybrid materials are generally industry-funded and driven. They show a concern for manufacturability and “integrative potential” in existing structures, as well as a desire to minimise cost. There is very little focus on the fundamental properties of the materials used. There are a number of notable examples in which composite materials and metallic coexist in the design and manufacture of cars [1,

10]. The Ford Focus C170 is one high volume manufactured example. A hybrid front end structure was produced using FRP injection moulded ribs to reinforce sheet steel, as shown in Figure 2-1 [21, 22].

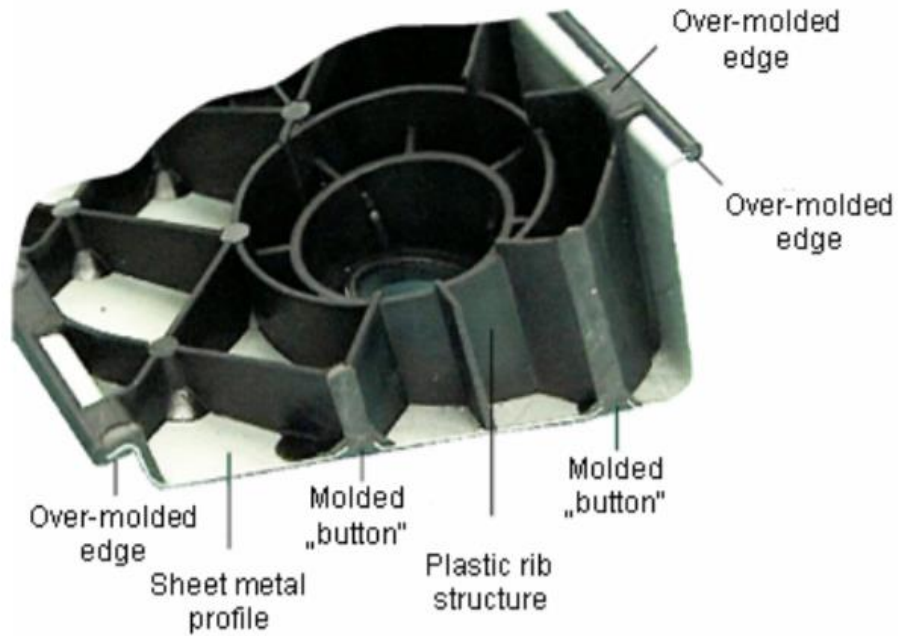


Figure 2-1: Profile cross-section of a hybrid structure with special structural parts labelled [21]

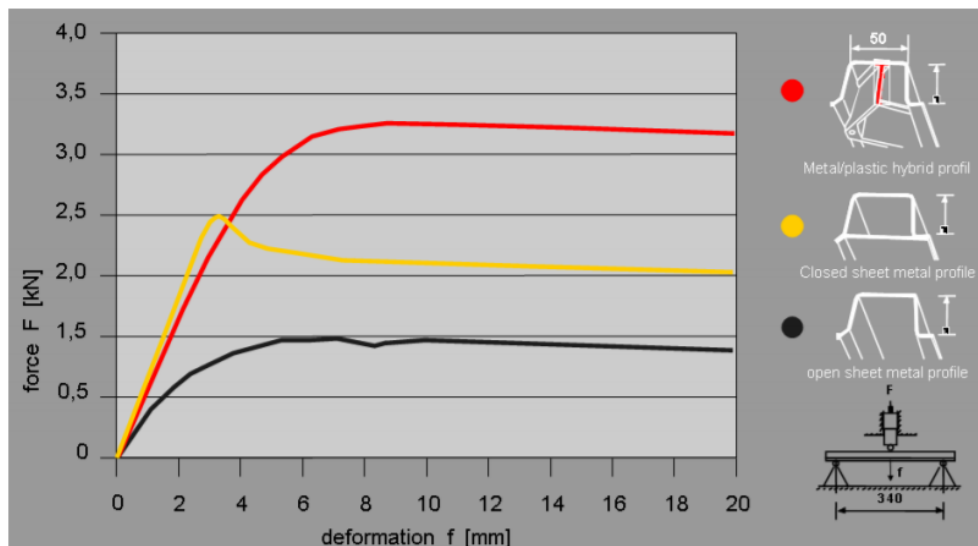
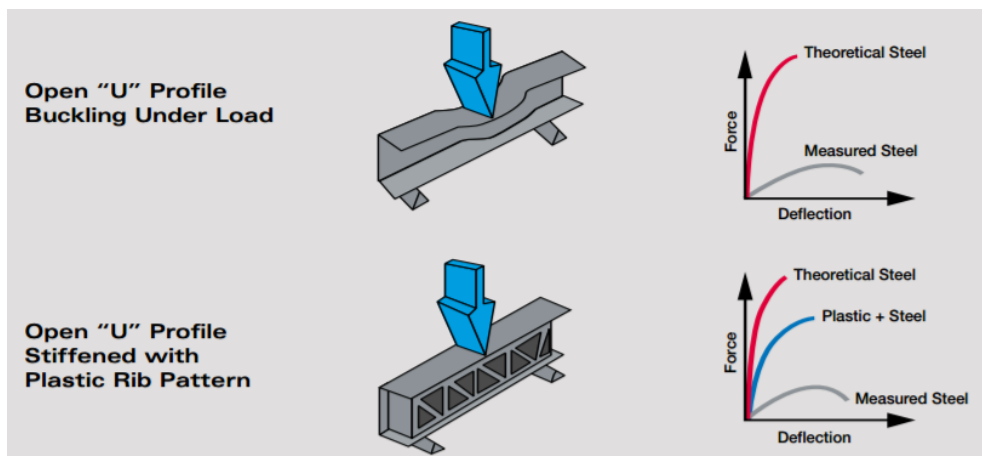


Figure 2-2: Load-deformation curve of the various profile sections tested in flexure [21]

Figure 2-2 shows an improved performance over an open sheet metal profile, and a slightly lower performance compared to a closed pure steel sheet metal profile. The studies on the part suggest a lightweighting for a given strength and stiffness, although they do not specify a value. They also suggest good recyclability. Lanxess [23] has additionally carried out further studies on plastic overmoulding of steel components. Their main findings are summarised in Figure 2-3. The thin, open, steel-only “U” section buckles under load, whereas the same profile stiffened with plastic ribbing has a performance approaching that of the theoretical steel performance.



*Figure 2-3: Load-deflection diagrams comparing an open “U” profile without and with plastic stiffeners [23]*

RWTH Aachen University in conjunction with VW and Daimler AG and funded by the Forschungsvereinigung Automobiltechnik (FAT) have researched a lightweight approach in which the sheet thickness of metals is reduced and local reinforcements of FRP (both glass fibre (GFRP) and CFRP) are added to compensate for the weakening of the structure [24]. The analysis is carried out on the floor structure of a representative middle class vehicle, specifically the rear tunnel bridge, the seat crossmembers, and the front and rear supports, as well as the floor long members. The materials used are PA 6.6 CFRP and PA 6 GFRP for composites and micro alloyed galvanized high strength steels (minimum yield strength from 260

to 340 MPa). Using the simulation model available from the SuperLightCar program [25], the reference behaviour of the structure was obtained. Using Optistruct and LS-DYNA (MAT\_058) as simulation software, “the analysis of 120 variations with adaption and optimisation of the parameter sheet thickness, laminate thickness of the FRP elements as well as number, position and length of the reinforcing elements, lead to a lightweight floor structure, where through the use of 1 kg CFRP/GFRP a total weight reduction of 2 kg was achieved. This corresponds to a weight reduction of 22 %.” [24]. This research does not present the fundamental and basic mechanical characterisation of the stiffness performance of the materials.

Universitat Paderborn investigated in 2010 a steel-composite hybrid structural component for cars, using specifically carbon fibres in a thermosetting resin. An epoxy-resin was used in conjunction with a nine-layer carbon fibre bi-directional scrim. The steel was a 22MnB5 alloy. They investigated primarily the manufacturability as the theoretical gain appears evident and claimed an overall potential 15 to 20 % weight save using an optimised steel-CFRP hybrid structure [26, 27]. They tested the application of a composite reinforcement in the inside of a top hat representative of an automotive pillar, in both quasi-static testing and crash. The geometry and application of the reinforcement can be seen in Figure 2-4.

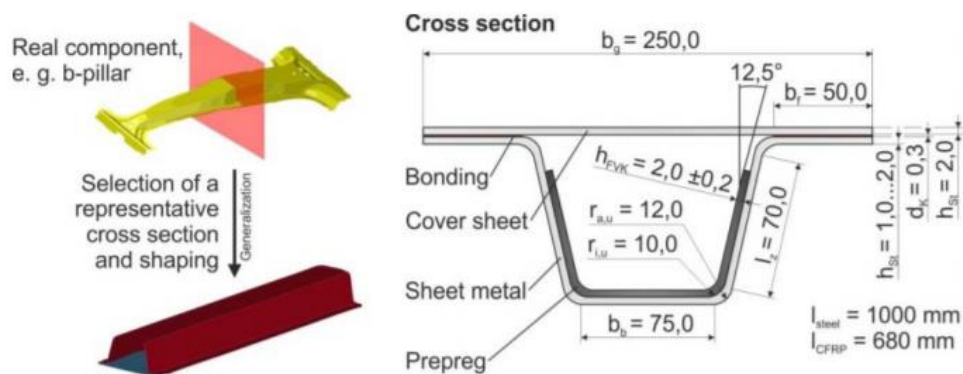


Figure 2-4: Geometry and location of composite reinforcement [27]

They noted a similar or improved performance from the hybrid material in all cases, as well as a potential lightweighting, which justified their research into the manufacturing techniques of steel-FRP hybrids for a high-volume application. Their work does not present the basic mechanical characterisation of the metallic-composite hybrid materials. Additionally, it does not show the lightweighting potential at a material level compared to the presented results of system application. There is also no simulation presented or discussed.

A number of studies using similar hybrid materials are present in the literature. However, the underlying focus was on the impact absorption and crashworthiness of hybrid structures. In the context of an ever increasing complexity of requirements for engineering structures, especially in crash applications, the latest developments in research focusing on lightweight materials have identified hybrid systems as one very promising way to realise advanced lightweight structures rather than one single “ideal” material [28]. Dlugosch [28], is the first to present the fundamental material properties of steel FRP hybrids, however his work is limited to a focus on energy absorption, and disregards any potential lightweighting application. The specimens used throughout his study are presented in Table 2-1. The fibre angle  $0^\circ$  indicates the specimen’s length axis. The steel sheets used in his research are of 1.5 mm constant thickness. The steel and composite are adhesively bonded together. His work, and its relevance to this project, is discussed in detail in later chapters as it was felt to be most beneficial. The samples were 190 mm in length, and 15 mm in width. The fibres were angled at  $0^\circ$ ,  $45^\circ$ ,  $90^\circ$  and  $135^\circ$ .

*Table 2-1: Specimen dimensions in study by Dlugosch [28]*

Number of plies	GFRP	CFRP
4	2.8 mm	3.1 mm
8	3.6 mm	4.6 mm
16	5.9 mm	6.8 mm

Bambach [29-31] has also focused on FRP reinforcement for both square and tubular beams in crash applications, noting that the presence of FRP modifies the overall failure mechanism and increases energy absorption.

As is highlighted from previous research, the main research focus appears to be on application to “complex engineering systems” rather than an investigation into the fundamental material characteristics. Dong [32] studied the strengthening of steel structures with FRP through flat coupons under tension, however limited his comparison to other steel-FRP hybrids rather than a comparison to steel structures only. Uriayer [33] tested steel-FRP coupons also under tension. He noted a response split into two main sections, one dominated by the performance of the composite (to failure) then a second dominated by the performance of the metal.

Sadighi [34] presented a review of the impact resistance of fibre-metal laminates (FMLs), studying flat coupons under tension and flexure (impact loading). He noted a global increase in performance and overall superior characteristics. His study was limited to the aerospace sector and applications relevant within; however, his findings are applicable to this study.

Dlugosch [28] additionally reports that a rather comprehensive study of hybrid materials on a coupon level was conducted by Mildner [35]. The title of this thesis indicates a focus of the work on crash behaviour of steel-FRP hybrid materials. Unfortunately, it has not been possible to source a copy of this work in English. Dlugosch reports: *“Specimens composed of aluminium or steel adhesively bonded to GFRP- or CFRP-laminates of different fibre layups were tested under quasistatic tension and 3-point-bending conditions. Although the vast majority of tension tests had to be aborted directly after the laminate fracture due to the failure of the clamping mechanism, several interesting observations were made. According to predictions based on rule-of-mixture calculations for non-unidirectional fibre orientations in the laminates the stiffness of hybrid specimens did not reach the levels*

of pure steel. The hybrids' stress-strain-curve also showed a bilinear behaviour except for unidirectional CFRP-steel specimens, which reached laminate fracture before reaching the yield stress of the steel. Hybrid specimens with laminates with mostly longitudinal ( $0^\circ$ ) fibre orientations outperformed pure steel specimens in terms of strength while predominantly transversally reinforced hybrid specimens did not." As stated by Dlugosch, Mildner's work appears to have been hampered by the specimen clamping mechanism and results and conclusions primarily drawn from performance predictions rather than experimental results. However, the predicted performance presents and correlates with the bilinear response also witnessed by Dlugosch is his work. The results showing a better performance in samples with a longitudinal fibre predominance over samples with a transversal fibre predominance additionally correlate with work supervised within WMG [36].

Hybrid composites, constructed of two or more types of fibres of different nature (such as a combination of carbon and glass fibres), are beginning to be used more regularly in the automotive industry, for applications to structural components. Hybridising composites based on fibre nature is a means to achieving a similar performance as a single natured composite for a lower cost, and also of reducing weight compared to the traditional steel materials used. Aston Martin used the Gurit Car Body Sheet material – CBS 96 – to manufacture the DBS body panels [37, 38]. CBS 96 is a sandwich construction with four layers, saving weight relative to steel.

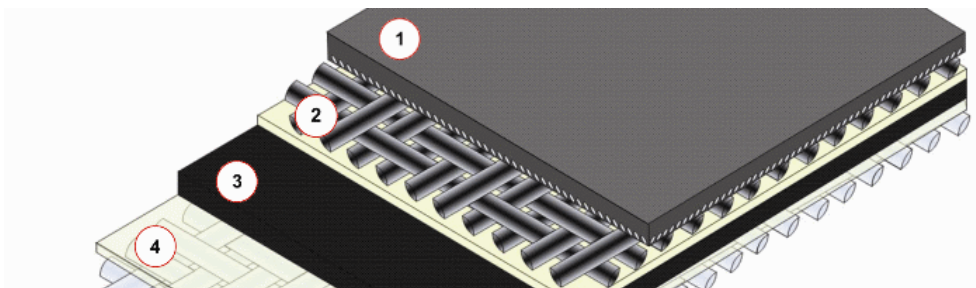


Figure 2-5: CBS 96, 1 – in-mould surface film, 2 – first fibre layer, 3 – resin core, 4 – second fibre layer [39]



The 2003 Dodge Viper used unidirectional carbon fibre sheet moulding compound (SMC) combined with glass fibre SMC in the windscreen surround [11]. The surround consists of two panels bonded together, both containing the two types of reinforcement in different places. The new design had 45 % less deflection compared to its previous design whilst also having only one edge requiring hand finishing rather than eight. The design also features in the 2013 SRT Viper [36, 39-41]. Research has been undertaken comparing hybrid composites to monolithic composites, with many of the largest benefits occurring when testing the flexural properties. Subagia [42] tested woven carbon/basalt hybrids as a sandwich in three-point bending. They found that the hybrids showed a drop in flexural modulus and flexural strength of 16 % and 14 % respectively compared to monolithic carbon fibre.

The literature shows industrial and research interests in the topic of metallic-FRP hybrid materials applications, for lightweighting purposes or otherwise. However, there has been no published evidence of a direct stiffness performance comparison of hybrid steel-FRP materials with their pure steel counterparts, specifically with a lightweighting focus. This work will focus primarily on quantifying the lightweight potential of a steel-FRP hybrid material over a pure steel material for a matched stiffness performance.

### **2.3 Other hybrid applications**

Lightweighting, and local reinforcement of structures using composite materials, is not confined to the automotive industry. Using FRP to reinforce structures was initially used in the aeronautical engineering industry. Here, the structures are not necessarily steel ones.

Notably, as early as 1987, research pioneered by the Aeronautical Research Laboratories (Australia) presented examples of practical applications using

composite patches to repair damaged aircraft. These examples use boron/epoxy patches with epoxy nitride structural film adhesives curing at about 120 °C, graphite/epoxy (cloth) patches with epoxy paste adhesives curing at ambient temperatures and boron/epoxy patches with modified acrylic adhesives curing at ambient temperature. The paper puts forward relevant material, mechanical and physical properties: modulus, shear modulus, critical strain, specific gravity and thermal expansion coefficient [43]. One of the primary advantages of the use of a thin patch of composite to patch and repair cracks is that the patches are approximately half to a third of the thickness of an equivalent aluminium alloy repair. The patching also minimises stress concentrations, corrosion and fretting. It causes no damage to the structure and minimises undesirable structural changes by tailoring the patch to suit the stress field. The patches are also easily formed to complex contours.

Meier, [44], highlights that the learning and technology used in aeronautical engineering can easily be applied to other areas of engineering such as civil engineering. Most research towards the application of steel-FRP materials focuses on the global reinforcement of steel beams using FRP materials, either pre-emptively through design or retrospectively. The DE-LIGHT Transport project run by the European Commission of research and innovation (Transport) highlights that other industries such as the marine and rail industries are investing in lightweighting research [45]. In the marine industry for example, Cao focuses on hybrid ship hulls, where steel beams are joined to composite beams [46-48].

Within civil engineering, research is split between applications to bridge structures, and applications to buildings. Indeed, a number of studies have been conducted investigating the use of composites as structural reinforcements to dissipate energy in seismic scenarios [49, 50]. The composite reinforcement properties are shown to have a positive effect on overall performance.

In the context of civil engineering, a number of review papers and books exist [51-53]. The use of composite reinforcements on structures is quasi-exclusively retrospective. Zhao in *FRP-Strengthened Metallic Structures* [51] gives an overview of the most prominent and relevant work performed in the civil engineering field in terms of FRP use in retrospective reinforcement. He highlights the milestone state-of-the-art papers published and provides a summary and an insight into the gaps in knowledge. There is also substantial literature on the use of FRP in reinforcing concrete. [54-68] all present different aspects of the on-going civil engineering research into this topic.

In addition to showing the positive outcomes of the local reinforcement, Schnerch et al, [54], discuss the durability of the CFRP-steel bond in environmental conditions including exposure to moisture and temperature fluctuations, galvanic corrosion and osmosis. The first two have an effect on the nature and performance of the bond and the third leads to debonding. The size and shape of the bonded patch is also studied, as the size of the reinforcement affects the stress and strain concentrations throughout the materials.

## **2.4 Joining mechanisms for dissimilar materials**

There are several obstacles to the joining of dissimilar materials which include high interfacial stresses, corrosion, heat, cold and differences in coefficients of thermal expansion. The use of joining can be structural, where the joint is load-bearing, or non-structural. In brief, these techniques are:

- Mechanical joining (bolts, rivets, etc.) - interlocking
- Welding (ultra-sonic, induction, laser) [69]
- Adhesive – chemical

Studies [70] have shown that adhesive bonds outperform spot-welded ones in three-point bend scenarios. However, adhesive methods can present issues with the manufacturing process (use of vacuum bagging, epoxy bleeding problems, shim cloth usage [71]) as well as present varying failure modes (peel, debonding) that can be complicated to predict. The AMRC Integrated Manufacturing group [72] has written a study on the current state of the art FRP surface preparation technology which examines these preparation techniques for their advantages and disadvantages. These have been described in the following bullet points:

- **Cleaning/Degreasing:** Removal of loose solids can be accomplished with a clean brush or blast of clean, dry air. Organic solvent or alkaline aqueous solution removes organic materials such as grease, oil and wax from adherend surfaces. This can be accomplished by wiping, dipping or spraying.
- **Surface Roughening:** The use of abrasive materials to remove unwanted layers and generate a roughened surface texture [72, 73].
- **Chemical Treatments:** Immersion of the adherend in an active solution which has the power to etch or dissolve a part of the adherend surface or change it in such a way that the free surface energy increases on the treated surface. An electrochemical reaction can also be included where current is transferred through an electrolyte between an auxiliary electrode and the adherend surface, e.g. anodising. This process introduces several additional factors to be controlled.
- **Physical Treatments:** Techniques where the adherend surface is cleaned and chemically modified by exposure to excited charges or species. Techniques such as corona discharge, plasma, flame or exposure to ultraviolet and ozone are examples in this group.

- **Primers:** Alternative surface treatments, often simpler than chemical or physical methods, applied by dipping, brush or spray. They can chemically alter the surface (e.g. silane coupling agents, chromate conversion coatings), or protect the preferred surface already generated by another method (e.g. aerospace primers after anodising).
- **Cold metal transfer:** small spikes are welded onto the surface of the steel which the fibres use as a fixation point during cure [74]. This can also be called z-pinning or 3-D weaving.

## 2.5 Theoretical analysis of the materials

There are a number of theoretical methods to expressing the stiffness performance of a hybrid material. An explanation of the rule of mixtures and Halpin-Tsai can be found in the Gurit Guide to Composites [71]. This is primarily used for pure composite structures however can be extended to a steel-FRP hybrid in situations where the steel is reinforced over its whole surface. The elastic material property calculations set forward by these two methods are based on the following assumptions:

- The matrix and fibres each behave as linear elastic materials. The non-linearity of the resin barely affects the material properties.
- The interface between the matrix and the fibres is infinitesimally thin
- The bond between the matrix and the fibres is perfect, thus the strains in each are identical. This implies the fibres are not slipping through the matrix, which close to failure is an invalid assumption.
- The matrix material close to the fibres has the same properties as the material in bulk form, implying no chemical interactions between the fibre and the matrix.

- The fibres are arranged in a regular array, which relies on high quality manufacturing.

The use of these assumptions, albeit flawed, provides reasonable predictions for stress and strain calculations in FRP structures, allowing the prediction of the elastic properties of the structure.

The main equations of the rule of mixtures are:

$$E_1 = E_f V_f + E_m V_m \quad \text{Equation 2-1}$$

$$E_2 = \frac{E_f V_f}{E_f V_m + E_m V_m} \quad \text{Equation 2-2}$$

Where  $E_1$  is the elastic modulus in the direction of the fibres, and  $E_2$  is the elastic modulus across the samples.  $E_f$  and  $E_m$  are the elastic modulus of the fibres and matrix respectively, and  $V_f$  and  $V_m$  the volume fraction of the fibres and matrix respectively.

The main Halpin-Tsai Equations calculates  $E_2$  differently:

$$E_2 = E_f \frac{1 + \alpha \varphi V_f}{1 - \varphi V_f} \quad \text{Equation 2-3}$$

$$\varphi = \frac{E_f/E_m - 1}{E_f/E_m + \alpha} \quad \text{Equation 2-4}$$

The coefficient  $\alpha$  is determined empirically by fitting curves to experimental data, and depends on the characteristics of the fibres and loading conditions. It is generally taken as a value of 2 for calculations of  $E_2$ .

Bruno Ludke [75], BMW Body Design specialist, identifies four areas for critical consideration: structural dynamics, static stiffness, crashworthiness, weight optimization. He developed a lightweight design material criterion for bending stiffness  $\sqrt[3]{E}/\rho$  [10] where  $E$  is Young's modulus and  $\rho$  is the density of the material. This expresses the relative bending stiffness of the sheets. As discussed in detail in Chapter 4, these rules have their limitations, as they are based on values of Young's

modulus, and limited when the reinforcement is a “patch” not covering the entire surface area.

Dong [76-80] uses the ASTM standard for a simply supported beam where

$$E_f = \frac{kL^3}{4bh^3} \quad \text{Equation 2-5}$$

In which  $k$  is the slope of the load extension curve,  $L$  is the span length,  $b$  the width and  $h$  the thickness. This is also used by Dlugosch [28] in the context of his preliminary work on steel-FRP hybrid materials for crash applications. Research [57] highlights and studies the gap that the standards leave when evaluating the stiffness and strength of a composite/metal adhesive joint. It concludes that, in terms of stiffness and strength, the highest impacting criteria is the overlap length, as adhesive thickness and stiffness ratio are negligible in comparison.

It was found, however, in the context of this work that using “ $k$ ”, the gradient of the load-extension curve, was the most appropriate means of expressing the stiffness of the coupon and component parts tested, as it enabled a direct comparison of the “engineering” performance of the samples tested, rather than an expression of the material performance. These are discussed within the context of their applications in Chapters 3, 4 and 5.

## **2.6 Purpose of this research**

This chapter has highlighted the gap in published knowledge relating to the stiffness performance and weight save potential offered by the local patching reinforcement of steels using FRPs over their pure steel counterparts. It is recognised in the literature that the lightweight and anisotropic properties of composite materials make them a viable solution for a lightweight retrospective reinforcement as they lend themselves to a “tailored” patch. There are emerging trends that promote the

use of “the right material at the right place, at the right time”. In part, automotive manufacturers have shown their interest in using multi-material combinations in their designs. Primarily, current research shows the use of hybrid materials where the composite is a global reinforcement, whereas this project focuses on global downgauging with a local patch reinforcement. However, there is a lack of fundamental research and supporting knowledge of the effect of the composite material on the steel.

It is intended that this project will seek to answer some of these questions, by focusing specifically on the stiffness and elastic performance of hybrid steel-FRP materials as well as pure steel and pure composite materials. Other characteristics will be noted throughout and discussed however the focus will remain on the elastic behaviour. As stiffness is defined by both the intrinsic material property and geometric aspect of the part, only the elastic region was studied so as to limit geometric interactions.

There are advantages to using composite materials, as, due to their anisotropic nature, they can be tailored to situation specific needs. Using a hybrid steel-FRP material enables the harnessing of both these materials’ advantages and properties towards an end benefit.

In other words, the purpose of this research is to quantify the lightweighting potential offered by the intelligent deployment of composite materials on steel parts, for a matched stiffness performance. The lightweighting potential of a hybrid steel-FRP material compared to a pure steel material will be investigated at both coupon and automotive component level. A systematic comparison of hybrid material samples with benchmark steel samples will be conducted, based on their stiffness performance and lightweighting potential.

The main focus of the work is to provide underpinning research to enable the further understanding of the opportunity of the stiffness performance of hybrid steel-



FRP materials, both experimentally and in simulation compared to their pure steel counterparts, and taking into account the lightweighting potential.

Hybrid specimens are fabricated from bonded DP600 and PA6 GF60 composite materials. Both flat coupon samples and automotive component samples are investigated – enabling an isolation of the material effects in the case of the coupon samples, and showing a global geometrical interaction in the case of the components. These samples are tested in quasi-static three-point bending to investigate lightweighting potential through matched stiffness performances.

### **3 MATERIALS AND METHODS**

This chapter will discuss the materials and methods used to carry out the experimental aspects of this research. This includes the materials studied, their relevant properties and the experimental and simulation programs carried out. It is intended that the reader, with a basic scientific knowledge, should be able to recreate the acquisition of data.

#### **3.1 Steel DP600**

As discussed in Chapter 1, “Drivers of the lightweighting trend”, advanced high strength steels or ultra high strength steels are increasingly in use alongside formable steel grades in the design and manufacture of BIW. This makes them a direct target for lightweighting efforts. This research concentrates on the automotive grade advanced high strength steel HTC600X (Euronorm – now known as CR3304590-DP), commonly known as DP600, a cold rolled Dual Phase (DP) steel with martensitic dispersion in a soft ferrite matrix [81].

Figure 3-1 shows the relative performance of the DP steels compared to their alternatives.

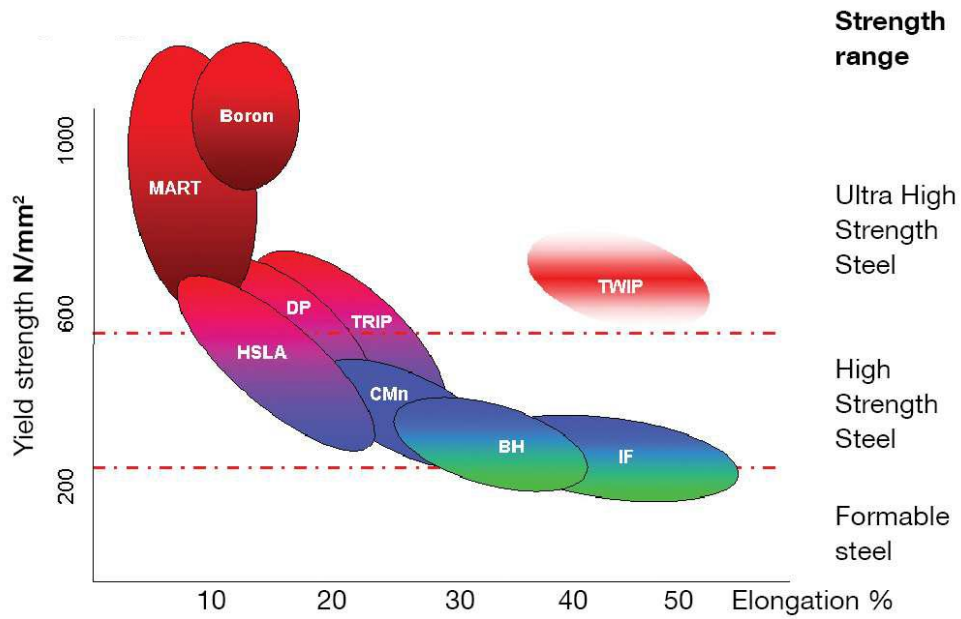


Figure 3-1: Strength - elongation graph of the different types of steel produced by Tata Steel [81]

### 3.1.1 DP600 properties

The DP600, provided by industrial sponsor Tata Steel, has been studied extensively and its properties, summarised (and normalised) in Table 3-1, are well known [82].

Table 3-1: DP600 properties obtained from tensile tests following standard BS EN ISO 6892-1 (2009) [83]

Engineering constant	Units	Values
Stiffness	[MPa]	205000
Poisson's ratio	–	0.3
Yield Strength	[MPa]	355
UTS	[MPa]	600+
$\rho$	[kg/m <sup>3</sup> ]	7850
Coefficient of Thermal Expansion	[10 <sup>-6</sup> m/(m K)]	11

The rolling direction is known [84, 85] to affect the performance of steels as it alters the crystal alignment. Personal communications with A. Carrado [100], indicate the rolling direction has a greatest affect when at 45 ° to the loading

direction. A full study of the effect of the rolling direction on the sample performance is suggested for further study, however, here, variations in results are considered to be small enough to be ignored in this research.

The thicknesses of DP600 used range from 0.5 mm to 1.6 mm. In the context of the coupon work (Chapter 4), the thicknesses used were 0.5 mm and 0.8 mm. In the context of the component work (Chapter 5), the thicknesses used in physical testing were 0.5 mm, 0.8 mm, 1.0 mm and 1.6 mm.

The chemical composition of the steel is guaranteed by the manufacturer as follows in Table 3-2.

*Table 3-2: Chemical composition of DP 600 as guaranteed by manufacturer [82]*

Product	C	Si	Mn	P	S	Al <sub>tot</sub>	Cr + Mo <sup>1</sup>	Nb + Ti <sup>2</sup>	V	B
	Max	Max	Max	Max	Max	Max	Max	Max	Max	Max
DP 600	0.17	0.80	2.20	0.080	0.015	≤2.00	1.00	0.15	0.20	0.005

### **3.1.2 DP600 coating**

The steel used in these experiments was uncoated as the coating of the steel affects its surface energy and therefore the bonding potential. It was considered that various surface treatments, such as galvanisation, zinc coating, etc. could provide a higher performing bond between the steel and FRP, however this investigation was deemed outside of the scope of the project. Results in Chapter 4 provide the observations and discussion supporting the use of uncoated steels. These concluded that the elastic region of the load extension curves was not affected by the nature of the bond, and when failure did occur, which was also considered outside the scope of this research, it was either by delamination of the composite or cohesively within

the adhesive layer. The nature of the coating of the steel was therefore excluded, and uncoated DP600 used throughout.

It was preserved from rust with an oil-based layer which was easily removed in surface preparation with the use of a solvent. The surface of the steel was mechanically roughened and cleaned in preparation for the adhesive bonding. A number of trials and literature studies [60, 61] showed this to provide the best bond. The abrasion is done manually using 180p emery cloth in circular motions to keep the abrasion regular over the whole surface. The steel was also lightly heated to approximately 60 °C to facilitate the spreading of the adhesive.

These techniques are discussed further in Chapter 4, Coupon program and Chapter 5, Component program.

## **3.2 Composite**

The choice of thermoplastic versus thermoset for the composite matrix was influenced by a number of factors, including life cycle analysis and recyclability, material procurement, ease of manufacturing, etc. It was also considered important that the fibres of the composite should run in a single direction, as that enables for a freedom of layup, where a woven composite would restrict the possible layup options. Unidirectional fabrics are generally in a pre-impregnated format, as this keeps the fibres in order. In terms of the nature of the fibre, glass is considered in a first measure, due to the lesser cost of manufacturing, with carbon being used in a second stage.

The final selection of thermoplastic composite PA6 GF60 and PA6 CF60 was supported at the most recent International Conference on Composite Materials 2015 which highlighted the industry's interest in the use and study of thermoplastic composite materials [86].

### 3.2.1 PA6 GF60 – Glass Fibre

The thermoplastic used in testing is a PA6 GF60 purchased from Ticona, the engineering polymer business of Celanese Corporation. This is a pre-impregnated polyamide 6 matrix with continuous glass fibres at  $V_f = 60\%$ ,  $T_m = 235\text{ }^\circ\text{C}$ ; additional properties summarised in Table 3-3. The fibre volume fraction of 60% is the highest fabricated by the producer Ticona, and provides higher material performance characteristics compared to lower fibre volume fractions. Additionally, it has the lowest coefficient of thermal expansion, due to the higher percentage of fibres. In order to best improve the stiffness performance of the hybrid material, this high-performing composite was selected.

As discussed previously, a thermoplastic composite is deemed most interesting to investigate. The current thermoplastic composite used is specifically selected due to the extensive research that it had already undergone within the WMG group and the corresponding knowledge base [87, 88]. It has also been the subject of previous automotive research. The material properties were established and rigorously tested over the course of the Low Carbon Vehicle Technology Programme (LCVTP) [88]. In that context, it was chosen for its combination of cost, performance, processability, and recyclability. An equivalent PA6 CF60 (carbon fibre) is commercially available, however it was not included in the experimental part of this study as its high cost (5 times higher than E-glass) was prohibitive.

Table 3-3: PA6 GF60 properties obtained from tensile and flexure testing [88, 89]

Engineering Constant		Units	Unidirectional (single ply)
Stiffness	$E_{11}$	[MPa]	28650
	$E_{22} \approx E_{33}$	[MPa]	6800
	$G_{12}$	[MPa]	200
	$G_{13} \approx G_{23}$	[MPa]	100
Poisson's ratio	$\nu_{12}$	-	0.36
Density	$\rho$	[kg/m <sup>3</sup> ]	1720
Thickness	T	[mm]	0.23- 0.26
Coefficient of Thermal expansion		[10 <sup>-6</sup> m/(m K)]	26.5

The composite is layed-up and consolidated by being heated to 240 °C. Heating the composite to 5 °C above the melting temperature ensures that the polyamide matrix reaches liquid state and all the layers merge. The surface finish to which the adhesive bonds to is achieved using a peel-ply fabric. Figure 3-2 is a micrograph of the adhesive-composite bond, and shows the surface well. From left to right, steel DP600, adhesive SAS 272, [0,90][90,0] PA6 GF60.

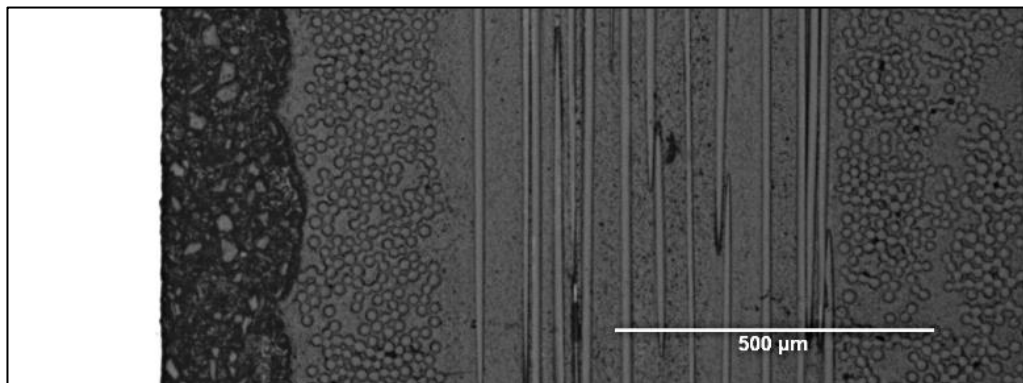
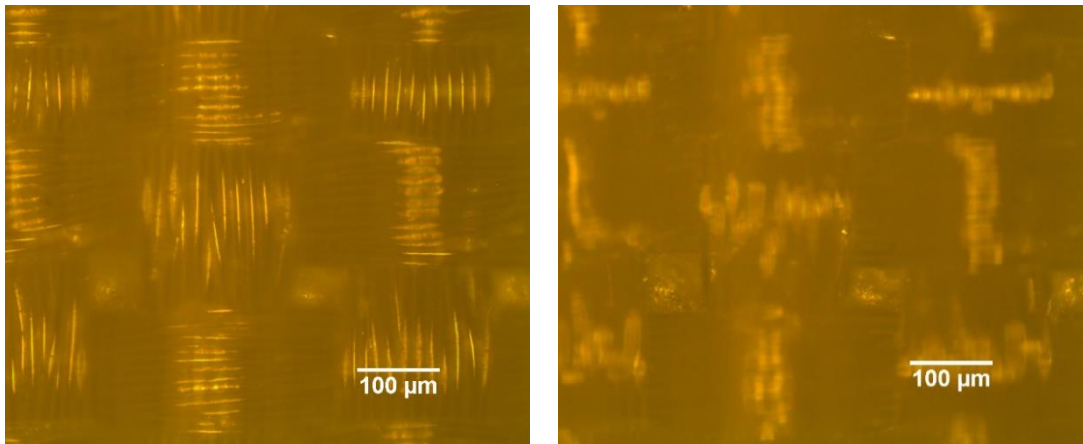


Figure 3-2: Micrograph image showing the layup of DP600, SAS 272 and [0,90][90,0] PA6 GF60

The micrograph highlights how the surface finish of the peel ply increases the surface energy and allows for an “interlocking” of the adhesive into the composite layer.

The following micrographs in Figure 3-3 shows the surface preparation of the PA6 GF60 which is the imprint of the peel-ply fabric in the matrix that occurs when

the matrix is heated past its melting temperature. The peel-ply moulds the matrix to its shape, leaving a roughened surface with varying heights that enables the adhesive to interlock with the surface and create a high quality bond. The two images in Figure 3-3 show the variation in height across the surface which allows for adhesive “lock-in”.



a) Top layer of peel-ply surface preparation

b) Bottom layer of peel-ply surface preparation

*Figure 3-3: Micrographs showing the depth of peel-ply surface preparation a) top layer of peel-ply surface preparation, b) bottom layer of peel-ply surface preparation*

The difference in focus in the two images highlights the difference in depth provided by the peel ply.

### **3.2.2 PA6 CF60 – Carbon Fibre**

As well as the PA6 GF60, a pre-impregnated polyamide 6 matrix with continuous carbon fibres (PA6 CF60) is used in the simulations. This is also a Ticona product, with relevant properties presented in Table 3-4 [90]. Due to the incurred costs of this material, it is used only in the simulation. A PA6 CF70 was available from the manufacturer, however, for continuity purposes a PA6 CF60 was also used.



Table 3-4: PA6 CF60 properties obtained from tensile and flexure testing

Engineering Constant		Units	Unidirectional (single ply)
Stiffness	$E_{11}$	[GPa]	100
	$E_{22} \approx E_{33}$	[GPa]	5.7
	$G_{12}$	[GPa]	2.5
	$G_{13} \approx G_{23}$	[GPa]	2.9
Poisson's ratio	$\nu_{12}$		0.37
Density	$\rho$	[kg/m <sup>3</sup> ]	1472
Thickness	T	[mm]	0.16

### 3.3 Adhesive

As the hybrid material performance was only considered within the elastic region, the adhesive simply needed to provide characteristics by which it would not fail within the elastic behaviour of the steel and the composite. In testing, none of the adhesives presented failure in the elastic regions of the tests. It is recognised that there could be a “sandwich” effect due to the presence of adhesive between the steel and the composite, however this is deemed outside the scope of the project. Three different adhesives were used in the sample preparation. Originally, S10, an Alpha Adhesive one-part epoxy based resin was used. The following iteration of adhesive was also an Alpha Adhesive one-part epoxy SAS 272. Initially, Alpha Adhesives were the manufacturer of choice due to their adhesive having been used in previous automotive studies. Additionally, they present an excellent working relationship with WMG and an ability to manufacture adhesives “on demand”. However, a change in their internal structure meant the supply of adhesive was discontinued and a Sika adhesive was used instead. The final adhesive used was a two-part Sika epoxy 490 C. This is one of the adhesives being considered for manufacturing with composites by Jaguar Land Rover, specifically in crash applications. All three adhesives present performances that are deemed suitable for the application. Lap shear test results for the SAS 272 adhesive and Sika 490 C adhesive (identical substrates) are presented and their performances compared as follows.

### 3.3.1 Alpha Adhesives S10 and SAS 272

Due to the product shelf life and slight iterations within the manufacturing company, Alpha Adhesive, the initial adhesive used was an S10, followed by an SAS 272. SAS 272 is an iteration of S10, with a lower viscosity to facilitate the handling performance in the fabrication phase. The performance as an adhesive is guaranteed by the company, therefore both are treated as having the same characteristics. However, some checks are run based on lap-shear tests and show a consistency in performance. The S10 was black in colour, the S272 was white.

Figure 3-4 shows the heat flow curve from the DSC [91]. It highlights the exothermic chemical reaction that occurs during cross-linking. When the curve stabilises, the chemical cross-linking is over. At 150 °C, the adhesive will be fully cured after 600 seconds.

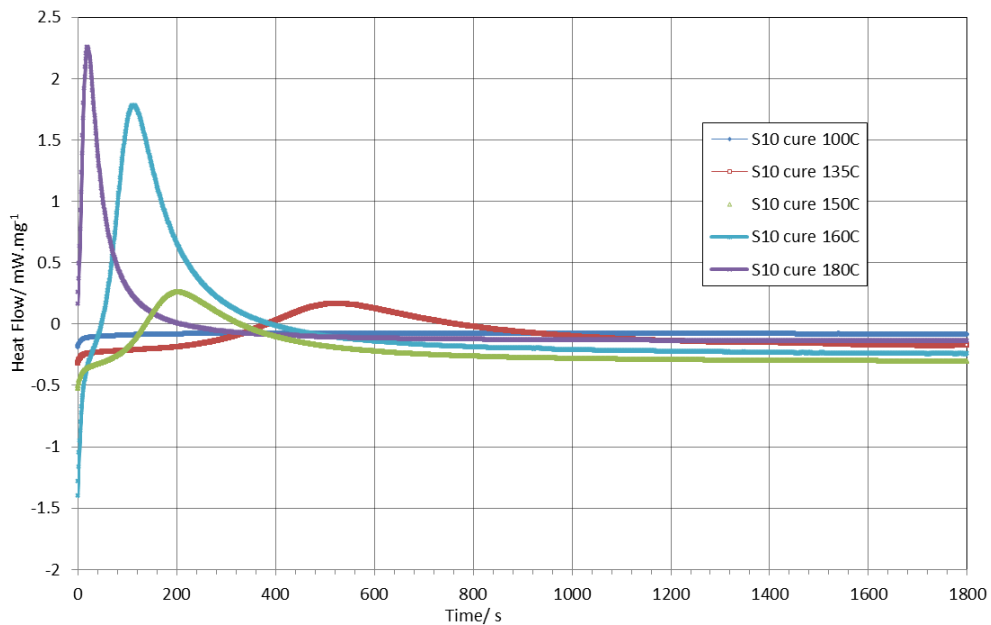


Figure 3-4: Heat flow curves for S10 adhesive [91]

This S10 adhesive was used for the first series of material testing, but was out of production for the remainder of the research. The SAS 272 one-part epoxy based resin is also dependant on heat to cure. The inclusions present in the micrograph

shown in Figure 3-2 were investigated. Results are presented in Appendix A. The adhesive contains aluminium tri-hydrate. A full chemical breakdown was not available from the manufacturer.

In addition to determining the nature of the adhesive at the micro-scale, some data is collected at the macro-scale enabling the comparison of the Alpha Adhesive with the Sika using lap-shear tests.

Lap shear tests for the SAS 272 adhesive between a CF MTM57 and AC600 E coated aluminium show a maximum shear strength of approximately 18 MPa, for a “stiffness” of 13 MPa/mm.

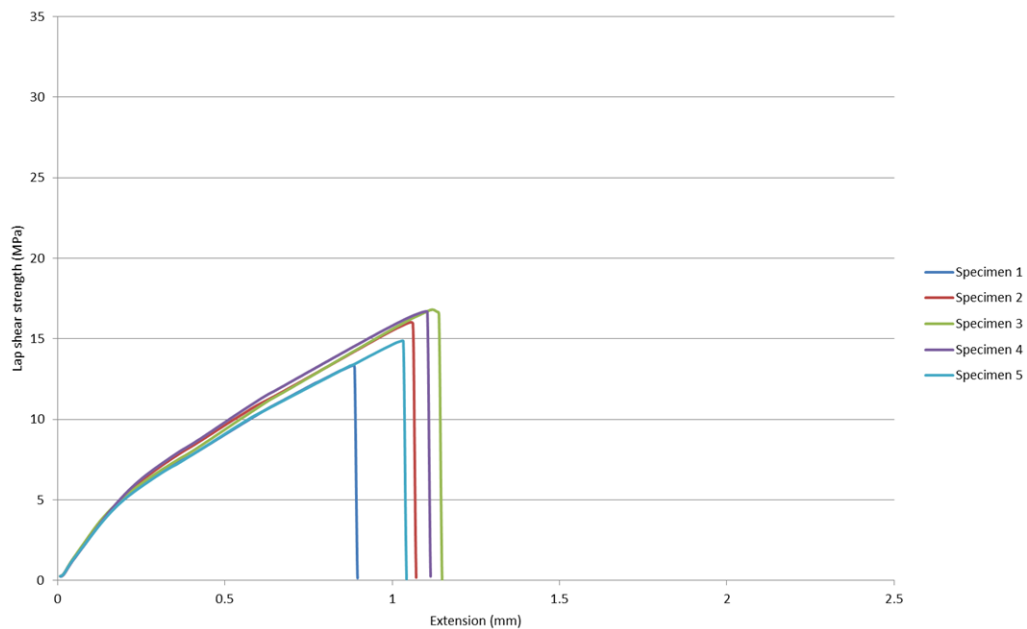


*Figure 3-5: Lap Shear strength extension curve for the SAS 272 adhesive between a carbon fibre MTM57 and AC600 E coated aluminium [92]*

### 3.3.2 Sika 490 C

The final adhesive used is the Sika 490C two-part epoxy. This adhesive cures at room temperature over 24 hours, however, for ease and rapidity in sample fabrication it is heated to 80 °C for 30 minutes. The Sika 490C is pink in colour, and contains

glass beads of 0.3 mm in diameter that ensure a constant thickness throughout the adhesive layer when spread. The datasheet is available in Appendix C.

The following graph shows the lap-shear curves to allow for a direct comparison with the SAS 272.

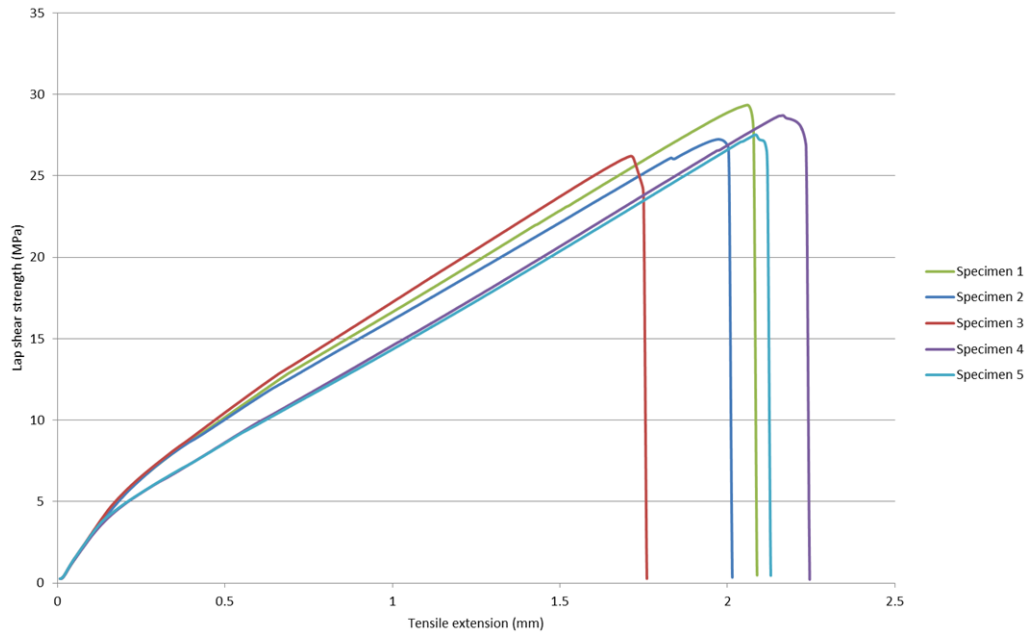


*Figure 3-6: Lap Shear strength extension curve for the Sika 490 C adhesive between carbon fibre MTM57 and AC600 E coated aluminium [92]*

The Sika 490 C shows a significantly greater performance to the SAS 272 in terms of strength, the Sika 490 C has a maximum lap shear strength of approximately 27 MPa, compared to approximately 18 MPa in the SAS 272. Both adhesives present a similar stiffness, approximately 13 MPa/mm.

The change in the adhesive was deemed acceptable as the performance of the adhesive in stiffness were comparable, and the Sika 490 C presented a higher bond strength compared to the SAS 272.

## **3.4 Testing**

This section discusses the equipment and methods used to cut, bend and test the materials and specimens. It also gives a brief overview of the standards used as guides through the experimental work.

### **3.4.1 Equipment**

#### *3.4.1.1 Cutting the specimens*

Cutting of the specimens is done using either a guillotine, water jet cutting or a CNC milling machine.

A guillotine was used to cut the steel sheets and the composite pre-preg tape to the required sizes. This is a rough cutting technique. Water jet cutting was used in cases where large samples, for example the components, needed to be cut to within 1 mm of a set shape. It can be a more damaging cutting technique for the steel as it removes the oil coating and allows the steel to rust. It offers the cutting of more complicated shapes compared to the guillotine, which can only handle flat sheets and straight cuts.

The CNC milling machine was used to cut out small sized specimens, where a high degree of precision is required. In the case of the coupon specimens, sheets of hybrid steel-composite of 500 mm x 500 mm in dimension were assembled and the specimens were cut using a Datron M7HP 3-axis high speed milling machine. The cutting technique was iteratively selected as initial samples had poor size consistency and surface finish. The final method required a spindle speed of 17000 rpm, using two 1.8 mm diameter diamond finished steel cutters, 2 or 3 flutes. The first cutter was used for the initial rough cut, and the second for the finishing cut. Pass depth on the rough cut were set to 0.5 mm and through the entire thickness on the final cut. The allowance between the rough and finishing cut was set at 0.05 mm. The samples

were cut with the composite face down so the cutters penetrated the steel first. This increased the quality of surface finish.

#### 3.4.1.2 *Shaping the specimens*

The component sections required pressing into shape. The equipment used for this task was the Interlaken SP 225 hydraulic 1000 kN press, using a final pressure of 800 kN, a rate of 100 kN/s holding for 30 seconds. The tooling used for the pressing was designed for 1.6 mm thick material, so in order to press the 0.5, 0.8, 1.0 mm thick steels, spacers were used. Appropriate thicknesses of steel were used to offset the samples to ensure the final geometry was correct. The geometry profile in all samples was of the female part of the press, to ensure all samples were identical. This was reflected in the simulations.

A brief springback investigation was carried out on 1.6 mm thick samples in order to determine the most successful forming method. A number of combinations of pressure, speed and hold time were attempted (presented in Table 3-5) and the spring back of the material comparatively quantified.

*Table 3-5: Variations of hold time, pressure and rate attempted to press samples*

Hold time	Option 1	10	s
	Option 2	30	s
Pressure	Option 1	100	kN
	Option 2	800	kN
Rate	Option 1	100	kN/s
	Option 2	800	kN/s

The samples were scanned by Dr. Abhishek Das, a member of WMG, to provide the following data points, indicating levels of springback (presented in Table 3-6). Full scans of the samples are available in Appendix B. He followed the following steps [93]:

- Data collection: Surface based measurement was necessary which provided large data points in terms of 3D Cloud-of-Points (CoPs). In this case, a laser scanner was used to capture surface data of the stamped parts. The scanner was attached as an end effector with one commercial measurement system, Romer (by Hexagon).
- Data processing: The captured data was processed with post-processing software PolyWorks (by InnovMetric) which had the following three steps:
  - Data Import: Nominal CAD model and CoP data were imported in the post processing platform.
  - Data Cleaning: The noisy data was removed with a data removal tool and the captured data was subsampled for faster computations.
  - Data Alignment: The cleaned part surface based data (i.e. CoP) was aligned with the CAD model for further analysis.
- Surface Deviation Computation: The surface deviation was computed at mesh node points. The surface colour map was generated for visual inspection

The samples scanned were all 1.6 mm in thickness, pressed at the rate of 800 kN/s; as this had provided the best results prior to the study of the effect of Pressure and Hold Time.

*Table 3-6: Maximum deflection from scans of samples after forming at varying pressures and hold times*

Rate, Pressure, Hold Time	Springback side profile
R: 800 kN/s, P: 100 kN; HT: 10 s	Max deflection ~14 mm
R: 800 kN/s, P: 100 kN; HT: 30 s	Max deflection ~14 mm
R: 800 kN/s, P: 800 kN; HT: 10 s	Max deflection ~13 mm
R: 800 kN/s, P: 800 kN; HT: 30 s	Max deflection ~11 mm

### 3.4.1.3 Three-point bend equipment

To investigate the stiffness of the hybrid material chosen, quasi-static three-point bend tests are undertaken. These are analogous to a side-impact automotive load case, where stiffness and energy absorption must be balanced to minimize intrusion and occupant accelerations. In the context of this work, stiffness will be the primary focus. The quasi-static testing was done using the 100 kN Instron Universal Tensile Testing machine in compression with a three-point bend fixture. Figure 3-7 shows an image of the set-up, where the top section is fixed and the bottom section moves along the red arrow (screw driven).

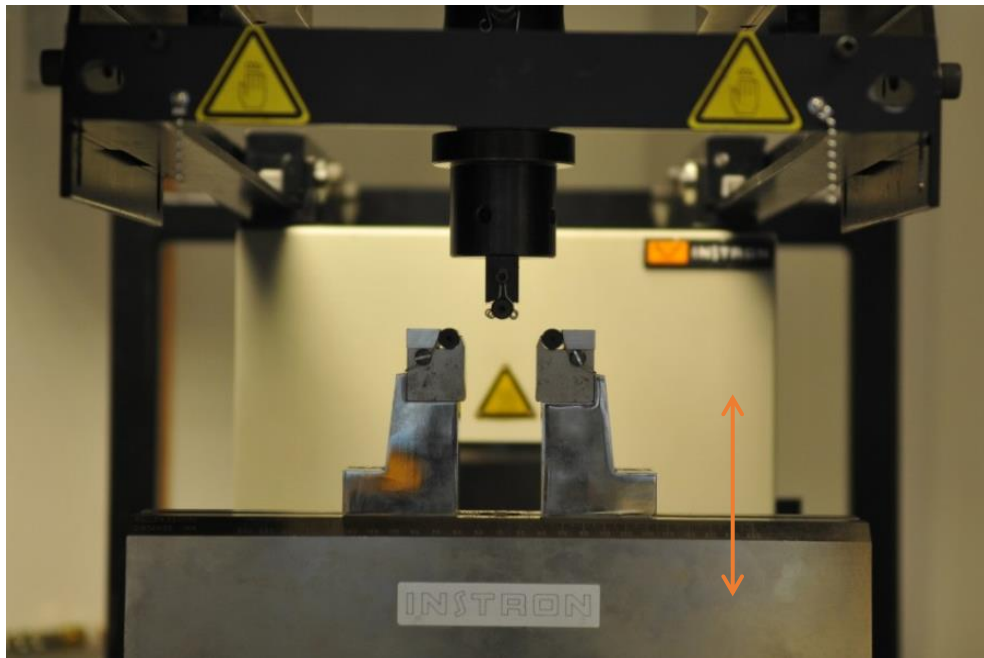


*Figure 3-7: Three-point bend test rig and fixture*

The speed was set according to the standards, at  $v_{\text{coupon}} = v_{\text{component}} = 1 \text{ mm/min}$  for both the coupon and component testing.

The data was recorded then exported to Microsoft Excel for post processing and analysis.



### **3.4.2 Standards**

There are no specific standards for the testing of hybrid materials. The closest standards available are used as the guideline for the testing of the material. The British Standards and ASTM standards are:

- BS EN ISO 14130:1998 – Fibre-reinforced plastic composites – Determination of apparent interlaminar shear strength by short beam method [94]
- BS EN ISO 14125:1998– Fibre-reinforced plastic composites – Determination of flexural properties [95]
- ASTM D7264/D7264M – 07 Flexural properties of polymer matrix composite material [96]

These state that at least five specimens shall be tested and set the size and aspect ratio of the samples based on their thickness. It was decided that the aspect ratio of the samples would remain the same for all tests regardless of the thickness. This simplifies the testing process and enables a direct comparison of performance.

The standards also give precisions as to the acceptable failure mode, defined as shear failure but this is considered outside the scope.

### **3.5 Simulation program**

Finite Element Analysis (FEA) is the widely accepted method to predict the performance of a known material under specific circumstances and perform a sensitivity or parametric analysis on the variables. It is used to predict the behaviour of large components, relying on a series of assumptions and known properties. The properties of the materials are incorporated into the FE model to simulate loading in bending of the samples. Once validated against the test results, this FE model is used to simulate, predict and evaluate coupon and component designs.

This chapter discusses the software packages used, with their advantages and limitations.

Initial simulation is performed using LS-DYNA, software developed by the Livermore Software Technology Corporation (LSTC). Following that the composite tailored software Genesis (Design Studio interface), developed by Vanderplaats R&D is used.

### **3.5.1 Element Selection and Meshing**

There are large number of mesh density analysis studies in the literature [84, 85]. These show the convergence of the predicted results as the mesh gets finer, as well as an increase in computational time.

As a result, only brief mesh density analysis was performed as part of this research, as the element size is small compared to the obtained deflections. Increasing the mesh density increases the detail and precision of the simulated part, at a computational cost. Here, the mesh density is “medium-high” and the computational time in the order of seconds. The overall deformed shape resembles a continuous curve and does not present the “discontinuous” aspect of a large element mesh. In both the case of the coupon simulation the mesh density “check” consisted of halving the size of the mesh to investigate possible changes in outputs. The results were found to be identical to the ones generated by the initial larger and less time consuming mesh. The original element size was deemed suitable and used throughout. The element size varied between the coupon and the component simulations.

There are two types of elements that could be used to model the geometries investigated: solid elements and shell elements. The choice of element type depends on the geometry analysed, expected stress state, software used, and theories

followed. Some material cards will also restrict the nature of the elements. Shell elements are essentially 2-dimensional elements and solid elements are 3-dimensional. Shell elements are comparatively thin to the length of the sample, and generally require a shorter computational time than solid elements.

In the case of composite modelling, most material cards require the elements defining them to be shells. Shell elements are also the easiest to apply, geometrically most accurate as there is little to no through thickness consideration.

There are two time integration scheme control methods that can be used to run a simulation, implicit and explicit. The support for LS-DYNA software users online explains it best as follows [97]: *“Explicit methods calculate the state of the system at a later time from the state of the system at the current time. Implicit methods solve an equation involving the state of the system at both the current and later times. In nonlinear implicit analysis, solution of each step requires a series of trial solutions (iterations) to establish equilibrium within a certain tolerance. In explicit analysis, no iteration is required as the nodal accelerations are solved directly”*. Due to the implicit methods using two state of system time factors, the calculations are computationally expensive compared to the explicit method. Static analysis, which presents smaller variable numbers than a dynamic analysis, is generally performed using an implicit solver. Dynamic analysis of a system can use either an implicit or an explicit solver.

Where it concerns time steps, explicit and implicit solvers vary. *“The time step in explicit analysis [takes the minimum] Courrant time step (time it takes a sound wave to travel across an element). Implicit transient analysis has no inherent limit on the size of the time step. As such, implicit time steps are generally several orders of magnitude larger than explicit time steps”* [97].

Implicit analysis requires a numerical solver to invert the stiffness matrix once or even several times over the course of a load or time step. This matrix inversion is an

expensive operation, particularly for large models. Explicit solvers do not follow these steps. Explicit analysis handles nonlinearities with relative ease as compared to implicit analysis. This would include treatment of contact and material nonlinearities.

LS-DYNA support explains furthermore [97]: *“In explicit dynamic analysis, nodal accelerations are solved directly, as opposed to iteratively. These are calculated as a multiplication of the inverse of the diagonal mass matrix by the net nodal force vector. The net nodal force includes contributions from exterior sources (body forces, applied pressure, contact, etc.), element stress, damping, bulk viscosity, and hourglass control. Once accelerations are known at time  $n$ , velocities are calculated at time  $n+1/2$ , and displacements at time  $n+1$ . Once the displacements are known, strain and stresses can be calculated, and the cycle repeated”*.

The material properties are defined using the experimental data as presented earlier in Chapter 3.

### **3.5.2 LS-DYNA**

The geometries modelled are broken down into parts, which contain the elements inherent to that section, and have assigned material characteristics and constraints. In LS-DYNA, the most straightforward way of modelling a multi-layered material is to use PART\_COMPOSITE. As explained in the user manual, PART\_COMPOSITE *“provides a simplified method of defining a composite material model for shell elements and thick shell elements that eliminates the need for user defined integration rules and part ID’s for each composite layer.”* [98].

LS-DYNA boasts nearly 300 material models of which 25 can be applied to the simulation of composite materials. These were all developed for different

applications. A material model is picked based on the availability of parameters and data from the experimental work that will fit into the mathematical model of the material card. The most suited to the modelling of this material and behaviour is MAT\_58 Laminated Composite Fabric [91].

Based on the assumption that the adhesive bond between the PA6GF60 and the DP600 is perfect in the elastic region, the simulations were performed in the LS-DYNA solver, using PART\_COMPOSITE, MAT\_58 Laminated Composite Fabric for the PA6GF60 and MAT\_2 Orthotropic Elastic for the DP600. MAT\_2 Orthotropic Elastic is a relatively simple material card, with limitations, however in the elastic simulation circumstances is appropriate. In more complex scenarios, MAT\_24 Piecewise Linear Plasticity should be used.

The detail of the simulation of the coupon and component systems are discussed in Chapters 4 and 6 respectively.

### **3.5.3 Genesis**

This software developed by VanderPlaats R&D is well suited for the elastic simulation of bodies and tailored for use with composite materials. It does not cater for dynamic analysis however is provided with an add-on which links it to LS-DYNA and allows for the simulations to run.

Similar assumptions were used here, P\_COMP was used as the equivalent to PART\_COMPOSITE, and the materials are defined within the software bounds. This can be used in conjunction with the Reinforcement Derivation Method and other optimisation add-in [99] for the optimisation placement of the composite reinforcing patches. The details are discussed in Chapters 4 and 6.

### **3.5.4 Optimisation Concept**

A model of the static stiffness and frequency response of a BIW could be used in further to assess potential locations for reinforcement. The focus should be on global stiffness behaviour.

- Areas where there is stress concentration and the direction of the stress is known
- Areas where the current gauge of steels allows for down gauging of steel: the overall thickness may increase but there is an opportunity for weight saving

## **4 COUPON PROGRAM**

This chapter discusses the initial experimental and simulation study, where the principle aim was to characterise the hybrid material stiffness performance and establish the viability of the concept for lightweighting. Using a coupon shape in quasi-static bending, the material was investigated and the data analysed. The manufacturing of the samples and the testing is discussed in detail. The assumptions and set-ups used to create the simulated FE model are also presented, as well as a validation of the model against experimental data.

The appellation “hybrid” refers to samples of DP600 reinforced with composite material. “Pure steel” refers to the un-reinforced DP600 samples. “0.5 mm hybrid” refer to hybrid samples with a 0.5 mm DP600 layer, and “0.8 mm hybrid” refer to hybrid samples with a 0.8 mm DP600 layer.

### **4.1 Testing**

This section concerns the production and testing of the benchmark pure steel and the hybrid samples. All aspects are covered in order to make the process as reproducible as possible by the reader.

#### **4.1.1 Sample production and hybrid preparation**

The optimised manufacturing of the hybrid and its applicability in an industrial context was considered outside the scope of this project. A simple, straightforward and repeatable preparation method was the aim and final outcome. The experimental approach to sample preparation was none-the-less an iterative process, until satisfactory samples were produced.

All hybrid coupon samples were produced using a vacuum bagging technique and cured at temperature in a Royce Industrial Oven.

Initially, a one-step technique was used. The composite pre-preg was prepared following the lay-up technique presented in Chapter 3. The steel was also prepared following the process described in Chapter 3 and the unconsolidated pre-preg, adhesive and steel placed in a vacuum bag. This was then cured at 240° C (the consolidation temperature of the PA6 GF60) for 10 minutes. This technique was discarded as, when tested, these samples disintegrated at the interface. It was believed that the consolidation temperature of the composite damaged the adhesive, causing a degradation and loss of properties. These samples provided a useful learning step towards the manufacturing, cutting and testing of the final specimens.

As the first method was unsatisfactory, a multi-step process was attempted. The steel surface was prepared for adhesion through manual abrasion. This increases the surface energy of the steel and is known to improve the bond strength [73]. In parallel, the composite was layed-up and consolidated under vacuum at 240 °C, using a removable peel ply fabric applied to one side as the surface preparation for adhesion. In the final step, the steel and consolidated composite were bonded together using a one-part epoxy (recommended in-house and from Alpha Adhesives) cured under vacuum at 150 °C for 3 hours. This finalised process provided satisfactory results discussed in Chapter 4, Results and Discussion. Detailed below are the material specific preparation steps.

#### *4.1.1.1 Steel preparation*

No specific attention was paid to the rolling direction as it is known to have negligible effects on performance, as discussed in Chapter 3. The steel was handled



in sheets of 500 mm<sup>2</sup>. This allowed for batch sample production and increased repeatability.

Multiple methods of surface preparation are possible. The Handbook of Adhesives and Surface Preparation [73] suggests that primers may be desirable if the bonds were subjected to rigid environmental exposure so as to prevent the bond from degrading. It also concludes that mechanical roughening techniques are preferred over chemical treatments. The adhesive manufacturer Sika also recommends the following surface preparation *“The surface to be bonded must be free of oil, grease and other impurities. The bonding area must be cleaned with a lint free towel and n-Heptane. It is advised to grind the bonding surface followed by cleaning with n-Heptane.”* Further instructions from the manufacturer can be found in the attached document in Appendix C. It is acknowledged that the bonding interface greatly affects the stability of the results, however the results generated in the context of this work have shown to be repeatable and provide confidence in the surface preparation. Additionally, surface preparations such as plasma or corona treatments can provide an equally high performing bond [100]. Here, it is speculated that the bonding is a combination of mechanical interlocking and covalent bonding. A full adhesive study is suggested in further work.

The steel surface was degreased using a generic multi surface cleaning agent and hot water. Care was taken to dry the sheet thoroughly (using either blue towel or a hot air dryer) after cleaning to avoid rapid corrosion. The steel sheet was then bathed in acetone to remove any soap residue then in isopropyl alcohol to remove acetone residue. The surface was then sanded manually as described in Chapter 3 using P180 sanding disk. This disk grain size provides a roughening neither too fine nor too coarse, shown to be adequate for adhesive bonding to steel [84].

Two thicknesses of steel were used in the hybrid coupon samples, 0.5 mm and 0.8 mm. Both were prepared following the same steps. The steel used in benchmarking tests did not require surface preparation.

#### *4.1.1.2 Adhesive preparation*

The hybrid coupon samples were produced using the Alpha Adhesive one-part epoxies, shown in Chapter 3 to be recommended for similar materials and applicable to PA based composites [101]. These were stored at 5 °C in order to prolong shelf life and were taken out approximately an hour before use to increase temperature and lower viscosity, making it easier to handle.

Additionally, it was found that heating of the steel allowed better flow of the adhesive on the surface, giving better coverage. When applied to the warm steel, the viscosity of the adhesive decreased. As can be seen from Section 3.3 “Adhesive”, at 60 °C, this does not significantly accelerate the curing cycle and enables a more consistent thickness throughout the adhesive layer. The roller pin used to spread the adhesive was also pre-heated, aiding the spreading.

The final hybrid was heated for 60 minutes at 150 °C, the curing temperature of the adhesive. This was to ensure that the heat has fully penetrated the sheet and that curing had occurred. This produced a hybrid plaque, where cutting at different angles provided the given lay-ups.

#### *4.1.1.3 Composite Preparation*

Throughout the experimental section of this coupon study, the composite used was the PA6 GF60 presented in Chapter 3.

A hand lay-up technique was used to produce the composite laminates. A 4-ply symmetrical laminate,  $[0,90][90,0]$ , was layed-up, where the individual unidirectional layers were tacked together using a soldering iron at 240 °C. The stack was then cured under vacuum bagging condition at 240 °C for 10 minutes. The peel-ply cloth spread over the top surface of the composite has a dual action, as detailed in Section 3.2 “Composite”, page 32. It prevents the matrix from attaching to the vacuum bag and when removed provides the ideal surface condition for the adhesive bonding.

Figure 4-1 shows the fibre direction convention used throughout this study. In the figure, the top layer, in grey, depicts the fibres running at 45° to the length of the sample. The middle layer, was pale blue, depicts the fibres running at 90°. The bottom layer, in pink, depicts the fibres running at 0° to the length.

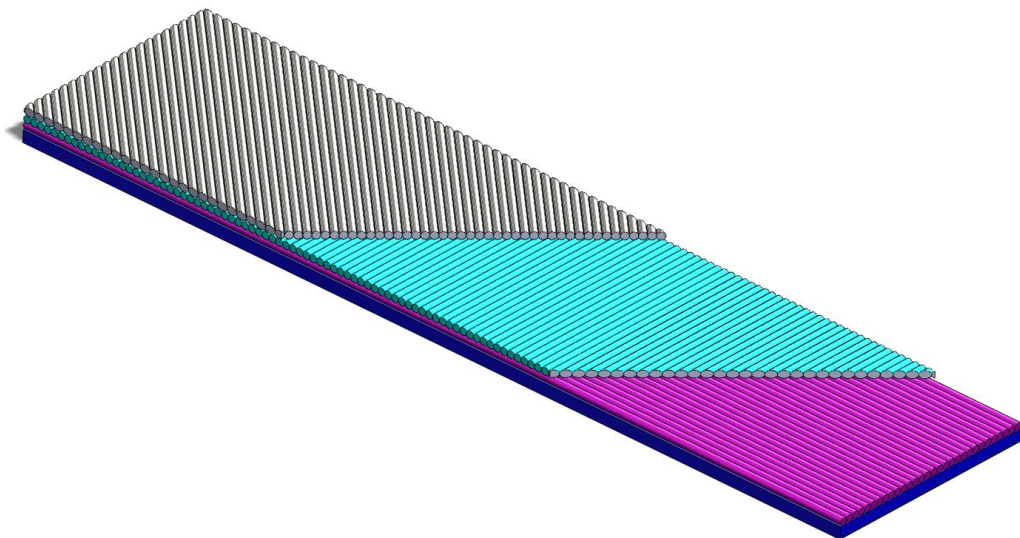


*Figure 4-1: Sketch defining fibre directionality in the three-point bending samples*

*(not to scale); from top to bottom 45° (grey), 90° (blue) and 0° (pink).*

#### 4.1.1.4 Hybrid preparation

In the finalised production of hybrid three-point bending samples, three different balanced composite layups were considered, [0,90][90,0], [45,-45][-45,45] and [90,0][0,90]. These shall be referred to here on as [0,90]<sub>s</sub>, [45,-45]<sub>s</sub> and [90,0]<sub>s</sub>. The standard ply directionality used for this work is depicted in Figure 4-1. These layups were selected as they are symmetrical and balanced, less affected by mismatches of coefficients of thermal expansion during production that leave residual stresses through-thickness, and can manifest by a warping of the samples. They are also non-isotropic, meaning the fibre directionality effect can be studied.

Table 4-1 presents the different fibre layups considered for the experimental coupon testing.

*Table 4-1: Fibre layups considered in study*

Steel	Composite
	[0,90] <sub>s</sub>
DP600	[45,-45] <sub>s</sub>
	[90,0] <sub>s</sub>

The coupon samples were cut from the bonded hybrid plaques using a Datron M7HP high speed milling machine. The cutting technique is presented in Chapter 3, 3.4.1.1 Cutting the specimens.

The sample dimensions for three-point bending were based on the recommendations given by the relevant ISO and ASTM standards [95, 96]. Note that all samples, regardless of their thickness, present the same geometry. This enables a direct physical comparison of the global bending stiffness. Table 4-2 and Table 4-3 present the sizing characteristics for the two batches of hybrid samples, based on the use of 0.8 mm DP600 and 0.5 mm DP600. Figure 4-2, Figure 4-3 and Figure 4-4 depict the hybrid composite lay-up, including fibre orientation based on the convention established above.

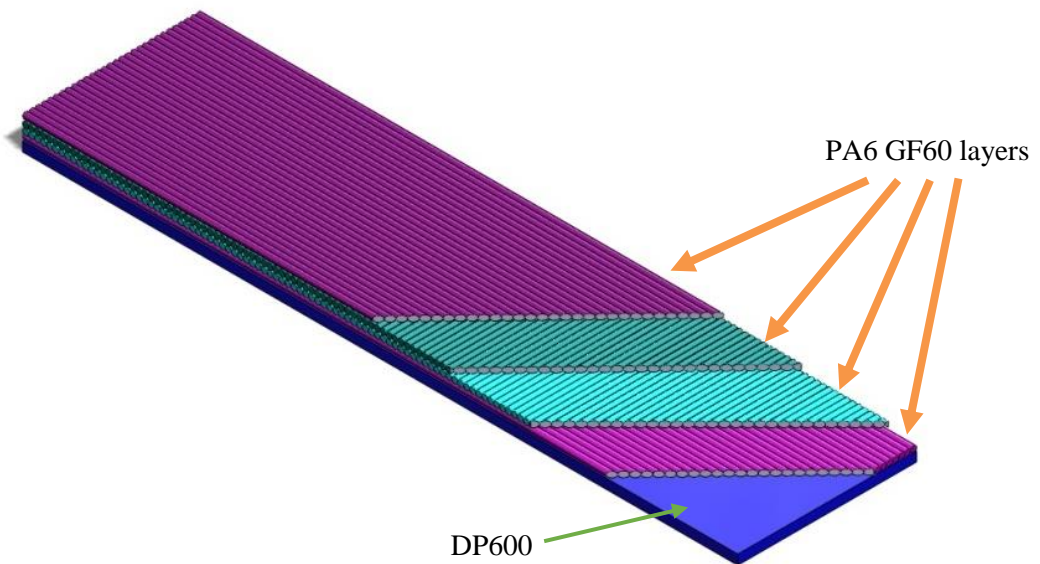
Given that the composite layer is 4-ply in every case, and that the only thickness variable is the thickness of the steel, hybrid samples using 0.8 mm DP600 will be referred to as 0.8 mm hybrid samples, and hybrid samples using 0.5 mm DP600 will be referred to as 0.5 mm hybrid samples.

*Table 4-2: Sizing of 0.8 mm hybrid samples for flexure tests*

Engineering constant	Units	Values	Uncertainty
Width	mm	15.00	±0.01
Length	mm	60.02	±0.01
Thickness	mm	2.20	±0.03
Weight	g	7.70	±0.03

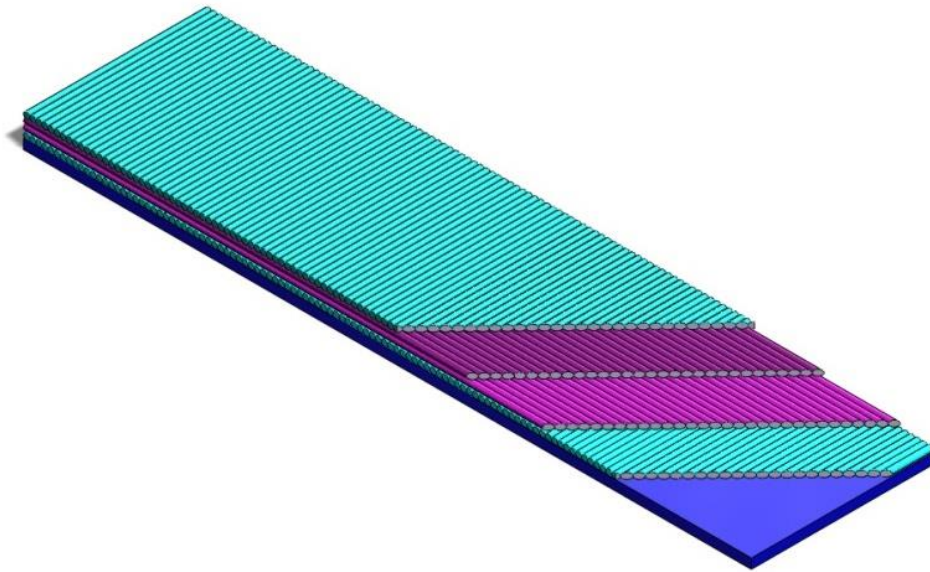
*Table 4-3: Sizing of 0.5 mm hybrid samples for flexure tests*

Engineering constant	Units	Values	Uncertainty
Width	mm	15.02	±0.01
Length	mm	60.02	±0.01
Thickness	mm	1.85	±0.04
Weight	g	5.53	±0.05



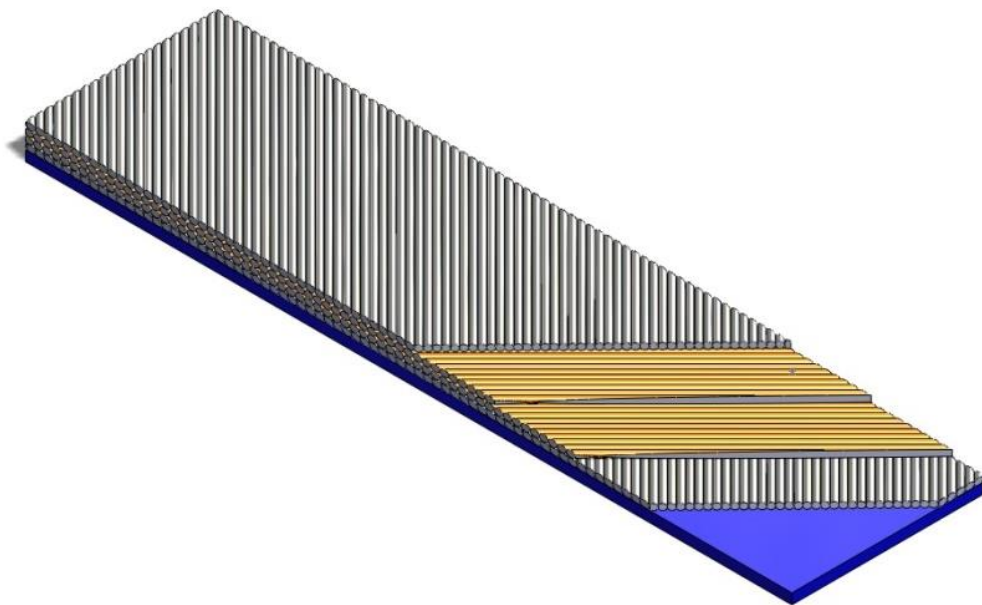
*Figure 4-2. Hybrid Composite/Steel [0,90]<sub>s</sub> ply directionality – not to scale*

Figure 4-2 depicts the composite-over-steel situation of the [0,90]<sub>s</sub> layup, where the fibres on the outer layers of composite run parallel to the length of the specimens.



*Figure 4-3: Hybrid Composite/Steel [90,0]<sub>s</sub> ply directionality – not to scale*

Figure 4-3 depicts the composite-over-steel situation on the [90,0]<sub>s</sub> layup, where the fibres on the outer layers of the composite run perpendicular to the length of the specimens.



*Figure 4-4: Hybrid Composite/Steel [45,-45]<sub>s</sub> ply directionality – not to scale*

Figure 4-4 depicts the hybrid composite-over-steel situation on the [45,-45]<sub>s</sub> layup, where the fibres on the outer layers of the composite run at 45° to the specimen length.

As the samples were manually manufactured, a check of the fibre orientation under a microscope was used to ensure reliability of the results and ensure the coherence between the tested and simulated samples. Figure 4-5 shows the cross section of a hybrid sample, highlighting the layer breakdown. The composite fibres are arranged in  $[0,90]_s$ , and seen as circular and “needle-like” shapes. The surface roughening provided by the removal of the peel-ply to the composite surface at the composite/adhesive interface, is also visible. As seen in Figure 4-5, the sample was mounted in a resin, to allow for micrograph images to be taken.

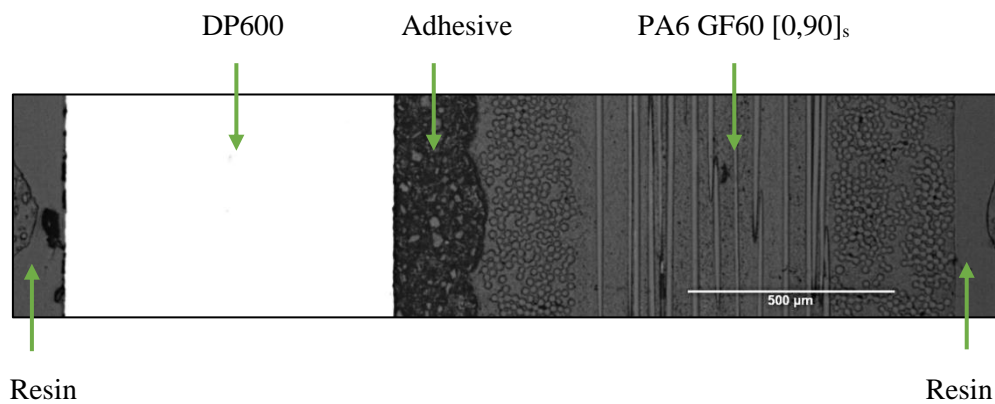


*Figure 4-5: Micrograph cross section of the hybrid sample DP600 and  $[0,90]_s$  PA6 GF60*

#### **4.1.2 Three-point bend instrumentation**

The principal aim of this study was to understand the stiffness performance of the hybrid material in relation to the benchmark steel. The testing used to that effect was quasi-static three-point bend, following the methodology set out by standard BS EN ISO 14125:1998 [95].

The tests were performed using an Instron 5800R universal testing machine, with a maximum load rating of 100 KN, grip faces of 25 mm or 50 mm for tensile tests and a three-point bend compressive fixture for bending. The rollers of the three-point bend fixture were sized at 5 mm according to standard [95], the span was constant

throughout, at 40 mm. The cross-head speed was set according to the standards, at  $v=1$  mm/min. The samples were pre-loaded to 20 N.

Figure 4-6 shows the fixture set-up in situ. The red arrow indicates the direction of travel of the screw driven platform, relative to the fixed middle roller.

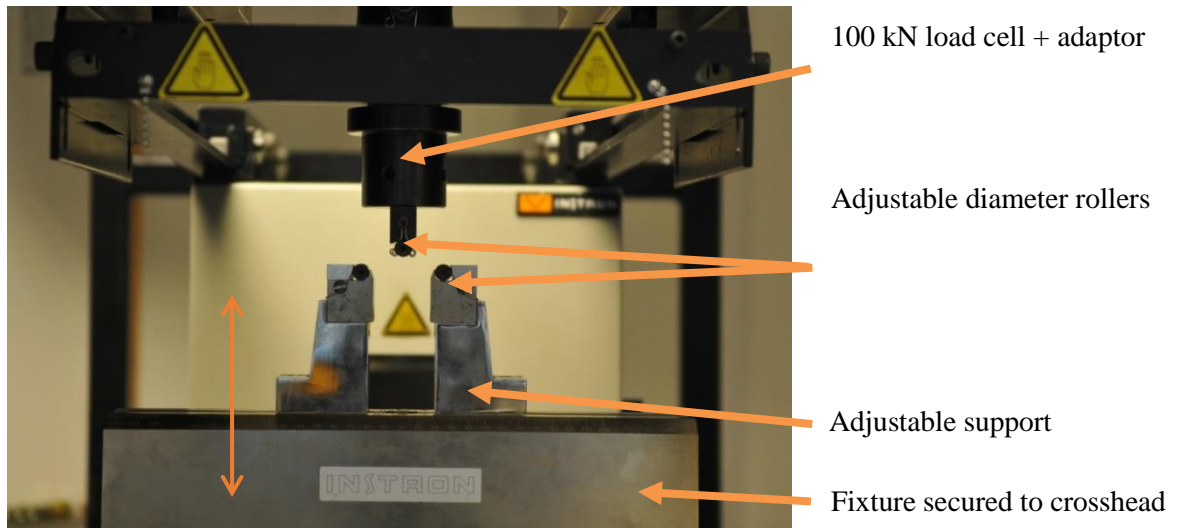


*Figure 4-6: Three-point flexure fixture set up – span length is 40 mm*

Three samples of each specimen type were tested as a trial run to establish confidence in the method set up in the Instron software and produce some initial data to outline the following steps. Once confidence was achieved in the method, and in order to establish the repeatability of the tests and ensure confidence in the results, five samples were tested for each condition, i.e. 60 hybrid samples in total, and 30 benchmarking samples (15 pure steel and 15 pure composite). Table 4-4 contains the overall summary of the family of tests.

### **4.1.3 Benchmarking**

In order to quantify the performance of the hybrid, the performance of the individual materials must be assessed separately. In benchmarking the steel, multiple thicknesses were used to create a broad coverage of data. PA6 GF60 balanced samples were also tested,  $[0,90]_s$ ,  $[90,0]_s$ ,  $[45,-45]_s$ . Table 4-4 includes a summary of



all the samples tested, both in benchmarking and hybrid scenarios. Note that 0.5 mm DP600 was not used in the benchmarking, as it is the thinnest material used, and considered “downgauged” and therefore reinforced with composite.

Interestingly, it was noted that the  $[45,-45]_s$  pure composite samples were slipping sideways as the load increased during the test. This is believed to be due to the sample rotating to align the fibre directionality away from the load path. As the fibres on the outer layer of composite are at an angle with the load path, it is believed that they rotate so as to create least resistance to the bending motion, and therefore the loads measured were sub-optimal. In further work, it would be recommended to repeat these tests and constrain the samples to prevent rotation or slip along the rollers. In the context of this study, despite the effect being minimal in the elastic region, the  $[45,-45]_s$  composite benchmarking results are treated with caution, and not used as a primary source of experimental validation.

#### **4.1.4 Hybrid**

As shown in Figure 4-7 and Figure 4-8, the samples were tested both in a situation of steel-over-composite (steel/composite – S/C) and composite-over-steel (composite/steel – C/S), where the loading path in the material is different, specifically in the fibres, either in tension or in compression. Table 4-4 summarises all samples tested in the context of the flexural work on coupon samples.



*Figure 4-7: Quasi-static three-point bend set up with composite face down (S/C) –  
sample length 60 mm, span 40 mm, width 15 mm*



*Figure 4-8: Quasi-static three-point bend set up with steel face down (C/S) –  
sample length 60 mm, span 40 mm, width 15 mm*

Table 4-4. Summary of the coupon samples tested, five repeats each. C/S refers to composite/steel, and S/C to steel/composite

Type of test	Material and Orientation		
	DP600 steel	PA6 GF60 Composite	
Benchmarking (60 mm by 15 mm)	-	[0,90] <sub>s</sub>	-
	-	[45,-45] <sub>s</sub>	-
	-	[90,0] <sub>s</sub>	-
	0.8 mm	-	-
	1.0 mm	-	-
	1.6 mm	-	-
Hybrid (60 mm by 15 mm)	0.5 mm	[0,90] <sub>s</sub>	C/S
		[45,-45] <sub>s</sub>	
		[90,0] <sub>s</sub>	
	0.8 mm	[0,90] <sub>s</sub>	S/C
		[45,-45] <sub>s</sub>	
		[90,0] <sub>s</sub>	
	0.8 mm	[0,90] <sub>s</sub>	C/S
		[45,-45] <sub>s</sub>	
		[90,0] <sub>s</sub>	
		[0,90] <sub>s</sub>	S/C
[45,-45] <sub>s</sub>			
[90,0] <sub>s</sub>			

## 4.2 Simulation

This section presents the campaign to create finite element models created to support and cross-validate against the experimental results. The modelling steps and consequent results are not presented here in their totality but discussed in small part to explain and justify certain choices.

At coupon level, the simulation was achieved in two parts. Two separate software packages, LS-DYNA and Genesis, presented in Chapter 3, were used. Initially, LS-DYNA was chosen as the software for the simulation, as it is also well documented within the literature for its use in modelling steel and composite structures [84, 85, 88, 98, 102, 103]. It is also widely supported within the home institution, WMG and it is extensively used within Tata Steel who provided guidance as a supervisory role. The coupon experimental work and simulations were therefore validated against each other, in a two-step process using LS-DYNA.

A later stage of this research was due to include composite optimisations which could be computationally expensive in LS-DYNA. A more detailed analysis, and a refining of the implicit LS-DYNA run could potentially mitigate this effect. However, an alternative was found in Genesis. Genesis, based on the MSC Nastran software, is more suited to this purpose and tailored to composite design and static-elastic composite optimisation. In Genesis, the computational time is a fraction of that required by LS-DYNA for the same model as Genesis is a purely linear software. LS-DYNA is not as readily prepared for a composite optimisation as Genesis. A primary application for LS-DYNA is automotive simulation [104] as is it a highly non-linear, transient dynamic FEA using explicit time integration. Genesis [105] is predominantly used for static, normal modes, direct and modal frequency analysis and system buckling and it presents a structural optimisation code.

Following initial studies, the nature of the part and coupon simulation indicated Genesis would be better suited to coupon simulations.

Having switched to Genesis, it was important to prove that the assumptions made in LS-DYNA were valid and could be carried forward. The validation iteration between the experimental and simulation results was therefore repeated. Both softwares present data that correlates closely with the experimental results (see later in Chapter 4), giving confidence not only in the results themselves but also in the assumptions made in creating the models.

Discussed below are the various models created in both software packages and indications of their correlations with the experimental work. All models were built around identical initial assumptions. The coordinate system for the modelled samples is defined as x running along the length of the sample, y running across the width and z through thickness. It is used consistently throughout all the simulations, in LS-DYNA and Genesis.

Figure 4-9 and Figure 4-10 show the directionality of the vectors normal to the shell element surface. This directionality is important, as it controls the direction in which the layers grow, either in thickness or within P\_COMPOSITE and PCOMP. Specifically, the “*integration points data should be given sequentially starting with the bottommost integration point*” [98]. This means that the shell elements pictured are the lowest in a composite stack. The colours and arrows indicate in which direction, in a “right hand” coordinate system, the vectors normal to the shell surface are pointing.

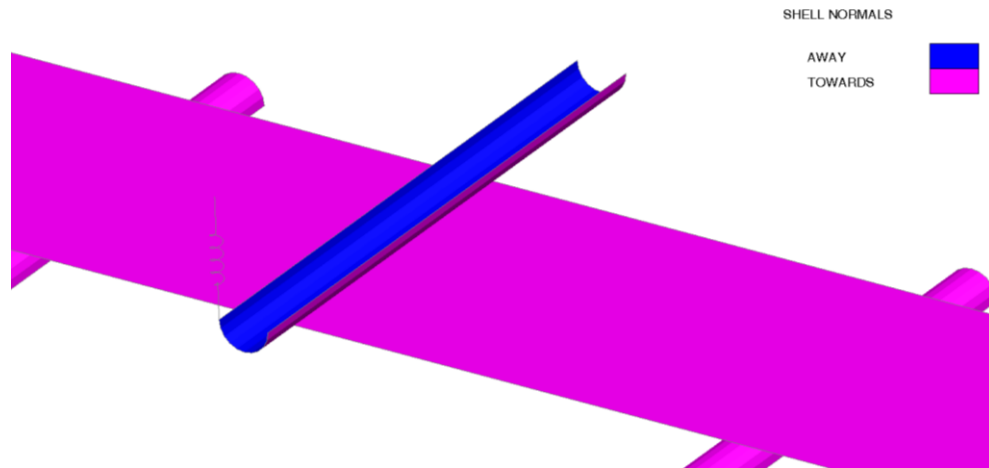


*Figure 4-9: LS-DYNA Model showing the directionality of the vectors normal to the shell elements from Primer*

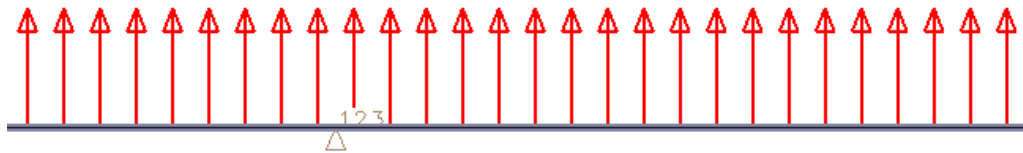


*Figure 4-10: Genesis model showing the directionality of the vectors normal to the shell elements*

Additionally, all theta vectors defining the longitudinal direction of the elements are aligned with the coordinate system, to ensure consistency in material orientation definitions.

The full results, experimental and simulated are discussed later in this chapter.

#### **4.2.1 FEA Model Creation in LS-DYNA**

The model of the coupon was drawn and meshed using Altair HyperMesh. The mesh size was 0.3 mm, or 200 elements along the 60 mm length of the samples, and 50 elements along the 15 mm width of the samples. This was set up using shell elements as they are compatible with all the material models and representative of the slender beam shape of the sample.

As the solver used in this simulation was LS-DYNA, the rollers of the three-point bend fixture were also modelled and meshed in HyperMesh. Figure 4-11 shows the initial model set up. The roller faces in contact with the sample were modelled.

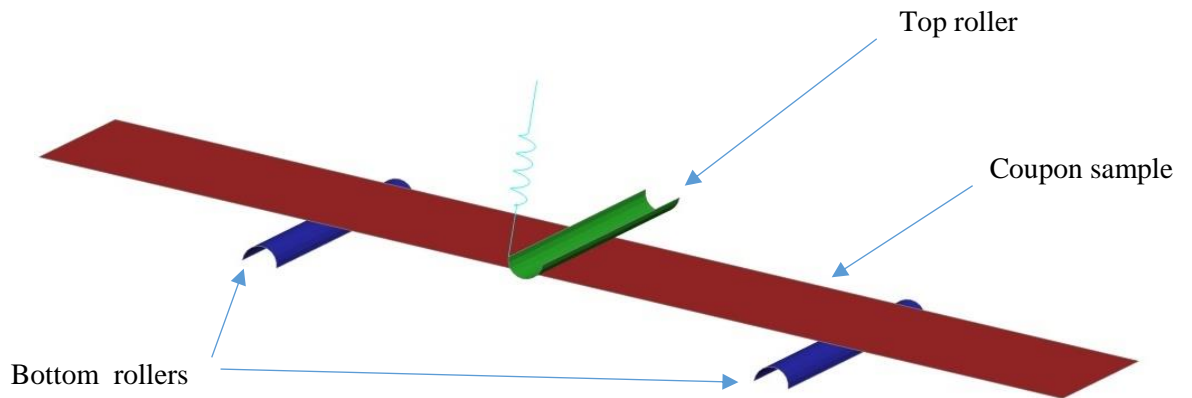


*Figure 4-11: HyperMesh model of the three-point bend test*

To model a hybrid material in a quasi-static bending situation, several models, theories and assumptions are possible. These all have inherent advantages and disadvantages. Three different models were investigated in this specific context. The first model included the steel and the composite in the same part. The second model assumed the steel and the composite in separate parts. The final model assumed all individual layers, be it steel or composite, to be in separate parts. The model with the highest correlation of results with the experimental work was taken forward to the later stages of modelling. In all models, constraints, initial state and required outputs were defined; as well as the material characteristics.

Assumption 1: Steel and Composite in the same part

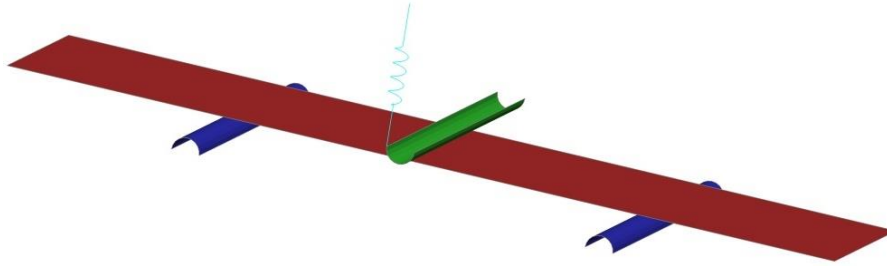


Figure 4-12: LS-DYNA model of the three-point bend test, with a single layer of shell elements

The overruling assumption for this model is that the adhesive bond behaviour between the composite to the steel is perfect, i.e. displays no failure in the elastic region and therefore does not require separate modelling. The steel and the composite are modelled together in an overall PART\_COMPOSITE, as in Figure 4-12. As explained in Chapter 3, the material cards used are MAT\_02 and MAT\_58 respectively. This material model is also used in the modelling of the benchmark materials, pure steel or composite alike. An underlying restrictive feature of PART\_COMPOSITE is the assumption that the interface between its layers to be perfect, implying a perfect interface between the steel and the composite material. It does not recognise incompatibilities between material interfaces, and therefore won't show true delamination failure modes.

Based on the vector directionality discussed previously, it is possible to define all six hybrid experimental cases separately and produce results. The layers are defined in the correct order and grown so that each sample can be represented.

Results for this type of model were within a 10% correlation to the experimental results, showing a high level of confidence in the model. Figure 4-13 shows the simulated and experimental load-extension graphs of the 0.8 mm hybrid samples. These are seen to present a high correlation, and provide confidence in the model set-up. The  $[0,90]_s$  and  $[90,0]_s$  hybrid samples show good agreement. The larger



difference in the  $[45,-45]_s$  hybrid samples is likely due to the slippage discussed earlier.

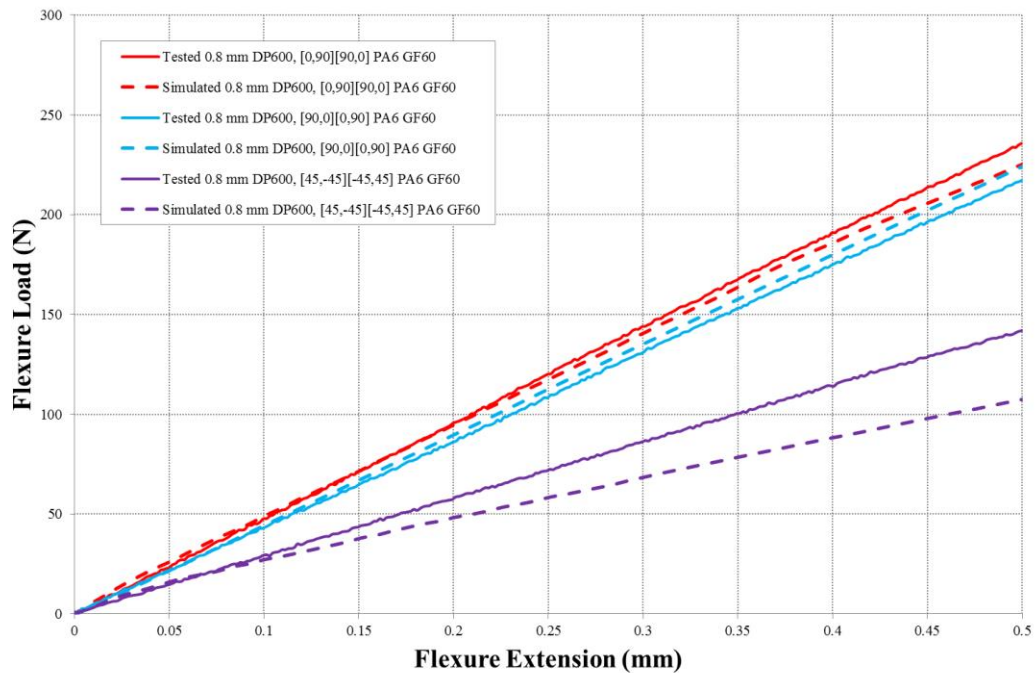
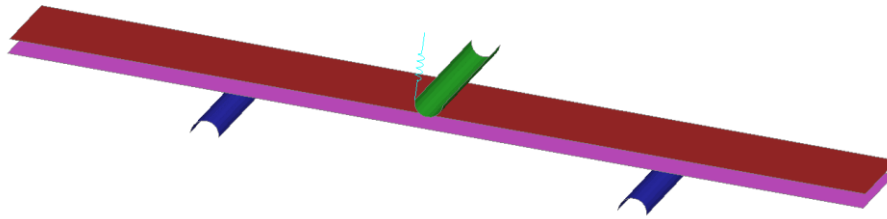


Figure 4-13: Representation of correlation between the experimental (solid lines) and simulated (dotted line) for the hybrid 0.8 mm DP600 GFRP samples

The two other assumptions were tested, however it was shown that Assumption 1 was the scenario that presented the highest level of correlation with the experimental model and the assumption taken forward through the simulations in LS-DYNA. The results are presented and discussed in detail in Chapter 4, Results. Once this assumption was selected it was then further verified through a second round of testing, where the results were predicted using the model and then checked experimentally. The correlation, as represented in Figure 4-13, was still found to be within 10 %, and the assumption carried forward to further simulations. The correlation is based on the values of stiffness gradient  $k$  calculated from the curves shown previously. The further two simulation set-ups tested are briefly presented and discussed as follows.

Assumption 2: Steel and Composite in separate parts



*Figure 4-14: LS-DYNA model with two layers of shell elements: Steel and composite model*

Two layers of shell elements were defined, one was given the properties of the steel and one was treated as a PART\_COMPOSITE with four layers of composite. A contact was created between the two layers to simulate the presence of the adhesive and avoid layer penetrations. This contact was either simulated as a contact card or using a layer of solid elements with basic adhesive properties.

In both cases, the model results did not correlate closely enough (over 15 %) with the experimental results, the stiffness of the overall structure was overestimated, and computational time increased.

Assumption 3: Five different shell layers

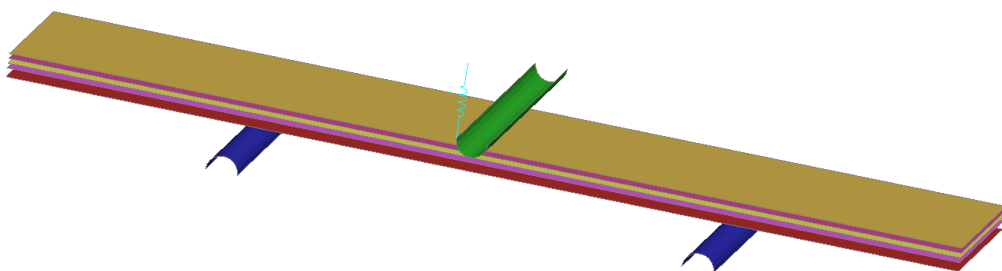


*Figure 4-15: Layers modelled individually*

Five layers of shell elements were defined, one was given the property of the steel and four were given individual composite properties. The fibre orientation was defined at a material property level and separate materials cards were created for

each fibre direction. Contacts were created between the layers simulating the presence of the adhesive and the nature of the matrix bond. This model had a high level of complication added to it, and inherent assumptions with every layer. This was also the most computationally expensive model. The results were the least convincing, the error was over 20 %. Additionally, this model did not profit from using MAT\_58 and PART\_COMPOSITE, as it did not use the in-built laminate function.

#### **4.2.2 FEA Model Creation in GENESIS**

The same Altair HyperMesh model as used in LS-DYNA was imported into Genesis as the software runs its models using shell elements. The rollers were not modelled or meshed, instead represented by a motion restriction and load in the location of the bottom rollers and impactor respectively. The nodes corresponding to support roller locations were given restricted degrees of freedom. On one end, the nodes were restricted in the x, y and z directions (1, 2, 3 as seen in Figure 4-16). This allowed for a rotation in alignment with test observations and simple beam theory. On the other end the nodes were restricted in the y and z directions (2, 3 as seen in Figure 4-16).

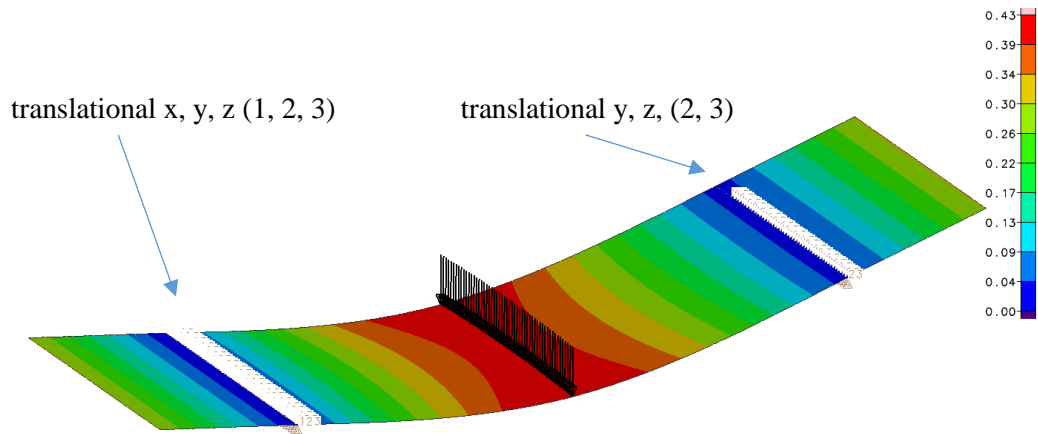


*Figure 4-16: Support and loading conditions on the coupon sample in Genesis – showing displacement (mm)*

This allows for rotation but also for the sample to “slip” over the roller in accordance with simple beam theory assumptions. It is also possible to restrict both sets of nodes simply in y and z; in the simulation of 1.6 mm DP600, hybrid 0.5 mm DP600 [0,90]<sub>s</sub> and hybrid 0.8 mm DP600 [0,90]<sub>s</sub>, the difference in deflection prediction was minimal – 0.01 %, 0.04 % and 0.09 % respectively. The difference was deemed small enough to be ignored, and Figure 4-16 shows the location of the rollers and load. Either roller constraint set up ([x, y, z and y, z] or [y, z and y, z]) may be used, so long as it is done consistently, throughout the modelling.

Genesis presents the option to represent the thickness of its materials, seemingly as solids, rather than the defined shell elements. This can be seen in Figure 4-17.

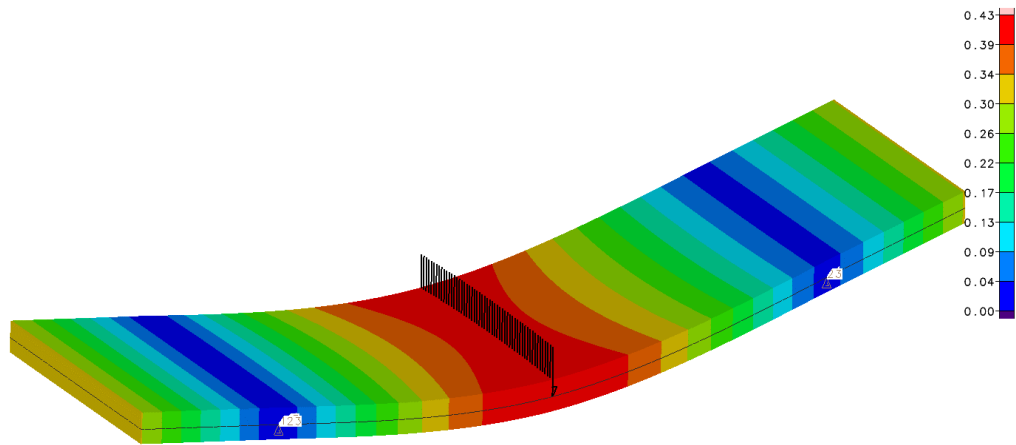


*Figure 4-17: Screenshot of the deflected 0.5 mm DP600 [0,90]s specimen –  
magnitude of deflection (mm)*

To ensure that the assumption carried in LS-DYNA that the adhesive bond behaves perfectly and that the materials can be modelled together within the same composite part was valid, the two first scenarios were reconsidered within Genesis. These are presented and discussed below.

Assumption 1: Steel and Composite in the same part

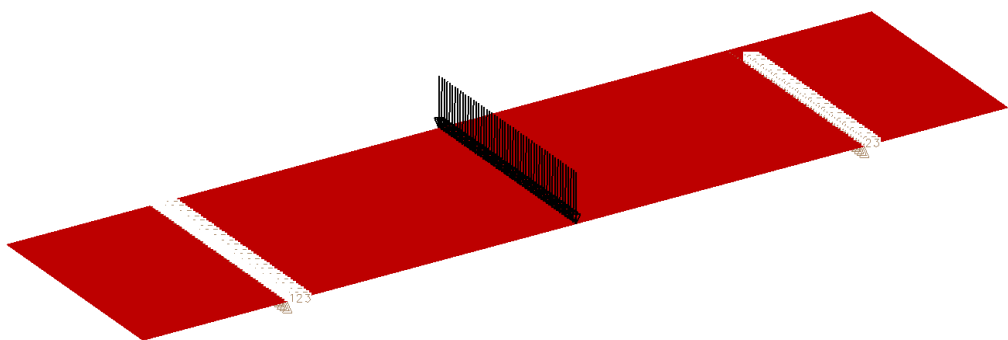


*Figure 4-18: Genesis model of the three-point bend test, with a single layer of shell elements*

The steel and the composite were modelled together in an overall PCOMP as in Figure 4-18. The material cards used were Isotropic MAT1 and PCOMP Orthotropic

MAT8 respectively. PCOMP suffers from the same flaws as PART\_COMPOSITE, as discussed in Section 654.2.1. In modelling the benchmark materials, pure steel and composite, this model was also used. The results for this model correlate to within 11 % of the experimental results. These results can be found in Table 4-5. Again, the largest discrepancy was seen in the [45,-45]<sub>s</sub> hybrid coupons.

*Table 4-5: Correlation of tested and Genesis simulated load-displacements for the benchmark DP600 material and both hybrids*

Material		Tested		Simulated			Correlation %
		Load (N)	Disp (mm)	Load (N)		Disp (mm)	
				Overall	Per Node		
1.6 mm DP600		380	0.50	380	7.2	0.48	-3.1
0.5 mm DP600	[0,90] <sub>s</sub>	139.2	0.50	139.2	2.6	0.55	9.3
	[45,-45] <sub>s</sub>	72.0	0.50	72.0	1.3	0.56	11.2
	[90,0] <sub>s</sub>	113.3	0.50	113.3	2.1	0.50	0.2
0.8 mm DP600	[0,90] <sub>s</sub>	229.3	0.50	229.3	4.3	0.52	4.5
	[45,-45] <sub>s</sub>	143.3	0.50	143.3	2.7	0.55	10.1
	[90,0] <sub>s</sub>	198.7	0.50	198.7	3.7	0.48	-3.5

Using the loads from the tested specimens, node-specific loads for the simulation were calculated. Due to the mesh size, there were 51 nodes across the width of the specimens. A single point load was applied to every node individually, with the overall load corresponding to that measured in testing. This simulated the action of the uniformly distributed loading of the roller against the specimen in testing. A brief investigation into the effect of the loading on the edge nodes was also run. The edge nodes only affect 2 elements where the centre nodes affect 4. The loading in the edge nodes should therefore logically be half that of a centre node. There was no difference in overall deflection between cases where the edge node carries half the loading of the central nodes and cases where all the nodes carry the same loading.

In the 0.5 mm hybrid simulations, thicknesses were set as 0.32 and 0.55 mm for the composite and steel layers respectively. In the 0.8 mm hybrid simulations thicknesses were set as 0.32 and 0.88 mm for the composite layers and steel respectively – this was done to incorporate the thickness of the adhesive in the

overall thickness. The thicknesses including the adhesive was 10 % higher than without, so the layers individually have seen their thicknesses increased by 10 % approximately to compensate.

Due to its correlation, this method was the one taken forward for the entirety of the Genesis based simulations. The alternative method investigated is described below.

Assumption 2: Steel and Composite in separate parts

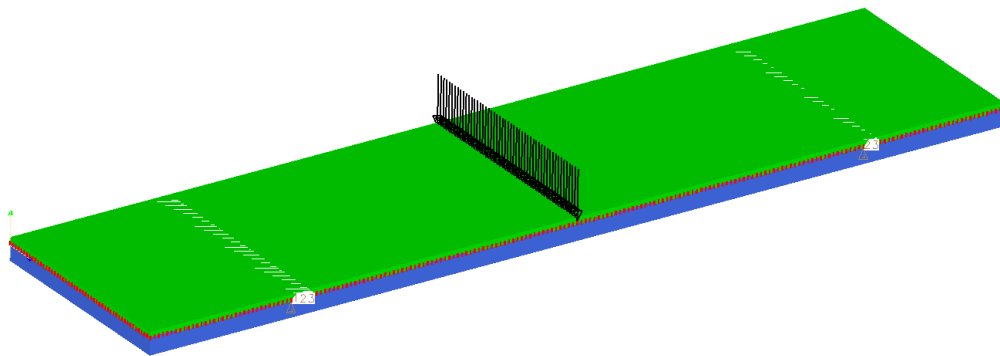


*Figure 4-19: Genesis model with two layers of shell elements joined by rigid body elements (RBE) – layer thickness shown*

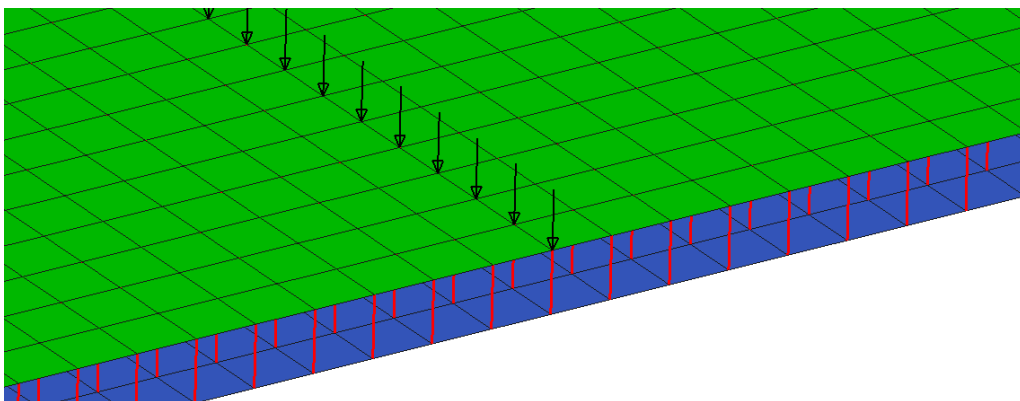


*Figure 4-20: Genesis model with two layers of shell elements – focus on RBEs*

The two layers of shell elements were given the properties of steel and composite separately. Bonding in Genesis was achieved using rigid body elements (RBE), which link the coincident nodes on each layer of shell elements together. The RBEs were given the option to move and rotate in all directions. This step was shown to not predict the stiffness behaviour of the coupon as accurately as the Assumption 1 method. This is due most likely to the inherent stiffness of the RBE bonds between the two layers and definitions of the location of  $z_0$ , the artificial “neutral axis” of the composite, around which the composite is bending. The results were outside the acceptable 10 % bracket of the experimental results, and deemed to be unacceptable.



### 4.3 Results and Discussion

In the following sections, the results of the experimental and simulated scenarios are presented. The validity of the results and their implications are discussed. Table 4-4 (page 62) presents the summary of all the physical tests run. Table 4-7 (page 85) presents a summary of all the results obtained.

#### 4.3.1 Expressing the results

The results obtained from the physical testing are a series of data points for the displacement of the screw driven platform and the load read by the load cell. These can be translated into load-extension curves which in turn can be interpreted to calculate values of the slope of the load-extension curve  $k$ , the values of Young's modulus  $E$ , as well as the normalised specific bending stiffness according to Ludke's lightweight design material criterion  $\sqrt[3]{E}/\rho$  [75]. There is also data available from the simulation software, either in the format of a load-extension curve in the case of the LS-DYNA models or as a single output value of extension for a given load in Genesis. Indeed, Genesis generates deflection values ( $x$ ,  $y$  and  $z$ ) for a specific loadcase, calculating the stiffness matrix of the parts prior to the application of load.

Depending on the context of the research, the different expressions of the results are best applicable to different situations.

Ludke's lightweight design material criterion [10, 75] is best suited to a material scientist investigating the performance of the global material. This criterion does not lend itself to the concept of "patching", as the values of Young's modulus  $E$  and density  $\rho$  are "rule of mixtures" type adaptations with an inherent assumption that the hybrid material is constant over the geometry tested. This criterion is not dependent on the thickness aspect of the geometry. All DP600 steels for example, regardless of their thickness in the coupon three-point bend situation should have a

Ludke criterion of 0.78. Figure 4-21 shows the relative performance of various materials according to the Ludke criterion, the Specific bending stiffness. The x-axis shows the performance of the specific strength of the materials, the y-axis shows the specific bending stiffness. The carbon fibre laminates have the highest specific bending stiffness, over twice that of steels. Sheet moulding compound composites (SMC) perform at a similar level to metals. PA6 GF60 has a specific bending stiffness over twice that of DP 600.

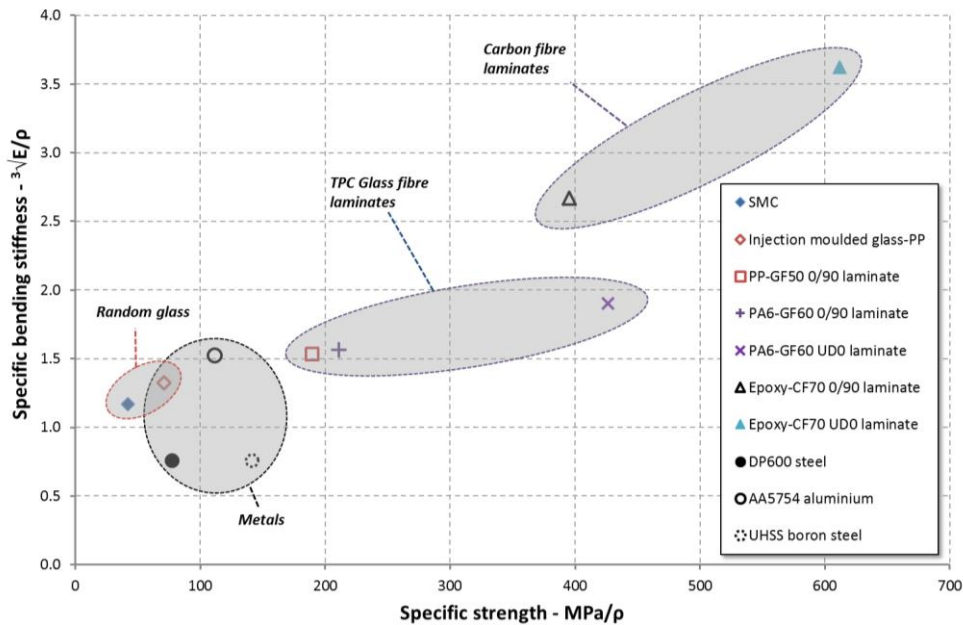


Figure 4-21: Specific stiffness diagram for various benchmark materials [87]

Young’s modulus values, based on “rule of mixture” type approximations, and calculated from the coupon testing, also do not readily lend themselves to a comparison of the performance of patched specimens. A single value of Young’s modulus cannot be used to express an overall stiffness in a scenario where only a section of the total geometry studied is a hybrid material.

In an engineering context, and with the patching application in mind, using the slope of the load-extension curve  $k$  gives a better insight and understanding of the situation. “ $k$ ” expresses the in-situ stiffness of the material regardless of the nature of the material or of the geometrical arrangements such as patching. For a

lightweighting study, this is most important as the weights can be compared directly in situations of where stiffness performance is matched.

The results of the coupon work have been expressed both in terms of the Ludke criterion and based on the slope  $k$ . Ludke's criterion and the slope  $k$  complement each other and provide a complete picture towards the lightweight potential of this hybrid material. These show the difference between investigating the material performance and the performance of the object in a situation specific context.

### 4.3.2 Full Results and Discussion

Table 4-4 presents the summary of all the experimental tests. As every sample set has five curves from the test repeats, there are 95 load-extension graphs for all the experimental tests completed. Of these, a selection of the 0.8 mm DP600 GFRP hybrid "average" curves for each situation are represented as shown below. Figure 4-22 below is a representative complete load-extension graph as it shows hybrid performance to failure.

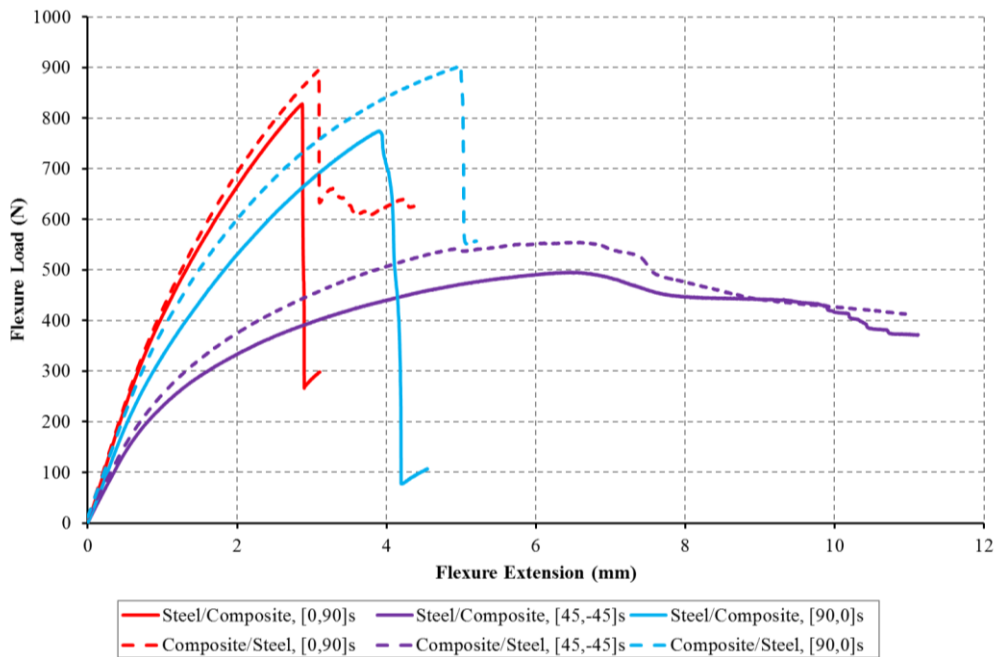


Figure 4-22: Load-extension diagram for the 0.8 mm hybrid coupon samples tested to failure

Figure 4-22, as it shows the coupons tested to failure, also includes notable information:

- stepwise failure of both the  $[0,90]_s$  and  $[90,0]_s$  hybrid samples
- $[0,90]_s$  has the highest stress to failure (outer layer of fibres has the greater effect)
- high strain to failure and low UTS in the case of the  $[45,-45]_s$  hybrid samples
- C/S presents a higher load in all cases

Of this data, only the section where both materials are known to be performing elastically is relevant to this study as we are interested in matching stiffness. This region is an extension of 0 mm to approximately 0.5 mm. The information contained within these full load-extension graphs on energy absorption and failure modes is discussed briefly in Appendix D. They are deemed out of the main scope of the current investigation.

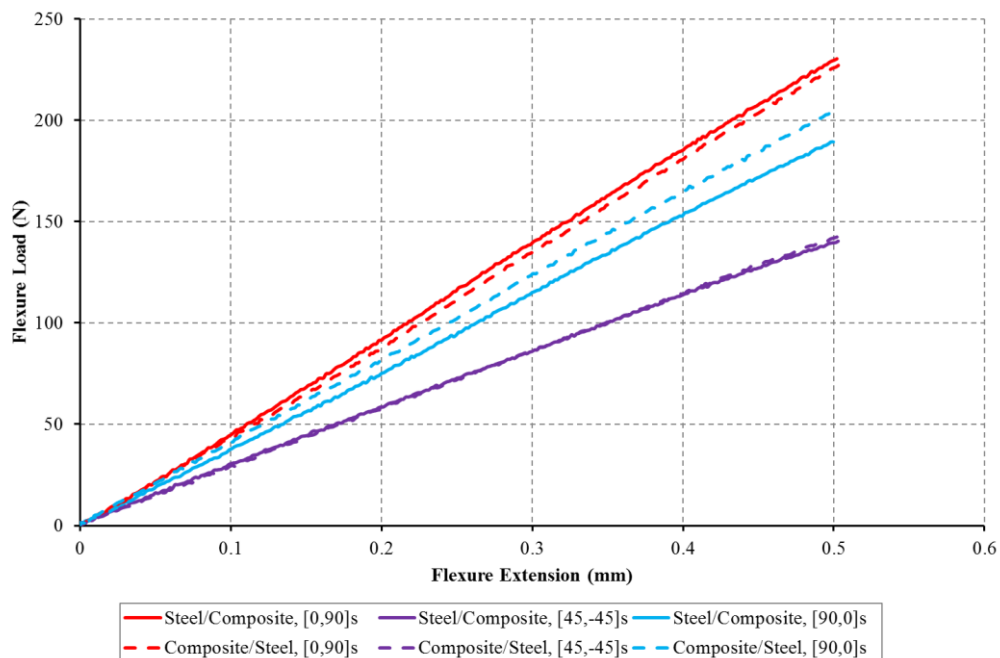


Figure 4-23: Elastic region relevant to the project, all 0.8 mm hybrid samples

Figure 4-23 shows the same samples within the elastic region. This is the section of data that the project is specifically interested in, adjusted to these tests from the suggested region from standards [95, 96], as it presents an elastic behaviour. All values of  $k$  and Ludke's criterion are calculated based on this elastic region of the data only. Figure 4-24 shows the specific bending stiffness of the materials, according to Ludke's criterion. The standard deviation for each value is small, highlighting the repeatability of the tests. In view of this repeatability, the results will be treated from here onwards as a single representative mean value of the full five tests.

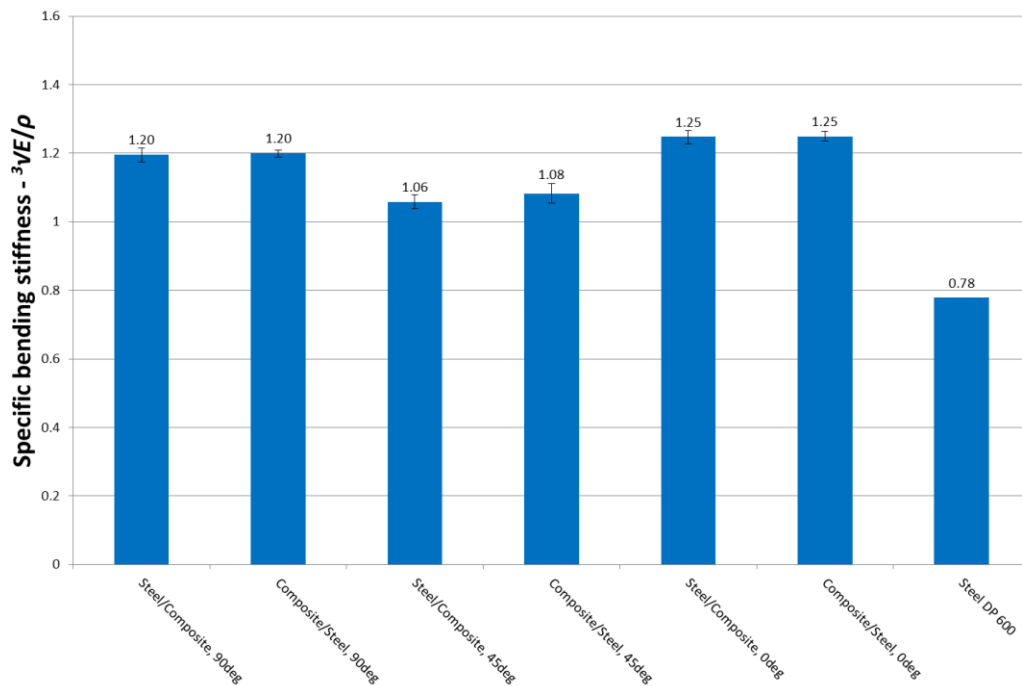


Figure 4-24: Specific bending stiffness for all 0.8 mm DP600 GFRP hybrids and steel

Figure 4-24 also highlights that despite the scenarios of steel-over-composite and composite-over-steel being tested separately, their performance in the elastic region is very similar for a given composite lay-up. To simplify matters in the context of the Ludke criterion analysis, samples are presented based only on their lay-up and all performance differences have been included in the standard deviation.

Figure 4-25 shows the load-extension graph for both the representative 0.8 mm hybrid samples presented previously, combined with the representative 0.5 mm hybrid samples. From these, the Ludke criterion is calculated, and Figure 4-26 shows the normalised performance (based on the Ludke criterion) of the hybrid GFRP materials to the performance of steel. It is worth noting that the  $[0,90]_s$  0.5 mm hybrid samples can be seen to outperform the  $[45,-45]_s$  0.8 mm hybrid samples.

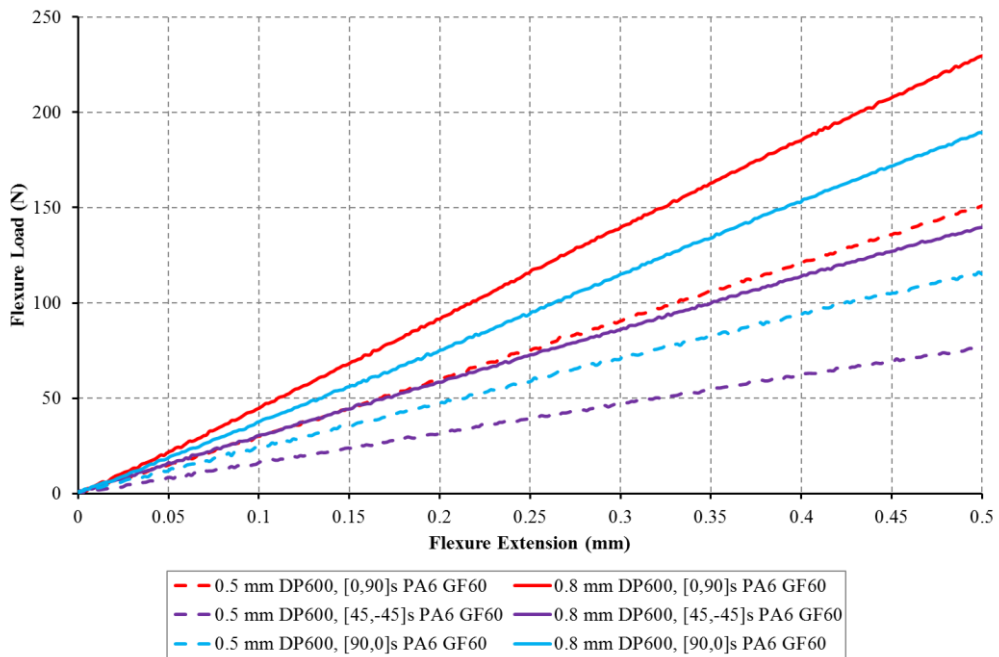


Figure 4-25: Graphical representation of all the hybrid samples

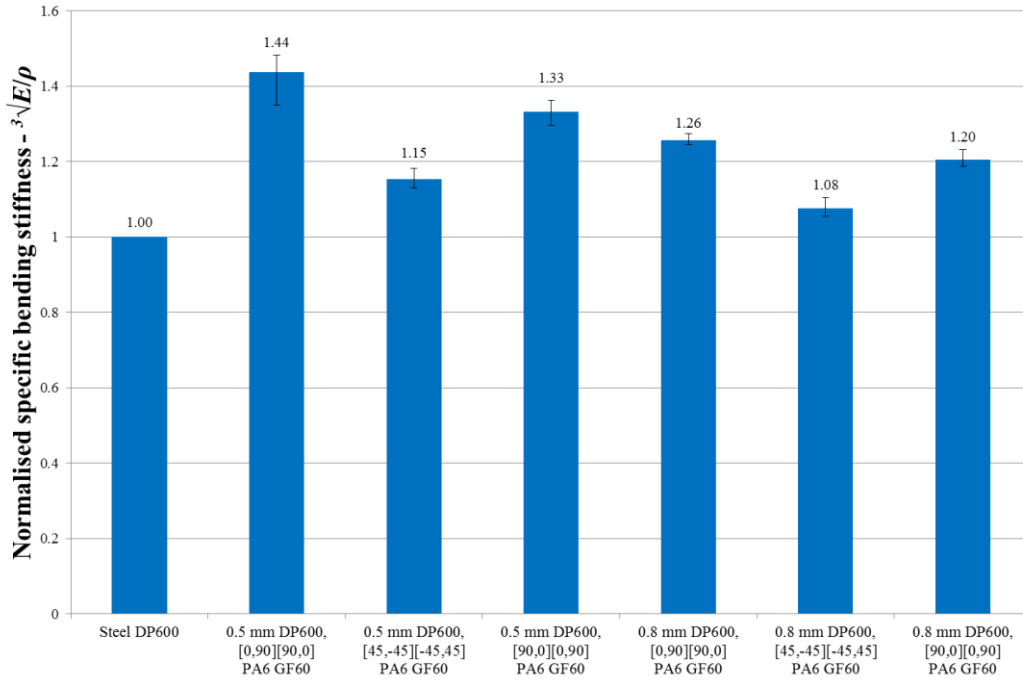


Figure 4-26: Ludke's criterion for the steel and GFRP samples, normalised to pure DP600 steel only

Based on the Ludke criterion, the potential weight save can be calculated using elastic analysis beam bending theory applied to the results.

$$E = \frac{\text{Force}}{\text{Deflection}} \frac{L^3}{48 I} \quad \text{Equation 4-1}$$

$$E = \frac{1}{4} k \frac{L^3}{bd^3} \quad \text{Equation 4-2}$$

where  $k$  is the slope of the elastic region of the force – deflection curve,  $L$  is the span,  $b$  is the breadth and  $d$  is the depth. This is based on an identical performance, ie,  $k$  is constant. These results are displayed in Table 4-6 below, and show the definite potential of lightweighting using FRP to reinforce steel.

To calculate the potential weight save, the same equations are used in reverse. The stiffness performance of the steel is set as a target for the hybrid samples and thickness decreased until the target is met. The weight of these samples is then calculated, and potential weight save estimated.

Table 4-6: Percentage increase in specific bending stiffness and percentage weight save for the equivalent performance in steel only

Material		% Increase in specific stiffness	% weight save for equivalent performance
Steel DP600		0	0
0.5 mm DP600	[0,90] <sub>s</sub>	44	30
	[45,-45] <sub>s</sub>	15	13
	[90,0] <sub>s</sub>	33	25
0.8 mm DP600	[0,90] <sub>s</sub>	26	20
	[45,-45] <sub>s</sub>	8	8
	[90,0] <sub>s</sub>	20	17

In addition to the results provided by the experimental tests, simulation data is available. At coupon level, it was most important to prove the concepts and assumptions behind the simulation and carry this knowledge forward to the component levels. Nevertheless, the simulation data is presented briefly as follows, and summarised in Table 4-7.

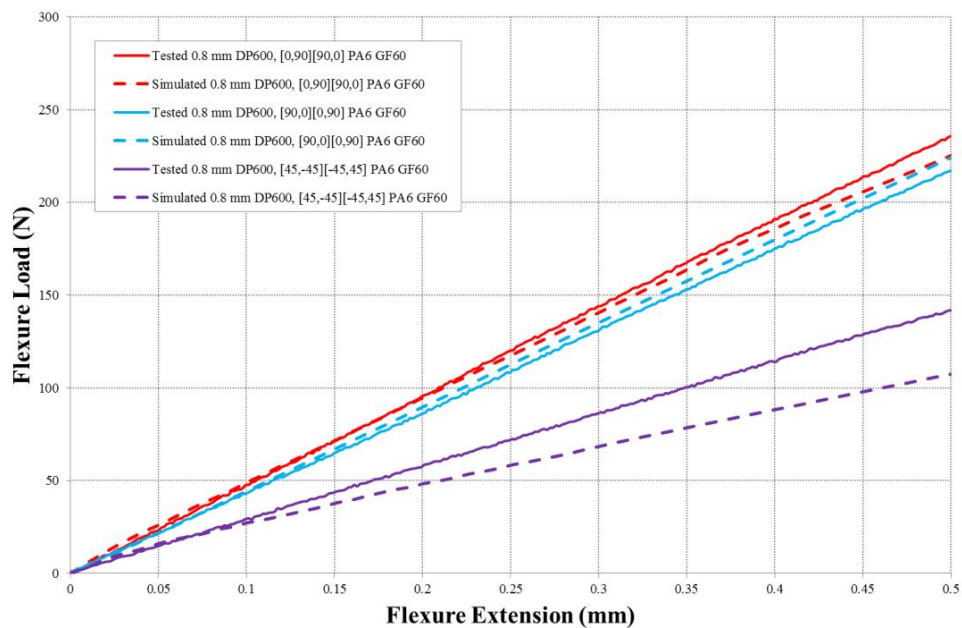


Figure 4-13 – Representation of correlation between the experimental and simulated for the hybrid 0.8 mm DP600 GFRP samples – reshown

Figure 4-13 shows the correlation between the tested and LS-DYNA simulated flexure for the case of the 0.8 mm DP600 with all three ply combinations PA6 GF60



in LS-DYNA. The slopes of the corresponding test-FE curves are well matched for the  $[0,90]_s$  and  $[90,0]_s$  composite layup situations. In the case of the  $[45,-45]_s$ , the small discrepancy seen are related to a shift of the specimen in the test environment. This could also be related to the small anisotropy in properties that arises at  $45^\circ$  to the rolling direction of the steel. The samples were consistently observed to rotate in alignment to the matrix direction, causing the stiffness to decrease.

Comparing the sample performance in terms of gradient of the load-extension curve  $k$ , means that a direct comparison can be achieved by simply analysing the graphs.

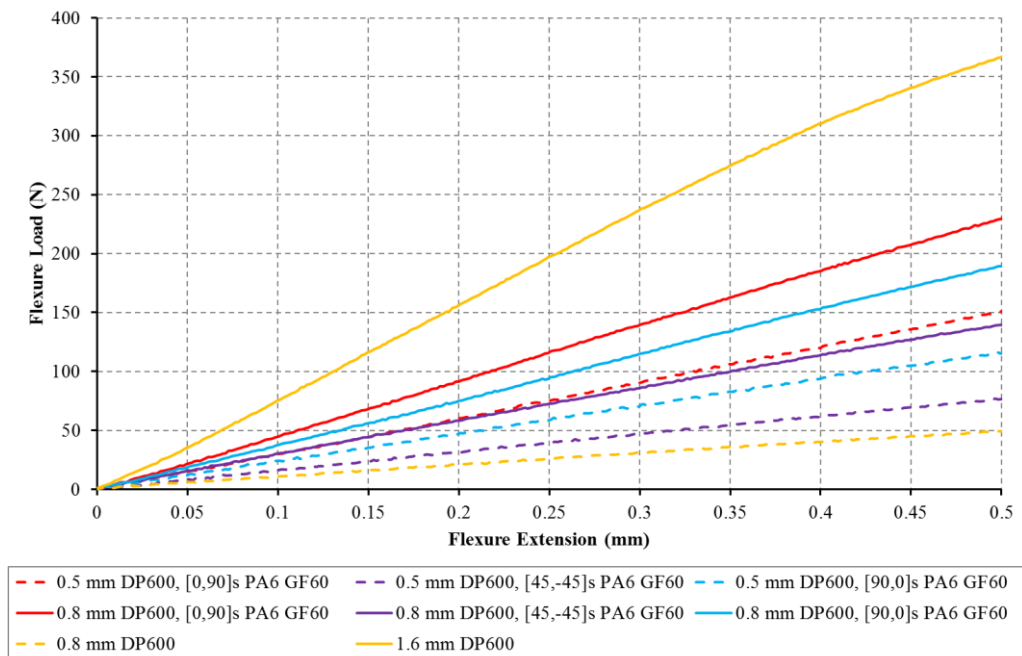


Figure 4-27: Load-extension graph showing the 0.5 and 0.8 mm hybrid samples and the benchmarked 0.8 and 1.6 mm pure steel sample

It can be seen from Figure 4-27 that the hybrids occasionally outperform each other (specifically here, the  $[0,90]_s$  0.5 mm hybrid outperforms the  $[45,-45]_s$  0.8 mm hybrid) due to the added performance of the composite material. The benchmarked 0.8 and 1.6 mm pure steel samples present the “envelope” within which the hybrid performances are contained.

The full results are presented in their “raw” form in Table 4-7. Table 4-8 presents the results obtained from simulations run on identical samples with a carbon fibre reinforcement. The carbon layers are 0.16 mm in thickness. Due to material cost constraints, the carbon samples performance was simulated only. The material properties were obtained from in-house testing on the PA6 CF60 pre-preg tape [90]. These were applied in Genesis so as to give an indication of the expected performance of a higher performance composite. The full GFRP and CFRP results from Table 4-7 and Table 4-8 are processed and presented in Table 4-9, Table 4-10, Table 4-12 and Table 4-13 as the performance of the hybrids relative to all samples. The dashed boxes represent the untested samples. These samples are all 60 mm in length, and 15 mm in width.

*Table 4-7: Summary of all the results obtained in testing and associated simulation*

Type of test	Material and Orientation		Weight (g)	Experimental k	Simulation k		
	Steel	GFRP			LS_DYNA	Genesis	
Benchmarking	-	[0,90] <sub>s</sub>	1.98	51.1	-	49.9	
	-	[45,-45] <sub>s</sub>		10.4	-	14.0	
	-	[90,0] <sub>s</sub>		12.5	-	18.5	
	0.8 mm	-	5.73	97.6	-	97.2	
	1.0 mm	-	7.11	185.2	-	194.2	
	1.1 mm	-	7.82	-	-	261.7	
	1.2 mm	-	8.55	-	-	337.6	
	1.6 mm	-	11.38	768.7	-	787.6	
GFRP Hybrid	0.5 mm DP600	[0,90] <sub>s</sub>	5.53	302.8	323.0	253.8	
		[45,-45] <sub>s</sub>		153.6	155.9	128.9	
		[90,0] <sub>s</sub>		208.0	323.0	225.4	
		[0,90] <sub>s</sub>		289.2	330.6	254.6	
		[45,-45] <sub>s</sub>		134.9	153.1	129.5	
		[90,0] <sub>s</sub>		232.0	330.6	226.2	
	0.8 mm DP600	[0,90] <sub>s</sub>	C/S	7.70	461.3	454.2	443.6
		[45,-45] <sub>s</sub>			286.3	210.1	261.4
		[90,0] <sub>s</sub>			410.0	450.8	404.8
		[0,90] <sub>s</sub>	S/C		465.3	450.8	438.8
		[45,-45] <sub>s</sub>			278.6	205.5	260.4
		[90,0] <sub>s</sub>			394.0	454.2	411.9

Table 4-8: Summary of simulated CFRP results

Type of test	Material and Orientation		Weight (g)	Experimental k	Simulation k	
	Steel	CFRP			LS_DYNA	Genesis
Benchmarking	-	[0,90] <sub>s</sub>	0.84	-	-	50.9
	-	[45,-45] <sub>s</sub>		-	-	4.4
	-	[90,0] <sub>s</sub>		-	-	8.6
CFRP Hybrid	0.5 mm DP600	[0,90] <sub>s</sub>	4.74	-	-	259.8
		[45,-45] <sub>s</sub>		-	-	78.5
		[90,0] <sub>s</sub>		-	-	220.5
	0.8 mm DP600	[0,90] <sub>s</sub>	7.07	-	-	524.8
		[45,-45] <sub>s</sub>		-	-	218.0
		[90,0] <sub>s</sub>		-	-	485.1

As the [0,90]<sub>s</sub> hybrid samples are seen to perform best in all tests, these are used throughout the analysis. This is reflected in Table 4-9 through to Table 4-13.

Table 4-9: Normalised performance of the GFRP 0.5 mm hybrid coupon samples relative to other samples

Type of test	Material and Orientation		Percentage difference %		
	Steel	GFRP	Weight (g)	Experimental k	Simulation k Genesis
Benchmarking	0.8 mm	-	-3.5	203.3	161.5
	1.0 mm	-	-22.2	59.8	30.9
	1.1 mm	-	-29.3	-	-2.9
	1.2 mm	-	-35.3	-	-24.7
	1.6 mm	-	-51.4	-61.5	-67.7
GFRP Hybrid	0.5 mm	[0,90] <sub>s</sub>	0.0	0.0	0.0
	0.8 mm	[0,90] <sub>s</sub>	-28.2	-36.1	-42.4
	Steel	CFRP			
CFRP Hybrid	0.5 mm	[0,90] <sub>s</sub>	16.7	-	-2.2
Hybrid	0.8 mm	[0,90] <sub>s</sub>	-21.8	-	-51.6

Table 4-9 shows the normalised performance of the GFRP 0.5 mm hybrid coupon samples relative to other samples using the values of weight and stiffness k presented in Table 4-7. These were calculated individually as

$$\% \text{ difference} = \frac{0.5 \text{ mm hybrid coupon performance} - \text{Compared sample}}{\text{Compared sample}}$$

Equation 4-3

So that the performance of the 0.5 mm hybrid sample is expressed relative to the benchmarked sample performances individually.

The samples highlighted in green show an improved performance, either in weight or in stiffness k values. The ones bordered in red show a marked increase in performance, for the relative weight save. The results bordered in blue, comparing the performance of the 0.5 mm hybrid samples to the 1.1 mm pure steel samples are particularly interesting as they show a near identical stiffness performance for a 29.3 % weight save, i.e., a 0.5 mm hybrid sample is able to match the elastic stiffness of a 1.1 mm pure steel sample but at a weight saving of nearly 30 %.

*Table 4-10: Normalised performance of the GFRP 0.8 mm hybrid coupon samples relative to other samples*

Type of test	Material and Orientation		Percentage difference %		
			Weight (g)	Experimental k	Simulation k
					Genesis
Steel	GFRP				
Benchmarking	0.8 mm	-	34.4	374.7	353.9
	1.0 mm	-	8.3	150.2	127.2
	1.1 mm	-	-1.5	-	68.6
	1.2 mm	-	-9.9	-	30.7
	1.6 mm	-	-32.3	-39.7	-44.0
GFRP Hybrid	0.5 mm	[0,90] <sub>s</sub>	39.2	56.5	73.6
	0.8 mm	[0,90] <sub>s</sub>	0.0	0.0	0.0
	Steel	CFRP			
CFRP Hybrid	0.5 mm	[0,90] <sub>s</sub>	62.4	-	69.8
Hybrid	0.8 mm	[0,90] <sub>s</sub>	8.9	-	-15.9

Table 4-10 shows the normalised performance of the GFRP 0.8 mm hybrid coupon samples relative to other samples using the values of weight and stiffness k presented in Table 4-7. These were calculated as per Table 4-9. The highlighted results are those indicating improved performance, either in weight or in stiffness. Again, results bordered in red indicate a weight save and a stiffness performance increase; here, over the 1.2 mm pure steel. The hybrid is shown to be nearly 10 % lighter and performing 30.7 % better. The results bordered in blue, indicate a like for

like weight performance between the 1.1 mm pure steel sample and the 0.8 mm hybrid. In this situation, the hybrid performs 68.6 % better. I.e., the 0.8 mm hybrid sample provides nearly a 70 % increase in stiffness performance for a matched weight.

*Table 4-11: Further simulated comparison of coupon samples*

Type of test	Material and Orientation		Percentage difference %		
			Weight (g)	Experimental k	Simulation k Genesis
	Steel	GFRP			
Benchmarking	1.2 mm	-	-9.9	-	30.7
	1.3 mm	-	-16.3	-	4.1
	1.6 mm	-	-32.3	-39.7	-44.0
Hybrid	0.8 mm	[0,90] <sub>s</sub>	0.0	0.0	0.0

It was found through further simulation, that the closest pure steel sample to the 0.8 mm hybrid would be a 1.3 mm sample. These would perform comparatively as indicated Table 4-11, where the 0.8 mm hybrid sample would present a weight save of 16.3 % for a near identical performance (hybrid performs 4 % better).

In a comparison of the GFRP hybrid coupons, it is worth noting that for an equivalent stiffness performance over steel, the 0.5 mm hybrid samples present a weight saving potential of approximately 30 %, where the 0.8 mm hybrid samples present a weight saving potential of approximately 17 %. This highlights the partial and hybrid effect of the composite on the steel's performance. The composite has impacted on the performance of the thinner steel to a larger extent.

Table 4-12: Normalised performance of the simulated CFRP 0.5 mm hybrid coupon samples relative to other samples

Type of test	Material and Orientation			Percentage difference %		
				Weight (g)	Experimental k	Simulation k
	Steel	GFRP				Genesis
Benchmarking	0.8 mm	-		-17.3	-	167.3
	1.0 mm	-		-33.3	-	33.8
	1.1 mm	-		-39.4	-	-0.7
	1.2 mm	-		-44.6	-	-23.0
	1.6 mm	-		-58.3	-	-67.0
GFRP	0.5 mm	[0,90] <sub>s</sub>	C/S	-14.3	-	2.2
Hybrid	0.8 mm	[0,90] <sub>s</sub>	C/S	-38.4	-	-41.1
	Steel	CFRP				
CFRP	0.5 mm	[0,90] <sub>s</sub>		0.0	-	0.0
Hybrid	0.8 mm	[0,90] <sub>s</sub>		-33.0	-	-50.5

Table 4-12 shows the normalised performance of the CFRP 0.5 mm hybrid coupon samples relative to other samples using the values of weight and stiffness k presented in Table 4-7 and Table 4-8. These were calculated as per Table 4-9. The highlighted results are those indicating improved performance, either in weight or in stiffness. Here, results bordered in red indicate a weight save and a stiffness performance increase; here, over the 0.8 and 1.0 mm pure steel. The hybrid is shown to be 17.3 and 33.3 % lighter and performing 167.3 and 33.8 % better respectively. The results bordered in blue, indicate a like for like stiffness performance between the 1.1 mm pure steel sample and the 0.5 mm CFRP hybrid. In this situation, the hybrid weighs nearly 40% less. The CFRP hybrid also presents a similar performance to the GFRP 0.5 mm hybrid, weighing 14.3 % less.

Table 4-13: Normalised performance of the simulated CFRP 0.8 mm hybrid coupon samples relative to other samples

Type of test	Material and Orientation		Percentage difference %		
			Weight (g)	Experimental k	Simulation k
	Steel	GFRP			Genesis
Benchmarking	0.8 mm	-	23.4	-	439.9
	1.0 mm	-	-0.6	-	170.2
	1.1 mm	-	-9.6	-	100.5
	1.2 mm	-	-17.3	-	55.5
	1.6 mm	-	-37.9	-	-33.4
Hybrid	0.5 mm	[0,90] <sub>s</sub>	27.8	-	106.5
	0.8 mm	[0,90] <sub>s</sub>	-8.2	-	18.9
	Steel	CFRP			
Hybrid	0.5 mm	[0,90] <sub>s</sub>	49.2	-	102.0
	0.8 mm	[0,90] <sub>s</sub>	0.0	-	0.0

Table 4-13 shows the normalised performance of the CFRP 0.8 mm hybrid coupon samples relative to other samples using the values of weight and stiffness k presented in Table 4-7 and Table 4-8. These were calculated as per Table 4-9. The highlighted results are those indicating improved performance, either in weight or in stiffness. Once again, results bordered in red indicate a weight save and a stiffness performance increase; here, over the 1.1 and 1.2 mm pure steel samples. The hybrid is shown to be nearly 10 and 20 % lighter and performing approximately 100 and 56 % better respectively. The results bordered in blue, indicate a like for like weight between the 1.0 mm pure steel sample and the 0.8 mm CFRP hybrid. In this situation, the hybrid performs 170 % better. The CFRP hybrid also presents a stiffness performance increase of 19 % on the GFRP 0.8 mm hybrid, weighing 8 % less.

Figure 4-28, Figure 4-29 and Figure 4-30 show a graphical representation of the tables discussed above. These figures show the optimal zone in which the hybrid samples perform better than the pure steel samples (positive stiffness k performance improvement % and positive weight improvement %). These graphs also show clearly the situations in which the hybrid samples vastly outperform the performance

of the pure steel samples but present no weight save, and situations in which the hybrid samples do not present a performance benefit over the pure steel samples.

Figure 4-28 shows the performance and weight improvement for the simulated GFRP samples. The 0.5 mm hybrid coupon presents a similar performance to a 1.1 mm pure steel counterpart, at approximately 30 % weight save and the 0.8 mm hybrid sample presents a similar performance to a 1.3 mm pure steel counterpart at an approximate 17 % weight save.



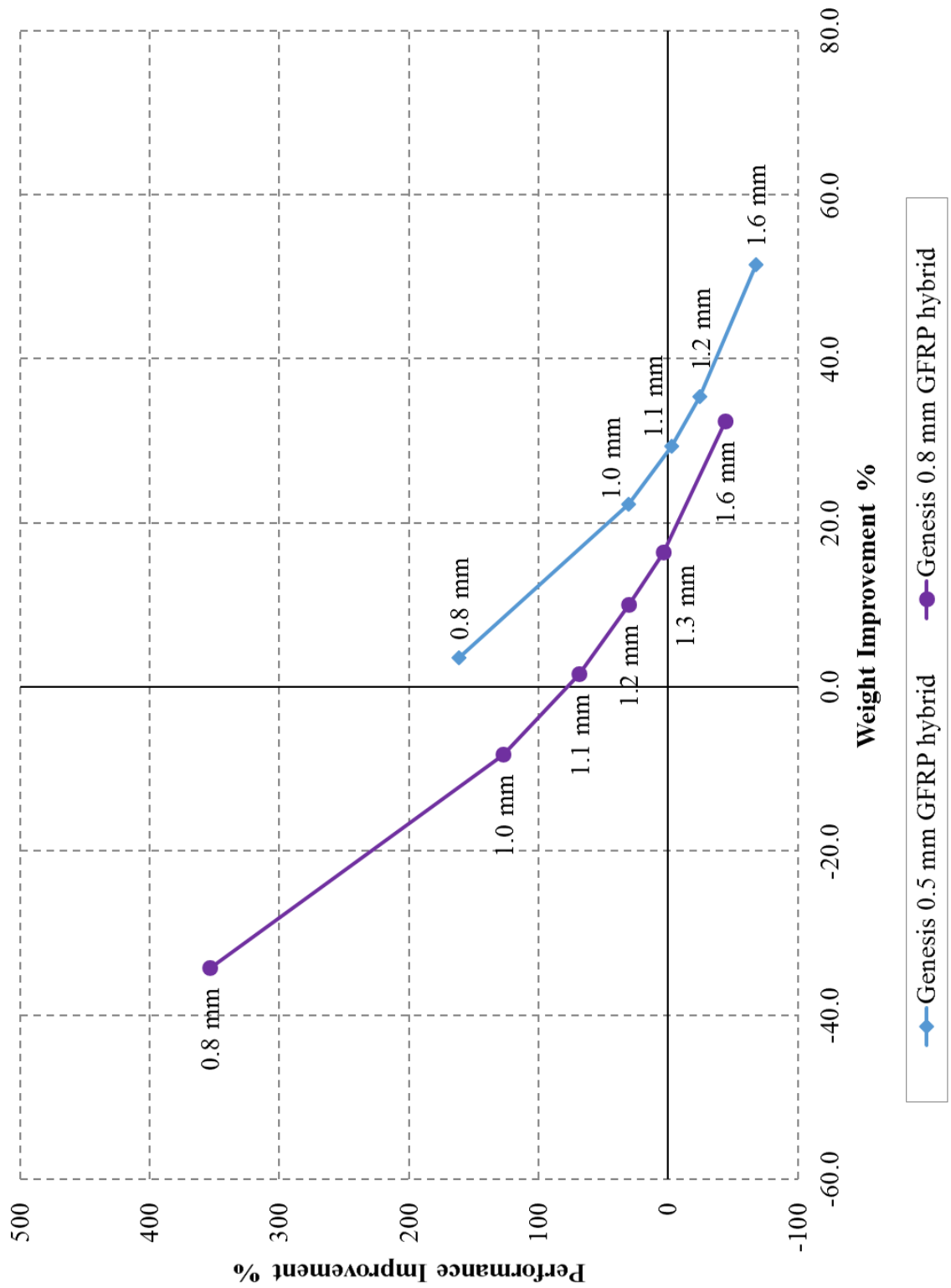


Figure 4-28: The performance and weight “improvements” of the GFRP hybrid samples compared to the pure steel ones

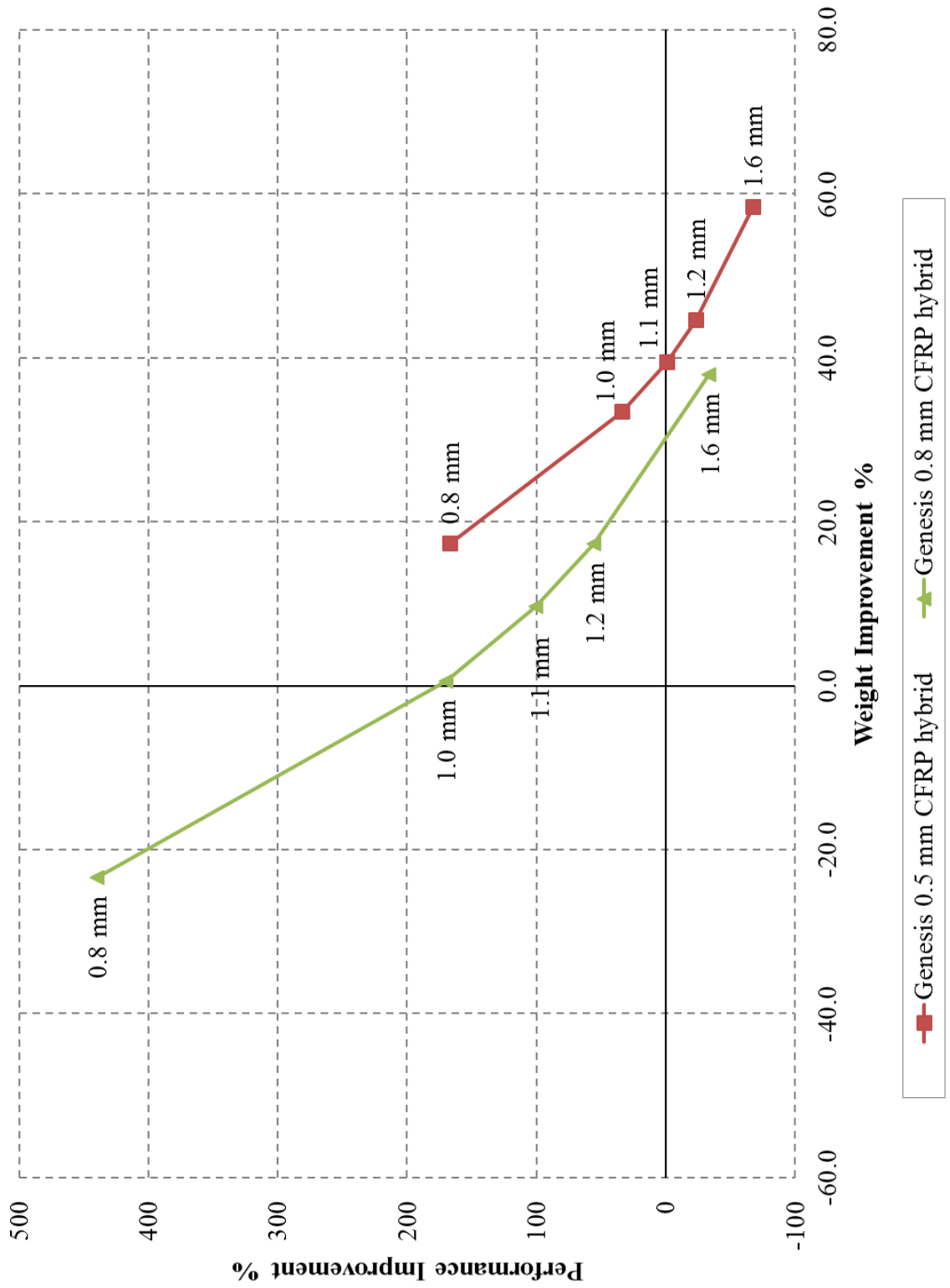


Figure 4-29: The performance and weight “improvements” of the CFRP hybrid samples compared to the pure steel ones

Figure 4-29 shows the performance and weight improvement for the simulated CFRP samples. The 0.5 mm hybrid coupon presents a similar performance to a 1.1 mm pure steel counterpart, at approximately 40 % weight save and the 0.8 mm hybrid sample presents an estimated similar performance to a 1.4 mm pure steel counterpart at an approximate 30 % weight save.

Figure 4-30 is the combination of both Figure 4-28 and Figure 4-29. From left to right, the 0.5 mm CFRP and GFRP and the 0.8 mm CFRP (red, blue and green) curves are from the comparative performance to the 1.6, 1.2, 1.1, 1.0 and 0.8 mm pure steel samples. The 0.8 mm GFRP curve (purple) is from the comparative performance to the 1.6, 1.3, 1.2, 1.1, 1.0 and 0.8 mm pure steel samples.

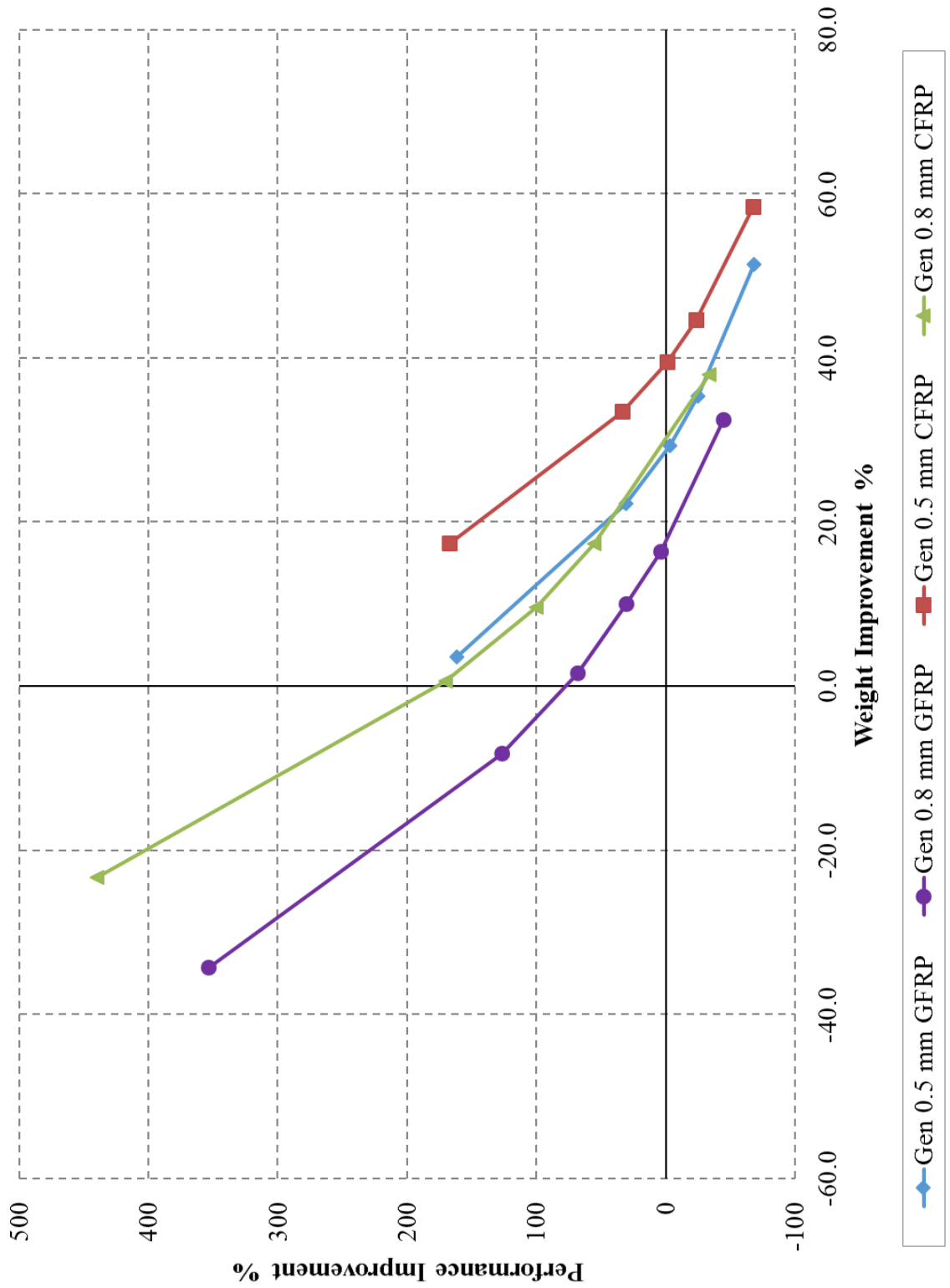


Figure 4-30: Comparative performance improvements between the GFRP and CFRP hybrids – combination of Figure 4-28 and Figure 4-29

This highlights the comparative performance of the Carbon reinforcements compared to the Glass reinforcements, showing that the 0.5 mm GFRP hybrid performs similarly to the 0.8 mm CFRP hybrid.

#### 4.4 Conclusions

The variations in hybrid results between the different lay-ups confirm that the orientation of the outer layer of composite fibres affects the performance of the specimens in bending. Considering the samples with a composite lay-up of  $[0, 90]_s$ , in which the outer layer of fibres runs in the direction of loading, the fibres are either in tension or in compression along their length. This is depending on whether the hybrid is being tested with the composite face up (compression) or the composite face down (tension). The performance of the  $[45, -45]_s$  shows the highest strain to failure, and lowest UTS. The difference in performance based on the fibre directionality indicates opportunity available due to fibre orientation effect, where the composite can be tailored to the situation due to its anisotropic nature. Tailored composite patches are an option when dealing with a structure in need of lightweighting. Indeed, the simulation can be taken further into an optimization context, and expanded to composite materials that have a higher Young's modulus, as these are likely to present a higher weight saving potential overall.

Set up as an iteration loop the testing and simulation results were used to counter-validate each other. Using two different thicknesses of steel and six different fibre orientations and layups, and repeatable results in the experimental section, it was possible to create a model with a high degree of confidence.

There is a good agreement between the results from the experimental and simulation program, providing confidence in the material model and assumptions made and allowing for the development and analysis of non-experimentally tested situations. The simulation results are consistent in LS-DYNA to within 10 % of the

experimental results, in every case an over-prediction (the [45,-45]<sub>s</sub> samples present the highest discrepancy in results). The analytical model in Gensis supports and correlates with these results, and they are within an acceptable 11 % correlation bracket of each other (again, the [45,-45]<sub>s</sub> present a higher discrepancy). This is attributed to the experimental uncertainty (machine lag) and approximations made in the extraction of the test data from the testing machine.

This high degree of correlation between the simulation and the testing reinforces the confidence in the validation and opens the possibility of using this model for a purpose filling application.

The greatest increase in specific bending stiffness in terms of Ludke criterion is 44 % (for the [0,90]<sub>s</sub> 0.5 mm hybrid samples), translating to a maximum weight saving potential of 30 %. This is a large enough potential for the concept to be investigated on a larger scale, as this weight save is expected to be lessened/diluted when applied in a situation where reinforced sections cohabit with unreinforced sections.

These results confirm that there is a potential for hybrid reinforcements in the lightweighting of steel. Indeed, as shown in the state of the art review Chapter 2, very little work has been done on the pre-design of structures using FRP with lightweighting in mind. The existing research concentrates mainly on a retrospective tensile reinforcement (bonding and strength effects) whereas this research investigates stiffness and location specific patching reinforcement.

As such, the coupon based results and analysis lead to the following conclusions:

1. There is potential for using FRP to reinforce steel in an intelligent deployment of composite material implying the structure can be optimised and lightweighted
2. Calculated using Ludke's criterion, the stiffness performance of the

hybrid can be improved by up to 44 % when reinforcing with a balanced 4 layer GF60 PA6

3. Additionally, for an identical stiffness performance, there is a potential 30 % weight save
4. The stiffness performance  $k$ , shows that for a matched stiffness performance, GFRP hybrid coupons can present a weight save of up to 30 % in tested samples
5. The orientation of the outer layer of fibres affects the stiffness greatly
6. The simulation and material model assumptions are acceptable for the modelling of the elastic region of hybrid steel composite coupons

## **CHAPTERS 5 AND 6; A BRIEF INTRODUCTION**

In order to assess the applicability of choices from the coupon program phase of the study, a demonstrator part was needed that could be subjected to a realistic performance evaluation. These results are compared against the performance of the benchmark materials (varying thicknesses of automotive-grade steel). These chapters discuss the application of the knowledge gained from the coupon testing presented in Chapter 4 on a larger and life-like realistic geometry. Using an idealised automotive top hat component from an OEM, the principal aim was to obtain an equally performing lightweighted part using a local intelligent deployment of composite patches in combination with a downgauging of the steel. The pillar design selected requires a combination of bending stiffness and strength. The focus here is on the bending performance. Although the structure chosen is a simplified design, similar sections are seen in other areas of vehicles including A and B pillars, sill structures and front longitudinal sections.

Using the material model that was validated in the previous chapter, samples are simulated in two parts: one which was mimicked experimentally and one where the application of composite reinforcement patches is evaluated in the loading scenario. The first set of simulations is validated experimentally to ensure a high degree of confidence in the model. The manufacturing of the samples is presented and the results and lightweighting opportunities discussed.



## 5 COMPONENT PROGRAM – EXPERIMENTAL APPROACH

This chapter presents the experimental approach to the component testing.

### 5.1 Geometry and dimensions

A scaled ( $\times 0.6$ ) top hat section with a closure plate (backplate) joined in a secondary operation, representative of the A, B, C/D pillars of a car was selected for the component level trials. This geometry was also used in studies found in the literature, such as those discussed earlier by Lanxess and Universitat Paderborn [23, 26, 27]. The final geometry selected is a top hat section and was provided by an automotive OEM, as shown in Figure 5-1. The overall length was modified to fit fabrication and test equipment and fixtures available. The final beam section design was approximately 43 mm tall, 132 mm wide, and 450 mm long.

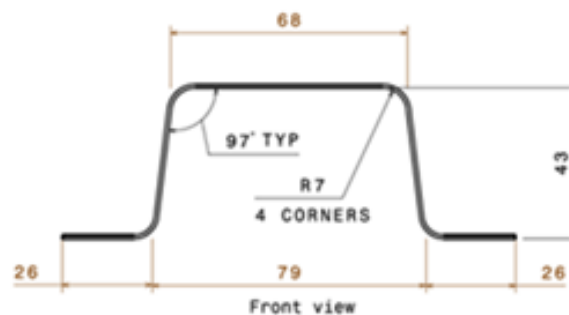


Figure 5-1: Selected top-hat geometry from an automotive OEM without backplate

The top hat geometry has two flanges, 26 mm in width each. The “top” section of the reinforcement is 68 mm in width, and the sides are at an angle enabling for the material to be cold pressed in the tool and removed post shaping. The corners have a radius of 7 mm, and the height of the top hat section from flanges to top is 43 mm. This cross section is constant throughout the length of the samples.

Flat sheets of DP 600 steel of 450 mm by 250 mm were delivered by Tata Steel. They were pressed into shape using the tools and methods described in Chapter 3.

Each top-hat section was then adhesively bonded to the backplate along the flanges after appropriate surface preparation, also discussed in Chapter 3. Finally, some of the samples were reinforced along the top section using a balanced  $[0,90]_s$  PA6 GF60 laminate as in Figure 5-2 below. The location of the reinforcement is discussed later in this chapter.

This geometry was recreated in Solidworks and HyperMesh to generate the model used throughout the simulations presented in Chapter 6, Section 6.1 “The basic model”. As can be seen from Figure 5-2, the flanges present some localised rust. This was due to the flanges being waterjet cut post shaping. The rust did not affect the bonding as it was removed in surface preparation.

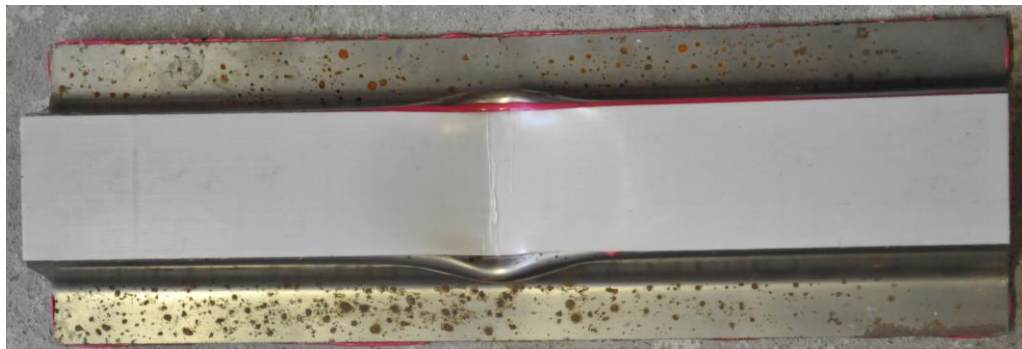


*Figure 5-2: Top hat showing local PA6 GF60 reinforcement on the top of the top-hat – sample is 450 mm in length, 132 mm in width, height ~ 43 mm*

## **5.2 Testing**

The simulation was used to predict the performance of the top hat specimens under varying reinforcement conditions. Some of these conditions were selected and the simulated model was validated using mechanical testing. Benchmarking tests were executed on pure steel samples. Due to practicality of manufacture, only hybrid samples with a top reinforcement were fabricated.

### 5.2.1 Sample production

Individually, the steel, composite and adhesive were prepared in a similar manner to that used for the coupon manufacturing.

The steel was provided by Tata Steel as industrial sponsor and cut to approximate sized sheets. The sheets were then cold pressed to shape in an Interlaken press at WMG following brief trials on time and pressure as presented in Chapter 3. These were run as there was an awareness that the material springback would be different in the varying thicknesses.

The tool set used to cold press the samples into shape was originally designed for sheets 1.6 mm thick. Due to the different thicknesses of the samples prepared within the scope of this project, a spacer was used to ensure the overall thickness was consistent with the designed thickness of the tool. The samples were all created to have matching inner geometries, growing outward from the inner-plane. This was reflected in the simulation.

As stated previously, once formed, the top hats were cut down to size along the flanges using a waterjet cutting technique. This also removed the oil-coatings and lead to a small amount of rust formation in time. In preparation for the joining, the samples were manually abraded, removing the localised surface rust. The thickness of the samples was not affected by this process.

The steel was abraded using a manual rotational sander, with a grit of 180P, and the sanded areas were measured pre and post-preparation to ensure there was no loss of thickness. Following abrasion, the steel was cleaned thoroughly using acetone and iso-propyl alcohol (IPA).

The Sika 490C adhesive was applied to the flanges and spread using a spatula. The adhesive contained glass beads (0.3 mm diameter) that ensured a constant bond thickness. The closure plates, cut to size, abraded and cleaned, were applied onto the

top-hat sections and secured into position using G-clamps. The overall beam product was then heated at 80 °C for 30 minutes in order to cure the adhesive.

Samples requiring reinforcement underwent a similar process. The finished beam was prepared (abraded and cleaned), as well as strips of [0,90]<sub>s</sub> PA6 GF60 cut to size (lay-up, consolidated, peel-ply surface preparation). Adhesive was applied on the top section of the hat, then the composite was applied and secured into place using clamps. The overall product was heated at 80 °C for 30 minutes in order to cure the adhesive. This curing time and temperature is known to not affect the composite (see Chapter 3). Figure 5-2 shows a finished sample with composite reinforcement.

### **5.2.2 Instrumentation set up**

The experiments were conducted using a similar set-up to that used for the coupon testing, described in Chapter 4. The fixture was a specifically made fixture for three-point bending of component sections such as top-hats. The span used for all samples was 350 mm. The rollers were 50 mm in diameter. Figure 5-3 shows the fixture set up with a sample in place. The quasi-static tests were run at a rate of 1 mm/min. The samples were pre-loaded to approximately 20 N, and the displacements used at baseline for result comparisons. The sample in Figure 5-3 is 450 mm in length, the top is reinforced with composite, and the presence of adhesive can be noted as the pink “line” along the length of the edge top face of the sample and along the flange. Figure 5-4 shows a schematic drawing of the three point bend experimental set-up with dimensions for the sample length, height, span and roller dimensions.

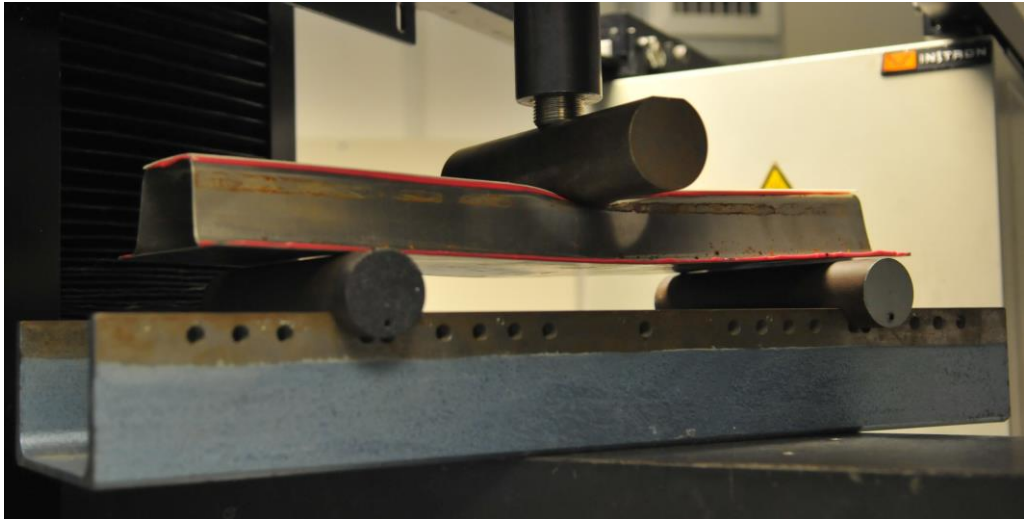


Figure 5-3: Three-point bend fixture set-up for the top-up static bending – sample length 450 mm, width 132 mm and height ~43 mm

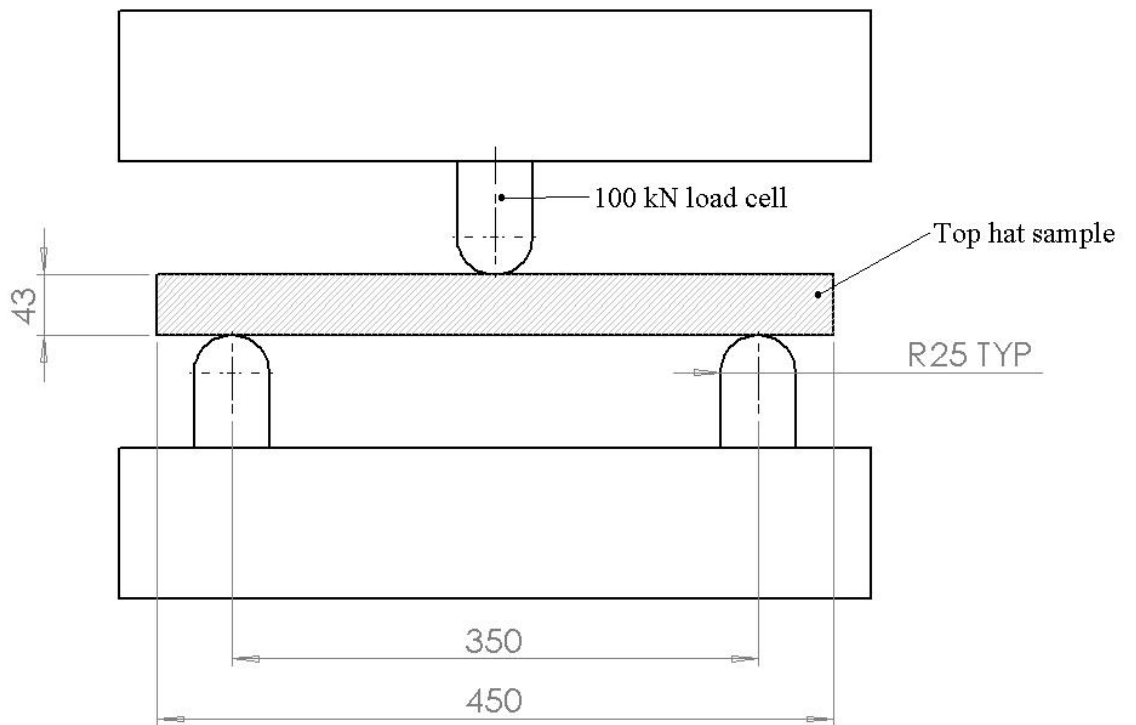


Figure 5-4: Schematic drawing showing the dimensions of the rollers and test set-

up

### 5.2.3 Samples

The data was benchmarked experimentally using 0.5, 0.8, 1.0 and 1.6 mm pure steel top hats. Guided by a simultaneous simulation (FE) program, explained in Chapter 6, the samples tested experimentally are presented in Table 5-1. The dashed lines represent samples where that material is not present. All samples were 450 mm in length, 132 mm in width and approximately 45 mm in height.

*Table 5-1: Summary of samples tested experimentally and their weights*

Type of test	Materials and Orientation		Weight (g)
	DP600	PA6 GF60	
Benchmarking (450 mm in length, 130 mm in width)	0.5 mm	-	651.3
	0.8 mm	-	983.7
	1.0 mm	-	1243.7
	1.6 mm	-	1963.3
Hybrid	0.5 mm	[0,90] <sub>s</sub>	689.7
	0.8 mm	[0,90] <sub>s</sub>	1060.7

The samples were tested so that the geometry was top-hat side up, and top-hat side down. The set-ups are shown in Figure 5-3 and Figure 5-5, top-hat side up scenario and top-hat side down scenario respectively. Figure 5-6 shows the samples post-testing where a) shows the top-hat side up scenario and b) shows the top-hat side down scenario. Samples are 450 mm in length.

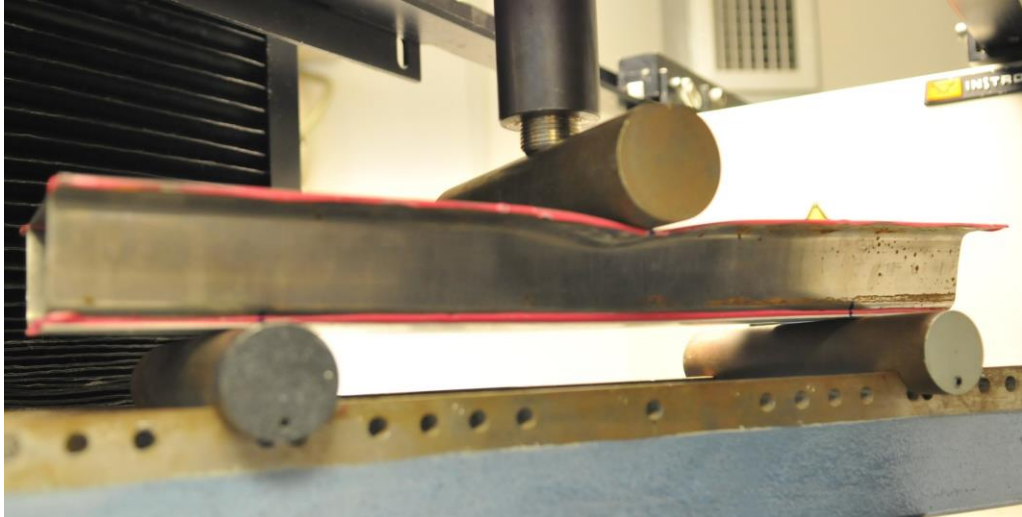
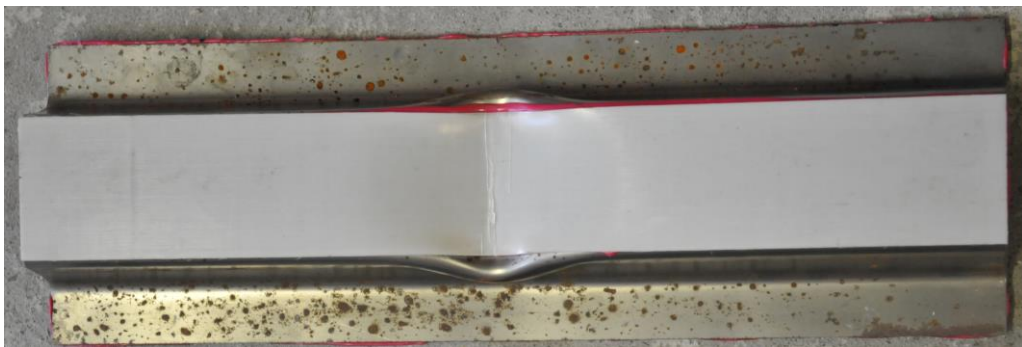


Figure 5-5: Sample with composite reinforcement in test rig; scenario with top-hat side down



a) Tested sample with composite reinforcement, top-hat side up scenario



b) Tested sample with composite reinforcement, top-hat side down scenario

Figure 5-6: Top-hat samples as tested, with composite reinforcement; a) scenario with top-hat side up; b) scenario with top-hat side down

From here on, the top-hat side up scenario will be referred to as “topside up” and the top-hat side down scenario will be referred to as “topside down”.

### 5.3 Results

The results presented as follows have been split into two parts. Initially, the samples are examined through photographic evidence, post testing, in both the topside up and down scenarios. In a second section, the load-displacement curves are presented and the values of effective bending stiffness calculated.

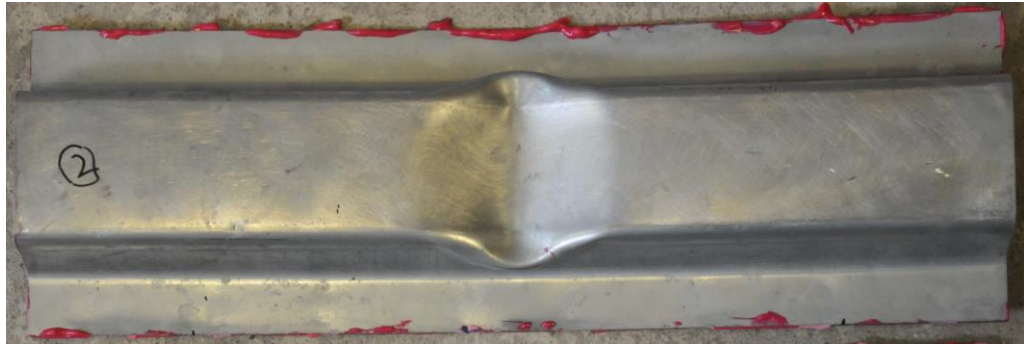
#### 5.3.1 Topside up

The samples considered in this section are the topside up samples. The images presented below are those of the 0.5 and 0.8 mm DP600 non reinforced (referred to as “pure steel”) and the 0.5 and 0.8 mm DP600 [0,90]<sub>s</sub> PA6 GF60 reinforced samples (referred to as “hybrid”). These were chosen as a direct comparison of sample deformations can be made. The 1.0 and 1.6 mm pure steel samples are not presented photographically as they do not add any additional information to that provided by the 0.5 and 0.8 mm pure steel samples.

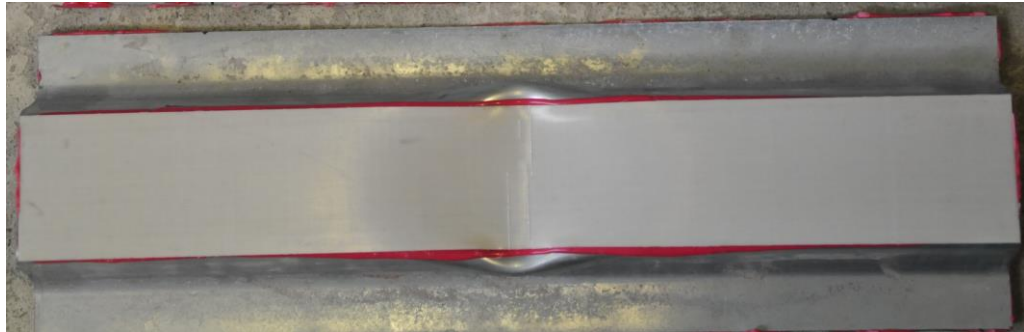
Figure 5-7 shows the samples in a top view. The samples are 450 mm in overall length. The images show the impactor location, and associated deflections. a) and b) show the 0.5 mm samples, whilst c) and d) show the 0.8 mm samples.

From these images, the impactor site appears to be subjected to plastic deformation and a “widening” effect on the samples, due to the local buckling of the side walls. Literature indicates that narrow beams in bending tend to be subjected to a “plastic hinging” effect [70, 106, 107]. Additionally, this view indicates that the deflections in the samples seem unaffected by the presence of the composite reinforcement, there is no distinctive or drastic change in deformation mechanism.

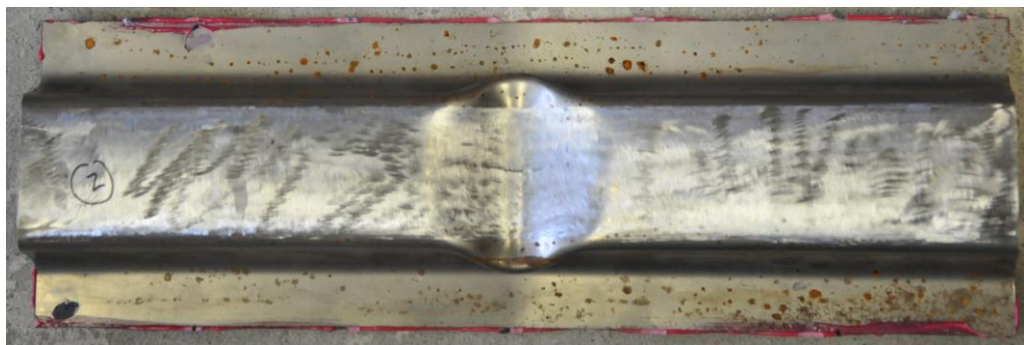




a) 0.5 mm pure steel sample



b) 0.5 mm hybrid sample



c) 0.8 mm pure steel sample



d) 0.8 mm hybrid sample

*Figure 5-7: 0.5 mm DP600, pure steel (a), hybrid (b); 0.8 mm DP600, pure steel (c), hybrid (d) – samples are 450 mm long*

Figure 5-8 shows the ISO view of the same samples. Here, some differences are notable. Comparing the pure steel and hybrid samples at the impactor site shows that

the presence of the composite material reduces the severity of the plastic deformation. Additionally, the hybrid samples show a plastic hinge deformation that is “flatter” towards the base. The “hinge” is less pronounced and sharp, and extends over a longer area across the length of the samples. The impactor site is approximately 75 to 80 mm in length in the case of the pure steel samples, and approximately 100 mm in the case of the hybrid samples. The length varied between samples, however, in all cases the hybrid site was larger than the equivalent pure steel site. This is visible in both the 0.5 and 0.8 mm samples. Figure 5-9 shows the side view of the affected area for the 0.8 mm pure and hybrid samples. This confirms the previous statements.

It is postulated that the composite serves to spread the loading across the top layer of the sample, therefore reducing the local plastic buckling effect in the side-walls.

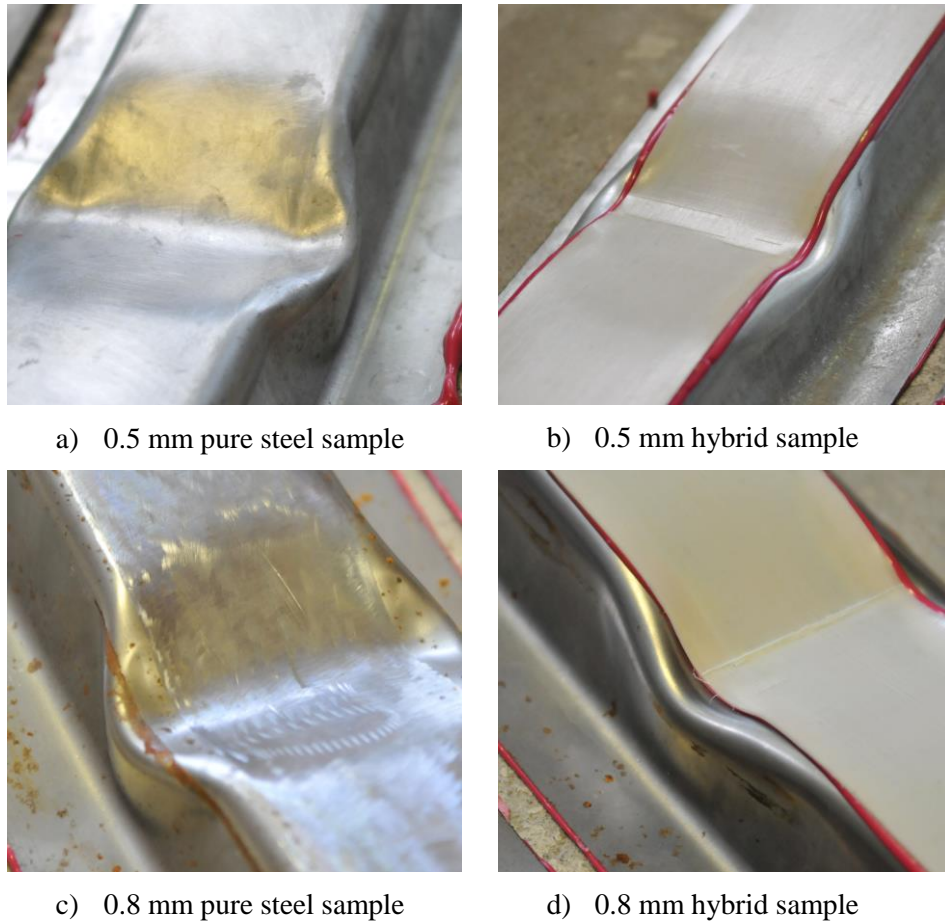


*Figure 5-8: ISO view of the deflection region of 0.5 mm DP600 pure (a) and hybrid (b); and 0.8 mm DP600 pure (c) and hybrid (d)*

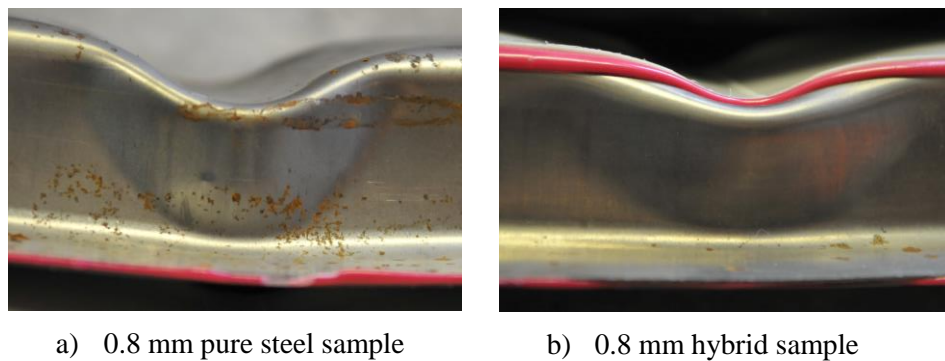


*Figure 5-9: Comparison of plastic hinge area in a) 0.8 mm DP600 pure steel sample and b) 0.8 mm DP600 hybrid sample*

Following on from the analysis of the images of the samples, the data was collected and is summarised graphically in Figure 5-10. The samples are referenced as: 0.5\_1, 0.5\_2, 0.5\_3 for the three repeats of the 0.5 mm pure steel samples; 0.8\_1,

0.8\_2, 0.8\_3 for the three repeats of the 0.8 mm pure steel samples; 1.0\_1, 1.0\_2 for the two repeats of the 1.0 mm pure steel sample; 1.6\_1 for the single 16 mm sample tested. Samples 14\_1 and 14\_4 stem are included for completeness and they were from testing related to the LCVTP project [87, 88]. These samples are 1.6 mm DP600 top hats of matching cold formed geometry. The backplate is attached using a combination of adhesive and self-piercing rivets. The samples were tested in comparable scenarios. These samples are discussed in Chapter 6. H0.5\_1, H0.5\_2, H0.5\_3 represent the tested 0.5 mm hybrid samples, and H0.8\_1, H0.8\_2, H0.8\_3 represent the 0.8 mm hybrid samples.

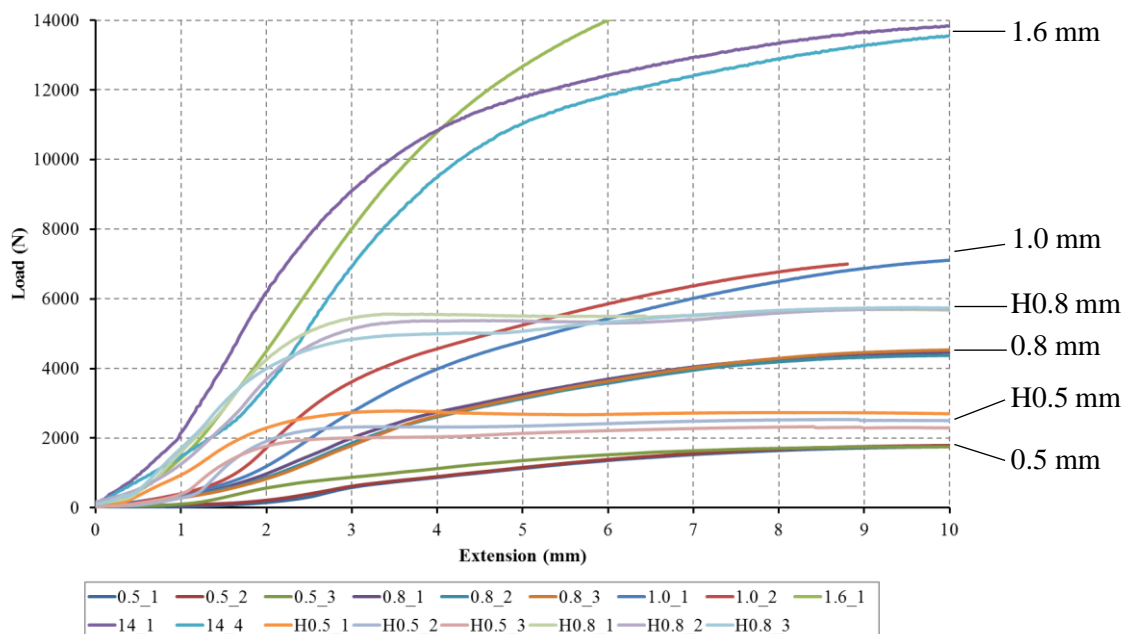


Figure 5-10: Summary of the load-extension curves for all samples tested in the topside up scenario

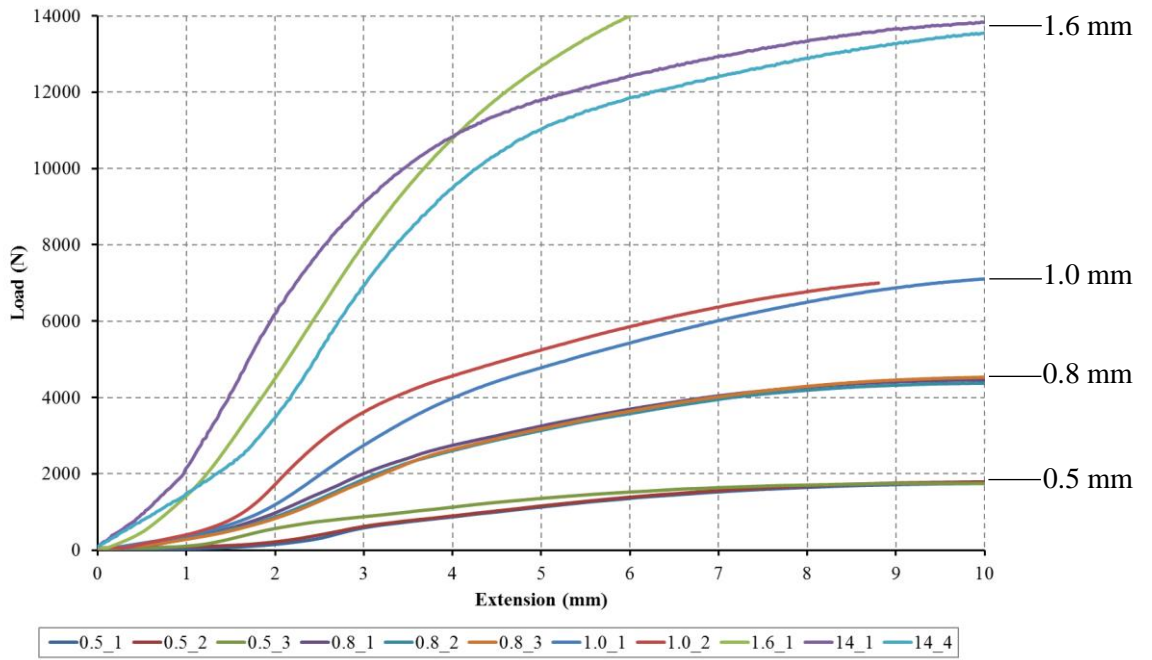


Figure 5-11: Load-extension curves for pure steel samples only

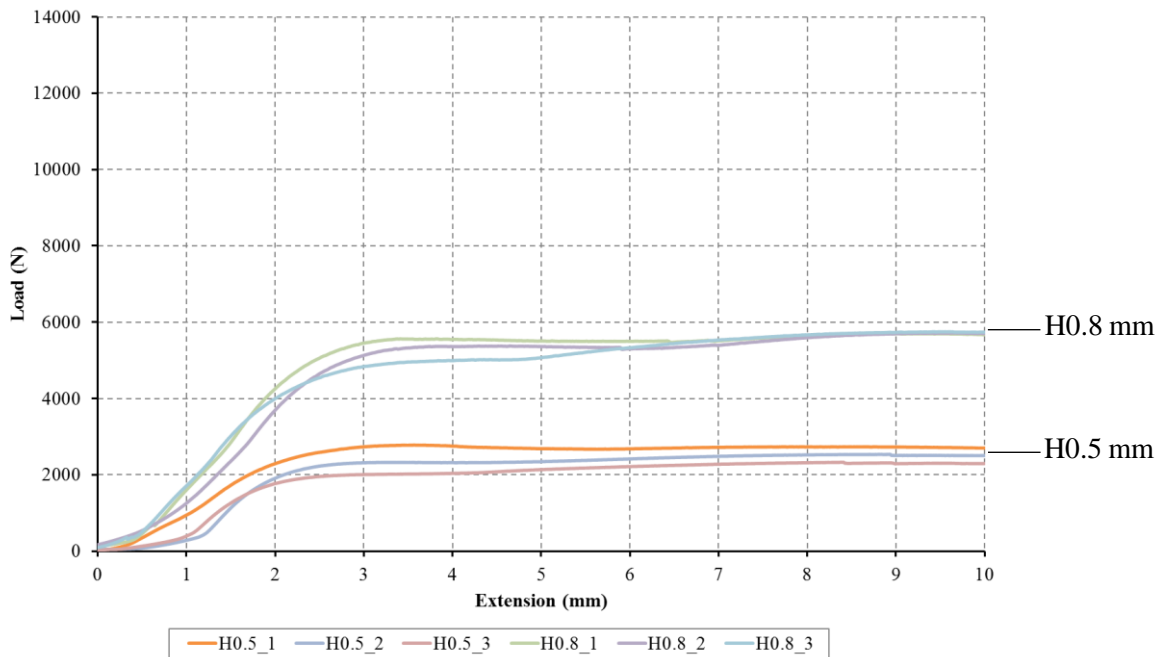


Figure 5-12: Load-extension graphs for hybrid samples only

Figure 5-11 and Figure 5-12 show the same samples, separated in pure steel and hybrid sample graphs.

The graphs show that the repeats of the tests are less consistent and more varied than at coupon level, which is to be expected as the samples are significantly larger. They also show however that the correlation levels are generally good, (especially over the elastic region) and sufficient for the data to be considered valid. In certain cases, however, such as the 0.5 mm pure steel samples, and the 0.5 mm hybrid samples, two of the samples correlate extremely well and the third presents a varying behaviour. In further studies, it would be interesting to determine the cause of this change, whether due to fabrication technique or otherwise.

The k values were calculated from the linear elastic sections of the curve, shown in Table 5-2. It is interesting to note that the 0.8 mm hybrid has an elastic behaviour that exceeds that of the 1.0 mm pure sample. The 0.5 mm hybrid sample presents a behaviour that exceeds that of the 0.8 mm sample, and when considering the values of k also exceeds the performance of the 1.0 mm sample and is 1.1 kg lighter.

*Table 5-2: Summary of topside up stiffness values and sample weights*

Type of test	Material		Value of k (N/mm)	Standard Deviation	Weight (g)
	Steel	Composite	Topside up		
Benchmarking	0.5 mm	-	648.6	54.1	651.3
	0.8 mm	-	1198.9	30.5	983.7
	1.0 mm	-	1828.0	388.6	1243.7
	1.6 mm	-	3861.5	-	1963.3
Hybrid	0.5 mm	[0,90]s	2106.9	134.1	689.7
	0.8 mm	[0,90]s	3062.5	120.2	1060.7

The complete data, to sample failure, although not analysed in the context of this thesis, also provides information on the energy absorption of the hybrid samples comparatively with the pure steel samples. This will be discussed in the further work section of Chapter 7. It is additionally worth noting the marked increase in beam yield values in the hybrid beams compared to their pure counterparts.

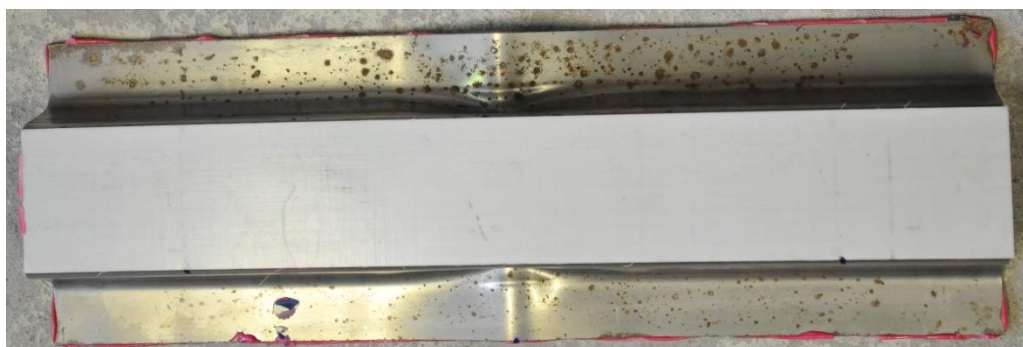
### 5.3.2 Topside down

The samples considered in this section are the topside down samples. The images presented below are those of the 0.8 mm DP600 non-reinforced (referred to as “pure steel”) and the 0.8 mm DP600 [0,90]<sub>s</sub> PA6 GF60 reinforced samples (referred to as “hybrid”). These were chosen as a direct comparison of the sample deformation can be made. The 0.5, 1.0 and 1.6 mm pure steel samples and 0.5 mm hybrid sample are not presented photographically as they do not add any additional information to that provided by the 0.8 mm samples.

Figure 5-13 shows the samples in a top view. This shows the impactor location, and associated deflections. a) shows the pure steel sample, b) shows the hybrid sample.



a) 0.8 mm pure steel sample



b) 0.8 mm hybrid sample

*Figure 5-13: Topside down 0.8 mm pure steel a) and hybrid samples b)*

Here again, the presence of composite does not appear to affect the overall performance or deflection pattern. A pinching effect is visible on the flanges at the location of the plastic hinge. The hybrid sample does not appear to display any

localised damage at the location of the lower rollers where the pure steel sample displays a small localised crushing. This was displayed on all pure steel samples, and in-situ of the test was only present after the onset of overall beam plasticity.

Figure 5-14 shows the detail of the plastic hinging in the two 0.8 mm samples; photos a), c) and e) referring to the pure steel sample, and b), d) and f) to the hybrid sample.



a) Impactor deformation on backplate of 0.8 mm pure steel sample



b) Impactor deformation on backplate of 0.8 mm hybrid sample



c) Impactor deformation top view, pure steel sample

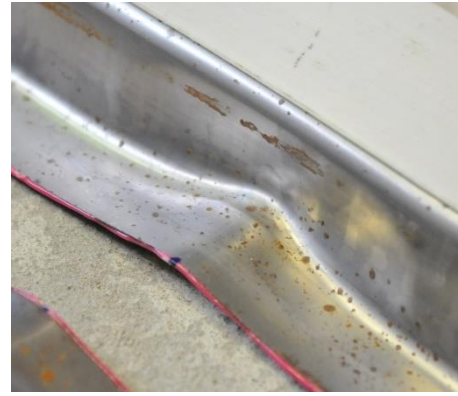


d) Impactor deformation top view, hybrid sample





e) ISO view of impactor deformation, pure steel sample



f) ISO view of impactor deformation, hybrid sample

*Figure 5-14: Detail of plastic hinging zone on 0.8 mm DP600 pure steel and hybrid samples for topside down*

The images suggest that the composite has a lesser effect on the plastic damage on these samples than the topside up ones, as expected as the impactor is on the steel backplate. A lessening of the plastic damage and severity of the hinge effect can be seen in images e) and f). Images a) and b) display a stretching of the backplate, however do not appear affected by the presence of composite. Figure 5-15 shows a summary of the load-extension graphs. This is again broken down into two separate graphs, presented in Figure 5-16 and Figure 5-17. The legend system used to refer to the samples and their repeats is the same as that used for the topside up scenario. The stiffness of the 0.8 mm samples is improved compared to its pure steel equivalent, however, past the yield point, both beams display a very similar behaviour.

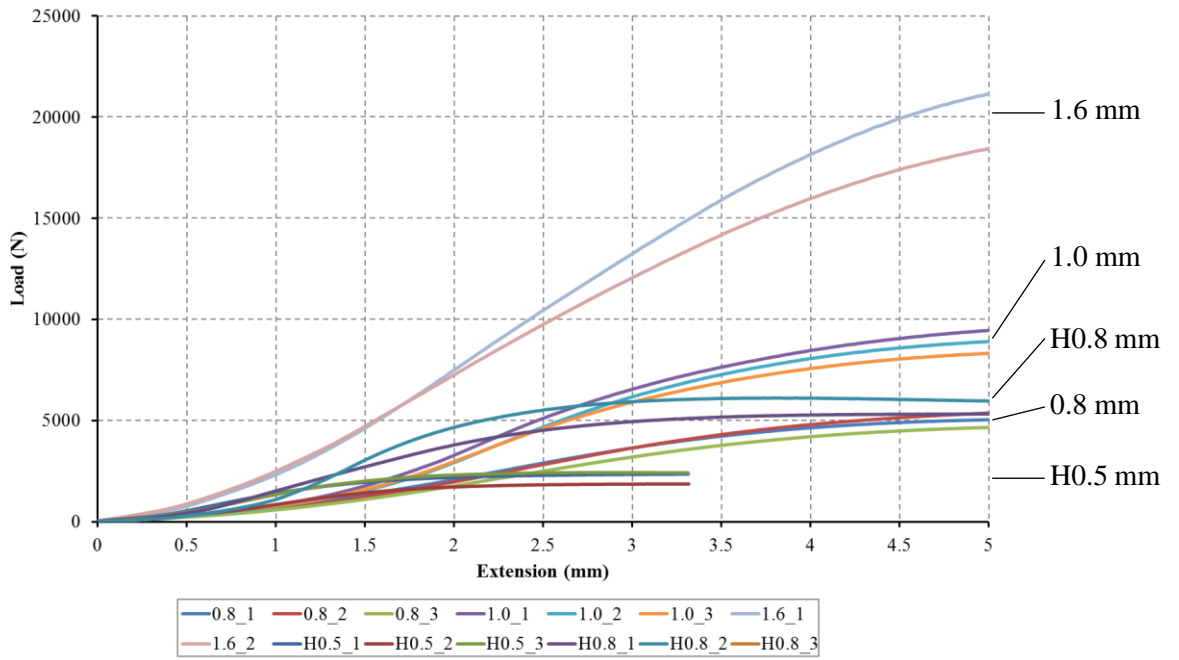


Figure 5-15: Load-extension graph for all samples tested topside down

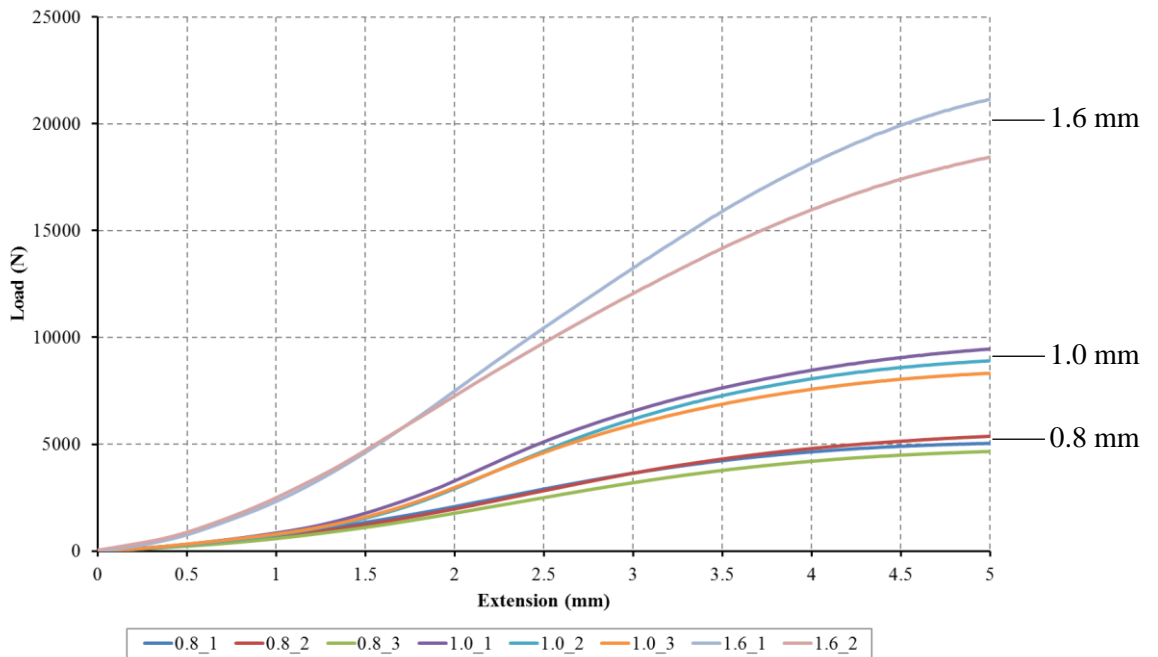


Figure 5-16: Load-extension graphs for pure steel samples only

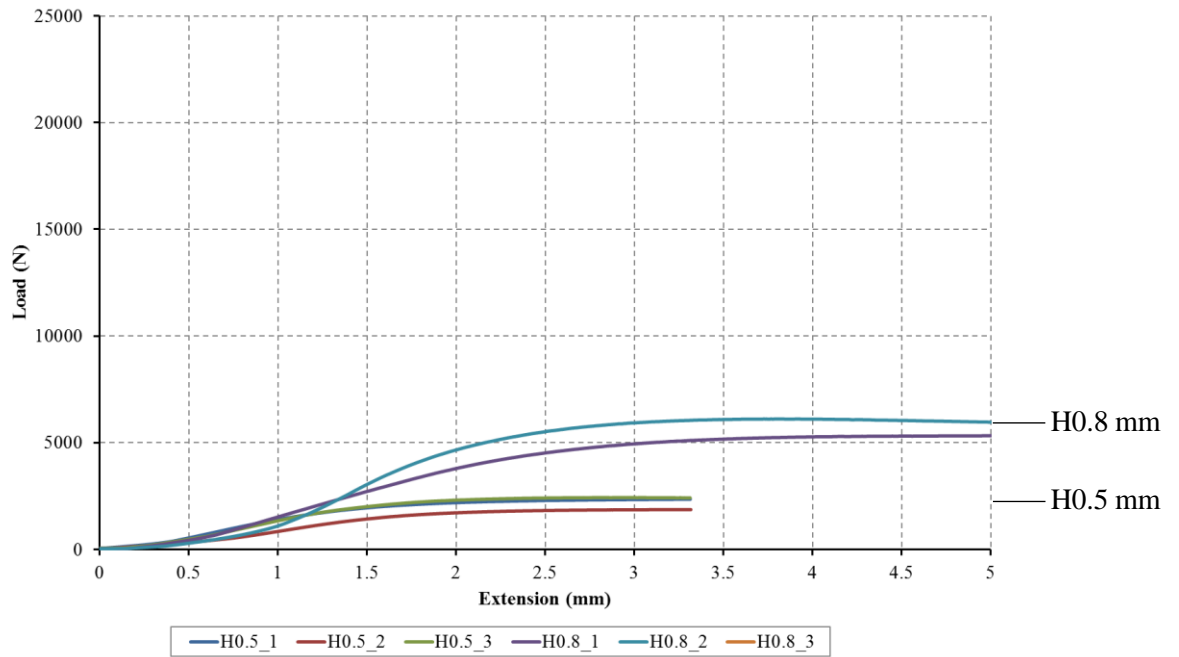


Figure 5-17: Load-extension graphs for hybrid samples only

Table 5-3 summarises the values of  $k$  and weight of the topside down samples. The 0.5 mm hybrid sample presents a behaviour that matches that of the 0.8 mm sample (in “ $k$ ”), and the 0.8 mm hybrid sample is seen to not quite achieve the same stiffness as the 1.0 mm pure steel sample. Dashes show samples not tested.

Table 5-3: Summary of topside down stiffness values and sample weights

Type of test	Material		Value of $k$ (N/mm)	Standard Deviation	Weight (g)
	Steel	Composite	Topside down		
Benchmarking	0.5 mm	-	-	-	651.3
	0.8 mm	-	1651.1	117.0	983.7
	1.0 mm	-	3595.9	173.0	1243.7
	1.6 mm	-	5641.6	444.1	1963.3
Hybrid	0.5 mm	[0,90]s	1686.6	203.2	689.7
	0.8 mm	[0,90]s	3194.8	754.6	1060.7

### 5.3.3 Discussion

The beams exhibited a failure mode of progressive localised crushing and plastic hinging under the central loading point of the impactor in both topside up and topside down scenarios. The local crushing and hinging effect began at moderately low loads, indicating that beam stiffness data is a measure of resistance both to global bending and to local crushing. All samples, both in pure steel and hybrid, provided similar performance in terms of this mixed-mode, flexure / crush.

The results presented previously are indicative of some very promising behavioural responses. Table 5-4 summarises the results from both the topside up and topside down series of tests. It is worth noting all values were calculated as averages of the performances of all the samples tested. As can be seen from the graphs above, the variance on all samples is small enough to be deemed acceptable.

*Table 5-4: Summary of topside up and topside down k values, as well as sample weights*

Type of test	Material		Value of k (N/mm)		Weight (g)
	Steel	Composite	Topside up	Topside down	
Benchmarking	0.5 mm		648.6	-	651.3
	0.8 mm		1198.9	1651.1	983.7
	1.0 mm		1828.0	3595.9	1243.7
	1.6 mm		3861.5	5641.6	1963.3
Hybrid	0.5 mm	[0,90] <sub>s</sub>	2106.9	1686.6	689.7
	0.8 mm	[0,90] <sub>s</sub>	3062.5	3194.8	1060.7

In the topside down experiments, the effect of the composite on the value of k is smaller, which is believed to be due to the geometrical dominance of the backplate. The backplate is the loaded surface, where the area of loading is nearly double that of the composite or steel surface in the topside up experiment. This also explains the overall increase in stiffness in the pure steel samples.

To calculate the bending stiffness of a quasi-static three-point bend set up the following Equation 5-1 can be used [96]:

$$E_{\text{bend}} = \frac{L^3 k}{48 I} \quad \text{Equation 5-1}$$

Where  $E_{\text{bend}}$  is the modulus of elasticity in bending (MPa),  $L$  the support span (mm),  $k$  the slope of the tangent to the initial straight-line portion of the load-deflection curve (N/mm) and  $I$  the second moment of area ( $\text{mm}^4$ ).

This bending stiffness is not truly representative of the performance of the material and beams however, but can be used to compare samples from different tests. As all the samples were tested in identical conditions throughout, the stiffness value  $k$ , gradient of the elastic section of the load-extension curve, is a better measure of the performance.

Table 5-5 and Table 5-6 present the comparative performances of the samples with respect to the 0.5 mm hybrid and the 0.8 mm hybrid respectively.

These were calculated individually as

$$\% \text{ difference} = \frac{\text{Hybrid coupon performance} - \text{Compared sample}}{\text{Compared sample}}$$

Equation 5-2

So that the performance of the hybrid sample is expressed relative to the benchmarked sample performances individually.

*Table 5-5: Comparative figures of the performance of the 0.5 mm hybrid samples to the benchmarked pure steel samples and 0.8 mm hybrid samples*

Type of test	Material		Percentage difference %		
			Value of k (N/mm)		Weight (g)
	Steel	Composite	Topside up	Topside down	
Benchmarking	0.5 mm		224.8	-	5.9
	0.8 mm		75.7	2.2	-29.9
	1.0 mm		15.3	-53.1	-44.5
	1.6 mm		-45.4	-70.1	-64.9
Hybrid	0.5 mm	[0,90] <sub>s</sub>	0.0	0.0	0.0
	0.8 mm	[0,90] <sub>s</sub>	-31.2	-47.2	-35.0

When considering the topside up scenario; the 0.5 mm hybrid beam presents an increased performance over three samples shown in green. These are the 0.5, 0.8 and 1.0 mm pure steel samples. When comparing their weight, two of these show the hybrid to be an improvement: the 0.8 and 1.0 mm pure steel samples, shown in red. In the topside down scenario, the 0.5 mm hybrid presents an improvement over only one sample, the 0.8 mm pure steel. The samples present near identical performances; however, the hybrid sample is nearly 30 % lighter.

*Table 5-6: Comparative figures of the performance of the 0.8 mm hybrid samples to the benchmarked pure steel samples and 0.5 mm hybrid samples*

Type of test	Material		Percentage difference %		
			Value of k (N/mm)		Weight (g)
			Topside up	Topside down	
Benchmarking	0.5 mm		372.2	-	62.9
	0.8 mm		155.4	93.5	7.8
	1.0 mm		67.5	-11.2	-14.7
	1.6 mm		-20.7	-43.4	-46.0
Hybrid	0.5 mm	[0,90]s	45.4	89.4	53.8
	0.8 mm	[0,90]s	0.0	0.0	0.0

When considering the topside up scenario; the 0.8 mm hybrid beam presents an increased performance over four samples. These are the 0.5, 0.8 and 1.0 mm pure steel samples and the 0.5 mm hybrid sample, highlighted in green. When comparing their weight, one of these shows the hybrid to be an improvement: the 1.0 mm pure steel sample, highlighted in red. In the topside down scenario, none of the samples are shown to be improved on by the addition of composite. The 0.8 mm hybrid seems to not be presenting as many solutions as the 0.5 mm hybrid, however it is important to highlight that this is most likely due to the sample batch tested. The 0.8 mm hybrid is expected to show improvements on the 1.2 mm and 1.4 mm pure steel samples, as shown Figure 5-18.

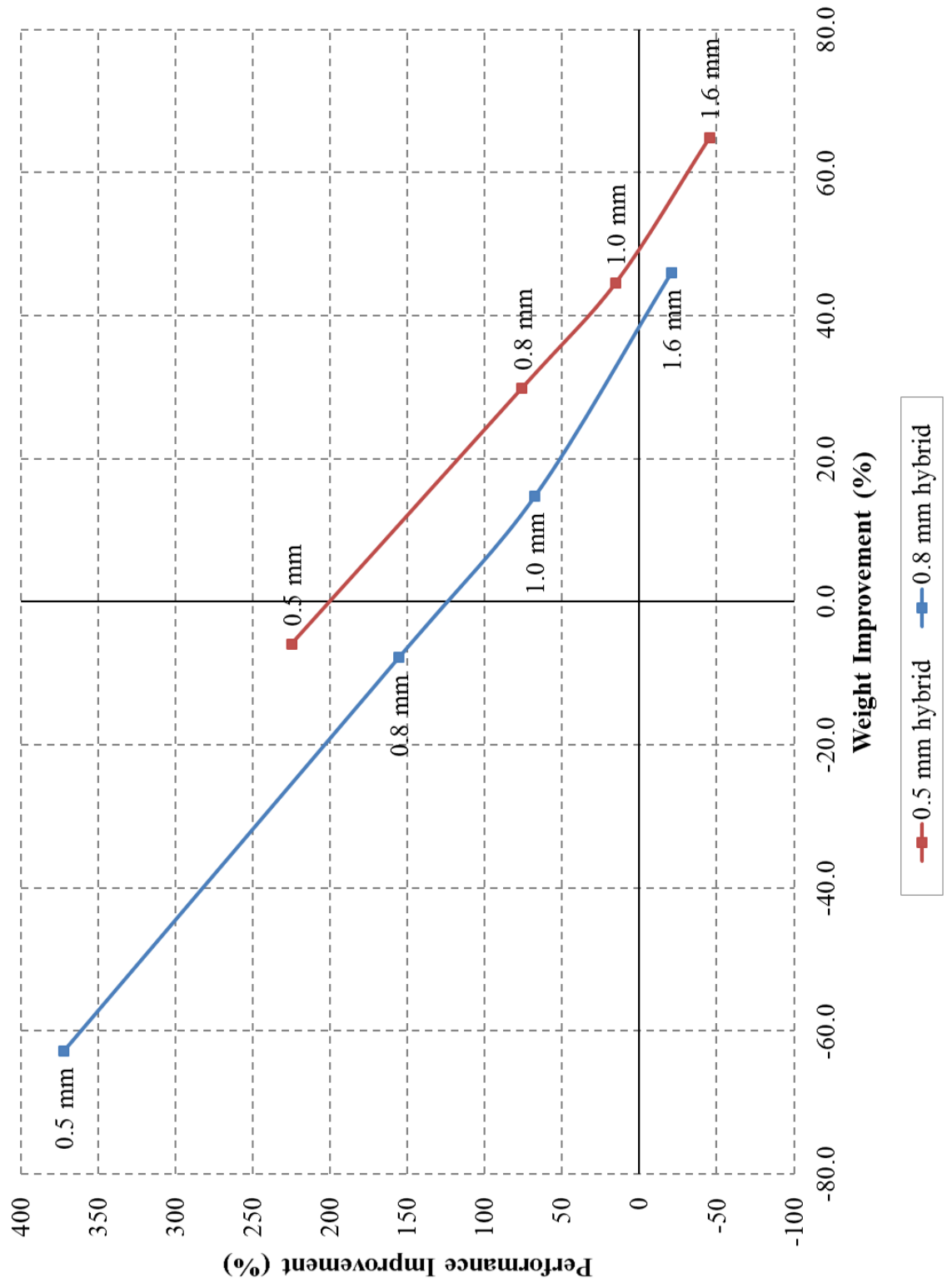


Figure 5-18: The performance and weight “improvements” of the hybrid samples compared to the pure steel ones, topside up

Figure 5-18 plots both the percentage weight and k benefit for the 0.5 and 0.8 mm hybrids compared to the pure steel. It indicates that for a given composite reinforcement, there is a near linearity in sample benefit, and a matching trend between the 0.5 mm hybrid benefits and the 0.8 mm hybrid ones. This graph also shows the “cut-off” areas. All samples falling in the quarter zone [positive weight, positive performance] are considered beneficial. For the 0.5 mm hybrid sample, this shows that matched stiffness is achieved for an approximate 1.2 mm pure steel sample with a weight save of nearly 50 %. Reading off the graph, for a 0.8 mm hybrid sample, matched stiffness can be achieved to an approximate 1.4 mm pure steel sample, saving nearly 40 % in weight.

It is worth noting that the samples do not improve linearly in their thickness. The trendline is parabolic, and showing a decreasing impact on performance per 0.1 mm thickness increase. This trendline is expected to plateau, as the hybrid samples only provide a given improvement on their pure steel counterparts. It is speculated that the nature of the composite reinforcement (lay-up, orientation, nature of fibres, etc.) would be able to further improve the performance effects.

The topside up experimental results show that in the comparison of the 0.5 mm hybrid and the 1.0 mm pure steel there is an increase in performance of 15.3 % and a lightweighting of 44 %. This proves that by downgauging the steel and adding a patch of composite to the load-bearing surface, it is possible not only to provide a lightweight solution but also to improve on the existing performance.

The topside up scenario is one which is most analogous to a side-impact automotive load case where stiffness and energy absorption must be balanced to minimise intrusion and occupant accelerations. As a result of this, only this scenario is investigated in the simulation program, with the aim to recreate the results and benefits shown here and engage in an optimisation of the patch location so as to further extend the benefits of the intelligent deployment of composite materials.



## 5.4 Conclusions

The GFRP local reinforcement of downgauged top-hat DP600 sections has shown in experimental testing the following conclusions:

1. There is potential for using FRP to reinforce steel in an intelligent deployment of composite material implying the structure can be optimised and lightweighted. An example of this, demonstrated in this Chapter, is that the 0.5 mm hybrid sample provides a 15 % increase in performance  $k$  over the 1.0 mm pure steel sample, whilst also providing a 44 % weight save.
2. For a given composite reinforcement, it is possible to create graphs indicating the “cut-off” areas of performance benefit.
3. The effect of the composite is larger in thinner samples, and in the current reinforcement is seen to have a lesser effect on the 0.8 mm steel than on the 0.5 mm steel. In further work, this could lead to the investigation of different lay-up, orientation or fibre reinforcements.

## 6 COMPONENT PROGRAM – SIMULATION APPROACH

This chapter will focus on the simulation work relating to the top-hat experiments discussed in Chapter 5. It will present the story and development of the simulation models, discuss the results, restrictions and learning outcomes.

### 6.1 The basic model

Chapter 4, Coupon Level simulation showed that both LS-DYNA and Genesis provide suitable results in the modelling of coupon hybrid steel-composite. Genesis provides its answers at a lower computational cost than LS-DYNA and is hence the primary software package used in the modelling of the top-hat section.

This initial simulation study was run prior to the experimental work, on all benchmark steel materials, and included a focus of the effect of the composite patch location on the performance. This was done in order to determine where best to locate the composite patches, and the varying effects of the composite patch locations and size. This justified the decision to test the top-reinforced hybrid samples so as to validate the simulated results, and ensure the accuracy of the simulated results.

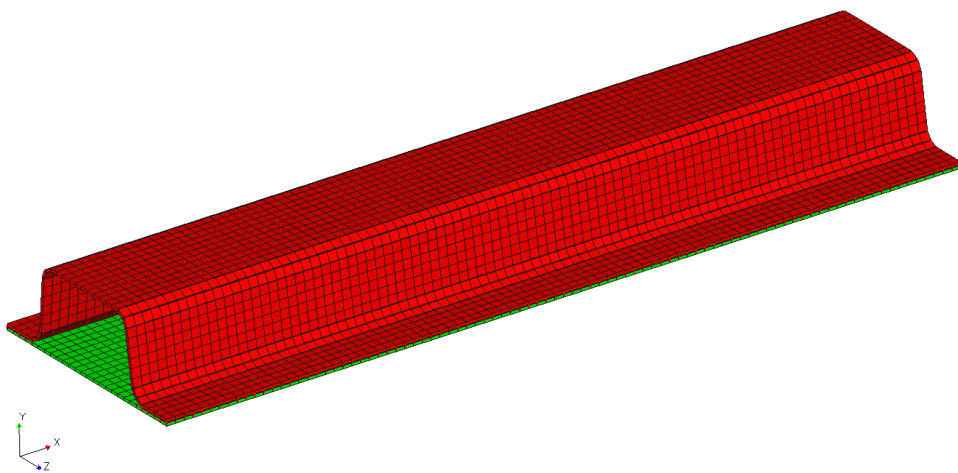
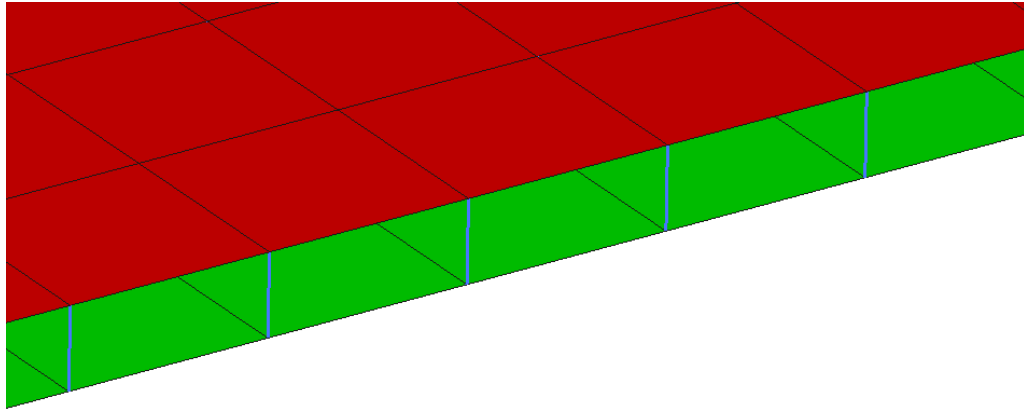


*Figure 6-1: Genesis FE model of the beams used in testing*

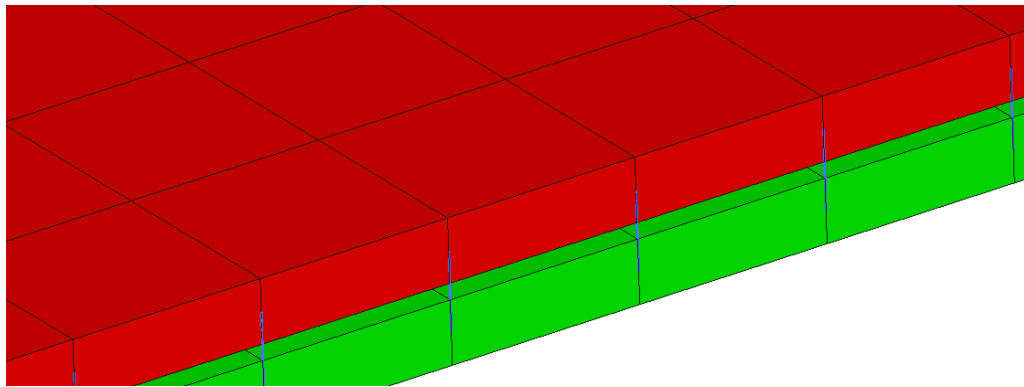
Figure 6-1 shows the model used for the simulation. The model was designed in Solidworks and meshed using HyperMesh. A number of studies [58, 102, 108, 109] show similar experiments and modelling using the axis of symmetry to reduce the size of the sample to  $\frac{1}{2}$  or  $\frac{1}{4}$  of the full model. These methods have the benefit of presenting smaller models that are less computationally, and therefore time, expensive. In the context of this work, it was felt that this would be more likely to induce errors than gain substantial time. The elements used were shell elements, and the mesh size was 5 mm. A mesh sensitivity analysis was briefly investigated, where the mesh size was decreased (increasing the mesh density), and concluded that the mesh size was not responsible for any variations in results. The hybrid material was simulated using PCOMP, the part composite within which both materials are defined. This will also be used in the context of top-hat modelling.

The coordinate system used throughout is defined as in Figure 6-1, by which the x-axis runs along the length of the sample, the y-axis is through the height of the sample and the z-axis runs along the width of the sample. This coordinate system was used in all simulations. The theta vectors (determining element directionality) were defined within this coordinate system to ensure that all composite fibre orientations match, both between the elements and along the overall component.

The backplate and top-hat sections were modelled separately. There are two primary options for joining the backplate to the flanges of the top-hat section without modelling the adhesive. One is to join every corresponding node using RBE's, the other is to take advantage of the Genesis defined "Glue Contact". Figure 6-2 shows a visual representation for the RBE connections used; a) and b) show the thickness representation in Genesis.



a) RBE2 connections with no layer thickness representation



b) RBE2 connections with layer thickness representation

*Figure 6-2: Showing the RBE2 links representing the adhesive bond between the top hat shape and the backplate; a) and b) with and without thickness representation*

In the coupon program, it was found that the inherent stiffness in the RBEs was sufficient to affect the overall stiffness of the material, although the behaviour is dominated by the steel. It was decided therefore to use the “glue contact” to go forward.

The top hat was initially modelled both topside up and topside down, however, following the results in the experimental tests showing a greater effect on the topside up samples, only these were modelled throughout. The loading is representative of the quasi-static three-point bend geometry used in the testing. Literature studies [88, 102, 107] imply that the loading conditions are not as straightforward as in the case of the coupon samples, as such, the variations were studied.

## 6.2 Study of the loading constraints

It is possible to use nodal forces, element pressures or a roller with one single force applied. In all cases, the bottom rollers were represented using nodal motion constraints that prevent the sample from behaviour non representative of the physical testing, such as a rotation around the z-axis. Two rows of nodes (one row at each support) were restricted in directions 2, 4 and 5; which in the context of this model was equivalent to a constraint in translational y and rotational x and y directions.

The forces simulated the top roller, and were applied as point loads to specific nodes. In testing, as the bending progresses, the centre section of the top hat experienced local deformation inwards, which lead to the forces only being applied to the outer section of the top hat top face and directly into the sides.

In order to accurately model this, a few variations of force locations were tested:

### 1) Nodal forces

Loadcase 1 saw forces applied on every node, equally distributed. This leads to a very large deformation of the sample top face. Figure 6-3 shows the deflection pattern, which is not an accurate representation of the experiment in terms of significant deflection in the central area of the top-hat. Following that, a series of different conditions were tested, where the forces were distributed to a number of nodes only (Loadcases 2 through 5). The force was equally distributed and equivalent to the total force, but limited to a specific area. A number of variations of these were trialled, as described in Table 6-1.

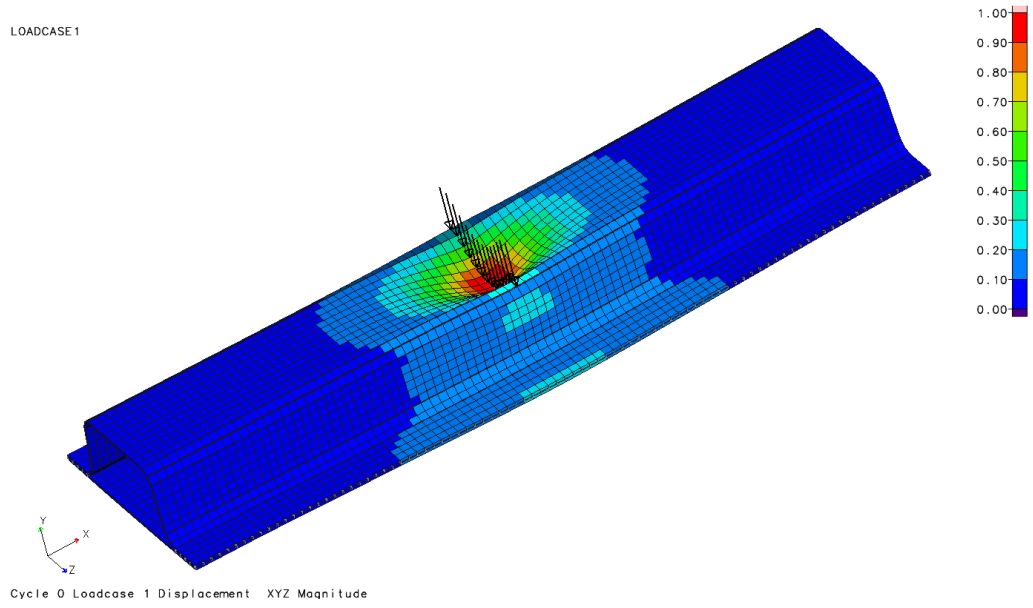
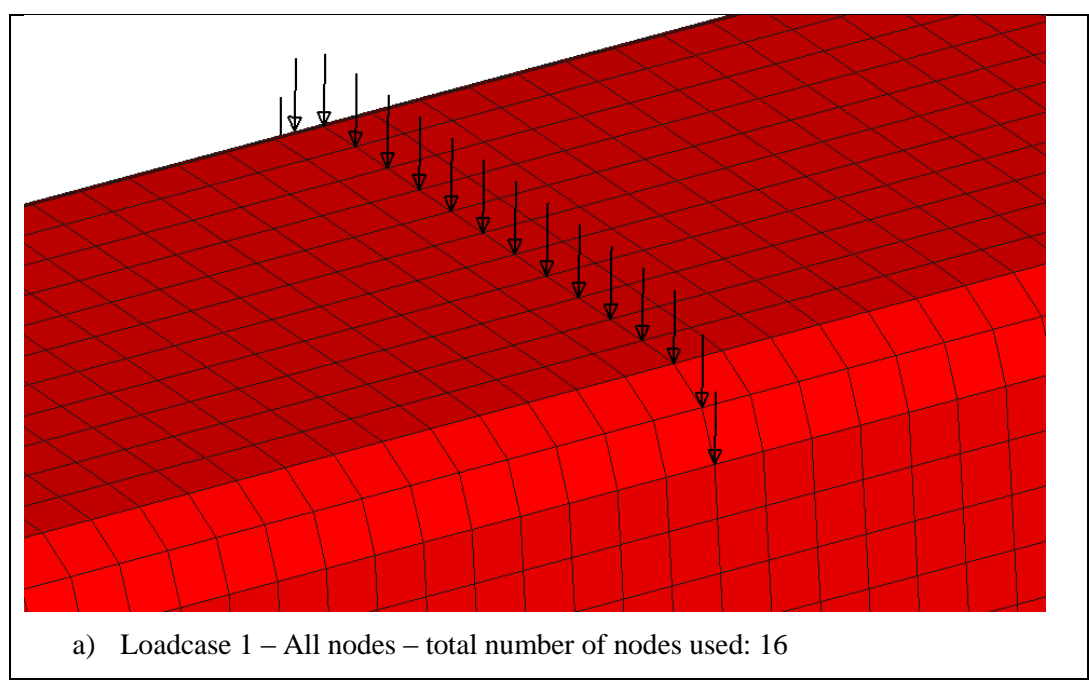
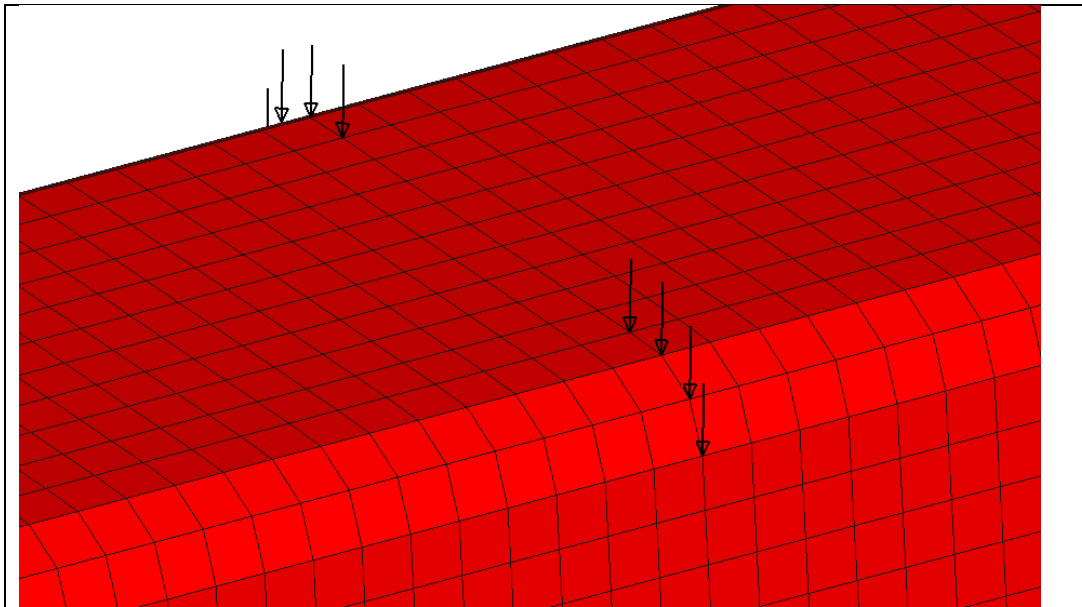


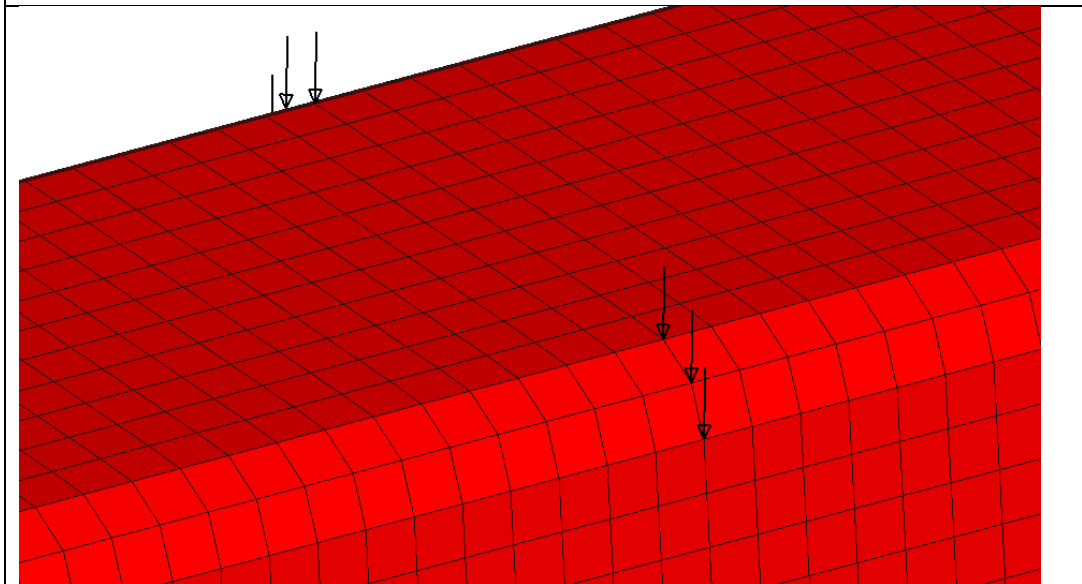
Figure 6-3: Deflection of beam under full nodal force distribution

Table 6-1: Description of loading conditions trialled

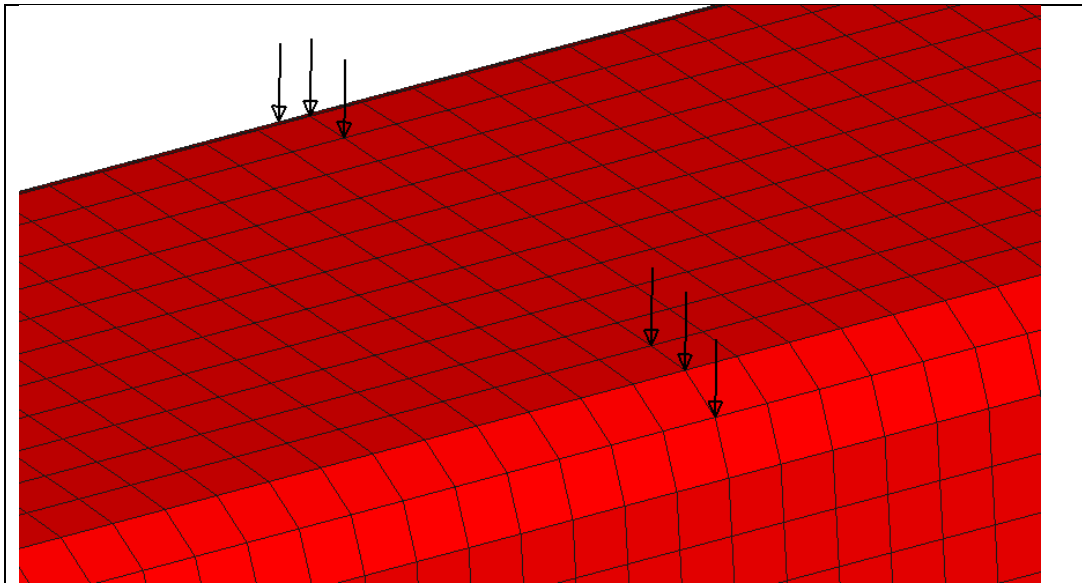




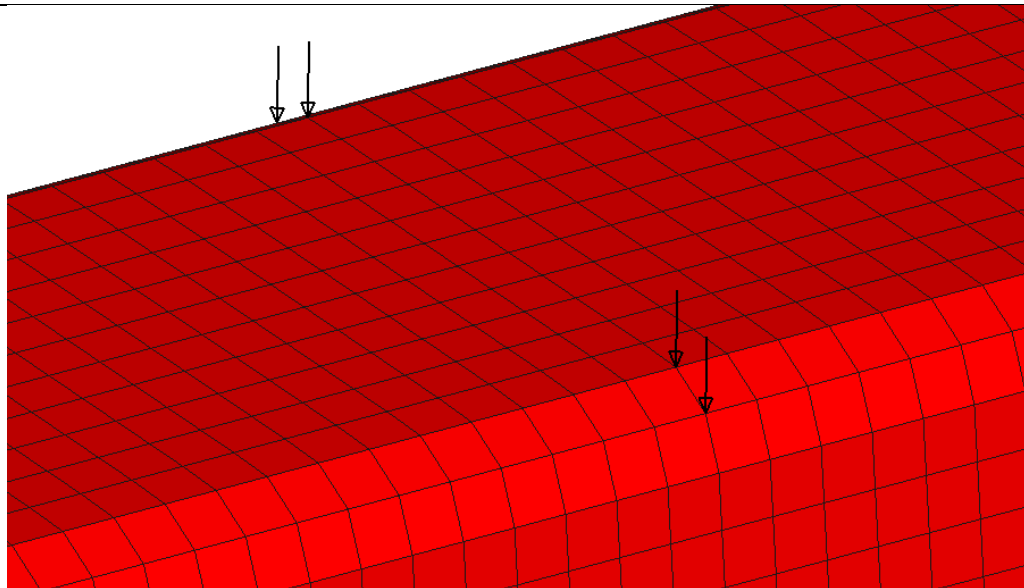
b) Loadcase 2 – 4 nodes on each side – total number of nodes used: 8



c) Loadcase 3 – 3 nodes on each side – total number of nodes used: 6



d) Loadcase 4 – 3 nodes on each side – total number of nodes used: 6



e) Loadcase 5 – 2 nodes on each corner – total number of nodes used: 4

## 2) Pressures

An identical trial was run using pressures on the centre of the elements instead of nodal forces.



### 3) Roller

In the coupon work, the application of nodal forces was a valid approximation of the effect of the impactor as the sample cross section is constant and the geometry is not affected by the bending (the only effect not considered is the anticlastic bending of the beam). Here the forces applied were not solely or evenly applied across the top surface as there was interaction between the side walls and top surface, as well as local geometrical effects.

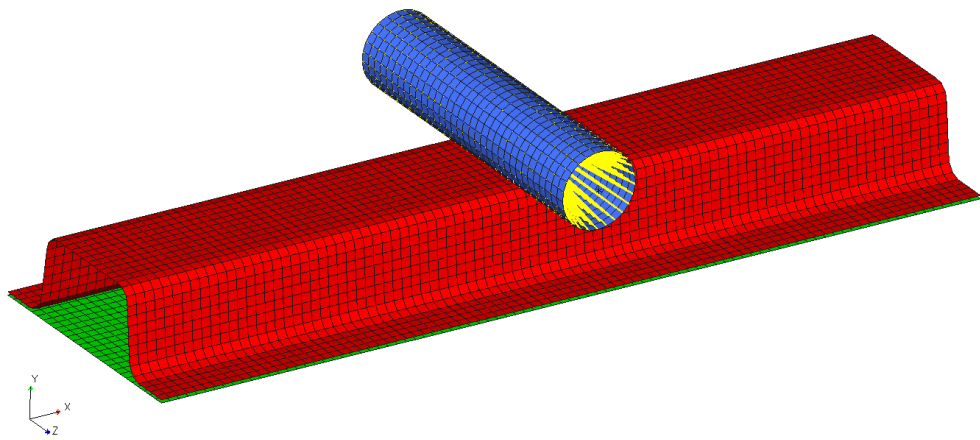


*Figure 6-4: Roller loading condition*

Figure 6-4 shows the roller loading condition. A centre force was applied to the roller, and motion is restricted through a combination of RBE's and degree of freedom constraints to ensure that the roller was rigid and replicated the motion of the test impactor. A contact was set-up between the roller and the top surface of the top-hat shape to avoid penetrations.

Figure 6-5 presents a graphical representation of the load-deflection curves for the different attempts, including the roller. The pressures are not included, as they gave a near identical response to the nodal loading.

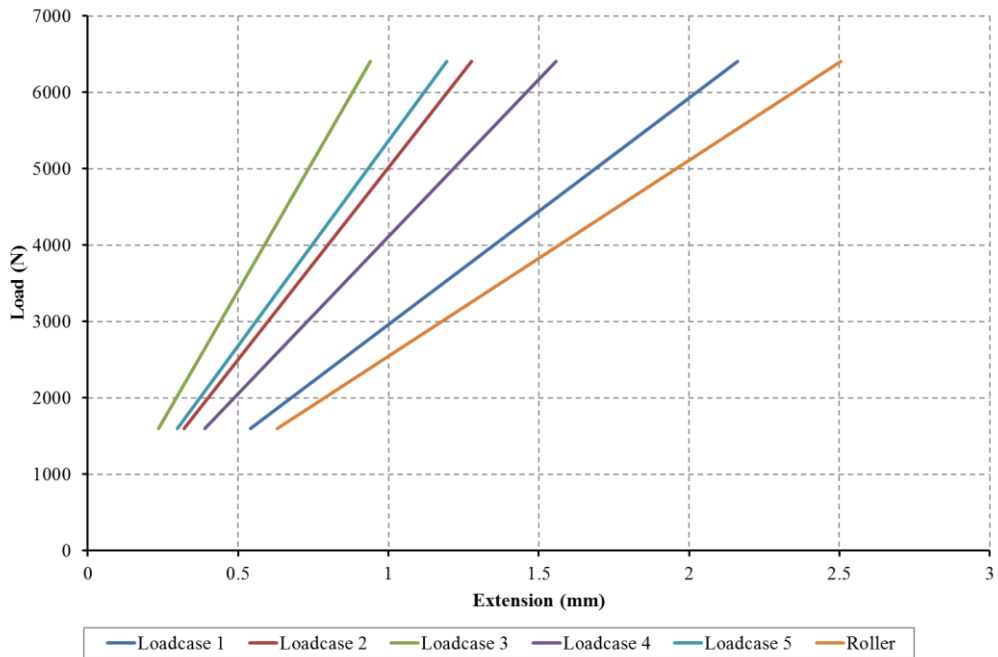


Figure 6-5: Graphical representation of the effect of the loading conditions of the load-extension performance

The LCVTP program [88] which studied a similar geometry beam used nodal forces on the corners only (loadcase 4) of their samples, and it was possible to obtain an identical reaction to their published results. However, as a solely localised nodal force had such a large number of variable possibilities, it was felt that the nodal forces were an approximation that could be incorrect, therefore the decision to use a roller, a closer representation of the experimental testing.

It is worth noting that the deformations measured in testing on all the samples were measured at the edge of the top-surface. Using the roller in simulation was additionally regarded as more accurate as, during the experimental tests, the extension/deflection measured was the motion of the impactor (contacting at the edges) rather than the maximum deflection of the beam.

Following the decision to simulate using the roller and nodal constraints as the impactor and supports, the local reinforcement effects were investigated.

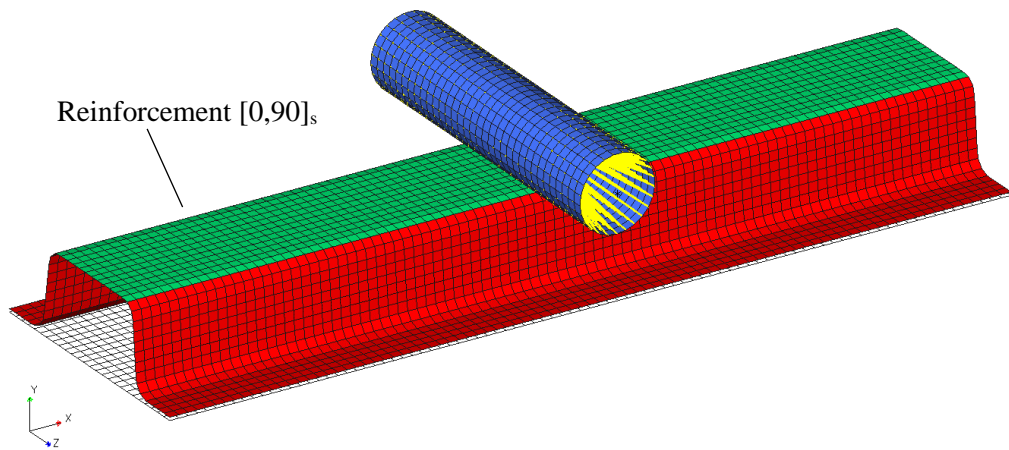
### 6.3 Local reinforcement

The concept of hybrid steel composite automotive beams is not a new one, and BMW is but the latest in a series of manufacturers to use a combination of materials to produce light weight, high end cars [2, 28]. Simply using composites to reinforce either concrete or steel beams in the civil engineering world is also not a breakthrough [51-53]. However, no studies have been published on the effect of localised composite reinforcement with regards to the stiffness performance of the overall beam. An initial approach to this is presented as follows.

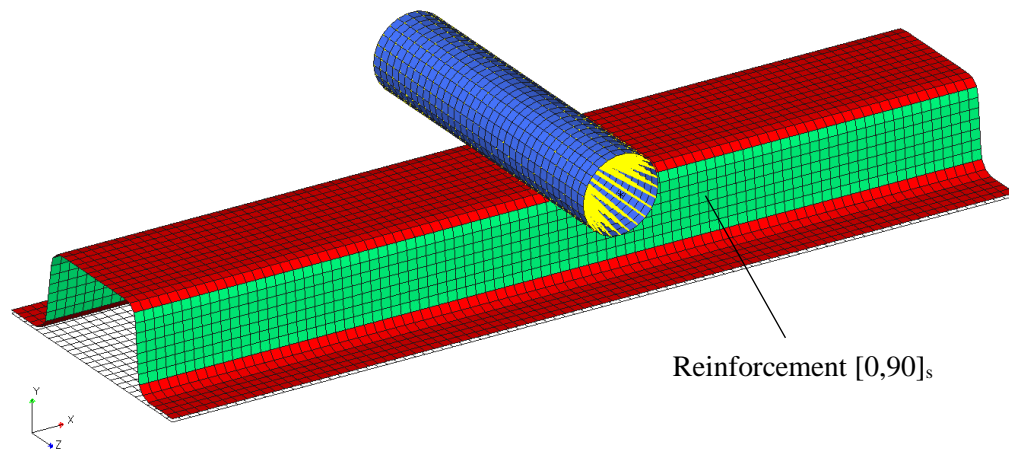
Local reinforcements of  $[0,90]_s$  and their effects were studied in the context of the pure elastic bending set-up, as summarised in Figure 6-6 and Table 6-2 below. The reinforcements are split in terms of location (top, sides, corner – see Figure 6-6). These reinforcement locations were used alone and also combined to study the effect of reinforcement location on the overall performance. Table 6-2 summarises the reinforcement location and combinations applied.

*Table 6-2: Summary of local reinforcement and combinations thereof*

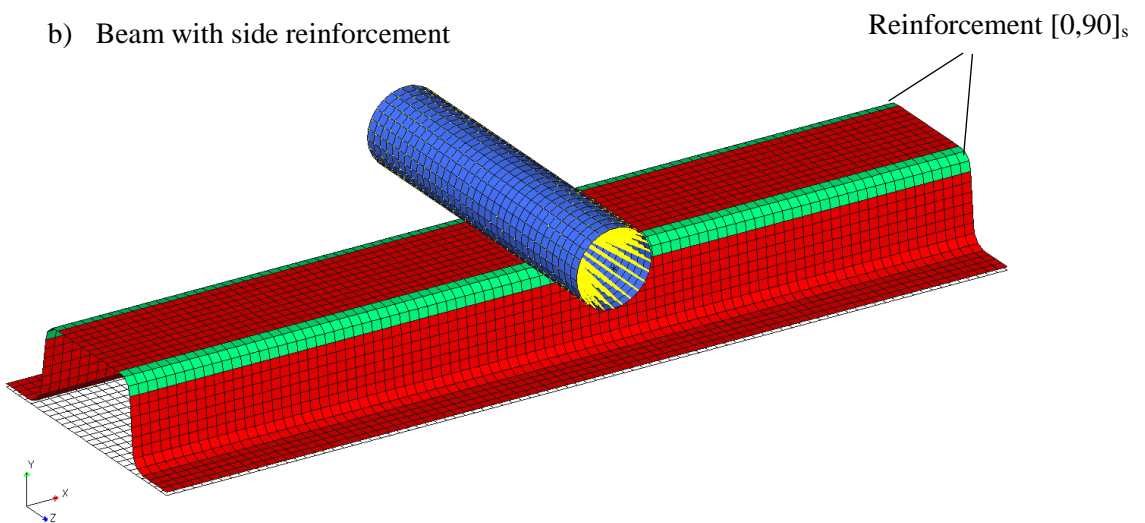
	Reinforcement Location and Combination
0.5 or 0.8 mm DP600	None
	Top
	Corners
	Sides
	Top + Corners
	Corners + Sides
	Top + Sides
	Top + Corners + Sides



a) Beam with top reinforcement (as used in testing)



b) Beam with side reinforcement



c) Beam with corner reinforcement

Figure 6-6: Shows the reinforcement locations; a) shows the top reinforcement, b) shows the side reinforcement, c) shows the corner reinforcement

## 6.4 Results

As a preliminary check to ensure the simulations were not incorrect, the sample weights were checked. As the simulations includes the use of the PCOMP card, and a simple glue contact to join the top hat to the backplate, the adhesive weight is not accounted for, and the experimental samples are expected to weight only slightly more than the simulated one. Using the 0.5 and 0.8 mm hybrid samples and their pure steel counterparts, it is possible to calculate the weight of the composite patch + adhesive on the top surface, as in Figure 6-6. An adhesive weight was estimated for the flanges (they show approximately the same surface area), and the weights output by the simulation were adjusted for comparison to the experimental ones. Table 6-3 shows that the simulated samples correlate well, to within 3.7% of the experimental ones. This gives a primary indication that the model can be trusted.

*Table 6-3: Summary of the weights of the samples, the “adjusted simulated” weights take into account the estimated weight of adhesive per sample.*

Sample Type	Weight (g)			Correlation %
	Experimental	Simulated	Adjusted Simulated	
0.8 mm DP600	983.67	923.8	957.81	2.6
1.0 mm DP600	1243.67	1154.7	1217.81	2.1
1.6 mm DP600	1963.33	1684.4	1937.48	1.3
0.5 mm DP600 [0,90]s	689.67	632.0	663.81	3.7
0.8 mm DP600 [0,90]s	1060.67	978.5	1034.81	2.4

Table 6-2 presents the summary of the simulated reinforcements initially run within this investigation. Table 6-4 presents the stiffness results of these simulations, in term both of stiffness and un-adjusted simulated weights. Figure 6-7 and Figure 6-8 give a graphical representation of the data from Table 6-4.

Table 6-4: Summary of stiffness values  $K$  based on samples make-up – pure DP600 or DP600 with specific reinforcements

Sample make-up		Stiffness $K$ (N/mm)	Weight (g)
DP 600	FRP		
0.5 mm	-	870.8	577.4
0.8 mm	-	2560.8	923.8
1.0 mm	-	4152.1	1154.7
1.6 mm	-	10590.1	1684.4
0.5 mm	Top	1601.2	632.0
	Corners	1047.8	604.8
	Sides	1343.0	641.0
	Top + Corners	1579.0	641.1
	Corners + Sides	1597.6	650.1
	Top + Sides	2174.4	695.5
	Top + Corners + Sides	2271.1	704.6
0.8 mm	Top	3616.6	978.5
	Corners	2415.8	920.1
	Sides	3236.2	987.5
	Top + Corners	3502.3	987.6
	Corners + Sides	3296.7	996.6
	Top + Sides	4299.7	1042.0
	Top + Corners + Sides	4262.3	1051.1

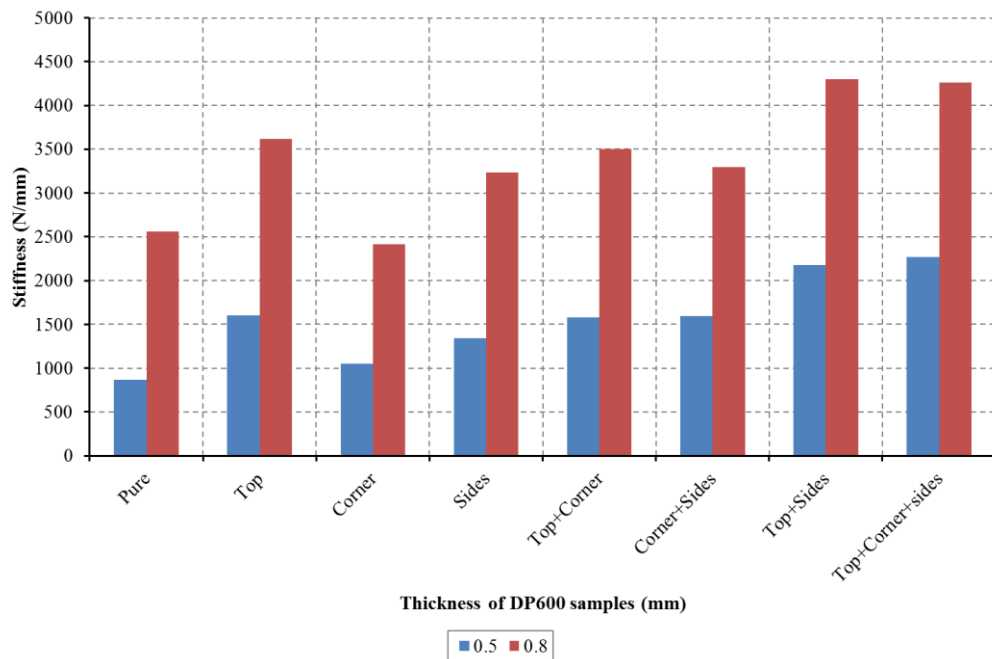


Figure 6-7: Bar chart showing the beam stiffness  $k$  based on steel thickness and composite reinforcement location, topside up

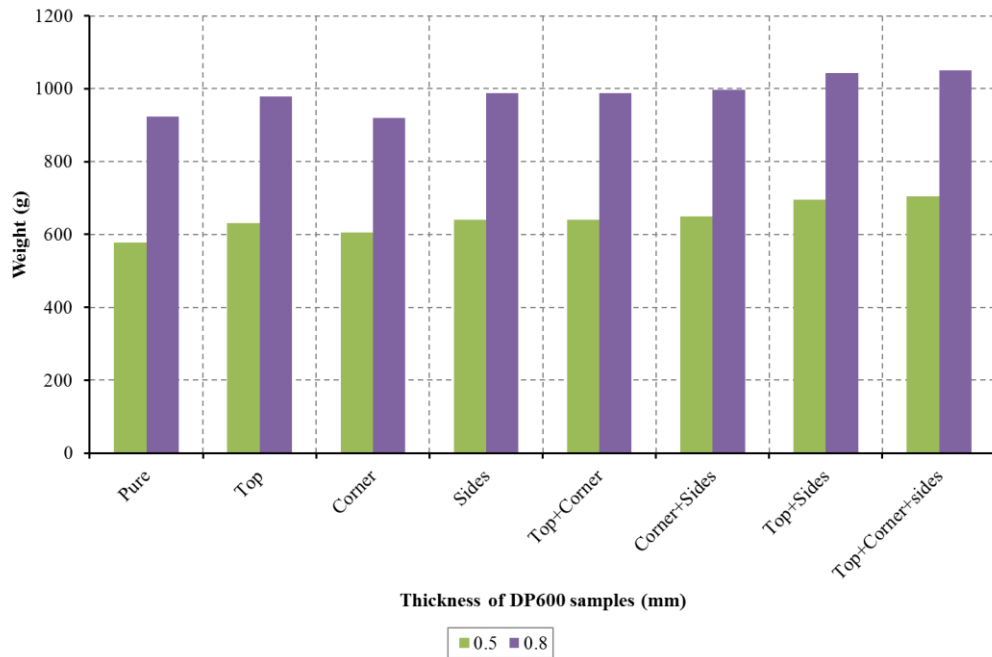


Figure 6-8: Bar chart showing the sample weights based on steel thickness and composite reinforcement location, topside up

A number of observations can be drawn from Figure 6-7 and Figure 6-8:

- The reinforcement with the largest effect on performance is the reinforcement of the top and sides. In the case of the 0.5 mm hybrid it more than doubles (2.6 times) the performance of its pure steel counterpart, and in the case of the 0.8 mm it multiplies it by approximately 1.6 although the mass increases by 118 g.
- Of the three individual options – top, corner, sides – the top has the greatest effect on performance, followed by the sides.
- Reinforcing the corner has no notable effect on the stiffness performance. It has a slightly more pronounced effect in the 0.5 mm samples compared to the 0.8 mm samples, however, this effect is too small to be considered beneficial.
- At the highest level of reinforcement (top + corners + sides) the weight of the samples only increases by 127.3 g. This corresponds to an increase in weight of 22 % and 13.8 % on the 0.5 and 0.8 mm pure steel samples

respectively. This is comparatively small increase in weight for the substantial stiffness gain (160 % and 64 % respectively).

Following the learning outcomes of the reinforcement location study, the results were compared to the experimental results from Chapter 5. Figure 6-9 shows the experimental and simulated stiffness performance for varying thicknesses in pure steel samples. It also shows the experimental and simulated performance of the hybrid samples. The simulation results appear to be consistently over-performing compared to the experimental results. The simulation results under-predict the performance of the 0.5 mm hybrid beams, and over-predict the results of the 0.8 mm beams. In the experimental results, the 0.5 and 0.8 mm hybrids improve the stiffness performance (disregarding weight) by 224.8 and 155.4 % over their respective pure steel counterparts. In the simulation results, the 0.5 and 0.8 mm hybrids improve by 160.8 and 66.4 % over their respective pure steel counterparts.

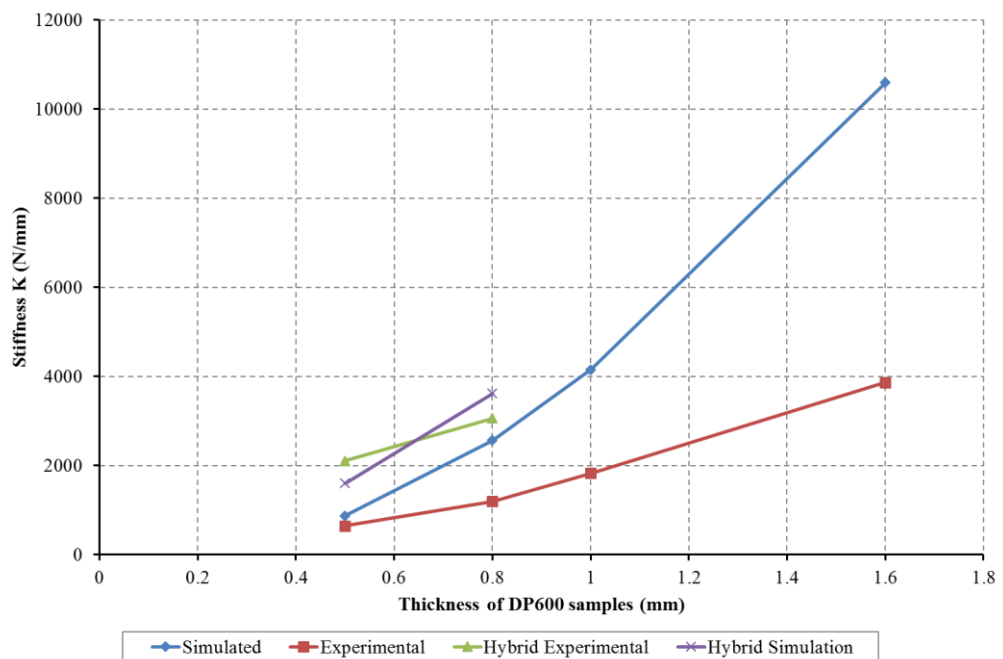


Figure 6-9: Pure steel and hybrid sample stiffness values in experimental and simulated cases



These discrepancies need some consideration. The software package Genesis assumes a complete elastic behaviour and response, and calculates its stiffness values at the onset of a problem, without taking into account the stiffness changes due to geometrical changes throughout a test. In this context, this was considered to be one of the main explanations of the lack of correlation between the tests and FEA. Indeed, Genesis is a software dedicated primarily to the modelling of composite structures, which are less prone to significant local plastic behaviour. Genesis provides an idealised stiffness performance which does not account for geometrical modifications throughout the test. The tests show samples with localised as well as globalised deflections, which the software does not take into account. As such, Genesis over-predicts the globalised stiffness performance of the samples, as they change geometrically through the tests.

Additionally, from a close observation of the samples in experimental testing, and comparison with the deflected simulated samples, it was hypothesised that the plastic localised deflections occur under the impactor of the three-point bend test and cause a weakening of the sample not taken into account by the linear bending. Literature studies support this hypothesis as a plastic-elastic thin walled structure, showing plastic hinges, buckling and crimping occur [70, 106, 107]. There was additionally a small concern over the validity of the samples measured, as experimental set-up errors could have been committed, and as such a means to verify those results was sought.

These concerns lead to an investigation of the simulation in the plastically-enabled LS-DYNA.

A number of hypotheses were made, and explained in the following steps:

1. If the experimental data can be verified, the error must lie with the simulation
2. If the plastic simulations in LS-DYNA can be correlated to the experimental data, the error lies with the use of the elastic-specific Genesis

3. If a study of the load concentrations in Genesis compared to the LS-DYNA simulations shows correlation, the previous work in Genesis has validity and presents an insight into full plastic composite optimisation behaviour

#### **6.4.1 Correlating the 1.6 mm DP600 samples**

An initial concern was that samples tested were possibly tested incorrectly, giving unsuitable results, and a solution was sought to check them. The sample results were compared to the results from the LCVTP program [87, 88]. The samples were produced using the same tooling as the LCVTP ones, ensuring that the geometries match. The material used in both studies includes cold-formed 1.6 mm DP600. The only notable difference between the two is the bonding method between the top-hat and backplate. Where the current study uses an adhesive, the LCVTP samples were bonded using a combination of adhesive and rivets where the adhesive is load-bearing. Figure 6-10 shows the load-extension graph for the topside up samples. Tests 14\_1 and 14\_4 are the LCVTP results, and Els 1 is the test corresponding to this research, see Figure 6-10. These are seen to correlate on the linear sections of the curve, between deflections of 1.5 and 2.5 mm, where the slopes of the curves seem comparable. The global performance of the curves are comparable, despite discrepancies seen in initial loading, and plastic deformation patterns. The whole sample behaviour was also compared in photographs, and correlates well. This gives confidence in the testing undergone in the context of this study, and suggests that the simulation results are over-predicting performance due to software restrictions.

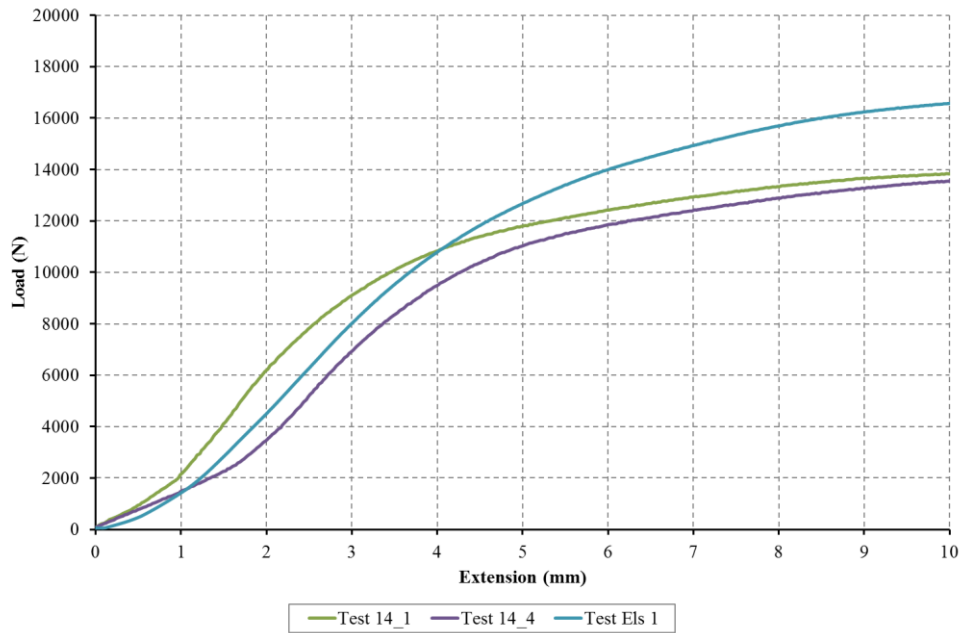


*Figure 6-10: Correlation of experimental testing from this work (Els 1) and LCVTP sources (14\_1 and 14\_4)*

The simulation work run in the context of the LCVTP program used a combination of both Genesis and LS-DYNA. It was possible to acquire the LS-DYNA models, and modify them to fit the assumptions of this study.

In total, three LS-DYNA models were run, one directly from LCVTP as a quarter beam model, and two modified to full beam samples.

#### LCVTP model – Quarter Beam model

Figure 6-11 shows the model as used in LCVTP. The beam is constrained at the “imaginary” open edges created by the symmetry. The flanges are connected through coincident nodes. The model was run through a displacement of 15 mm, and the load-extension graph analysed.

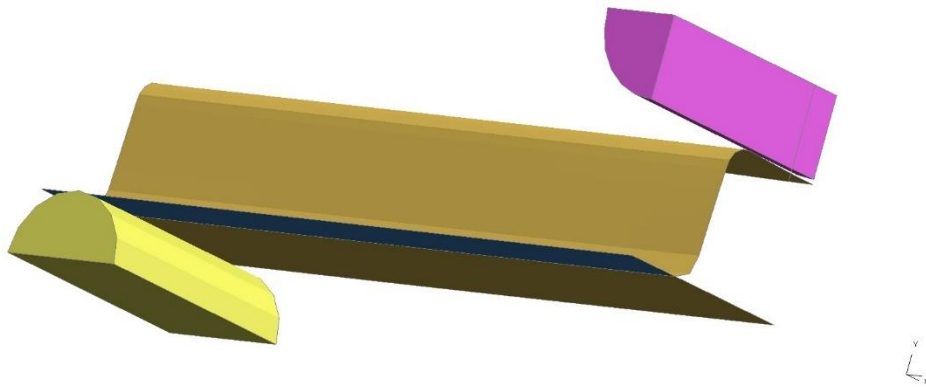


Figure 6-11: Quarter-beam model as used in LCVTP

Figure 6-12 and Figure 6-13 respectively show the Von Mises stress and plastic strain at the onset of beam deformation. They show that in areas the Von Mises stress exceeds yield stress (approximately 360 MPa for DP600) and additionally plastic strain is present in the corner of the beam. They confirm the previous assumption that plasticity is reached very early in the beam deformation causing a localised crushing and the formation of a plastic hinge.

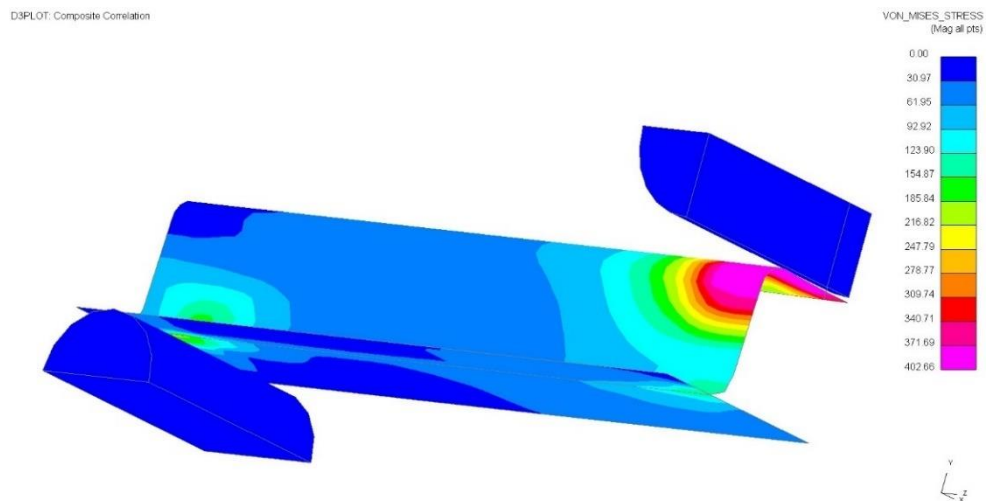
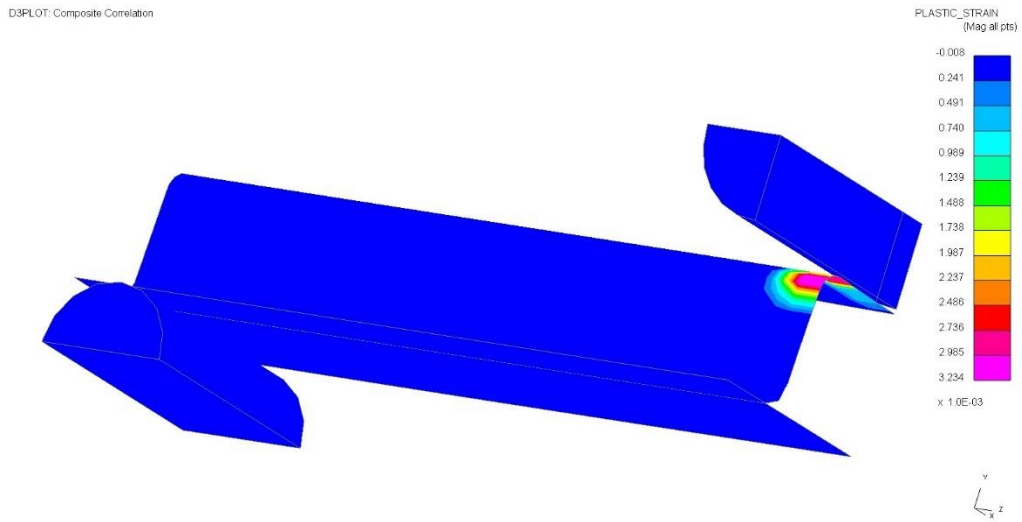


Figure 6-12: Von Mises stress values at onset of displacement – when impactor first connects with beam



*Figure 6-13: Plastic strain values at onset of displacement – when impactor first connects with beam*

### *Full Beam 1*

Two full beam models were also run, as it was felt that they would best represent the experimental procedure, and remove uncertainties due to assumptions and constraints that due to time-restrictions, could not be evaluated in detail.

Figure 6-14 and Figure 6-15 shows the Von Mises stress values and plastic strain values at the onset of displacement.

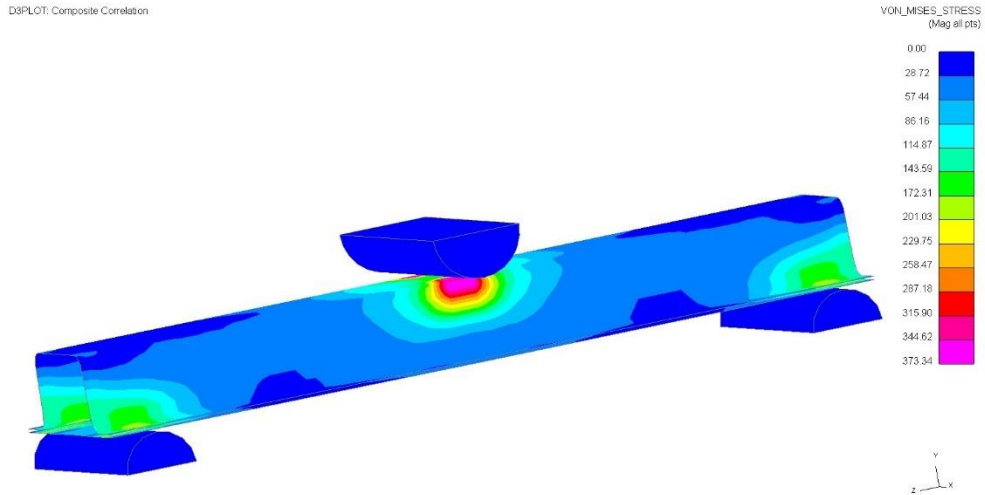


Figure 6-14: Von Mises stress values at onset of displacement

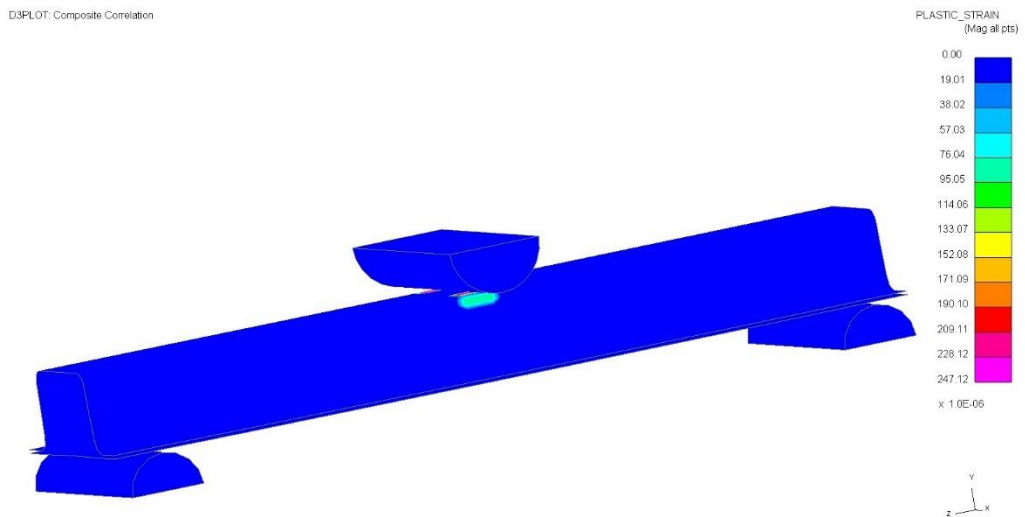


Figure 6-15: Plastic strain values at onset of displacement

The plots again indicate plasticity at the onset, and the Von Mises values exceed yield stress values. Again, these reinforce the conclusions from the experimental testing observations and differences to the simulation indicating the early onset of plasticity and its effect on the overall beam stiffness.

## Full Beam 2

This model presented a higher level of geometrical detail in both the beam and the supports. The visual results are similar to the previous two, and also confirm early onset of plasticity under the impactor.

## Results

Figure 6-16 and Figure 6-17 show the results of the simulated LS-DYNA tests presented above, overlain with the experimental results. The overall results show a likeness in both shape and order of magnitude. They fit within the envelope of the experimental samples.

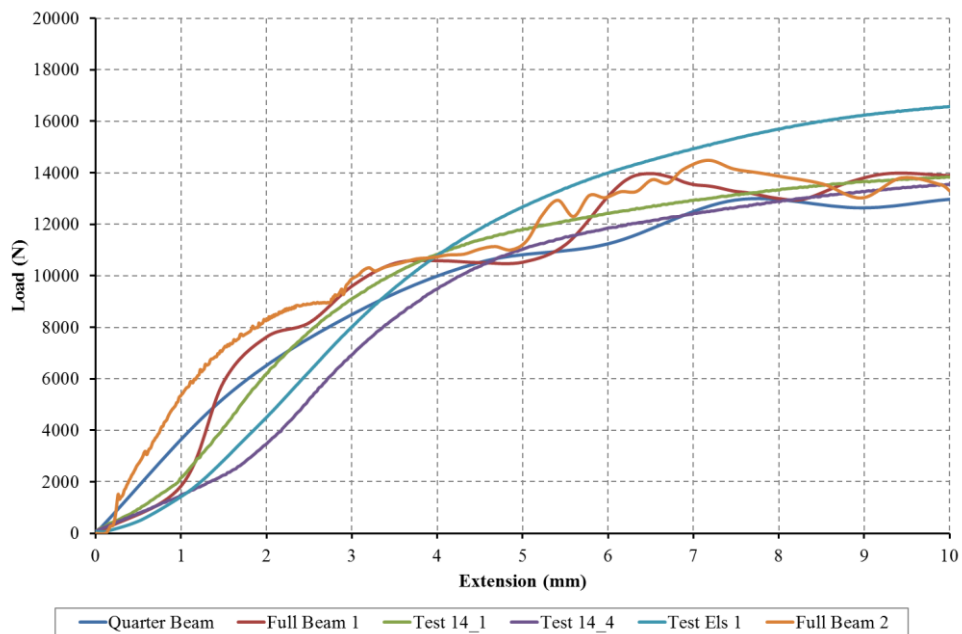


*Figure 6-16: Load-extension graph showing the correlation of the experimental and simulated results*

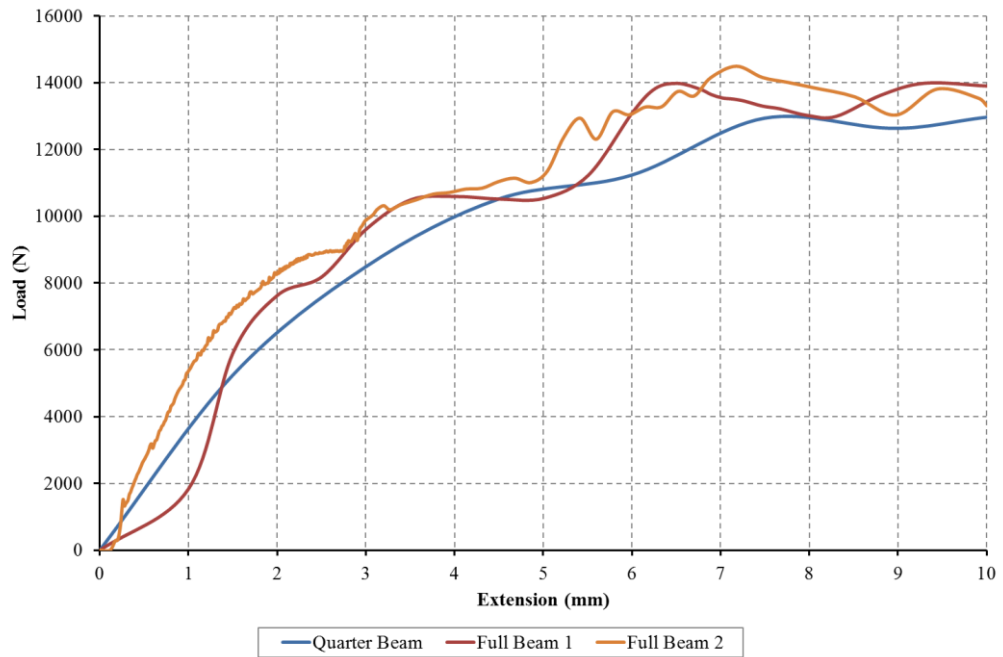


Figure 6-17: Load-extension graph of the simulated results only

It can be seen that the experimental results present a smooth response, where the simulated response, shown in Figure 6-17, presents some fluctuation of the sample in the response. The motion is confirmed by a close inspection (every timestep) of the D3PLOT results. This could be due to a number of factors including the implicit run, velocity of impactor, etc. Ramaswamy [102] noted in his work that the fluctuation was a difficult aspect to manage and noted that the predictions were still indicative of the expected behaviour. This was the only work relating to simulation of parts of an identical geometry found within the literature review. The work was conducted within the context of the LCVTP work conducted at WMG, and used comparable processes for sample production. Discussions with the industrial leads of the LCVTP program also indicated that the fluctuations were a flaw of the simulation, due to the presence of a spring system measuring the displacement response of the samples.



Figure 6-17 also shows that the quarter beam model presents a smoother response to the two full beam models. However, the full beam model 1 shows an initial deformation pattern, from 0 to 1 mm, most resembling that of the experimental results.

A case study was run on the 0.8 mm hybrid models to determine whether the experimental results could be recreated in LS-DYNA. This was also to ensure that the hybrid experimental results were offset in Genesis due to the early onset of plasticity. The two models used were a full beam model (simulation 1) and a quarter beam model (simulation 2). Figure 6-18 shows the graphical results. The models correlate well in the elastic region, however show an under prediction of the overall performance. The models also display the “bouncing” phenomenon observed in the pure steel models, to a lesser extent.

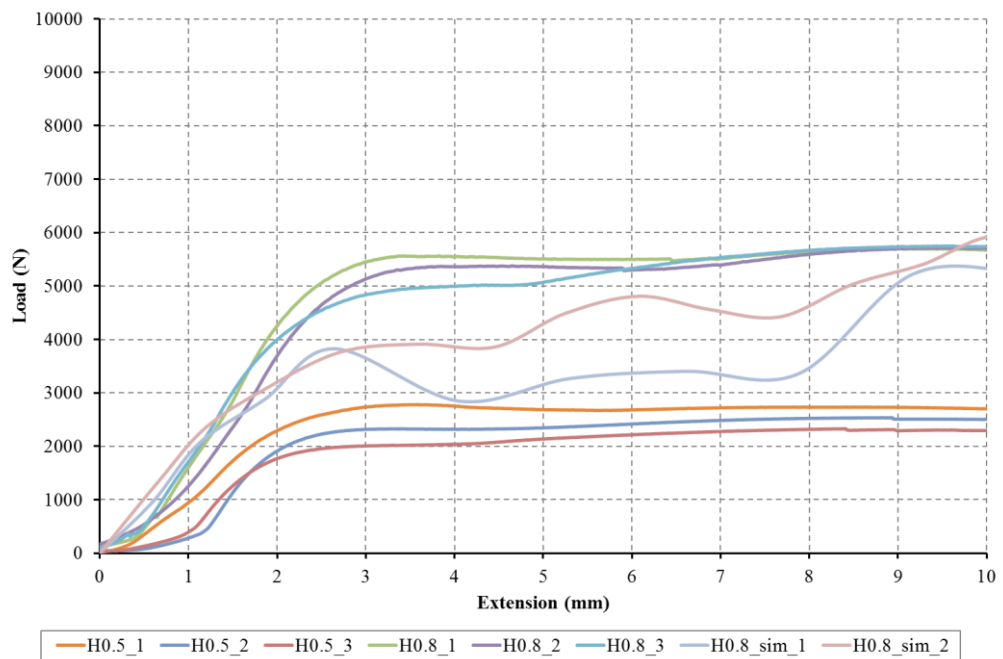


Figure 6-18: Load-extension graph of the hybrid experimental and simulated results

The results, as presented, stand to demonstrate that the early onset of plasticity and continued presence throughout caused the lack of correlation between the initial Genesis simulated results and the experimental results. The Genesis models present the correct deflection patterns, localised stress and strain concentrations but simply do not account for the decrease in load bearing capability due to the plastic behaviour in the materials and geometry. It is acknowledged however that further time should be spent on the LS-DYNA models to optimise them and obtain closer correlation between the tested and simulated load-extension curves.

## **6.5 A manual localisation optimisation – pure elastic bending**

In light of all the simulation challenges, a short manual optimisation of the reinforcement location was run. From the deflection and stress plots of the previous samples, it can be seen that there are localised areas of high stress. These simulations are based on the original three point bend simulations, as seen page 125, and are an intelligent deployment of composite materials, where the location and size of the patches was picked based on areas of high stress concentration, and deformations.

It was speculated that even in the pure geometrical bending, it would be possible to show that a small addition of composite material on these areas of high stress would alter the performance significantly. As a result, the following model, as seen in Figure 6-19, was proposed to be studied. The patches on the sides are 40 mm in height and 30 mm across, and the top patch is 80 mm along the width of the top hat beam, and 30 mm across.

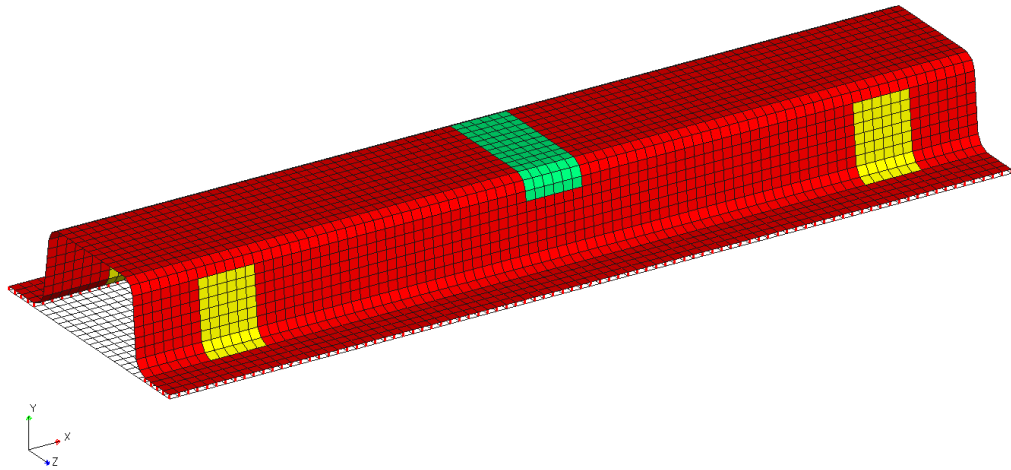


*Figure 6-19: Localised reinforcement using patches of composite material*

*Table 6-5: Stiffness performance of the hybrid samples with local reinforcements compared to the previously tested ones*

Sample make-up		Stiffness K (N/mm)	Weight (g)
DP600	FRP		
0.5 mm	-	870.8	577.4
0.5 mm	Top (full strip)	1601.2	632.0
0.5 mm	Local Reinforcement	1691.6	592.6
0.8 mm	-	2560.8	923.8
0.8 mm	Top (full strip)	3616.6	978.5
0.8 mm	Local Reinforcement	3852.3	939.1

Table 6-5 shows the performance results. These highlight that with a simple, intelligent deployment of composite material it is possible to out-perform a large reinforcement patch, as well as lowering the overall weight. Not only do the samples with local reinforcement have an increased stiffness compared with the hybrid top reinforcement ones, but the composite also covers a smaller surface area, meaning the samples weight less.

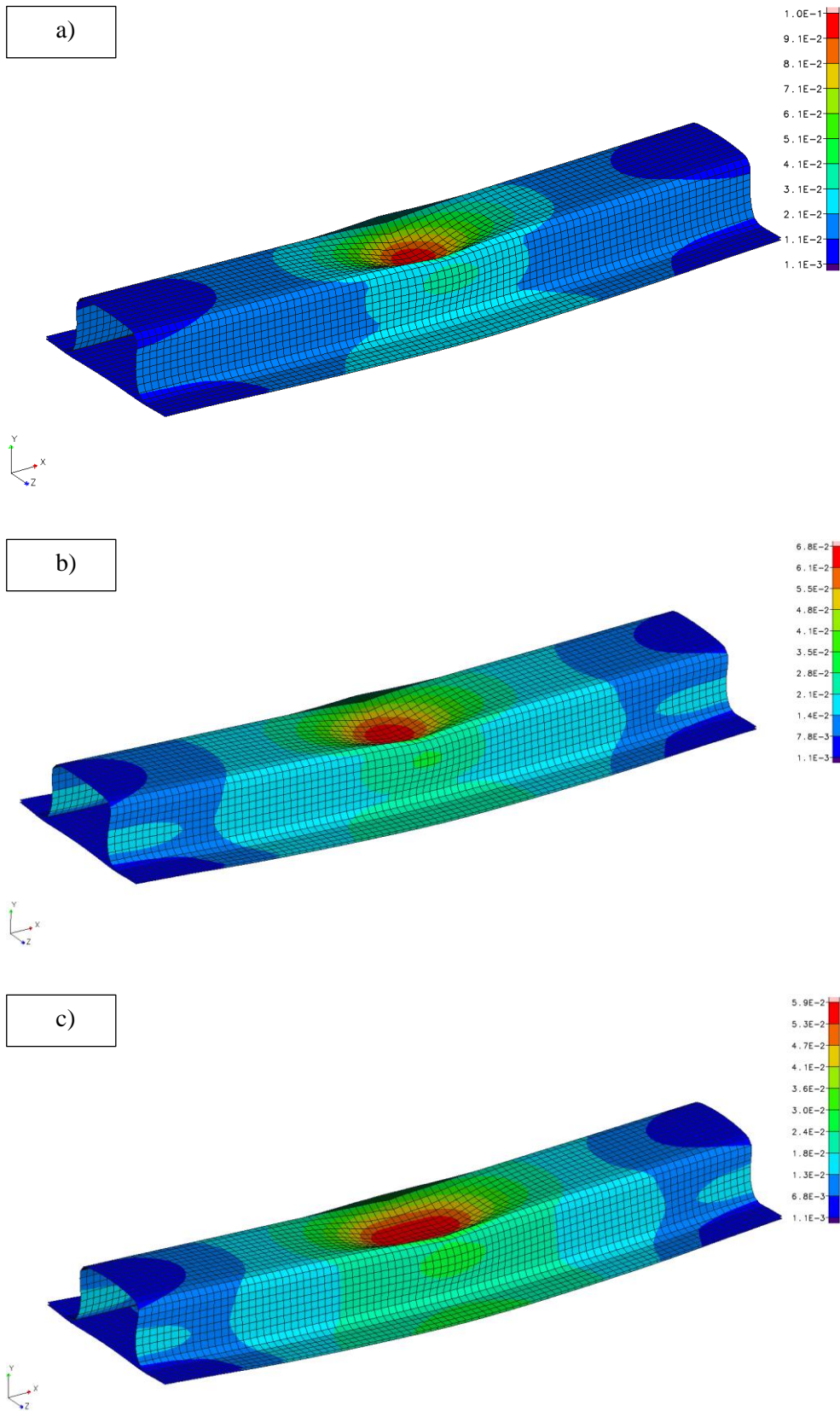


Figure 6-20: Deflection plot for 0.8 mm samples at identical load; a) pure steel, b) top reinforcement, c) local reinforcement – deflections not to scale

Figure 6-20, showing the deflection of the beam with no plastic hinging, also shows that the presence of composite as a localised patch affects the overall localised deflection of the beam.

The pure steel beam displays a maximum deflection 30 % larger than that of the beam with a top reinforcement and 40 % larger than that displayed by the locally reinforced beam. The presence of localised reinforcement allows a spreading of the loading and smaller localised deflections. These deflections are not to scale.

## 6.6 Limitations, Conclusions and Further work

From the results in Chapter 5, a clear benefit is found in terms of stiffness  $k$  in downgauging a steel part and adding a local reinforcement of composite material to the top surface. This also agrees with the findings of Chapter 4.

In light of these experiments, the difficulties in obtaining pure bending in the chosen experimental case without the localised effects of plasticity appear prominent. It is suggested that in further work a detailed investigation of the pure bending in experimental circumstances of this specific geometry would be carried out. It would be interesting for example to study experimental cases that suppress the plastic deformation, either by four-point bend, which provides a section of pure bending between the two impactors, or by creating an impactor with an altered geometry capable of constraining the beam and preventing the plastic hinging. It could be additionally feasible to use a localised composite reinforcement with the same goals. The case tested relates to an intrusion case, which was not the case envisaged by the project in terms of stiffness performance and pure elastic behaviour.

Chapter 6 has highlighted the issues and unforeseen difficulties of creating a model that can accurately predict the performance of the beams given the chosen experiments. The simulation trials and manual optimisation run in Genesis provide vital information as to the effect of the composite patching on the overall beam performance. However, there are limitations inherent to the software which have proven difficult to circumvent, as Genesis is ideal for composite optimisation but proves inadequate for plasticity modelling, and LS-DYNA has the capabilities to model the plasticity problem but does not lend itself as directly to a composite optimisation in terms of topological optimisation as well as layer orientation and thickness.

However, the simulation has shown that the behaviour can be predicted, all-be-it here in a “rough” and slightly unstable manner, giving confidence in both the

material model assumptions from Chapter 4 and the experimental results showing the lightweighting potentials discussed on both the coupon work in Chapter 4 and the component work in Chapter 5.

## 7 SUMMARY

This chapter discusses and summarises the learning outcomes from this body of work.

### 7.1 Discussion of outcomes and limitations to the research

There is a recognised lack of knowledge concerning the fundamental stiffness performance of downgauged steel structures locally reinforced with FRP. Much of research in the field of localised steel FRP reinforced hybrid materials is focused on the retrospective reinforcing of civil engineering structures. Major OEM's in the automotive industry, BMW, JLR, VW to name but a few [2], have shown to use composite and steel combinations in their vehicles. Published research however, either does not provide the overall insight into material performance or focuses on energy absorption and crash scenarios.

This thesis has sought to help fill this gap in knowledge. The aim of this project was to perform fundamental research into the stiffness performance of hybrid metal-FRP materials and quantify the potential for lightweighting through an initial coupon program, followed by a component program, all the while supported by FE. With the trend in the automotive industry towards lightweighting and the effective reducing of vehicle mass, this research is applicable and relevant to both academic and industrial circles, providing under-pinning knowledge and allowing the uptake of hybrid materials in a different form and application.

In the context of this study specifically, an advanced high strength steel DP600 was used. The hybrid samples were made up of 0.5 and 0.8 mm DP600 with a composite reinforcement. The composite reinforcement was a polyamide 6, at 60 % weight fraction (PA6 GF60) of varying lay-ups  $[0,90]_s$ ,  $[45,-45]_s$  and  $[90,0]_s$ .



The following are a summary of the overall outcomes and contributions to knowledge. Additionally, points of interest and further work are discussed. The manufacturing of the samples is presented first, followed by a discussion relevant to the expression of the results followed by a focus on the coupon and component work. This chapter finishes on the outcomes of the simulation and the relevant further work.

### **7.1.1 Manufacture of the hybrid materials**

The manufacturing methods for the hybrid materials were detailed in Chapter 3. Chapters 4 and 5 presented the work specific to the coupon and component samples respectively. The DP600 used in the testing was uncoated, so as to avoid complications relating to bonding. The samples were prepared in the following steps: both materials were prepared for bonding, the steel surface was manually abraded whereas the PA6 GF60 composite used the peel-ply as a surface preparation. All materials were joined using adhesive bonding, three different adhesives were used, all providing satisfactory results. In the context of the component structures, the steel sheets were press-formed prior to the composite reinforcement being added. Monolithic steel samples, referred throughout the thesis as “pure steel samples”, were also produced for benchmarking purposes. Samples produced are summarised Table 7-1 for both the component and coupon test programmes.

The samples produced repeatable results in testing, giving confidence in the techniques used. The process, however, was manually intensive and time consuming, and would not be applicable to a high volume manufacturing environment. A similar process would need to be trialled and optimised for such an application, although this was out of scope for this project.

Type of test	Material	Orientation	Coupon	Component
	DP600 steel	PA6 GF60		
Benchmarking	-	[0,90] <sub>s</sub>	✓	
	-	[45,-45] <sub>s</sub>	✓	
	-	[90,0] <sub>s</sub>	✓	
	0.8 mm	-	✓	✓
	1.0 mm	-	✓	✓
	1.6 mm	-	✓	✓
Hybrid		[0,90] <sub>s</sub>	✓	✓
	0.5 mm	[45,-45] <sub>s</sub>	✓	
		[90,0] <sub>s</sub>	✓	
		[0,90] <sub>s</sub>	✓	✓
	0.8 mm	[45,-45] <sub>s</sub>	✓	
		[90,0] <sub>s</sub>	✓	

*Table 7-1: Summary of all fabricated samples*

All testing was undertaken following adapted standard procedures [95, 96], at quasi-static speeds of  $v = 1$  mm/min in three-point bend fixtures tailored to the samples.

### 7.1.2 Expressing the stiffness performance

The results were difficult to express consistently throughout the thesis, not only to ensure a direct comparison of results amongst themselves but to provide a useful tool to both the reader and industrial partners. There are subtleties associated with expressing the stiffness of the parts tested as there is a double stiffness effect due to the sample hybridisation. The samples present both a material stiffness and a geometric stiffness. As such, the stiffness is either a material property, expressed well by the Ludke criterion  $\sqrt[3]{E}/\rho$  or by the bending modulus  $E_{\text{bend}} = L^3 k/48 I$ ; or a geometrical (and material) property, expressed well by  $k$ , the gradient of the elastic region of the load-extension curve of such samples, and the measure of the sample's ability to resist deformation.

Neither Ludke's criterion or the bending modulus are particularly adapted to the expressing of stiffness of a locally reinforced part as Ludke's criterion depends on a

value of Young's modulus and density averaged over the component, the bending modulus is dependent on the span, modulus and value of  $I$ . Ludke's criterion, when normalised to steel, enables the expression of the material performance from a characteristic perspective. It shows a comparative performance of the materials. It is applicable only to materials with a constant cross-section. The bending modulus  $E_{\text{bend}}$  presents itself with the same issue, and required the materials used to be of a constant cross-section. The gradient of the load-extension curve  $k$ , presents itself throughout as the best expression of stiffness. In identical test environments, it gives an accurate understanding of the hybrid sample performance, and provides data applicable to industrial needs.

Regarding industrial applications of this knowledge, in a scenario where size and geometry are likely to be primary considerations, a combination of all three stiffness expressions would provide thorough information regarding the selection of materials.

In further work, it would be interesting to investigate the creation of a mathematical concept or graph expressing the stiffness of a complex geometry in terms of its gradient  $k$ , the "engineering" stiffness, as well as the weight of the samples, and the nature of the reinforcement patch (thickness, orientation, etc).

### **7.1.3 Quasi-static coupon testing**

Hybrid coupon samples were produced, from 0.5 and 0.8 mm DP600 and composite lay-ups of  $[0,90]_s$ ,  $[45,-45]_s$  and  $[90,0]_s$  orientation. These were tested in quasi-static three-point bend to assess the performances of the material in stiffness. The results were expressed both in terms of Ludke's criterion (showing the stiffness performance of the steel can be improved by up to 44 % when reinforcing with a balanced 4 layer GF60 PA6) and engineering stiffness  $k$  (showing that for a matched

stiffness performance, GFRP hybrid coupons can present a weight save of up to 30 % in tested samples).

Simulation was done in both LS-DYNA and Genesis, giving a generally trustworthy prediction of the performance, always within 11 % of the experimental data. This predicted data is shown in Figure 7-1.

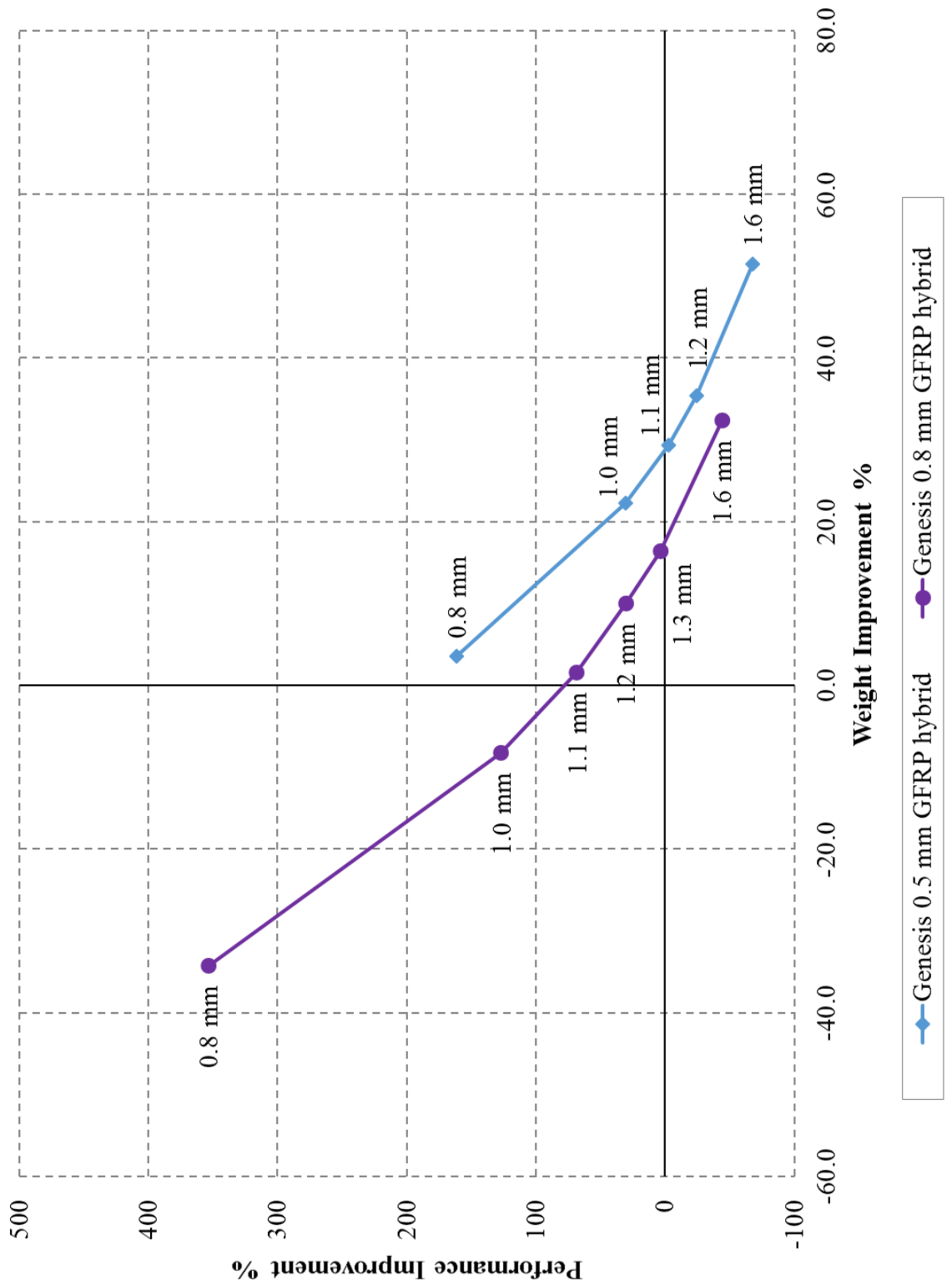


Figure 7-1: The performance and weight “improvements” of the GFRP hybrid samples compared to the pure steel ones (reshown Figure 4-28)

Figure 7-1 highlights the main conclusions from the GFRP coupon stage testing (1.6 and 0.8 mm pure steel samples) and simulation (1.3, 1.2, 1.1 and 1.0 mm pure steel samples), explained as follows. Every data point on the curve represents the performance of the hybrid sample compared to the performance of the labelled thickness of pure steel sample. The values used for 1.6 and 0.8 mm pure steel samples were obtained experimentally, and the values used for 1.3, 1.2, 1.1, 1.0 mm pure steel samples were obtained through simulation. The 0.5 mm hybrid coupon presents a similar stiffness performance to a 1.1 mm pure steel counterpart, at approximately 30 % weight save and the 0.8 mm hybrid sample presents a similar performance to a 1.3 mm pure steel counterpart at an approximate 17 % weight save.

Additionally, it was noted that the orientation of the outer layer of fibres has a large effect on the stiffness and on the energy absorption mechanism and failure of the samples. The  $[0,90]_s$  hybrid samples out-performed the  $[90,0]_s$  and  $[45,-45]_s$ . The  $[45,-45]_s$  presented the lowest yield strength, no sharp fibre failure and were observed in tests to rotate so as to present a lower resistance to the deflection (lower energy state).

The simulation and material model assumptions were deemed acceptable for the modelling of the elastic region of hybrid steel composite coupons as they presented a satisfactory level of correlation.

From the literature review, Michael Dlugosch presents work closest related to that presented here. His work [28], in partnership with BMW, focuses mainly on the energy absorption of hybrid materials for front impact. He presents initial coupon work which is comparable to that performed here, although never focuses on the lightweighting potential, only on the increase in energy absorbed. His tests use a dual phased steel and a hardened boron steel as well as glass and carbon fibre pre-pregs. His samples were 1.5 mm steel and varying thicknesses and lay-ups of composite.

His work correlated with results presented here on a number of points:

- the orientation of the composite affects the performance of the coupons
- the hybridisation of a sample increases the UTS load and extension to failure of both the steel and the composite when combined
- a stepwise laminate fracture is observed through failure, in the composite layers
- the coupons in steel-over-composite and composite-over-steel scenarios present very similar responses

His work noted the gap in literature when considering fundamental understandings of hybrid steel-FRP materials, as well as a lack of standardised means of expressing stiffness, although he picked the use of  $E_{\text{bend}}$  to express his results in the context of his coupon-only work.

His work included useful notes to the extended and further work on coupon samples where “the overall stiffness decreases with a rising cross-sectional share of the less stiff FRP-phase”. It would be suggested that in further work to this thesis both the 0.5 mm and 0.8 mm hybrids be tested with varying thicknesses of composites, to replicate this finding and further quantify this effect with reference to lightweighting. His results also indicate that the hybrid performance difference between GFRP and CFRP reinforced samples is minimal, as the behaviour is dominated by the steel. This is also noted in the context of this thesis, where the samples perform similarly, however the CFRP samples are notably lighter (0.5 mm hybrids 14.3 % lighter CFRP compared to GFRP and 0.8 mm hybrids 19 % better performance for 8 % lighter CFRP compared to GFRP – See Tables 4-11 and 4-12). This differing performance between fibres of varying nature highlights another area needing further investigation contributing to the thorough understanding of the lightweighting potential in a stiffness critical performance of hybrid steel-FRP materials. However, the work in this thesis has shown, for the first time, a

quantification of the lightweighting potential associated with the use of FRP combined with a downgauged steel whilst matching the stiffness performance of the pure steel equivalent. It has also provided an associated material simulation for the use of FRP composites reinforcing a downgauged steel coupon. It has been noted that other literature focuses on the hybridisation of coupon shaped composites, using glass and carbon in conjunction, focusing on stiffness for energy absorption and cost [76-80]. In further studies, these hybrid composites could be used in conjunction with the steel in a global hybrid study.

#### **7.1.4 Quasi-static component testing**

Using an idealised automotive component geometry, hybrid component samples were produced. These were from 0.5 and 0.8 mm DP600, and [0,90]<sub>s</sub> PA6 GF60 GFRP reinforcement along the top section of the component. The components were tested in quasi-static three-point bend to assess overall performance. This component geometry and test method is also used in published literature, providing benchmark data and adding confidence in the results [87, 88]. There has however been no literature found directly studying the stiffness performance of hybrid steel-FRP beams. There have been studies investigating both the pure steel and pure composite equivalents, as well as other materials [87, 88].

In the context of component testing, the results were analysed and compared based on the value of stiffness  $k$ . The samples were tested in identical conditions so that the results could be directly compared. The component is seen to plastically deform around the impactor site, causing a plastic hinge to form. The bending stiffness as expressed by  $k$  is a reflection of both the material stiffness and geometrical stiffness.



The samples were not tested to global failure; however, the deformation patterns were observed as well as the effect of the hybridisation. The presence of composite reinforcement is seen to alleviate some of the plastic hinging damage that the beams incur during the tests. The areas affected are larger, however the damage is less severe. [70, 88, 106, 108] are but a few to have noted this plastic-elastic kinking hinge effect appearing on thin walled structures during deformation.

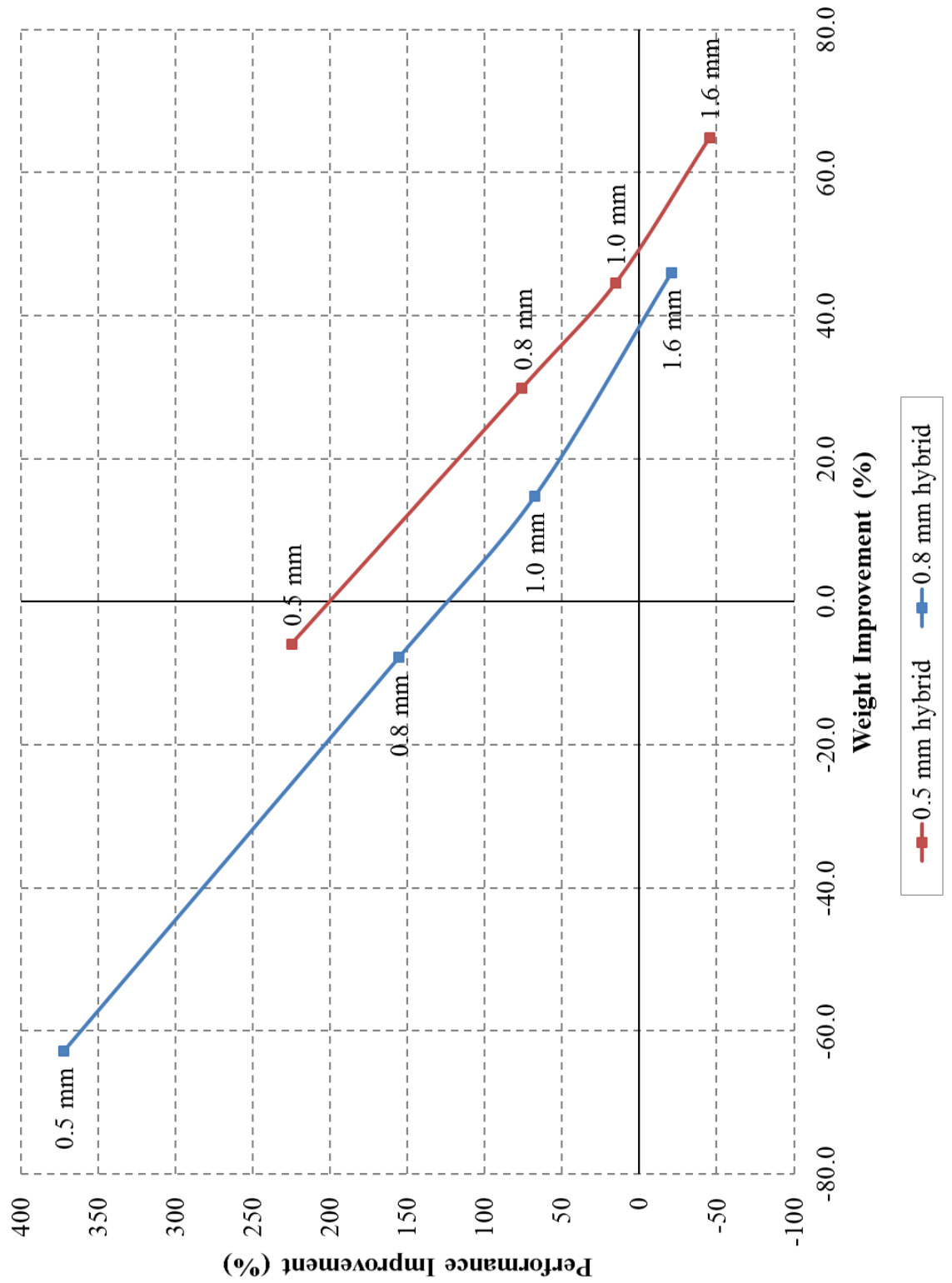


Figure 7-2: The performance and weight “improvements” of the hybrid samples compared to the pure steel ones – reshown Figure 5-18

Figure 7-2 plots both percentage weight gain and stiffness  $k$  benefit for the 0.5 and 0.8 mm hybrid samples compared to the pure steel ones. It shows that there is a distinct potential for using FRP to reinforce steel in an intelligent deployment of composite material implying the structure can be optimised and lightweighted. Indeed, the 0.5 mm hybrid sample provides a 15 % (y-axis reading) increase in performance over the 1.0 mm pure steel sample, whilst also providing a 44 % (x-axis reading) weight save. It is estimated from Figure 7-2 that a 1.1 mm pure steel sample would provide an identical stiffness response as the 0.5 mm hybrid, where the hybrid would weigh up to 50 % less.

The data collected has shown that for a given composite reinforcement, it is possible to create graphs indicating the “cut-off” areas of performance benefit, Figure 7-2 being such an example.

In further work, it would be interesting to investigate the nature of the composite reinforcement in terms of thickness, as the comparative effect of a 1.2 mm FRP patch would be more notable on a 0.5 mm steel than on a 0.8 mm steel. There are a range of scenarios where the hybrids would be dominated by a specific material, and establishing the boundary between material effect domination (either steel or composite) and geometrical domination would be a valuable area of further research leading towards an application to manufacturing.

### **7.1.5 FEA predictions**

Finite element modelling was used to simulate the stiffness behaviour of the tested models and to predict the performance of the hybrid and monolithic materials. Two software packages were used, LS-DYNA and Genesis.

In the coupon stage of the simulation, the material model was shown in both LS-DYNA and Genesis to predict the results with reasonable confidence (within 11 %).

Several assumptions were trialled, with the most successful being the assumption to model both materials inside a singular part (P\_COMP and PART\_COMPOSITE), ignoring the presence of adhesive and taking advantage of the inbuilt function of the software. As it presented the highest level of correlation, the model created following this assumption was carried forward and used to model the elastic region of the hybrid steel composite coupons. Additionally, as it provided the most accurate and least computationally expensive results, the simulation was carried forward in Genesis.

At component level, geometric interactions proved the idealised pure elastic Genesis model to be insufficient. The purely elastic model run by the software over-predicted the performance. Additionally, Genesis does not include an ongoing calculation of stiffness as it is calculated at the start of the simulation and does not consider any later changes in geometry. In LS-DYNA, it was shown to be possible to create a model that considers the early onset of plasticity. Literature [102] has shown that the FE modelling of a quasi-static component in terms of geometry, contacts, etc. is a complex process. Achieving a stable and accurate model is possible through a lengthy iterative process. The models used in the context of this work show the prediction of the plasticity to be unstable but within the envelope spread of the experimental results.

In light of these experiments, the difficulties in obtaining experimental pure bending without the localised effects of plasticity were prominent. In further work, a detailed investigation of experimental pure bending scenarios is recommended. This could involve for example four-point bend scenarios, a modification of the impactor or a geometrical alteration in the sample allowing for pure bending in testing. It would be interesting to study experimental cases that suppress the plastic deformation, either by four-point bend, which provides a section of pure bending between the two impactors, or by creating an impactor with an altered geometry

capable of constraining the beam and preventing the plastic hinging. It could be additionally feasible to use a localised composite reinforcement with the same goals.

It is worth noting that a material model has been proven to be effective at the prediction of the hybrid material performance, but that further simulations were hampered by the software limitations and unforeseen geometrical effects. This is additionally an indication of the potential application of this intelligent deployment of composite materials, as by downgauging the steel, the structure is more vulnerable to intrusions, therefore the application would need to be to a structure in global bending with limited localised effects.

## **8 CONCLUSIONS AND PERCEIVED CONTRIBUTION TO KNOWLEDGE**

This thesis has examined the potential for lightweighting provided by the intelligent deployment of composite materials on steel parts for matched stiffness performance. This is previously undescribed in the literature.

The results show that hybrid materials can provide a matched stiffness performance to their pure steel counterparts whilst being lighter. This lightweighting potential was shown both at coupon level as well as applied to an idealised automotive part. Simulation models for the hybrid material proved performance to be predictable when deformations were entirely constrained to an elastic behaviour. However, despite the hybrid material being accurately predicted, geometrical effects presented additional complications, and the hybrid effects on the global performance are indicative only.

The thesis, in combination with the literature review shows that this is an industry-relevant topic, and with potential to find its application in future optimised lightweight vehicles.

For the materials studied, DP600 and PA6 GF60, it was shown that:

- The intelligent deployment of FRP offers significant lightweighting potential compared to steel-only structures
- It is possible to downgauge a steel component and then locally reinforce with FRP patches to achieve matched stiffness at 30 % overall weight save
- It has been shown that a 30 % weight save is valid for both coupon and component level tests
- Coupon and component simulation has been developed which cross-validates experimental tests

- The simulated material model could be exploited by CAE automotive design for lightweight vehicles

The lightweight potential of 30 % would be expected to rise when reinforcing with other materials, such as CFRP. Early investigations indicate a 40 % lightweighting potential.

## **9 WIDER IMPLICATIONS OF FRP STEEL HYBRID UPTAKE IN BIW**

Uptake of steel-FRP hybrids, in the form of patches, in BIW application as well as other automotive parts would also need to undertake the following testing and investigations. Note these are only a representation of the research that could be applied to the topic, and are a reflection of the feedback and discussions that arose throughout the duration of the thesis.

- Full material properties – all samples were investigated purely in stiffness, a full characterisation would be necessary prior to industrial uptake.
- Bond strength – the bonds would need evaluating to establish performance and optimise their nature (UTS and fatigue). A full study of the adhesive bonding to both the steel and composite substrates would be needed (mechanical locking vs covalent bonding) as well as a surface preparation study.
- Noise and vibration – the used of specially designed composite patches could not only provide a stiffness reinforcement but also a noise and vibration damper.
- Fatigue – the fatigue life of a composite material is different to that of steel, and self-healing nano-composites could be a viable solution – a full life cycle assessment would be needed. Additionally, composite materials and steel have differing degradations of their properties through their lifetimes.
- Corrosion – the presence of both glass and carbon fibres near a steel surface could cause additional corrosion issues that would need further investigating and mitigating.
- Thermal mismatch – the composite and steel have varying coefficients of thermal expansion, and although those have not been an issue through the tests performed here, they could become problematic in an automotive build



cycle, where the BIW undergoes heating and cooling (paint cycle for example).

- Varying fibres – varying the nature of the fibres and the matrix would provide further knowledge towards the optimal choice of material, as well as location, size and nature. An Ashby-type diagram of all hybrid performance would be invaluable.
- Varying metallic substrate - the effect of gauge changes on the “thin walled effect” [110] and their vulnerability to intrusion and localised damage must be taken into consideration, showing that the weight advantage of aluminium over steel can be decreased by properly locating reinforcements on downgauged steel sections. Again, an Ashby-type diagram of all hybrid performance would be invaluable.
- Cost analysis – an investigation into the cost benefit of the application of hybrid materials to BIW structures over the lifetime of the vehicle.
- Recycling – an environmental impact assessment would provide the knowledge towards the end-of-life aspect of hybrid applications.
- Risk Based Design – approaching the design of the vehicle from a risk-based and probabilistic approach rather than the current empirical one would yield interesting results, and potentially show areas where hybrid materials are at their most effective.
- Manufacturing aspects – a study into the implementation and applicability of the knowledge to a high volume manufacturing environment.

A third year Master’s thesis study is proposed on the effect of rolling direction and fibre direction on the stiffness and strength performance of geometrically identical samples. In addition to the fibre directions presented in this work, the rolling direction would vary in each case, at 0°, 45° and 90° to the sample length.

Additionally, a study into the surface preparation and conditioning for adhesive bonding would contribute to the understanding of the hybrid bond.

## 10 REFERENCES

1. Clough, A. and T. Baxter, *Past, current and future automotive markets for carbon fibre reinforced plastics*. 2013, Tata Steel.
2. Clough, A., *European automotive materials, current material choice and long term trends*. 2015, Tata Steel: Tata Steel.
3. Audi. *Audi A5 Sportback*. 2009 [cited 2013 12/12].
4. United Nations Framework Convention on Climate Change. *United Nations Framework Convention on Climate Change*. 2013 [cited 2013 11/12/2013].
5. UNFCCC. *Kyoto Protocol*. 2013 [cited 2013 11/12/2013].
6. UNFCCC. *Paris Agreement*. 2015 [cited 2016 02/11/2016].
7. National Association of Clean Air Agencies, *Background and History of EPA Regulation of Greenhouse Gas (GHG) Emissions Under the Clean Air Act & National Association of Clean Air Agencies' Comments on EPA GHG Regulatory and Policy Proposals*. 2013, National Association of Clean Air Agencies.
8. An, F., Gordon, D., He, H., Kodjak, D., Rutherford, D., *Passenger vehicle greenhouse gas and fuel economy standards: a global update*. 2007, The International Council on Clean Transportation: [www.theicct.org](http://www.theicct.org).
9. SMMT, *New Car CO2 Report 2013*, The Society of Motor Manufacturers and Traders Limited, Editor. 2013.
10. Davies, G., *Materials for Automotive Bodies*. 2nd Revised edition ed. 2012: Butterworth Heinemann.
11. Stewart, R., *Lightweighting the automotive market*. Reinforced Plastics, 2009. 53(2): p. 14-21.
12. Messler Jr, R.W., *The challenges for joining to keep pace with advancing materials and designs*. Materials & Design, 1995. 16(5): p. 261 - 270.
13. Cui, X., Zhang, H., Wang, S., Zhang, L., Ko, J., *Design of lightweight multi-material automotive bodies using new material performance indices of thin-walled beams for the material selection with crashworthiness consideration*. Materials and Design, 2011. 32: p. 815 - 821.
14. Burgess, S.C., Pasini, D., Smith, D., J. Alemzadeh, K., *A general solution to the material performance index for bending strength design*. Materials and Design, 2006. 27: p. 1046 - 1054.
15. Das, S., *The cost of automotive polymer composites: a review and assessment of the Department of Energy's lightweight materials composite research*, U.S. Department of Energy, Editor. 2001, Oak Ridge National Laboratory.
16. European Parliament and Council, *Directive 2000/53/EC of the European Parliament and of the Council of 18 September 2000 on end-of life vehicles* - Commission Statements OJ L 269, 21.10.2000, p. 34-43 2000: <http://eur-lex.europa.eu/LexUriServ/LexUriServ.do?uri=CELEX:32000L0053:EN:NOT>.

17. Lake, K. *The Importance of Educating our Future Engineers in Optimisation*. in 2013 Optimised Product Engineering Conference. 2013. Motor Heritage Centre, Gaydon: <http://www.grm-consulting.co.uk/index.php/conf-agenda/>.
18. Catapult. *Introducing the Catapults*. 2016 [cited 2016 13/06/2016].
19. Mayyas, A.T., Qattawi, A., Mayyas, A. R., Omar, Mohammed A., *Life cycle assessment-based selection for a sustainable lightweight body-in-white design*. Energy, 2012. 39(1): p. 412-425.
20. Mallick, P.K., Horvath, C. D., Benedyk, J. C., Powell, B. R., Kridli, G. T., Boileau, J. M., Das, S., Deb, A., *Materials, Design and Manufacturing for Lightweight Vehicles*. 2010: Woodhead Publishing Ltd.
21. LANXESS, *Hybrid-Front End Ford Focus*, Technical information, Semi-Crystalline Products. 2008: [www.durethan.com](http://www.durethan.com).
22. Marechal, L., *New metal plastic technology for front end modules*. Thermal Systems & Climate control, re-printed by SAE Technical Paper Series, 2006.
23. Corporation, L. *Plastic/Metal Hybrid Technology*. 2005 [cited 2016].
24. Eckstein, L., Ickert, L., Goede, M., Dölle, N., *Lightweight floor structure with reinforcements of CFRP and GFRP*, in ATZ Worldwide. 2011.
25. Goede, M. and M. Stehlin. *SuperLIGHT-Car project - An integrated research approach for lightweight car body innovations*. in Innovative Developments for Lightweight Vehicle Structures. 2009. Wolfsburg, Germany: Volkswagen AG.
26. Frantz, M., C. Lauter, and T. Troster, *Advanced manufacturing technologies for automotive structures in multi-material design consisting of high-strength steels and CFRP*, in 56th International Scientific Colloquium, Ilmenau University of Technology. 2011, TU Ilmenau.
27. Lauter, C., J. Niewel, and T. Troester, *Quasistatic and crash tests of steel-CFRP hybrid pillar structures for automotive applications*. Int. J. Automotive Composites, 2014. 1(1).
28. Dlugosch, M., Lukaszewicz, D., Fritsch, J., Hiermaier, S. *Mechanical characterization of hybrid material systems consisting of sheet metal and advanced composites*. in 20th International Conference on Composite Materials. 2015. Copenhagen.
29. Bambach, M.R. and M. Elchalakani, *Plastic mechanism analysis of steel SHS strengthened with CFRP under large axial deformation*. Thin-Walled Structures, 2007. 45(2): p. 159-170.
30. Haedir, J., Zhao, X-L., Grzebieta, R. H., Bambach, M. R., *Non-linear analysis to predict the moment–curvature response of CFRP-strengthened steel CHS tubular beams*. Thin-Walled Structures, 2011. 49(8): p. 997-1006.
31. Haedir, J., Bambach, M. R., Zhao, X. L., Grzebieta, R. H., *Strength of circular hollow sections (CHS) tubular beams externally reinforced by carbon FRP sheets in pure bending*. Thin-Walled Structures, 2009. 47(10): p. 1136-1147.

32. Dong, C., *Experimental Study of Strengthening of Steel Structures with Fiber Reinforced Plastic*. Curtin University of Technology.
33. Uriayer, F.A.J., *The new Steel-CFRP composite specimen (CFRP laminates sandwiches between two strips) and its behaviour under uniaxial tension*. International Journal of Civil, Environmental, Structural, Construction and Architectural Engineering, 2013. 7(1).
34. Sadighi, M., R.C. Alderliesten, and R. Benedictus, *Impact resistance of fiber-metal laminates: A review*. International Journal of Impact Engineering, 2012. 49: p. 77-90.
35. Mildner, C., *Numerische und experimentelle Untersuchungen des Crashverhaltens von FVK-verstärkten Metallstrukturbauteilen*. 2013, Technische Universität München.
36. Sachan, S., *Effect of Fibre Directionality on the Strength of Adhesively Bonded Joints*. 2015: School of Mechanical Sciences, Indian Institute of Technology, Bhubaneshwar, Odisha.
37. Marsh, G. *Carbon composite car body panels gain traction with Gurit Automotive*. 2011 [cited 2015 May 2015].
38. Griffiths, D. *Gurit CBS for Aston Martin DBS*. 2010 [cited 2016.]
39. Gurit. *Automotive Materials Sprint Car Body Sheet*. 2016 [cited 2016.]
40. Brosius, D. *Carbon Fiber Goes Mainstream Automotive*. 2003 [cited 2016 November].
41. Jacob, A. *Composites-intensive Chrysler SRT Viper wins SPE award*. 8 November 2012 [cited 2016 November].
42. Ary Subagia, I.D.G., Kim, Y., Tijjing, L. D., Kim, C. S., Shon, H. K., *Effect of stacking sequence on the flexural properties of hybrid composites reinforced with carbon and basalt fibers*. Composites Part B: Engineering, 2014. 58: p. 251-258.
43. Baker, A.A., *Fibre composite repair of cracked metallic aircraft components - practical and basic aspects*. Composites Part A: Applied Science and Manufacturing, 1987. 18(4): p. 293 - 308.
44. Meier, U., *Strengthening of structures using carbon fibre/epoxy composites*. Construction and Building Materials, 1995. 9(6): p. 341-351.
45. Frank, R. *Developing Lightweight Modules for Transport Systems featuring Efficient Production and Life-cycle Benefits at Structural and Functional Integrity using Risk-based Design*. 2006 [cited 2013 March 2013].
46. Cao, J. and J.L. Grenestedt, *Design and testing of joints for composite sandwich/steel hybrid ship hulls*. Composites Part A: Applied Science and Manufacturing, 2004. 35(9): p. 1091 - 1105.
47. Cao, J., J.L. Grenestedt, and W.J. Maroun, *Steel truss/composite skin hybrid ship hull. Part I: Design and analysis*. Composites Part A: Applied Science and Manufacturing, 2007. 38(7): p. 1755-1762.

48. Maroun, W.J., J. Cao, and J.L. Grenestedt, *Steel truss/composite skin hybrid ship hull, Part II: Manufacturing and sagging testing*. Composites Part A: Applied Science and Manufacturing, 2007. 38(7): p. 1763-1772.
49. Nateghi-Alahi, F. and M. Khazaei-Poul, *Experimental study of steel plate shear walls with infill plates strengthened by GFRP laminates*. Journal of Constructional Steel Research, 2012. 78: p. 159-172.
50. Nestmann, F., Schlangen, E., As'ad, S., Nateghi-Alahi, F., Khazaei-Poul, M., *The 2nd International Conference on Rehabilitation and Maintenance in Civil Engineering (ICRMCE) Analytical Study on the Strengthened Steel Plate Shear Walls by FRP Laminate*. Procedia Engineering, 2013. 54: p. 377-386.
51. Zhao, X.-L., *FRP-Strengthened Metallic Structures*. 2014: CRC Press, Taylor & Francis Group.
52. Zhao, X.-L. and L. Zhang, *State-of-the-art review on FRP strengthened steel structures*. *Engineering Structures*, 2007. 29(8): p. 1808 - 1823.
53. Teng, J.C., T. Yu, and D. Fernando, *Strengthening of steel structures with fibre-reinforced polymer composites*. Journal of Constructional Steel Research, 2012. 78: p. 131 - 143.
54. Schnerch, D., Dawood, M., Rizkalla, S., Sumner, E., Stanford, K., *Bond Behavior of CFRP Strengthened Steel Structures*. *Advances in Structural Engineering*, 2006. 9(6): p. 805 - 817.
55. Haghani, R. and M. Al-Emrani, *A new design model for adhesive joints used to bond FRP laminates to steel beams – Part A: Background and theory*. Construction and Building Materials, 2012. 34(0): p. 486-493.
56. Haghani, R. and M. Al-Emrani, *A new design model for adhesive joints used to bond FRP laminates to steel beams: Part B: Experimental verification*. Construction and Building Materials, 2012. 30(0): p. 686-694.
57. Anyfantis, K.N. and N.G. Tsouvalis, *Loading and fracture response of CFRP-to-steel adhesively bonded joints with thick adherents - Part I: Experiments*. Composite Structures, 2013. 96: p. 850-857.
58. Anyfantis, K.N. and N.G. Tsouvalis, *Loading and fracture response of CFRP-to-steel adhesively bonded joints with thick adherents - Part II: Numerical simulation*. Composite Structures, 2013. 96: p. 858-868.
59. Colombi, P. and C. Poggi, *Strengthening of tensile steel members and bolted joints using adhesively bonded CFRP plates*. Construction and Building Materials, 2006. 20(1–2): p. 22-33.
60. Hollaway, L.C. and J. Cadei, *Progress in the technique of upgrading metallic structures with advanced polymer composites*. Progress in Structural Engineering and Materials, 2002. 4(2): p. 131–148.
61. Cadei, J.M.C., Stratford, T. J., Hollaway L. C., Duckett, W. G., *Strengthening metallic structures using externally bonded fibre-reinforced polymers*. Vol. C 595. 2004, London: CIRIA.

62. Photiou, N., L.C. Hollaway, and M.K. Chryssanthopoulos, *Strengthening of an artificially degraded steel beam using a carbon/glass composite system*, in *Advanced Polymer Composites for Structural Applications in Construction*. 2004, Woodhead Publishing. p. 274-283.
63. Dawood, M., *Fiber-reinforced polymer (FRP) composites for strengthening steel structures*, in *Developments in Fiber-Reinforced Polymer (FRP) Composites for Civil Engineering*. 2013, Woodhead Publishing. p. 382-409.
64. Dawood, M., *Durability of steel components strengthened with fiber-reinforced polymer (FRP) composites*, in *Rehabilitation of Metallic Civil Infrastructure Using Fiber Reinforced Polymer (FRP) Composites*. 2014, Woodhead Publishing. p. 96-114.
65. Matta, F. and Dawood, M., *Rehabilitation of steel tension members using fiber-reinforced polymer (FRP) composites*, in *Rehabilitation of Metallic Civil Infrastructure Using Fiber Reinforced Polymer (FRP) Composites*. 2014, Woodhead Publishing. p. 169-200.
66. Dawood, M., M.W. El-Tahan, and B. Zheng, *Bond behavior of superelastic shape memory alloys to carbon fiber reinforced polymer composites*. *Composites Part B: Engineering*, 2015. 77: p. 238-247.
67. Rizkalla, S., M. Dawood, and D. Schnerch, *Development of a carbon fiber reinforced polymer system for strengthening steel structures*. *Composites Part A: Applied Science and Manufacturing*, 2008. 39(2): p. 388-397.
68. Schnerch, D., Dawood, M., Rizkalla, S., Sumner, E., *Proposed design guidelines for strengthening of steel bridges with FRP materials*. *Construction and Building Materials*, 2007. 21(5): p. 1001-1010.
69. Jung, K.W., Kawahito, Y., Takahashi, M., Katayama, S., *Laser direct joining of carbon fiber reinforced plastic to zinc-coated steel*. *Materials & Design*, 2013. 47(0): p. 179-188.
70. Belingardi, G. and A. Scattina, *Experimental investigation on the bending behaviour of hybrid and steel thin walled box beams— The role of adhesive joints*. *International Journal of Adhesion and Adhesives*, 2013. 40: p. 31-37.
71. Gurit, *Guide to composites*. 2013, Gurit: <http://www.gurit.com/guide-to-composites.aspx>.
72. Hughes, D.J., *Trade study on current state-of-art composite surface preparation technology*, 2013, AMRC Integrated Manufacturing Group: WMG, Personal communications.
73. Ebnesajjad, S., *Handbook of Adhesives and Surface Preparation*. PDL Handbook Series, ed. S. Ebnesajjad. 2011, Oxford: William Andrew Publishing. ii.
74. Ucsnik, S., Scheerer, M., Zaremba, S., Pahr, D. H., *Experimental investigation of a novel hybrid metal-composite joining technology*. *Composites Part A: Applied Science and Manufacturing*, 2009. 41(3): p. 369-374.
75. Lüdke, B., *Funktionaler Rohkarosserie-Leichtbau am Beispiel der neuen BMW-Generation*. *Stahl und Eisen*, 1999. 119(5): p. 123-128.

76. Dong, C. and I.J. Davies, *Flexural and tensile moduli of unidirectional hybrid epoxy composites reinforced by S-2 glass and T700S carbon fibres*. *Materials & Design* (1980-2015), 2014. 54: p. 893-899.
77. Dong, C., H.A. Ranaweera-Jayawardena, and I.J. Davies, *Flexural properties of hybrid composites reinforced by S-2 glass and T700S carbon fibres*. *Composites Part B: Engineering*, 2012. 43(2): p. 573-581.
78. Kalantari, M., C. Dong, and I.J. Davies, *Multi-objective robust optimisation of unidirectional carbon/glass fibre reinforced hybrid composites under flexural loading*. *Composite Structures*, 2016. 138: p. 264-275.
79. Dong, C. and I.J. Davies, *Optimal design for the flexural behaviour of glass and carbon fibre reinforced polymer hybrid composites*. *Materials & Design*, 2012. 37: p. 450-457.
80. Dong, C., *Uncertainties in flexural strength of carbon/glass fibre reinforced hybrid epoxy composites*. *Composites Part B: Engineering*, 2016. 98: p. 176-181.
81. Tata Steel, *Pocket book of steel*. 3rd ed, ed. T. Steel. 2009, University of Warwick: Tata Steel.
82. Tata Steel, *DP600 Data Sheet*. 2013, Tata Steel: [www.tatasteelautomotive.com/aurora](http://www.tatasteelautomotive.com/aurora).
83. Standards, B., *Metallic materials. Tensile testing. Method of test at ambient temperature* BS EN ISO 6892-1:2009. 2009.
84. Sharma, S., *Sandwich steels for crash energy absorption applications*, in WMG. 2014, University of Warwick, PhD Thesis.
85. Beaumont, R., *Determining the Effect of Strain Rate on the Fracture of Sheet Steel* in WMG. 2012, University of Warwick, PhD Thesis.
86. ICCM. 20th International Conference on Composite Materials. in 20th International Conference on Composite Materials. 2015. <http://www.iccm20.org/proceedings>: MCI Scandinavia.
87. Reynolds, N. and A.B. Ramamohan, *High volume thermoplastic composite technology for automotive structures*. 2013, WMG: Materials and Manufacturing Group, Unpublished material.
88. Tomlin, O. and N. Reynolds, *Validation of a Thermoplastic Composite Material Model for Low Carbon Vehicle Applications*, in 9th European LS-DYNA Conference. 2013: Manchester.
89. Reynolds, N., *PA6-GF60 UD ply properties*. 2013, WMG: Materials and Manufacturing Group, Personal communications.
90. Reynolds, N., *PA6-CF60 UD ply properties*. 2014, WMG: Materials and Manufacturing Group, Personal communications.
91. Hughes, D.J., *DSC S10 cures*. 2013, Materials and Manufacturing Group, Personal Communications, WMG.
92. Ascroft, H., *Lap-shear extension curves*. 2014: Materials and Manufacturing Group, Personal communications, WMG .



93. Das, A., *Springback investigation through scanning and deviation map creation*. 2016: Materials and Manufacturing Group, Personal communications, WMG.
94. British\_Standards, *Fibre-reinforced plastic composites — Determination of apparent interlaminar shear strength by short-beam method*. 1998.
95. British\_Standards, *Fibre-reinforced plastic composites — Determination of flexural properties* BS EN ISO 14125:1998 + A1:2011. 1998.
96. ASTM, D7264/D7264 M Flexural properties of polymer matrix composite materials. 2007, ASTM International.
97. LSTC. The differences between implicit and explicit control cards. 2016 [cited 2016 March 2016].
98. LSTC, *LS DYNA Keyword User's Manual*, Version 970. 2003.
99. Tomlin, O. *A Case Study in Applying RDM® to Automotive BIW Design*. in *2013 Optimised Product Engineering Conference*. 2013. Motor Heritage Centre, Gaydon: <http://www.grm-consulting.co.uk/index.php/conf-agenda/>.
100. Palkowski, H., O. Sokolova, and A. Carrado, *Encyclopedia of Automotive Engineering Chapter: Sandwich Materials*. 2015: John Wiley & Sons.
101. Emerson, D., *Energy absorption characteristics of automotive-type beam structures in high-speed crush testing*, in *SPE Automotive Composites Conference and Exhibition*. 2013, Society of Plastic Engineers.
102. Ramaswamy, K., Radhakrishnan, J., Patham, B., Savic, V., *Fast and Stable Quasi-Static Bending Simulations in LS-DYNA: Identification of Optimal Finite Element Model Parameters*. 2016, SAE International.
103. LSTC, *Modeling of composites* in LS-DYNA. 2012, LSTC.
104. LSTC. LS-DYNA. 2016 [cited 2016 03/06/2016].
105. Vanderplaats R&D, I. *GENESIS Software for Structural Analysis and Optimization* 2016 [cited 2016 03/06/2016].
106. Kecman, D., Special Issue Structural Crashworthiness Conference, *Bending collapse of rectangular and square section tubes*. International Journal of Mechanical Sciences, 1983. 25(9): p. 623-636.
107. Youssef, M.A., *Analytical prediction of the linear and nonlinear behaviour of steel beams rehabilitated using FRP sheets*. Engineering Structures, 2006. 28(6): p. 903-911.
108. Štok, B. and M. Halilović, *Analytical solutions in elasto-plastic bending of beams with rectangular cross section*. Applied Mathematical Modelling, 2009. 33(3): p. 1749-1760.
109. Pastor, M.M. and F. Roure, *Open cross-section beams under pure bending II. Finite element simulation*. Thin-Walled Structures, 2009. 47(5): p. 514-521.
110. Patton, R., F. Li, and M. Edwards, *Causes of weight reduction effect of material substitution on constant stiffness components*. Thin-Walled Structures, 2004. 42: p. 613 - 637.

## APPENDIX A

### Study of the nature of the adhesive S10 – Chapter 3, Section 3.3 “Adhesive”

Microscopy images, as shown in Figure 3-2 and reshown in Figure A-1 of the coupon specimen from testing in Chapter 4 were used to confirm layup ahead of simulation runs and offer the opportunity to investigate the nature of the adhesive further. The cross sectional image of the final material shows inclusions in the adhesive. The manufacturer’s formulation indicates that the adhesive contains aluminium tri-hydrate. This was verified using Scanning Electron Microscopy (Energy-dispersive X-ray spectroscopy – EDS) methods. The SEM used is a Philips x130 FEG SEM with Oxford Inca software.

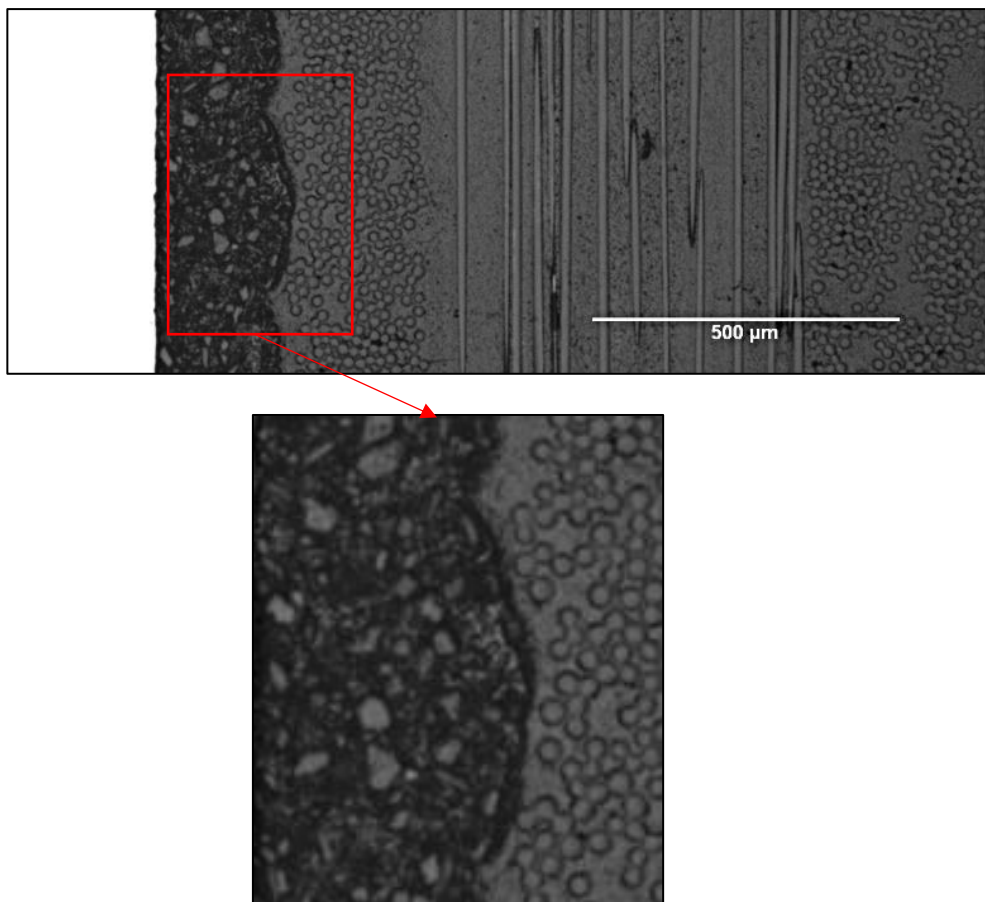


*Figure A-1: Optical microscopy image of the cross section of a hybrid DP600 PA6 GF60 specimen showing the adhesive (top) and composite (bottom) layers – scale*

*>500 μm*

The following are a series of SEM images used to identify the inclusions in the adhesive.

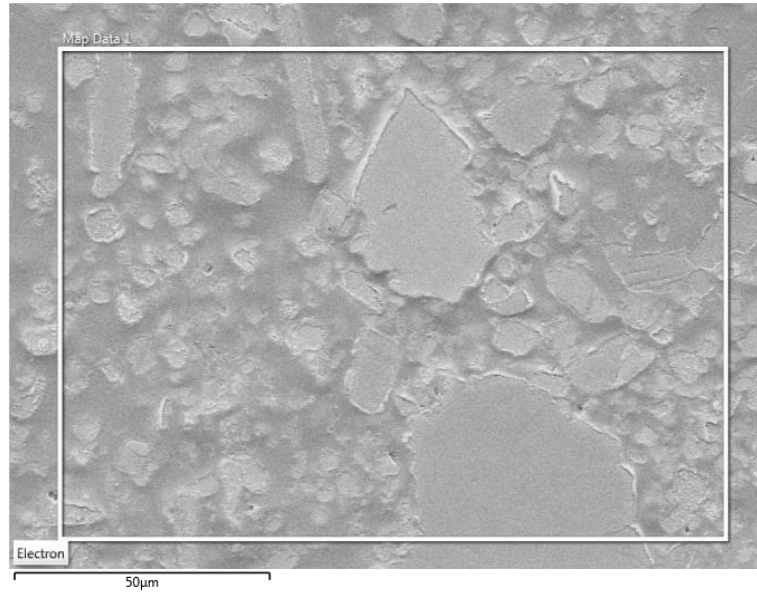


*Image A-1: SEM image of the adhesive*

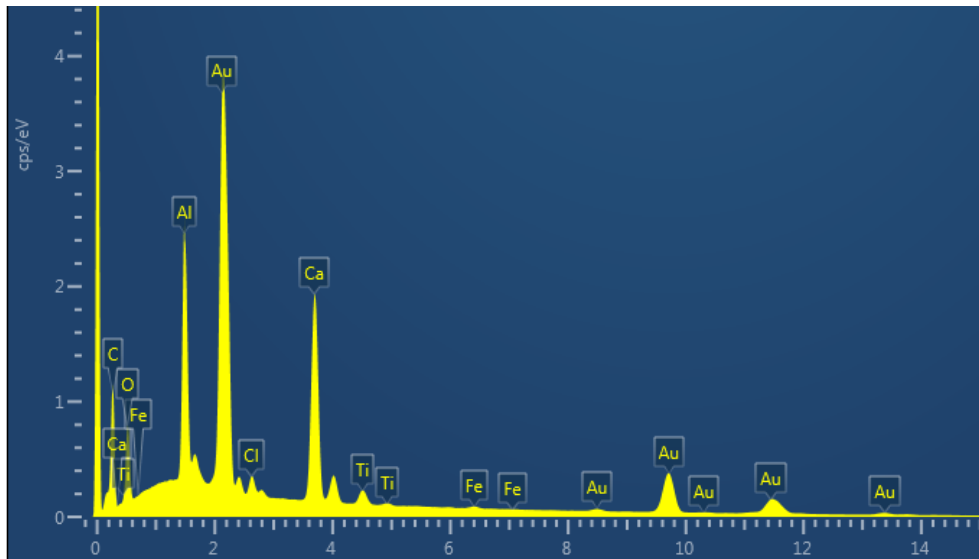


*Figure A-2: EDS graph showing the elements present in the adhesive*

Image A-1 highlights the presence of inclusions in the cured adhesive. The scanning reveals the presence of carbon, oxygen, calcium, aluminium, titanium,

chlorine and iron. Table A-1 summarises the element weight distribution as calculated by the SEM.

*Table A-1: Element weight distribution in the adhesive layer SAS 272*

Element	Weight %
C	41.2
O	28.3
Ca	16.3
Al	10.9
Ti	1.8
Cl	1.2
Fe	0.4

The presence of gold on the spectrum, as shown in Figure A-2, is explained by the coating applied to the specimen in order to carry out the scanning. Without the coating, the beam damages the specimen and does not provide readings. The element distribution images show that the nuggets are composed either of a combination of aluminium and oxygen or calcium.

These results confirm the presence of aluminium tri-hydroxide, as stated by the manufacturer.

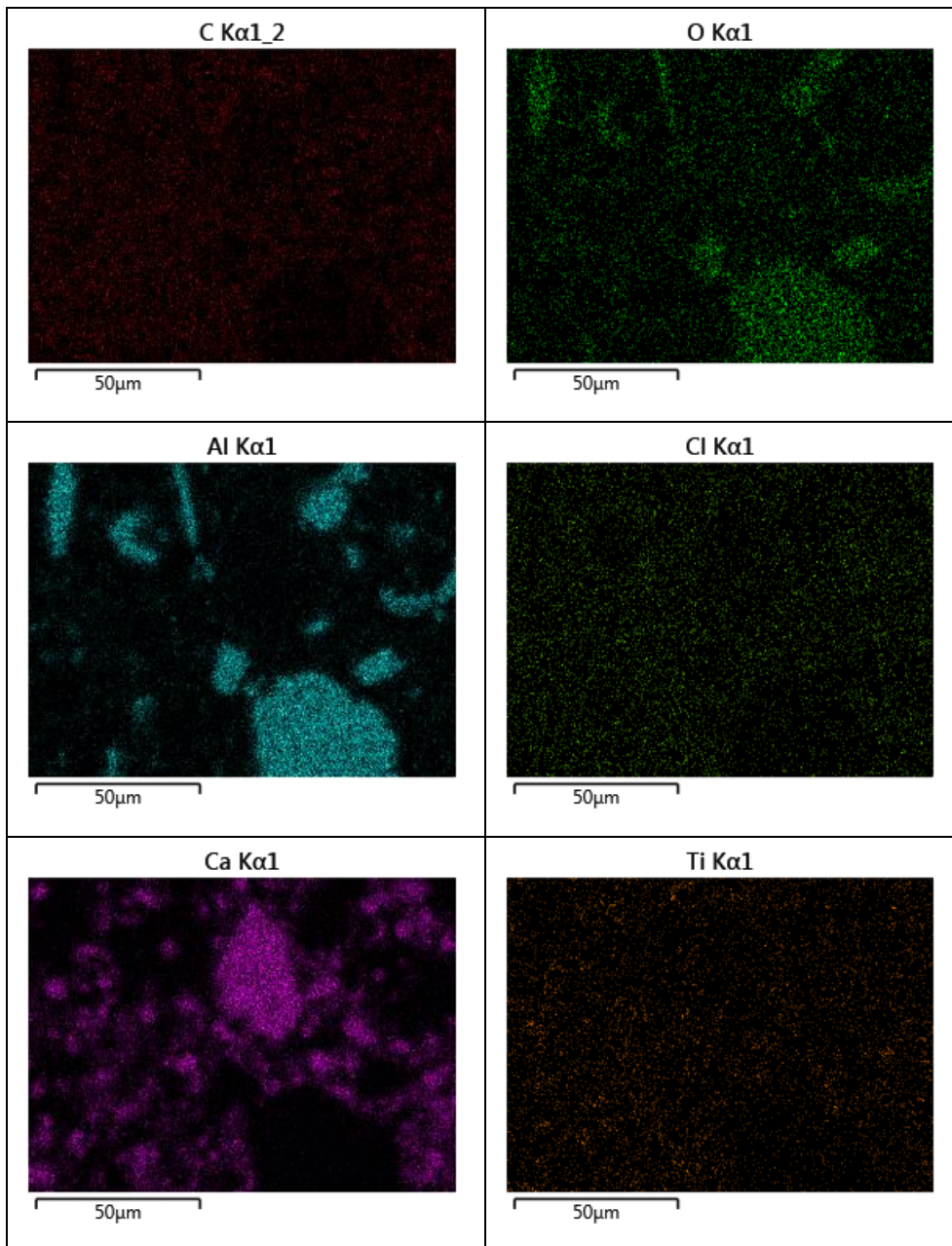


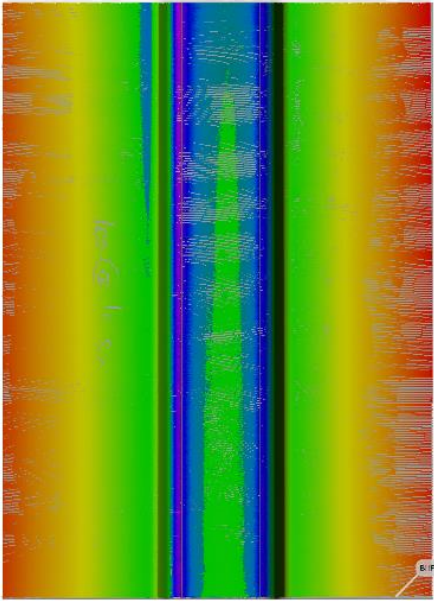
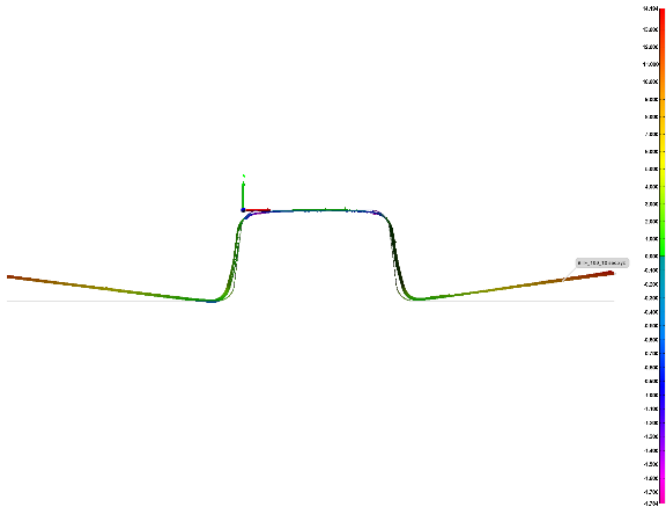
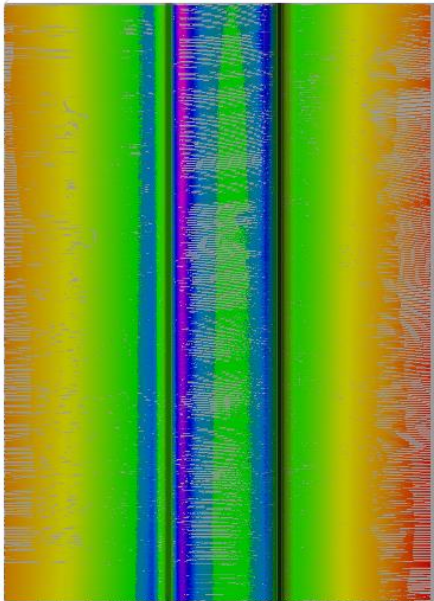
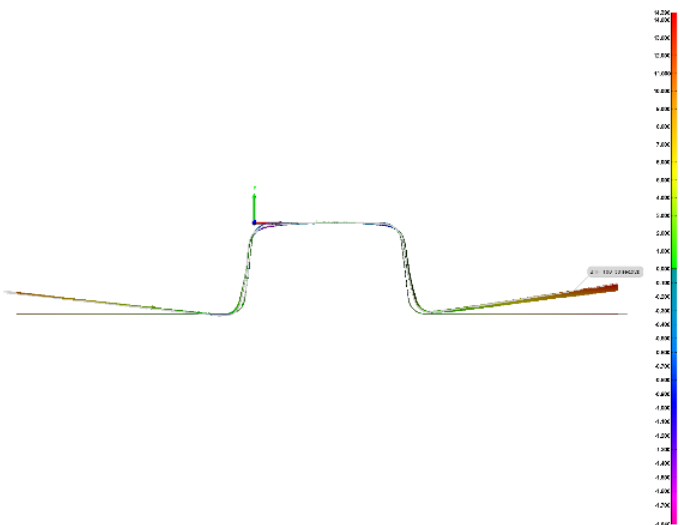
*Figure A-3: Scans showing presence of elements in inclusions*

## APPENDIX B

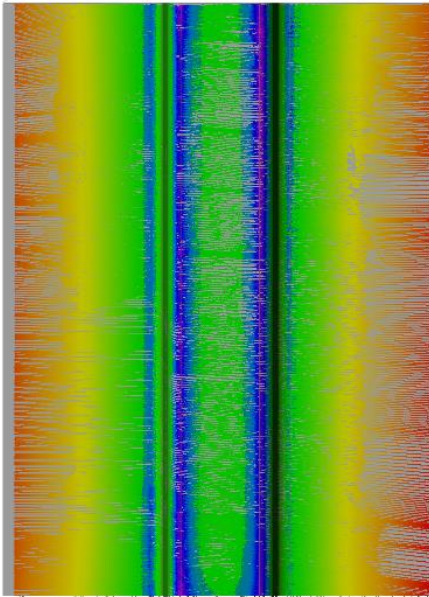
### Springback study, Chapter 3, 3.4.1.2 “Shaping the specimens”

Table B-1 shows the scans produced in the springback study.

*Table B-1: Scans of springback samples, with associated rate, pressure and hold time information*

Rate, Pressure, Hold Time Top view of samples	Rate, Pressure, Hold Time Springback side profile (mm)
<p>R: 800 kN/s, P: 100 kN; HT: 10 s</p> 	<p>800_100_10</p>  <p>Max deflection ~14 mm</p>
<p>R: 800 kN/s, P: 100 kN; HT: 30 s</p> 	<p>800_100_30</p>  <p>Max deflection ~14 mm</p>

R: 800 kN/s, P: 800 kN; HT: 10 s

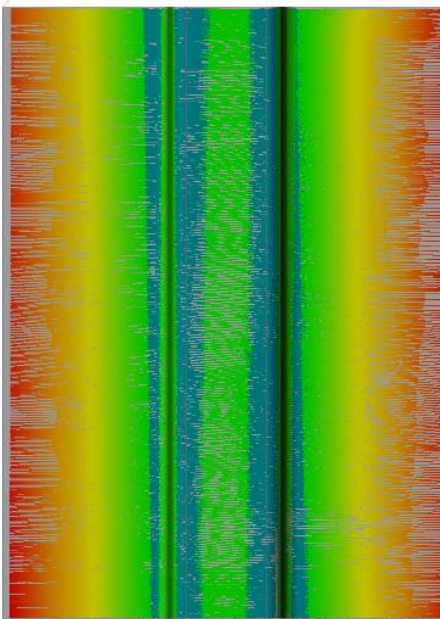


800\_800\_10



Max deflection ~13 mm

R: 800 kN/s, P: 800 kN; HT: 30 s



800\_800\_30



Max deflection ~11 mm

## APPENDIX C

### Sika Adhesive Data Sheet



# PRODUCT DATA SHEET

## SikaPower®-490 C

### STRUCTURAL AND CRASH RESISTANT 2 COMPONENT ADHESIVE

#### PROVISIONAL TECHNICAL PRODUCT DATA

Properties	Component A	Component B
	SikaPower®-490 C	SikaPower®-490 C
Chemical base	Epoxy	Amine
Color	red	white
Non-volatile compounds (CQP <sup>1</sup> 576-1)	99 % approx.	99 % approx.
Particle size	maximum 150 µm approx.	300 µm approx.
Density before curing (CQP 576-1)	1.1 kg/l	1.1 kg/l
Density after curing (CQP 576-1)	1.1 kg/l	
Mixing ratio (weight)	2	1
Mixing ratio (volume)	2	1
Viscosity; 20 °C, P/P 25 mm, 1 mm gap, Shear rate 10 s <sup>-1</sup>	430 Pa·s approx.	80 Pa·s approx.
Application temperature	15 – 35 °C	
Curing time (object temperature)	7 days at room temperature or 4 hours room temperature plus 30 min at 85 °C	
Lap shear strength <sup>2,3</sup> (CQP 580-1,-6 / EN 1465)	Curing 7 d room temperature Curing 4 h RT+ 30 min 85 °C	28 MPa approx. 28 MPa approx.
Dynamic resistance <sup>2,4</sup> (CQP 580-3,-6 / ISO 11343)	Curing 7 d room temperature Curing 4 h RT+ 30 min 85 °C	30 N/mm approx. 30 N/mm approx.
E-Modulus <sup>2,5</sup> (CQP 580-5,-6 / ISO 527)	1700 MPa approx.	
Tensile strength <sup>3</sup> (CQP 580-5,-6 / ISO 527)	28 MPa approx.	
Elongation at break <sup>5</sup> (CQP 580-5,-6 / ISO 527)	3 % approx.	
Glass transition temperature, DMTA 1Hz (CQP 509-1 / DIN EN ISO 6721)	Curing 7 d room temperature Curing 4 h RT+ 30 min 85 °C	65 °C approx. 95 °C approx.
Shelf life <sup>2</sup>	12 month	

1) Corporate Quality Procedure

2) 23°C

3) H420LAD + Z 1.5 mm, adhesive layer: 25 x 10 x 0.3 mm

4) DC 04 ZE 75/75 0.8 mm; adhesive layer: 20 x 30 x 0.3 mm; Impact speed : 2.0 m/s

5) Curing 4h RT + 30 min 85 °C

#### DESCRIPTION

SikaPower®-490 C is a two component ambient temperature applied adhesive based on Epoxy/Amin and is designed for steel, aluminium and CFRP bonding. The adhesive cures at ambient temperature, at higher temperatures (e.g. 30 min at 85 °C) the curing is accelerated. SikaPower®-490 C is manufactured in accordance with ISO 9001/ 14001 quality assurance system and with the Responsible Care program.

#### PRODUCT BENEFITS

- Can be applied with 1C application gun
- Increased stiffness
- Structural and crash resistant application
- Inhibits corrosion
- Bonding of different substrates
- Contains glass beads (0.3 mm) to ensure defined bonding thickness
- Does not contain solvents or PVC

#### APPLICATION AREAS

SikaPower®-490 C adheres on various metals and CFRP substrates and enables structural and crash resistant bonding applications on substrates free of oil, grease and dirt. The adhesive is suitable for applications in combination with spot welding, riveting or clinching. This product is suitable for professional experienced users only.

Product Data Sheet

SikaPower®-490 C

02/2014, Version 1

CH



## CURING MECHANISM

The SikaPower®-490 C cartridge contains two separate chambers, one with an epoxy respectively an amine component. While extruding through the static mixer both components are getting mixed and the curing takes place at room temperature through reaction of the two components. The curing speed depends on temperature as well as time. An increased curing temperature of 80 °C – 180 °C increases the thermo-dependent mechanical properties of the adhesive.

## APPLICATION METHOD

### Application tools

In order to extrude the adhesive an electrical 1 component application gun with piston and driving rod is required. Suitable mixers are supplied together with the adhesive.

### Surface preparation

The surface to be bonded must be free of oil, grease and other impurities. The bonding area must be cleaned with a lint free towel and n-Heptane. It is advised to grind the bonding surface followed by cleaning with n-Heptane.

### Application of the adhesive

Apply a small amount of adhesive until both components start to flow evenly. Clean off the adhesive from both outlet with a clean spatula and dispose it. Attach the static mixer, press out the adhesive and ensure that both components emerge uniformly. Press out and discard at least an amount equal to the length of the mixer.

The adhesive has to be applied on both substrates to be bonded. Spreading the adhesive prior to joining with a clean spatula will guarantee that the entire ground surface will be covered to ensure corrosion protection. The parts must be joint and fixed together within the open time of maximum 60 minutes. The adhesive cures at room temperature. An increased curing speed can be achieved by heating up the parts to 85 °C for 30 minutes. This process provides shorter curing time and higher strength is achieved.

In case the application is interrupted for 30 minutes or more, the mixer has to be purged once again prior application.

### Removal of adhesive residuals

Uncured adhesive residuals can be removed with isopropyl alcohol. Cured material can be removed mechanically only. Hands/Body must be cleaned immediately with Sika®Handclean or with a suitable hand cleaning paste and water. Do not use solvents!  
For specific advice contact Sika Automotive.

## FURTHER INFORMATION

Following documentation is available upon request:

- Material safety data sheet

## PACKAGING INFORMATION

cartridge 2 in 1	195 ml
------------------	--------

## VALUE BASE

All technical data stated in this Product Data Sheet are based on laboratory tests. Actual measured data may vary due to circumstances beyond our control.

## HEALTH AND SAFETY INFORMATION

For information and advice on the safe handling, storage and disposal of the chemical products, users shall refer to the most recent Material Safety Data Sheet containing physical, ecological, toxicological and other safety-related data.

## LEGAL NOTES

The information, and, in particular, the recommendations relating to the application and end-use of Sika products, are given in good faith based on Sika's current knowledge and experience of the products when properly stored, handled and applied under normal conditions in accordance with Sika's recommendations. In practice, the differences in materials, substrates and actual site conditions are such that no warranty in respect of merchantability or of fitness for a particular purpose, nor any liability arising out of any legal relationship whatsoever, can be inferred either from this information, or from any written recommendations, or from any other advice offered. The user of the product must test the product's suitability for the intended application and purpose. Sika reserves the right to change the properties of its product. The proprietary rights of third parties must be observed. All orders are accepted subject to our current terms of sale and delivery. Users must always refer to the most recent issue of the local Product Data Sheet for the product concerned, copies of which will be supplied on

Product DataSheet  
SikaPower®-490 C  
02/2014, Version 1  
CHE

Sika Schweiz AG  
Tueffenwies 16  
8048 Zurich  
Switzerland  
[www.sika.com/automotive](http://www.sika.com/automotive)



**BUILDING TRUST**



## APPENDIX D

### Additional notes on coupon performance, Chapter 4

During the coupon tests, the samples were monitored throughout, leading to the observation that there was no delamination or failure of the composite and adhesive layers in the elastic region of the test i.e. a deformation of up to 0.5 mm.

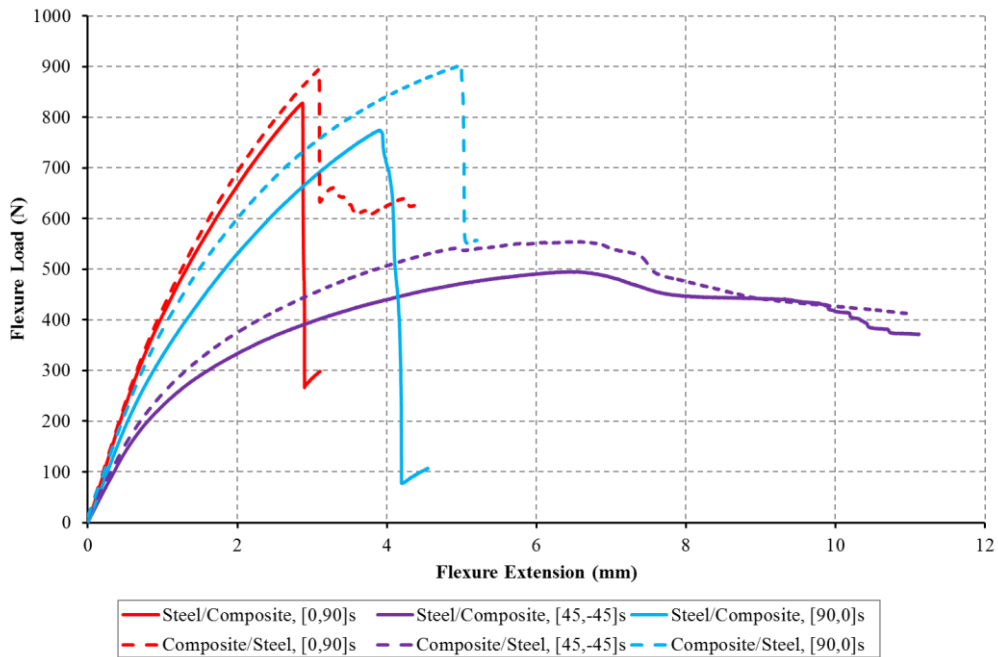


*Figure D-1: Load-extension diagram for the 0.8 mm hybrid coupon samples tested to failure - reshown*

In the reshown Figure D-1, it is apparent that the samples where the composite is in compression outperform the samples where the composite is in tension. They also show variations in failure modes.

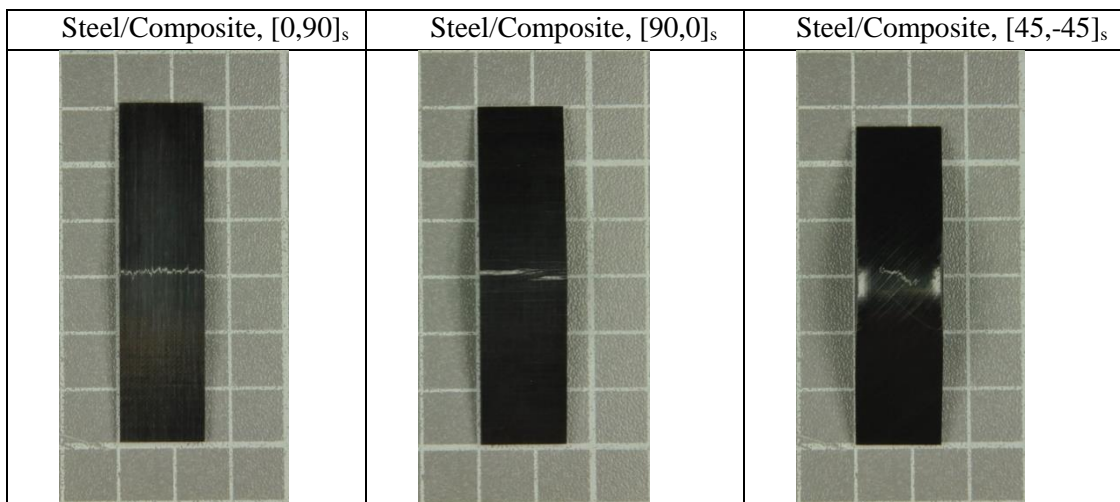
An initial observation (Table D-1) of the samples provided information on the failure modes; additionally, highlighting the tensile versus compressive nature of the loading through the composite layer.

Table D-1: Notes on sample failure patterns

Sample	Notes
Steel/Composite [0,90] <sub>s</sub>	tensile fibre failure, delamination from adhesive
Steel/Composite [45,-45] <sub>s</sub>	matrix failure in shear, tensile fibre failure, strain “pinching” of the composite layer (slight anticlastic bending), adhesive failure
Steel/Composite [90,0] <sub>s</sub>	matrix failure in the outer layers, adhesive failure at matrix failure
Composite/Steel [0,90] <sub>s</sub>	compressive fibre failure, delamination on 3 samples only
Composite/Steel [45,-45] <sub>s</sub>	matrix failure in shear, compressive fibre failure, “expansion” of the composite layer
Composite/Steel [90,0] <sub>s</sub> :	delamination between layers, composite compressive failure

Images in Table D-2, representative of the Steel/Composite failure modes for [0,90]<sub>s</sub>, [90,0]<sub>s</sub> and [45,-45]<sub>s</sub> respectively confirm the observations above. The background grid seen in the images is 10 mm by 10 mm.

Table D-2: Representative failure (photographic documentation)



Further assessments would be possible if failure was a major focus of the research where digital image correlation, acoustic emissions, optical microscopy techniques and specialist resins could be used in parallel to provide detailed information as to the nature of the failure and propagation patterns within the samples.

During the analysis of the results, it was also noted that samples tested in composite-over-steel set-ups presented a higher load at failure than the samples tested in steel-over-composite. In the C/S tests, the fibres in the composite are mainly in compression, whereas in S/C tests, the fibres are primarily in tension. This was also witnessed by Dlugosch [28]. It is speculated that the failure mechanism and presence of the impactor plays a role in this. Indeed, considering only the outer layer of composite fibres in tension, once failure occurs, there is minimal load transfer from the surrounding material. In compression however, careful examination of the samples shows that although there is complete fibre failure, the failure surfaces are still in contact, compressed together as the samples bend.

Table D-3 shows images of the samples in composite compression. The broken fibres are seen to overlap which implies that even though the fibres are now discontinuous, the load can still be carried through the layers. There is also possibility that the presence of the roller from the testing rig delays the failure as it prevents sample disintegration. The geometrical cross section of the samples also increases, which would increase the stiffness of the overall sample.

Table D-3: Image captures of the compressive zone of the samples – fibre overlap

show

